

DESIGN OF A LOW COST, HIGH SPEED ROBOT FOR
POULTRY PROCESSING

A Thesis
Presented to
The Academic Faculty

By

Eric Anderson

In Partial Fulfillment
Of the Requirements for the Degree
Master of Science in Mechanical Engineering

Georgia Institute of Technology
July, 2004

DESIGN OF A LOW COST, HIGH SPEED ROBOT FOR
POULTRY PROCESSING

Approved By:

Dr. Harvey Lipkin

Dr. Imme Ebert-Uphoff

Dr. Wayne Book

Date Approved: 7/7/2004

Acknowledgement

First and foremost I would like to express my deep gratitude towards my co-advisors on this project, Dr. Harvey Lipkin and Mr. Gary McMurray. They each provided a wealth of knowledge, creative ideas, and encouragement during the course of this project. They provided guidance when I needed it and let me explore things on my own when it was appropriate. I learned a great deal working on this project and much of the credit for that should go to them. I would also like to thank them for letting me take on this project and for providing such a pleasant work environment. It was a pleasure working with each of them and working on this project. I would also like to thank the thesis committee members, Dr. Wayne J. Book and Dr. Imme Ebert-Uphoff, for their expertise and assistance in shaping the final version of this thesis.

I would like to thank the Students and Staff of the Georgia Tech Research Institute. They were always willing to offer help and advice when I needed it. Wiley Holcombe deserves special thanks for willingness to share his expert knowledge of all things related to mechanical design. He helped me with many aspects of this thesis and was always eager to do so. Special thanks also go to Alain Gaillard and Alex Debais for assistance building the proof of concept mockup.

Funding for this research was provided by the U.S. poultry and Egg Association. Thanks to the U.S. Poultry and Egg Association, as well as all of the local poultry processing facilities, and members of the poultry processing industry who provided information and assistance.

Last but not least I would like to acknowledge all the family members and friends who provided insight, encouragement, and advice throughout the project. Their help was crucial to the completion of this thesis, and to maintaining a positive outlook when things got difficult. I would like to extend special thanks to my parents Mr. William Anderson, and Mrs. Susan Anderson, as well as to my friend Mathias Craig.

Table of Contents

LIST OF TABLES.....	ix
LIST OF FIGURES	xii
SUMMARY	xxiii
CHAPTER 1, INTRODUCTION	1
1.1 Background and Motivation	1
1.2 Review of Previous Work.....	9
1.2.1 General Robotics.....	9
1.2.2 Robots in Poultry Processing.....	15
1.3 Goals of This Research	20
1.4 Design Methodology.....	21
1.5 Organization of the Thesis.....	21
CHAPTER 2, PLANNING AND CLARIFYING THE TASK.....	24
2.1 Overview of Poultry Processing Operations.....	24
2.2 Current WOG Hanging Process.....	26
2.3 Quantifying the Task.....	30
2.3.1 Assumptions.....	30
2.3.2 Defining Coordinate Frames.....	32
2.3.3 WOG Characterization.....	35
2.3.4 Constraints	36
2.3.5 Robot Motion.....	39
2.4 Requirement List.....	42
CHAPTER 3, CONCEPTUAL DESIGN	46
3.1 Establishment of the Function Structure.....	46
3.1.1 Tree Diagram	47
3.1.2 Flow Chart Diagram	50
3.2 Concept Development.....	52
3.2.1 Decomposition of Ideas	54
3.2.2 Construction of a Morphological Matrix	59
3.2.3 Refinement of the Morphological Matrix	61
3.2.4 Synthesis of a Representative Group of Solutions.....	66
3.3 Evaluation of Concepts.....	73
3.3.1 Evaluation Criteria.....	74
3.3.2 Evaluation Criteria Weighting Factors	79
3.3.3 Evaluation of Solutions for <i>X</i> , <i>Y</i> and <i>Z</i> Motions.....	82
3.3.4 Evaluation of Solutions for <i>Rotate</i> and <i>Flip</i> Motions.....	86

3.4 Concept Selection	90
CHAPTER 4, KINEMATIC DESIGN	94
4.1 Introduction.....	94
4.2 Design of Parallel Base.....	95
4.2.1 Structural Synthesis of Parallel Base Using Group Theory.....	95
4.2.2 Reverse Kinematics	110
4.2.3 Forward Kinematics.....	118
4.2.4 Angles of Passive Joints of the Parallel Mechanism	125
4.3 Overview of Specialized End Effector Design.....	130
4.4 Design and Integration of Robotic Wrist.....	135
4.4.1 General Design.....	135
4.4.2 Kinematics of the Wrist	140
4.5 Jacobian and Singularity analysis of the Parallel Mechanism	142
4.5.1 Two Part Jacobian of Parallel Mechanism.....	144
4.5.2 Singularity Analysis.....	146
CHAPTER 5, OPTIMIZATION OF ROBOT PARAMETERS	151
5.1 Characterization of Parameters.....	151
5.2 Characterization of Workspace.....	154
5.3 Qualitative Work Space Study.....	155
5.4 Quantitative Work Space Study.....	160
5.4.1 Concerns About Singular and Near-Singular Configurations	161
5.4.2 Study Procedure and Results	162
5.5 Range of Motion	169
5.6 Wrist Vectors \overline{FG} and \overline{EF}	170
5.7 Conclusion	174
CHAPTER 6, MODELING AND DETAIL DESIGN	176
6.1 Introduction.....	176
6.2 Proof of Concept Mockup.....	177
6.2.1 Constructability Issues.....	178
6.2.2 Confirmation of Robot Behavior	182
6.3 Comments on Materials and Joint Construction.....	184
6.4 Dynamic Model	187
6.4.1 Dynamic Wrist Model.....	187
6.4.2 Dynamic Parallel Mechanism Model.....	194
6.5 Dynamic Analysis.....	198
6.5.1 Defining the Tasks	199
6.5.2 Motion Planning.....	202
6.5.3 Generating CAD Prototypes	204
6.5.4 First Dynamic Prototype	206
6.5.5 Second Dynamic Prototype.....	209
6.5.6 Third Dynamic Prototype	212
6.6 Motor Selection.....	217
6.7 Cost Analysis	220

CHAPTER 7, CLOSURE	223
7.1 Summary	223
7.2 Critical Review of Design	224
7.3 Future Work	225
APPENDIX A, COMPLETE ROBOT SOLUTION MATRIX	227
APPENDIX B, SOLUTION EVALUATION MATRIX	233
B.1 Evaluation of Solutions for the X, Y, and Z Motions	234
B.2 Evaluation of Solutions for the Flip and Rotate Motions	240
APPENDIX C, MATLAB CODE	244
C.1 Matlab Code for Qualitative Workspace Study	245
C.1.1 RotDeltVar.m	245
C.1.2 RotDeltVar2.m	248
C.1.3 RDeltWSRKin.m	250
C.1.4 rKinRot.m	252
C.1.5 WSplotRKin.m	253
C.2 Matlab Code for Quantitative Workspace Study	253
C.2.1 LinkVar.m	254
C.2.2 robotscale3.m	255
C.2.3 FaceinWS2.m	256
C.2.4 inWS2.m	257
C.2.5 WSboundary2.m	258
C.2.6 RDeltWSRKin2.m	260
C.3 Matlab Code for Calculating Range of Joint Angles	260
C.3.1 JointRange.m	261
C.4 Matlab Code for Dynamic Analysis of Robot	262
C.4.1 DynamicModel.m	262
C.4.2 wristsim.m	268
C.4.3 PlatBal.m	269
C.4.4 armBal.m	270
C.4.5 dif.m	271
APPENDIX D, WORKSPACE PLOTS FOR THE QUALITATIVE WORKSPACE STUDY	272
D.1 First Round of Qualitative Workspace Study	273
D.2 Second Round of Qualitative Study, (c-e) is Positive	288
D.3 Second Round of Qualitative Study, (c-e) is Negative	294
APPENDIX E, RESULTS OF THE DYNAMIC ANALYSIS	300
E.1 Dynamic Analysis of First Prototype for Breast Up WOG Acquisition	301
E.2 Dynamic Analysis of First Prototype for Breast Down WOG Acquisition	305
E.3 Dynamic Analysis of Second Prototype for Breast Up WOG Acquisition	309
E.4 Dynamic Analysis of Second Prototype for Breast Down WOG Acquisition	313

E.5 Dynamic Analysis of Third Prototype for Breast Up WOG Acquisition.....	317
E.6 Dynamic Analysis of Third Prototype for Breast Down WOG Acquisition.....	321
APPENDIX F, ACTUATOR CUTSHEETS	325
F.1 Parallel Mechanism Actuator Cutsheets.....	326
F.2 Flip Motion Generating Wrist Actuator Cutsheets.....	331
F.3 Rotate Motion Generating Wrist Actuator Cutsheets.....	333
REFERENCES	335

LIST OF TABLES

Table 1.1: Comparison of robot and human worker.	3
Table 2.1: Summary of initial and final conditions of WOGs.....	42
Table 2.2: Requirements list.	43
Table 3.1: Basic robot ideas.....	55
Table 3.2: Morphological matrix.....	60
Table 3.3: Refined morphological matrix.....	64
Table 3.4: Final morphological matrix.	66
Table 3.5: Actuation concepts.....	68
Table 3.6: First 12 rows of the robot solution matrix.	70
Table 3.7: Refined robot solution matrix.....	72
Table 3.8: Representative group of robot solutions.....	73
Table 3.9: Descriptions of subtask specific evaluation criteria.	77
Table 3.10: Evaluation criteria importance matrix.	81
Table 3.11: Evaluation matrix for X , Y , and Z motion solutions.	83
Table 3.12: Reference geometries for evaluation of the X , Y , and Z motion solutions.....	84
Table 3.13: Results of evaluation of X , Y , and Z motion solutions.....	85
Table 3.14: Reference points for evaluation of the <i>Flip</i> and <i>Rotate</i> motion solutions.	87
Table 3.15: Evaluation matrix for <i>Flip</i> and <i>Rotate</i> motion solutions.	88
Table 3.16: Results of evaluation of <i>Flip</i> and <i>Rotate</i> motion solutions.....	89

Table 4.1: Subgroups of $\{D\}$.	96
Table 5.1: Single parameter variation for $(c-e)>0$.	158
Table 5.2: Two parameter variation for $(c-e)>0$.	158
Table 5.3: Single parameter variation for $(c-e)<0$.	159
Table 5.4: Two parameter variation for $(c-e)<0$.	159
Table 5.5: First set of results for secondary workspace study.	165
Table 5.6: Results from round two of quantitative workspace study.	166
Table 5.7: Rounded results from round two of quantitative workspace study.	167
Table 5.8: results of final round of quantitative workspace study.	168
Table 5.9: Location and range of mechanism workspace.	169
Table 5.10: Range of joint angles for parallel mechanism.	170
Table 6.1: Task definition for breast up WOG capture.	201
Table 6.2: Task definition for breast down WOG capture.	202
Table 6.3: Revised task definition for breast up WOG capture.	214
Table 6.4: Revised task definition for breast down WOG capture.	214
Table 6.5: Analysis of selected parallel mechanism actuator.	218
Table 6.6: Analysis of Selected <i>Flip</i> motion Actuator.	220
Table 6.7: Robot cost estimate.	220
Table A.1: Complete robot solution matrix (five pages).	228
Table B.1: First evaluation matrix for X , Y , and Z motion solutions.	234
Table B.2: Second evaluation matrix for X , Y , and Z motion solutions.	235
Table B.3: Third evaluation matrix for X , Y , and Z motion solutions.	236
Table B.4: Fourth evaluation matrix for X , Y , and Z motion solutions.	237

Table B.5: Fifth evaluation matrix for X , Y , and Z motion solutions.....	238
Table B.6: Weighted and summed evaluation matrix for X , Y , and Z motion solutions.	239
Table B.7: First evaluation matrix for <i>Flip</i> and <i>Rotate</i> motion solutions.....	240
Table B.8: Second evaluation matrix for <i>Flip</i> and <i>Rotate</i> motion solutions.	241
Table B.9: Third evaluation matrix for <i>Flip</i> and <i>Rotate</i> motion solutions.	242
Table B.10: Weighted and summed evaluation matrix for <i>Flip</i> and <i>Rotate</i> motion solutions.	243

LIST OF FIGURES

Figure 1.1: WOG	2
Figure 1.2: WOG rehang station.....	2
Figure 1.3: Per capita meat consumption in the U.S.....	7
Figure 1.4: ABB robot range, IRB 1400.....	11
Figure 1.5 ABB Flexpicker: an industrial Delta robot.....	12
Figure 1.6: ABB 940 Tricept.	14
Figure 1.7: Early prototype workcell loading traypacks.....	16
Figure 1.8: poultry back half being automatically loaded onto a spine removal machine.	18
Figure 1.9: Prototype for automatic loading of breast pieces into traypacks.....	19
Figure 1.10: DSI 512 water jet portioner.....	20
Figure 1.11: Outline of design process by thesis chapter.	23
Figure 2.1: Overview of poultry processing operation.	26
Figure 2.2: WOGs discharged from the chiller.....	27
Figure 2.3: WOGs circulating on the conveyor belt system.....	28
Figure 2.4: Typical conveyor belt system and shackle lines.	29
Figure 2.5: Proposed robot positions (top view).....	32
Figure 2.6: Global coordinate frame.....	33
Figure 2.7: WOG coordinate frame.....	34

Figure 2.8: Representation of Euler angles ZYZ.....	34
Figure 2.9: Inertial Properties of an ellipsoid	36
Figure 3.1: Overall function structure.....	47
Figure 3.2: Tree diagram.....	48
Figure 3.3: Flow chart diagram.....	51
Figure 4.1: SCARA Robot.....	99
Figure 4.2: Revolute pair and plane hinged parallelogram.....	103
Figure 4.3: RRPaR and RPaRR kinematic chains.	104
Figure 4.4: Translation-only parallel mechanism with two $\{X(w)\}$ chains.....	106
Figure 4.5: $\{X(w)\}$ and $\{D\}$ generating chains with same translational workspaces. ..	108
Figure 4.6: Parallel mechanism.....	109
Figure 4.7: Single leg of the parallel mechanism.	111
Figure 4.8: Distances between points used in the reverse kinematics.	112
Figure 4.9: Global coordinate frame and $X_{1i}Y_{1i}Z_{1i}$ coordinate frames.....	113
Figure 4.10: Constraints on the location of L_i	114
Figure 4.11: Elbow out and elbow in solutions to the reverse kinematics.	118
Figure 4.12: Constraint on the position of D_i	120
Figure 4.13: Constraint on the position of E	121
Figure 4.14: Intersection of three spheres.....	124
Figure 4.15: Platform up and platform down solutions to the forward kinematics.	125
Figure 4.16: Angles of the joints of the i th leg (viewed along Y_{1i}).....	128
Figure 4.17: Angles of the joints of the i th leg (viewed along Z_{3i}).....	129
Figure 4.18: CAD rendering of specialized end effector.....	131

Figure 4.19: Specialized end effector in operation.	131
Figure 4.20: Release method when WOG is acquired breast up.	133
Figure 4.21: Release method when WOG is acquired breast down.	134
Figure 4.22: First example of a <i>Rotate</i> then <i>Flip</i> wrist.	138
Figure 4.23: Second example of a <i>Rotate</i> then <i>Flip</i> wrist.	139
Figure 4.24: One possible <i>Flip</i> then <i>Rotate</i> wrist.	140
Figure 4.25: 2 DOF wrist.	142
Figure 4.26: Platform singularity due to two parallel $\overline{L_i D_i}$ vectors.	148
Figure 4.27: Platform singularity due to three co-planar $\overline{L_i D_i}$ vectors.	148
Figure 4.28: $\theta_{2i} = 180^\circ$ arm singularity.	149
Figure 4.29: $\theta_{2i} = 0^\circ$ arm singularity.	150
Figure 4.30: $\rho_{3i} = -90^\circ$ arm singularity.	150
Figure 5.1: Illustration of ρ_{0i} angles.	152
Figure 5.2: Link lengths of the i th arm of the parallel mechanism.	153
Figure 5.3: vectors \overline{EF} and \overline{FG}	154
Figure 5.4: Workspace plot for $\rho_{0i} = 30^\circ, 150^\circ, 270^\circ, l = 1, d = 1, c = 1, e = 1$	156
Figure 5.5: Check points on the top and bottom face of the required workspace.	164
Figure 5.6: Wrist vectors.	170
Figure 5.7: Top view schematic of parallel mechanism and shackle line for $\theta_{11} = \theta_{12} =$ $\theta_{13} = 0^\circ$ (lower links not shown).	173
Figure 5.8: Top view of arm one and shackle line for $\theta_{11} = 0^\circ$ (lower links not shown).	174

Figure 6.1: Spherical joint at point D_3	179
Figure 6.2: Spherical motion generator made from a revolute pair and a universal joint.	179
Figure 6.3: Connections of arms and moving platform of the parallel mechanism.....	181
Figure 6.4: Regular arm and shifted arm.	181
Figure 6.5: Proof of concept model.	182
Figure 6.6: Proof of concept model and end effector placing a WOG in a shackle.	183
Figure 6.7: Acceptable construction for a part with an internal angle $<135^\circ$	185
Figure 6.8: Acceptable construction for a shaft in a product contact area.....	186
Figure 6.9: Objects rotating with the wrist.	188
Figure 6.10: Wrist coordinate frames.	189
Figure 6.11: One moving object, required moment and force at center of mass.....	191
Figure 6.12: One moving object, required moment and force at center of wrist.....	192
Figure 6.13: Required force and moment at the wrist.	193
Figure 6.14: Forces acting on the moving platform.....	195
Figure 6.15: Objects included in the platform force balance.....	196
Figure 6.16: Upper link of i th arm.	198
Figure 6.17: Most demanding WOG transport for breast up WOG acquisition.	200
Figure 6.18: Most demanding WOG transport for breast down WOG acquisition.	201
Figure 6.19: Results of fitting a 3rd order polynomial to the X position of the moving platform.....	203
Figure 6.20: 3-D CAD model of first dynamic prototype.	207

Figure 6.21: Actuator moments for the first prototype when the WOG begins breast up.	208
Figure 6.22: Actuator moments for the first prototype when the WOG begins breast down.....	209
Figure 6.23: 3D CAD model of second dynamic prototype.	210
Figure 6.24: Actuator moments for second prototype when the WOG begins breast up.	211
Figure 6.25: Actuator moments for the second prototype when the WOG begins breast down.....	212
Figure 6.26: 3D CAD model of third dynamic prototype.....	213
Figure 6.27: Actuator moments for third prototype when the WOG begins breast up...	215
Figure 6.28: Actuator moments for third prototype when the WOG begins breast down.	216
Figure D.1: Variation of c : $l = 1, e = 1, d = 1, \rho_{0i} = [30^\circ, 150^\circ, 270^\circ]$	273
Figure D.2: Variation of l : $c = 1, e = 1, d = 1, \rho_{0i} = [30^\circ, 150^\circ, 270^\circ]$	274
Figure D.3: Variation of d : $l = 1, e = 1, c = 1, \rho_{0i} = [30^\circ, 150^\circ, 270^\circ]$	275
Figure D.4: Variation of e : $l = 1, d = 1, c = 1, \rho_{0i} = [30^\circ, 150^\circ, 270^\circ]$	276
Figure D.5: Variation of ρ_{0i} : $l = 1, e = 1, c = 1, d = 1$	277
Figure D.6: Variation of c and l : $d = 1, e = 1, \rho_{0i} = [30^\circ, 150^\circ, 270^\circ]$	278
Figure D.7: Variation of c and d : $l = 1, e = 1, \rho_{0i} = [30^\circ, 150^\circ, 270^\circ]$	279
Figure D.8: Variation of c and e : $d = 1, l = 1, \rho_{0i} = [30^\circ, 150^\circ, 270^\circ]$	280
Figure D.9: Variation of l and d : $c = 1, e = 1, \rho_{0i} = [30^\circ, 150^\circ, 270^\circ]$	281

Figure D.10: Variation of l and e : $c = 1, d = 1, \rho_{0i} = [30^\circ, 150^\circ, 270^\circ]$	282
Figure D.11: Variation of d and e : $c = 1, l = 1, \rho_{0i} = [30^\circ, 150^\circ, 270^\circ]$	283
Figure D.12: Variation of c, l and d : $e = 1, \rho_{0i} = [30^\circ, 150^\circ, 270^\circ]$	284
Figure D.13: Variation of c, l and e : $d = 1, \rho_{0i} = [30^\circ, 150^\circ, 270^\circ]$	285
Figure D.14: Variation of c, d and e : $l = 1, \rho_{0i} = [30^\circ, 150^\circ, 270^\circ]$	286
Figure D.15: Variation of l, d and e : $c = 1, \rho_{0i} = [30^\circ, 150^\circ, 270^\circ]$	287
Figure D.16: Positive variation of $(c-e)$: $l = 1, d = 1$	288
Figure D.17: Variation of l : $(c-e) = 0.5, d = 1$	289
Figure D.18: Variation of d : $(c-e) = 0.5, l = 1$	290
Figure D.19: Variation of l and positive variation of $(c-e)$: $d = 1$	291
Figure D.20: Variation of d and positive variation of $(c-e)$: $l = 1$	292
Figure D.21: Variation of l and d : $(c-e) = 0.5$	293
Figure D.22: Negative variation of $(c-e)$: $l = 1, d = 1$	294
Figure D.23: Variation of l : $d = 1, (c-e) = -0.5$	295
Figure D.24: Variation of d : $l = 1, (c-e) = -0.5$	296
Figure D.25: Variation of l and negative variation of $(c-e)$: $d = 1$	297
Figure D.26: Variation of d and negative variation of $(c-e)$: $l = 1$	298
Figure D.27: Variation of l and d : $(c-e) = -0.5$	299
Figure E.1: Motion of the moving platform in the global X direction (1 st prototype, breast up).	301
Figure E.2: Motion of the moving platform in the global Y direction (1 st prototype, breast up).	301

Figure E.3: Motion of the moving platform in the global Z direction (1 st prototype, Breast up).	302
Figure E.4: Motion and moment provided by the parallel mechanism actuator at point C_1 (1 st prototype, breast up).	302
Figure E.5: Motion and moment provided by the parallel mechanism actuator at point C_2 (1 st prototype, breast up).	303
Figure E.6: Motion and moment provided by the parallel mechanism actuator at point C_3 (1 st prototype, breast up).	303
Figure E.7: Motion and moment provided by the <i>Flip</i> motion wrist actuator at point F (1 st prototype, breast up).	304
Figure E.8: Motion and moment provided by the <i>Rotate</i> motion wrist actuator at point F (1 st prototype, breast up).	304
Figure E.9: Motion of the moving platform in the global X direction (1 st prototype, breast down).	305
Figure E.10: Motion of the moving platform in the global Y direction (1 st prototype, breast down).	305
Figure E.11: Motion of the moving platform in the global Z direction (1 st prototype, breast down).	306
Figure E.12: Motion and moment provided by the parallel mechanism actuator at point C_1 (1 st prototype, breast down).	306
Figure E.13: Motion and moment provided by the parallel mechanism actuator at point C_2 (1 st prototype, breast down).	307

Figure E.14: Motion and moment provided by the parallel mechanism actuator at point C_3 (1 st prototype, breast down).	307
Figure E.15: Motion and moment provided by the <i>Flip</i> motion wrist actuator at point F (1 st prototype, breast down).	308
Figure E.16: Motion and moment provided by the <i>Rotate</i> motion wrist actuator at point F (1 st prototype, breast down).	308
Figure E.17: Motion of the moving platform in the global X direction (2 nd prototype, breast up).....	309
Figure E.18: Motion of the moving platform in the global Y direction (2 nd prototype, breast up).....	309
Figure E.19: Motion of the moving platform in the global Z direction (2 nd prototype, breast up).....	310
Figure E.20: Motion and moment provided by the parallel mechanism actuator at point C_1 (2 nd prototype, breast up).	310
Figure E.21: Motion and moment provided by the parallel mechanism actuator at point C_2 (2 nd prototype, breast up).	311
Figure E.22: Motion and moment provided by the parallel mechanism actuator at point C_3 (2 nd prototype, breast up).	311
Figure E.23: Motion and moment provided by the <i>Flip</i> motion wrist actuator at point F (2 nd prototype, breast up).	312
Figure E.24: Motion and moment provided by the <i>Rotate</i> motion wrist actuator at point F (2 nd prototype, breast up).	312

Figure E.25: Motion of the moving platform in the global X direction (2 nd prototype, breast down).....	313
Figure E.26: Motion of the moving platform in the global Y direction (2 nd prototype, breast down).....	313
Figure E.27: Motion of the moving platform in the global Z direction (2 nd prototype, breast down).....	314
Figure E.28: Motion and moment provided by the parallel mechanism actuator at point C_1 (2 nd prototype, breast down).	314
Figure E.29: Motion and moment provided by the parallel mechanism actuator at point C_2 (2 nd prototype, breast down).	315
Figure E.30: Motion and moment provided by the parallel mechanism actuator at point C_3 (2 nd prototype, breast down).	315
Figure E.31: Motion and moment provided by the <i>Flip</i> motion wrist actuator at point F (2 nd prototype, breast down).	316
Figure E.32: Motion and moment provided by the <i>Rotate</i> motion wrist actuator at point F (2 nd prototype, breast down).	316
Figure E.33: Motion of the moving platform in the global X direction (3 rd prototype, breast up).....	317
Figure E.34: Motion of the moving platform in the global Y direction (3 rd prototype, breast up).....	317
Figure E.35: Motion of the moving platform in the global Z direction (3 rd prototype, breast up).....	318

Figure E.36: Motion and moment provided by the parallel mechanism actuator at point C_1 (3 rd prototype, breast up).....	318
Figure E.37: Motion and moment provided by the parallel mechanism actuator at point C_2 (3 rd prototype, breast up).....	319
Figure E.38: Motion and moment provided by the parallel mechanism actuator at point C_3 (3 rd prototype, breast up).....	319
Figure E.39: Motion and moment provided by the <i>Flip</i> motion wrist actuator at point F (3 rd prototype, breast up).....	320
Figure E.40: Motion and moment provided by the <i>Rotate</i> motion wrist actuator at point F (3 rd prototype, breast up).....	320
Figure E.41: Motion of the moving platform in the global X direction (3 rd prototype, breast down).....	321
Figure E.42: Motion of the moving platform in the global Y direction (3 rd prototype, breast down).....	321
Figure E.43: Motion of the moving platform in the global Z direction (3 rd prototype, breast down).....	322
Figure E.44: Motion and moment provided by the parallel mechanism actuator at point C_1 (3 rd prototype, breast down).....	322
Figure E.45: Motion and moment provided by the parallel mechanism actuator at point C_2 (3 rd prototype, breast down).....	323
Figure E.46: Motion and moment provided by the parallel mechanism actuator at point C_3 (3 rd prototype, breast down).....	323

Figure E.47: Motion and moment provided by the <i>Flip</i> motion wrist actuator at point <i>F</i> (3 rd prototype, breast down).....	324
Figure E.48: Motion and moment provided by the <i>Rotate</i> motion wrist actuator at point <i>F</i> (3 rd prototype, breast up).....	324
Figure F.1: Baldor ZDWNM3546T 1 hp washdown vector motor features.....	326
Figure F.2: Baldor ZDWNM3546T 1 hp washdown vector motor performance data. ..	326
Figure F.3: Baldor ZDWNM3546T 1hp washdown vector motor mechanical characteristics.....	327
Figure F.4: Baldor ZDWNM3546T 1 hp washdown vector motor dimensions.	328
Figure F.5: Baldor WDF6032AG 60:1 washdown gearbox features.....	329
Figure F.6: 60:1 Baldor WDF6032AG washdown gearbox performance.	329
Figure F.7: Baldor WDF6032AG 60:1 washdown gearbox dimensions.	330
Figure F.8: Atlas Copco LZB 34RL AR004.....	331
Figure F.9: Atlas Copco LZB 34RL AR004 product data.....	331
Figure F.10: Atlas Copco LZB 34RL AR004 performance curve: 81 psi.....	332
Figure F.11: Atlas Copco LZB 34RL AR004 dimensions.	332
Figure F.12: Pacific scientific PMA 23 washdown servo motor characteristics.	333
Figure F.13: Pacific scientific PMA 23 washdown servo motor dimensions.....	334

SUMMARY

In poultry plants in the United States, a water chiller is used to chill WOGs (de-feathered birds without giblets). After exiting the chiller these WOGs are manually transferred from a conveyor belt to shackles for further processing. The current process is less than ideal. The labor pool for jobs such as these is continuing to shrink and labor turnover is a constant problem. The rates of repetitive motion injury reported are high and are continuing to rise. In addition, many poultry producers see this as a bottleneck in the process. Automation has the potential to alleviate these problems.

The high variability of this task, cost restrictions, and special design considerations associated with meat handling equipment make automation of this task challenging. Industrial robots have traditionally been limited to tasks with low variability. These tasks usually involve moving rigid bodies with well-defined sizes and shapes between well-defined positions and orientations. WOGs are compliant bodies. They come in a wide variety of sizes and shapes. They are presented on the conveyor belt in a wide variety of positions and orientations. In addition the shackles onto which the WOGs are hung are compliant. The shackles are free to swing several inches in any horizontal direction and are free to rotate in the horizontal plane. Most robotic automation systems consist of a commercially available industrial robot, a specialized end effector and a control scheme. The economics of this task prohibit the use of a

commercially available industrial robot, as there are no industrial robots on the market that will offer a short enough payback. Robots have not yet been adapted to meat handling processes, and existing robotic designs are not well suited to the task. A meat processing robot must meet stringent USDA design criteria to prevent the robot from imparting any taste, color, bacteria, or foreign particles on the meat. In addition, a meat processing robot must be able to withstand the relatively hostile environment of a meat-processing plant, with high humidity and frequent washdowns with high pressure chlorinated water.

The design of a robotic system for picking up WOGs and hanging them on shackles is broken up into three areas: specialized end effector design, robot design, and machine vision system design. This thesis presents the robot design.

In designing a low cost, high-speed robot for poultry processing the requirements of the robot are defined and a variety of robot architectures, constructions, and materials are explored. Simple modifications to the existing shackle and conveyor setup to make the task easier for a robot are also explored. After the robot requirements are defined a large group of possible designs is developed. The possible designs are systematically evaluated and/or eliminated until a single design is selected. A hybrid serial-parallel robot consisting of a 3 DOF translation-only parallel base with a two DOF robotic wrist attached to the end is selected as the best solution. This robot is determined to provide low cost (installed cost of the robot and all support structures it requires, as well as ongoing maintenance costs), while achieving high reliability, and high speed. The forward and reverse kinematics for this robot are developed. A singularity analysis is carried out. A proof of concept mockup is built. A series of CAD prototypes are modeled

dynamically. Preliminary motor selections are made and a cost analysis of the final prototype is carried out.

CHAPTER 1

INTRODUCTION

1.1 Background and Motivation

In poultry plants in the United States, a water chiller is used to chill WOGs (de-feathered birds without giblets, see Figure 1.1). After exiting the chiller these WOGs are manually transferred from a conveyor belt to a moving shackle line for further processing (Figure 1.2). The current process is less than ideal. The labor pool for jobs such as these is continuing to shrink and labor turnover is a constant problem. The rates of repetitive motion injury reported are high and are continuing to rise. In addition, many poultry producers see this as a bottleneck in the process. Automation has the potential to alleviate these problems but the high variability of this task, cost restrictions, and special design considerations associated with meat handling equipment make automation of this task challenging.



Figure 1.1: WOG



Figure 1.2: WOG rehang station

Industrial robots have traditionally been limited to tasks with low variability. The use of industrial robots is well established in the automotive and semiconductor industries. The tasks required of these industrial robots usually involve moving nearly rigid bodies from one well-defined position and orientation to another. Generally, the size, shape, weight, rotational inertia, texture, and structural strength of the payload are also relatively well-defined. Currently available industrial robots are designed to perform well-defined repetitive tasks where high precision, high repeatability and high speed are needed. The downside of this is an intimidating cost structure. Industrial robots are often used when the task at hand requires precision that can not be achieved by a human, or when a mistake would be very costly. Table 1.1 shows a comparison of a typical industrial robot and a typical human worker [9].

Table 1.1: Comparison of robot and human worker.

	Industrial Robots	Human Worker
Cost	\$70,000 +	\$30,000 per year per 8-hour shift
Accuracy	<0.025 mm	2-3 mm
Speed	12.5 rad/s	≥ 7 rad/s
Flexibility	May need fixtures and calibration for each task	Versatile end-effector
Adaptability	Requires reprogramming for new task	Able to learn and perform a wide variety of tasks
System Intelligence	Limited to programmed routines	Ability to sense and respond to a wide variety of scenarios

Picking up WOGs from a conveyor belt and transferring them to shackles is a task with high variability and high compliance. Tasks such as this are performed almost exclusively by human workers. WOGs are compliant bodies; when forces are applied to them they deform significantly. They are both slippery, making a successful grasp difficult, and fragile, limiting the force that can be used for grasping. They come in a wide variety of sizes and shapes. Occasionally they arrive on the conveyor belt damaged or incomplete. They are presented on the conveyor belt in a wide variety of positions and orientations. In addition, the shackles onto which the WOGs are hung are free to swing several inches in any horizontal direction and are free to rotate about the vertical axis passing through the middle of the shackle.

Most robotic work cells consist of a commercially available industrial robot, a specialized end effector, a control scheme, and a sensor system. The economics of this task prohibit the use of a commercially available industrial robot, as there are no industrial robots on the market that will offer a short enough payback. For automation of this task to be feasible the automation system must have a one year payback. The yearly pay of a person who transfers WOGs from a conveyor to shackles is approximately \$30,000. There are two shifts per day. If we assume that the robotic workcell will do the work of one human worker, but that it will work both shifts, then the maximum cost of the robot, the end effector, the vision/sensor system, and the implementation of the robot is \$60,000. Robots that are currently available are far too expensive for a one year payback to be possible. A typical 6 degree of freedom industrial robot, such as the ABB Robot Range IRB 1040, costs approximately \$70,000, and can cost as much as \$70,000 to implement. Even without the specialized end effector and the vision/sensor system

that would put us well over the \$60,000 limit. For WOG hang process to be automated a much less expensive industrial robot must be developed.

For the transfer of WOGs from a conveyor belt to a moving shackle line, the high precision, and high repeatability of available industrial robots are not assets. The objects the robot interacts with in the WOG hang process are often compliant and are designed to work properly with the high variability inherent in the task. As a result the precision and repeatability tolerances for this task are low. By taking advantage of these low tolerances the robot can be designed to be lighter, to be less rigid, and to use materials that might be unsuitable for high precision industrial robots. All of these can result in a less expensive robot.

Robots have not yet been adapted to meat handling processes, and existing robotic designs are not well suited to the task. A meat-processing robot must meet stringent USDA design criteria to prevent the robot from imparting any taste, color, bacteria, or foreign particles on the meat. The USDA restricts the material that meat processing equipment can be made from, the types of connectors that can be used, the types of lubrication that can be used, and the shapes of parts used in meat processing equipment. Though some industrial robots have been retrofitted to meet USDA standards no industrial robots have been designed for meat processing. The few industrial robots available that meet USDA requirements meet them by coating the links of the robot in USDA approved materials and placing billows over the joints. If the coating chips or if one of the billows cracks then the robot no longer meets USDA requirements. In addition, a meat-processing robot must be able to withstand the relatively hostile environment of a plant with high humidity and frequent washdowns. No currently

available industrial robots are equipped to operate well in this environment. Robots used in such an environment have a history of frequent maintenance problems and high downtime. To work well, meat processing robots need to be designed specifically for the task. This has not yet been done by the robotics industry.

Chicken is one of the most consumed meats in the United States and chicken consumption continues to rise. Figure 1.3 shows the per capita consumption of red meats and chicken between 1970 and 2000 [11]. In 2000 Americans consumed more chicken than any other meat (retail cut equivalent). The per capita consumption of chicken was 81.7 lbs and the total consumption was 22.5 billion lbs. Chicken consumption has steadily increased over the last 30 years and is expected to steadily increase in the future. Automation has the potential to decrease the cost of transferring WOGs from a conveyor belt to shackles, and to increase throughput of this process. Lowered processing costs will allow the poultry industry to make larger profits and/or lower the cost of chicken. Higher throughput will allow the poultry industry to increase production capacity without building new facilities. This could save a lot of money as the demand for poultry increases in the future.

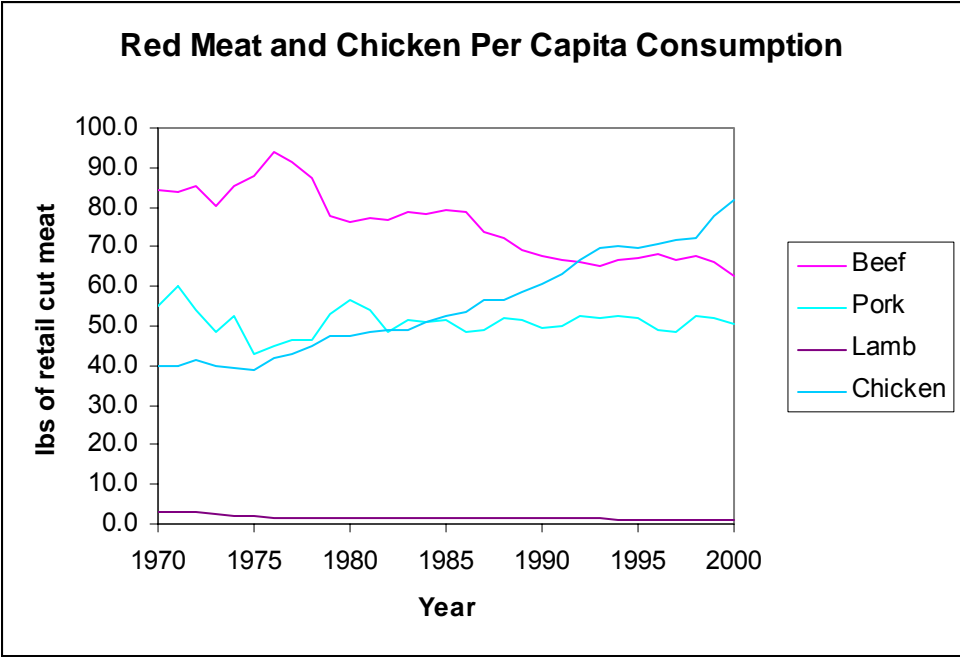


Figure 1.3: Per capita meat consumption in the U.S.

Though transferring WOGs from a conveyor belt to shackles is a task with high variability from an industrial robotics point of view, the motion required is still highly repetitive when compared to most human activity. Whenever people are required to perform highly repetitive tasks the risk of Repetitive Stress Injuries (RSI) arise. RSIs are caused by excessive and repetitive demands placed on the body and RSIs can lead to pain, inability to work, and permanent injury [7].

The poultry industry has greatly decreased the rates of occupational injuries and illnesses over the last decade, but the rates of RSI are still much higher than in other industries. Occupational Injuries and Illnesses in poultry processing have decreased from 2320 per 10,000 full time employees in 1992 to 1270 per 10,000 full time employees in 2001[7]. The rates of RSI in poultry processing have fallen in that time period as well,

but they remain higher than most other industries. From 1994 to 2001 the poultry processing industry ranked 3rd, 4th or 5th on the list of industries with the highest rates of disorders associated with repeated trauma. In 2001 (the most recent year for which data was available) poultry processing ranked 5th with an incident rate of 320.2 per 10,000 full time workers. This is 13.4 times higher than the national average of 23.8 per 10,000 full time employees [8]. The high rates of RSI in poultry processing provide a further incentive to automate the transfer of WOGs from a conveyor belt to shackles.

Previous work has provided a framework for applying robotics to tasks such as transferring WOGs from a conveyor to shackles where human level performance [10] is required. The development of sophisticated machine vision algorithms has made it possible to identify the position, orientation, and trajectory of work pieces. The development of a variety of reliable actuators and the extensive research into robot geometry has given robot designers a large number of viable options to choose from or to build upon. Sophisticated control systems allow robots to achieve high precision and high load capacity with links that are not as rigid, heavy, or expensive to produce as those used in most industrial robots. Research into specialized end effectors has shown that it is possible to grasp and secure slippery, compliant, fragile objects, such as WOGs, without damaging them. These advances make it possible to automate many unstructured poultry processing tasks effectively, and inexpensively.

1.2 Review of Previous Work

1.2.1 General Robotics

For this thesis, a robot is a multi-degree of freedom manipulator capable of being re-programmed through the use of a high level language. The motion of a robot is provided by revolute and/or prismatic actuators. A revolute actuator creates torque along a specified axis and rotational motion about that axis while a prismatic actuator creates force along a specified axis and linear motion parallel to that axis. The power that makes these actuators work can be supplied by a variety of sources, however most industrial actuators use electric, pneumatic, or hydraulic power. The geometry of a robot allows it to be categorized as belonging to one of three types: serial, parallel, or serial-parallel hybrid. Each type has its strengths and weaknesses, and there has been extensive research conducted on each of these types of robot. Both serial and parallel robots have been successfully developed and utilized as industrial robots. Though they are not yet widely used in industry serial-parallel hybrid robots are now being developed by some industrial robot manufacturers.

The basic structure of a serial robot is the open kinematic chain. A kinematic chain is open if there is only one sequence of links connecting the two ends of the chain. Each of the mechanical links in a serial robot is connected to the link before it by either a revolute or a prismatic joint. In an open kinematic chain each joint provides the structure with a single degree of freedom. Six degrees of freedom, three rotational and three translational, are needed to arbitrarily position and orient an object in 3-dimensional

space. Serial robots are much more common in industrial robotics than any other type of robot. In addition, the geometry of serial robots has been more extensively studied than the geometries of parallel robots or serial-parallel hybrid robots.

The geometry of a serial robot is primarily characterized by the actuators that connect the links of the open kinematic chain. The type and sequence of actuators allow a serial robot to be classified as one of five types: Cartesian, cylindrical, spherical, SCARA, and anthropomorphic. Figure 1.4 shows a typical industrial anthropomorphic arm with a three degree of freedom robotic wrist attached to the end. Starting from the base of the robot and moving towards the end effector a Cartesian robot starts with three prismatic actuators, a cylindrical robot starts with a revolute joint then two prismatic joints, a spherical robot starts with a revolute, a prismatic, then a revolute joint, a SCARA robot starts with two revolute joints then a prismatic joint, and an anthropomorphic robot starts with three revolute joints. Each of these robots is able to provide arbitrary positioning in a three dimensional work space. Most of them also provide some rotation, however the rotation is not decoupled from the translation. If a task requires orientations that can not be achieved with the first three links, a robotic wrist is generally added to the end of the chain. A robotic wrist is a set of revolute joints whose axes of rotation all intersect at a single point. A robotic wrist provides arbitrary rotation about that point.

The performance of serial robots is characterized by a large workspace and high dexterity. A disadvantage of serial robots is that each joint and each link must support the weight and loads of all of the following links of the kinematic chain. As a result serial robots tend to be constructed of very rigid, heavy links and they tend to have low maximum load to weight ratios.



Figure 1.4: ABB robot range, IRB 1400.

The basic structure of the parallel robot is the closed kinematic chain. A kinematic chain is closed if there is more than one sequence of links connecting the end of the chain to the base. There is one important difference between the kinematic chain that makes up a parallel robot and the kinematic chain that makes up a serial robot. The chain of a parallel robot can have non-actuated joints.

The first parallel mechanism, the Gough platform, was developed in 1947 [2]. The end of the Gough platform is attached to the base of the Gough platform by six legs whose lengths can be varied by prismatic actuators. Gough platforms have six degrees of freedom, high accuracy, and high load capacities, but small workspaces. The most famous and most commercially successful parallel robot is the Delta robot (see Figure

1.5). The Delta robot is part of a whole family of robots that provide three translational degrees of freedom with no rotation. These parallel manipulators usually have a much larger workspace than Gough platforms. There are also many three degree of freedom parallel mechanisms that provide rotational motion or some combination of rotational and translational motion. However, the rotations that these mechanisms provide are small when compared to the rotations that can be provided by a serial mechanism.



Figure 1.5 ABB Flexpicker: an industrial Delta robot.

Research has also been conducted into redundant parallel mechanisms. These mechanisms have more actuators than end effector degrees of freedom. Two noteworthy examples are the articulated truss, which is an example of kinematic redundancy, and the redundant wire driven robot, which is an example of force redundancy. An articulated truss is essentially several Gough platforms stacked on top of one another. The

articulated truss is a strong, lightweight structure that can move like an elephant's trunk or a snake. These robots are expensive but they combine the light weight and strength of the Gough platform with a much larger workspace. In a redundant wire driven robot the moving end of the mechanism is attached to the base by several wires. Actuators reel in or let out the wires to control the position of the end effector. It is necessary to have more actuated wires than degrees of freedom to insure that the wires always remain in tension. Redundant wire driven robots are very light and fast moving mechanisms.

Parallel robots are characterized by high accuracy, high rigidity and a high load to weight ratio because the end effector load is shared between several kinematic chains. Even though parallel robots are more mechanically complex, having more links and joints than serial robots with the same number of degrees of freedom, parallel robots can often be made from far less material. As a result a parallel robot can often be less expensive to manufacture than a serial robot that has the same maximum load. A disadvantage of parallel robots is that they generally have a smaller workspace and smaller range of rotation than serial robots.

Serial-parallel hybrid robots are made from combinations of both serial and parallel mechanisms. They are generally formed by attaching a parallel platform to the end of a serial robotic arm, or by attaching a serial chain to the end of a parallel mechanism. These robots combine the strengths and weaknesses of both serial robots and parallel robots. Lee and Arjunan [13] suggested attaching a high precision 3 degree of freedom micro-motion piezoelectric actuated parallel platform to the end of a serial robotic arm. They suggested using a course-fine positioning strategy that would allow the robot to have the large range of motion of the serial arm, but the high precision

positioning of the micro-motion parallel platform. Figure 1.6 shows a version of the ABB Tricept, a serial-parallel hybrid industrial robot. It is comprised of a three degree of freedom parallel platform with a three degree of freedom serial robotic wrist attached to the end. The parallel base provides high precision placement of the end effector and allows the robot to be very rigid. The three degree of freedom serial robotic wrist provides a much larger range of rotation than any parallel mechanism could provide. This industrial robot is intended for machining operations. It is relatively light and low cost when compared to the machine tools that would normally perform these operations.



Figure 1.6: ABB 940 Tricept.

1.2.2 Robots in Poultry Processing

There are many tasks in poultry processing that do not require sophisticated automation. The poultry processing industry has embraced the automation of these tasks, and as a result poultry processing has become highly automated. Tasks such as the transportation of bird carcasses, simple butchering tasks, and de-feathering are all automated in modern poultry plants. Many other tasks, however, involve too much variability to be automated with available industrial robotic systems. Though few robots are currently used in poultry processing, robotics has the potential to automate many of these tasks. Much research into the automation of highly variable, poultry processing tasks has been focused on the development of robotic workcells that can meet human level performance requirements. In this research robots, specialized end effectors, control schemes, and/or sensor systems are investigated in attempts to find robotic workcells that will work better and cheaper than human workers.

Researchers at the Georgia Tech Research Institute are currently working to automate the loading of poultry traypacks into bins. A traypack is a Styrofoam tray of meat that has been sealed in shrink-wrapped plastic. These traypacks have various weights, centers of mass and rotational properties. In addition, the contents of the traypacks are free to shift around. Traditionally these traypacks are loaded into bins manually, but GTRI is developing a workcell to make automation possible and feasible. First a sensor system and a specialized end effector were developed. Using these developments and a SCARA type serial robot it was shown that automation is possible. Figure 1.7 shows an early prototype workcell loading traypacks into bins. The traypacks start out by traveling down a conveyor belt. An encoder determines the speed of the

conveyor belt, while a photo sensor senses the presence of a traypack on the conveyor belt. Using the information from the encoder and photo sensor the robot intercepts the traypack and picks it up using the specialized end effector. The specialized end effector consists of a plate with several compliant suction grippers. The robot then transports the traypack to an empty spot in the bin and releases it. More recent work has gone into developing a robot that will be less expensive than the ADEPT SCARA type robot and will be able to perform the task more quickly. The current prototype workcell uses a Cartesian type robot with three degrees of translational freedom and one degree of rotational freedom at the end effector.

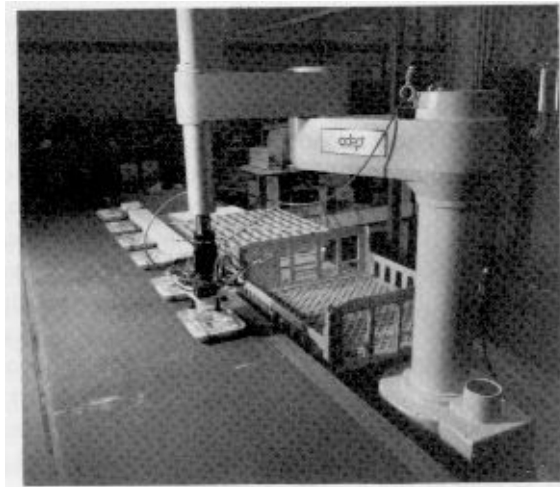


Figure 1.7: Early prototype workcell loading traypacks.

GTRI also developed a workcell to automate removing poultry back-halves from a shackle and loading them onto a machine for further processing. Figure 1.8 shows a prototype of this robot. A poultry back-half is the portion of a poultry carcass formed by

the two legs and thighs connected by a short section of backbone. Further processing of the poultry back-halves requires the backbone to be separated from the thighs. The poultry industry uses a machine to automatically separate the thighs from the backbone, but loading the back halves into the machine is done manually. The poultry back halves are presented on a moving shackle line. A worker removes a poultry back half from the shackle line and feeds it into the spine removal machine making sure the spine is aligned with guides on the machine and making sure the poultry back half is engaged by the drive chain of the machine. A rate of 40 back-halves per minute is desired.

As in the traypacking task there is a lot of variation in this task. The back-halves vary in weight, size, and to some extent shape. The task is further complicated because the back halves are slippery and compliant. GTRI developed a specialized end effector that allowed this task to be carried out by a robot. For the prototype system a 6 degree of freedom PUMA 560 articulated arm was used. Even though the robot was able to successfully complete the task this system never made it past the prototype phase of development. The system could not meet the desired rate of 40 back halves per minute and the PUMA robot would have made the workcell too expensive to be practical.

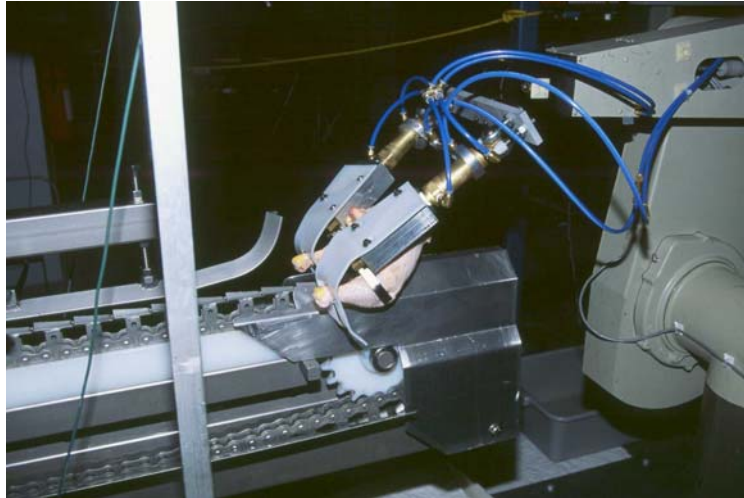


Figure 1.8: poultry back half being automatically loaded onto a spine removal machine.

K. Khodabandehloo [5] has shown that a robot can be used to package small poultry parts such as drumsticks and thigh pieces. Packaging these portions can mean simply placing them in a bag until the bag has the right weight then sealing the bag, or it can mean arranging them neatly in a Styrofoam traypacks. Khodabandehloo researched a variety of end effectors, a vision system, and a control scheme for the packaging of these poultry portions. He also constructed a prototype system for one such packaging task. The prototype is illustrated in Figure 1.9. After cutting and de-boning, breast fillets travel down a conveyor belt and are weighed by an in-line weigh system. The breasts are eventually loaded into Styrofoam trays, but first the control system determines which combinations of breast fillets will yield a tray pack that is as close to the target weight as possible. A vision system identifies the locations and orientations of the breast fillets. Next a SCARA robot equipped with a specialized end effector picks up each of the breast fillets and places it into the predetermined Styrofoam tray. Once a tray is full it is carried away on another conveyor belt.

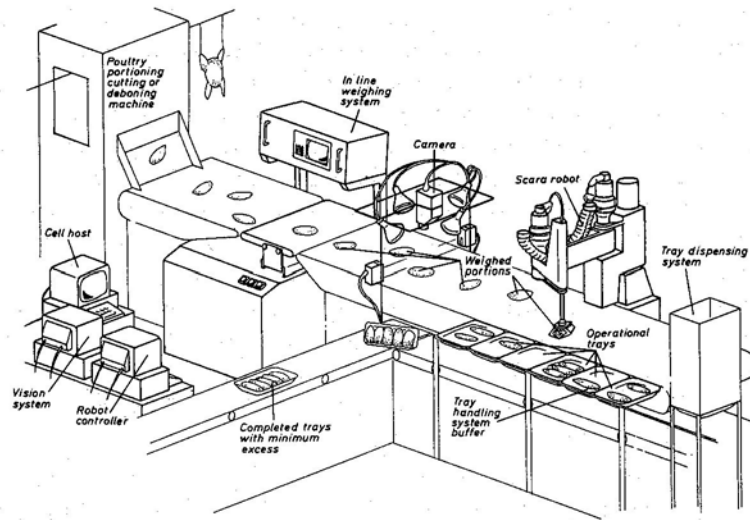


Figure 1.9: Prototype for automatic loading of breast pieces into traypacks.

One poultry processing robot that has been successfully implemented in industry is the DSI water jet portioner. Figure 1.10 shows one version of the DSI water jet portioner. The water jet portioner has applications in the processing of several types of meat. In poultry processing it is used to cut butterfly filleted chicken breasts into desired shapes and sizes. For example, it may be asked to cut sandwich pieces and nugget pieces for Chick-fil-A. Workers take butterfly filleted chicken breasts and align them on a conveyor belt using a laser guide that is projected on the conveyor belt. The conveyor belt carries the breast pieces into the machine where a three dimensional vision system determines the shape of the breast piece. The machine has been pre-programmed with a prioritized list of desired product sizes shapes and weights, and it determines the cutting pattern that will result in the most desirable combination of end products. The breast

pieces move onto a grated conveyor where high pressure water jets cut the breast pieces in the pre-determined pattern. When the portioned breast pieces leave the cutting area a variety of manual and automatic methods are used to sort the end product. This machine is expensive. It costs approximately one million dollars. The cost of this machine is easily justified however because it does the job of several workers and the percentage yield of the cutting operation is higher than it was when this task was done by hand.



Figure 1.10: DSI 512 water jet portioner.

1.3 Goals of This Research

The goal of this research is to automate the task of transferring WOGs from a conveyor belt to a moving shackle line. In particular a low cost, high speed robot will be designed for this task. The robot will be part of a work cell that includes the robot, a specialized end effector for grasping WOGs, and a vision system. The development of a low cost, high speed robot for transferring WOGs from a conveyor to a shackle line will

show that it is possible and feasible to automate unstructured meat handling tasks with robotics. To be feasible the robot and the workcell must meet a paradigm for the design of robots known as human level performance [9]. The performance criteria for a human level performance robot are defined by the capabilities of a human worker. Cost, cycle time, accuracy, and flexibility are included in the criteria.

1.4 Design Methodology

The robot is designed using a systematic design methodology. The overall design procedure is loosely based on a methodology outlined by Pahl and Beitz [10]. The Pahl and Beitz methodology breaks the design into four steps: planning and clarifying the task, conceptual design, embodiment design, and detail design. Within each of these steps design tools presented by Pahl and Beitz, Yan [3], and my adviser Dr. Harvey Lipkin, as well as design tools developed specifically for this design are used. A systematic design methodology provides assistance in the design process as well as justification and support for design decisions.

1.5 Organization of the Thesis

In this thesis there are one or more chapters corresponding to each step of the Pahl and Beitz design methodology. Figure 1.11 shows an outline of the design methodology as well as a breakdown of thesis chapter contents.

Chapter 2 plans and clarifies the task. It provides a thorough evaluation of the problem and generates the specifications that will be used for the rest of the design process. First an overview of the poultry processing environment and the current WOG hanging procedure are given. The task is then quantified and a requirements list is generated.

In Chapter 3, Conceptual Design, the principal solution is generated. First the structure of the task is developed and evaluated. A large number of possible solutions to the task are then generated and evaluated to determine the principal solution.

In Chapter 4 the kinematic design of the principal solution is carried out. The structure of the principal solution is developed including the number, order, and orientation of joints. The equations governing the position and motion of the principal solution are then derived and evaluated.

In Chapter 5 the dimensions of the robot developed in Chapter 4 are optimized. First the workspace required by the task is determined. Robot dimensions are then determined based on the required workspace and the layout of the conveyor belt and shackle line.

In Chapter 6 robot prototypes are generated and used to finalize many of the details of the design. Both a physical mockup and CAD models are generated and used to simulate the performance of the robot. Actuator selections and a cost analysis are also carried out.

In Chapter 7 the thesis is summarized and critically reviewed. Further work is also discussed.

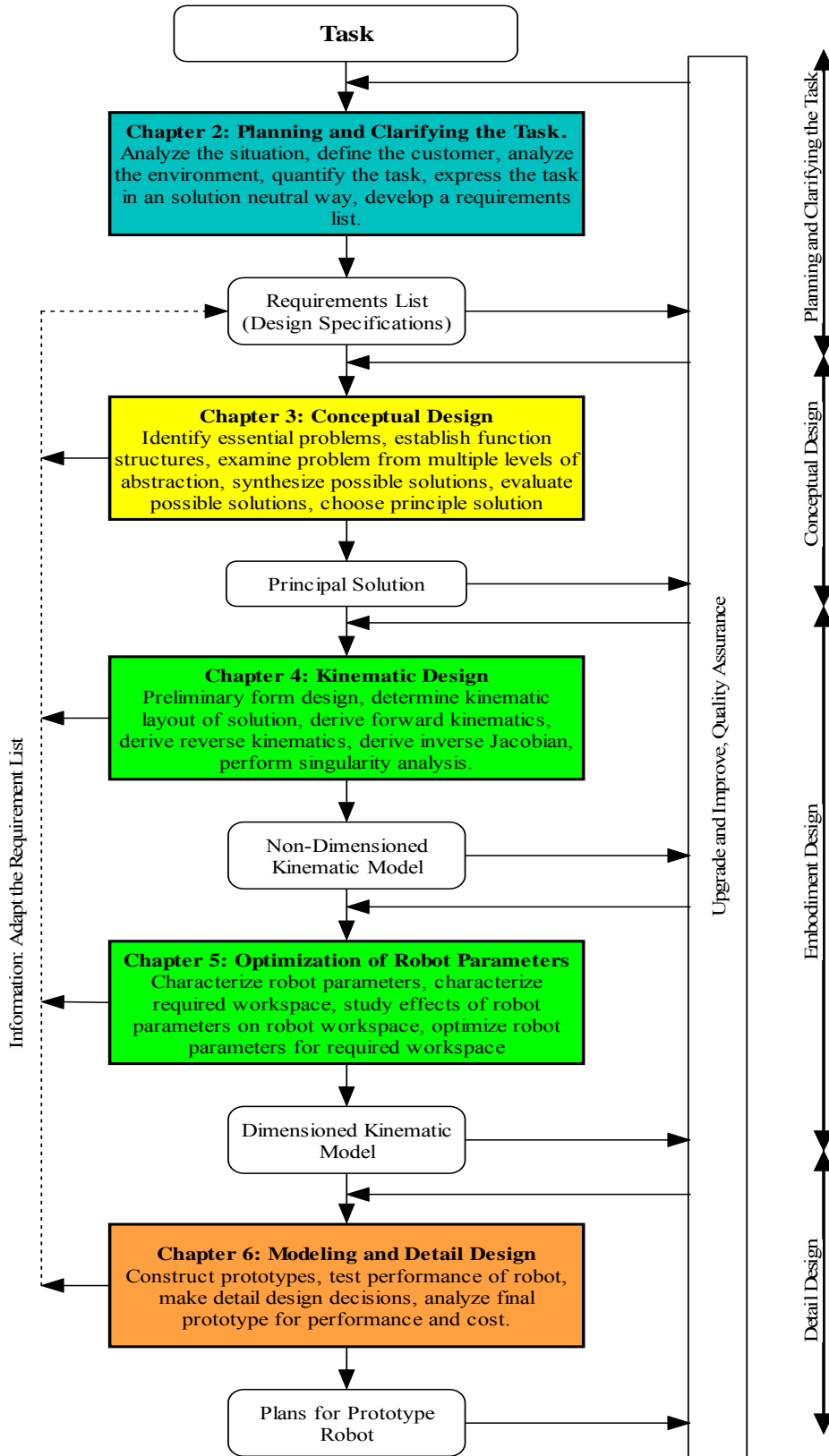


Figure 1.11: Outline of design process by thesis chapter.

CHAPTER 2

PLANNING AND CLARIFYING THE TASK

In this chapter the task of transferring a WOG from conveyor belt to a moving shackle line is planned and clarified. First, a detailed quantitative description of the task is developed to determine exactly what the robot must do. The demands and wishes for the robot are then developed. The demands are requirements that the robot must fulfill in order to successfully complete the task. Wishes are desired robot properties that are above and beyond what is absolutely necessary to complete the task. The robot will be designed to meet all of the demands and as many wishes as possible.

This chapter begins with an overview of poultry processing operations in the United States. Section 2.2 describes the task of hanging WOGs on shackles as it is currently carried out, while Section 2.3 quantifies the task. In Section 2.4 a requirement list, containing the demands and wishes for the robot, is developed.

2.1 Overview of Poultry Processing Operations

Most poultry plants consist of a slaughter or first processing section and a further or second processing section. The processing that takes place in a typical plant is shown in Figure 2.1. Processing begins when cages of live chickens are trucked in. These cages

of chickens are automatically dumped onto a conveyor line. The chickens are then manually hung on an overhead moving shackle line. While on the shackle line the chickens are stunned, killed, scalded, and de-feathered. Next the chickens heads and feet are removed. The processing steps up to this point are sometimes referred to as pre-processing. The second half of the first processing is sometimes called whole bird processing. The whole birds are manually hung on an evisceration line, where they are mechanically opened, eviscerated then inspected for wholesomeness. After inspection the remaining viscera and any other remaining internal items are removed. These whole birds without giblets or WOGs are then washed and dumped into an immersion chiller for final washing and cooling to an average temperature of no more than 40 degrees F (4 C). After exiting the chiller the WOGs are manually re-hung on an overhead moving shackle line. Depending on the grade of a WOG it is either sent to whole bird packout, or to further processing. Second processing includes a large number of cutting and deboning processes, but all second processing tasks are not carried out on all WOGs. Second processing is where whole birds are processed into the many varieties of chicken parts that are available for consumption such as chicken quarters, eight piece, and deboned chicken breasts. Additional processing such as marinating, breading, cooking, and processing chicken into lunch meat can also be carried out in second processing. The chicken is then refrigerated for 24 hours, packaged and shipped.

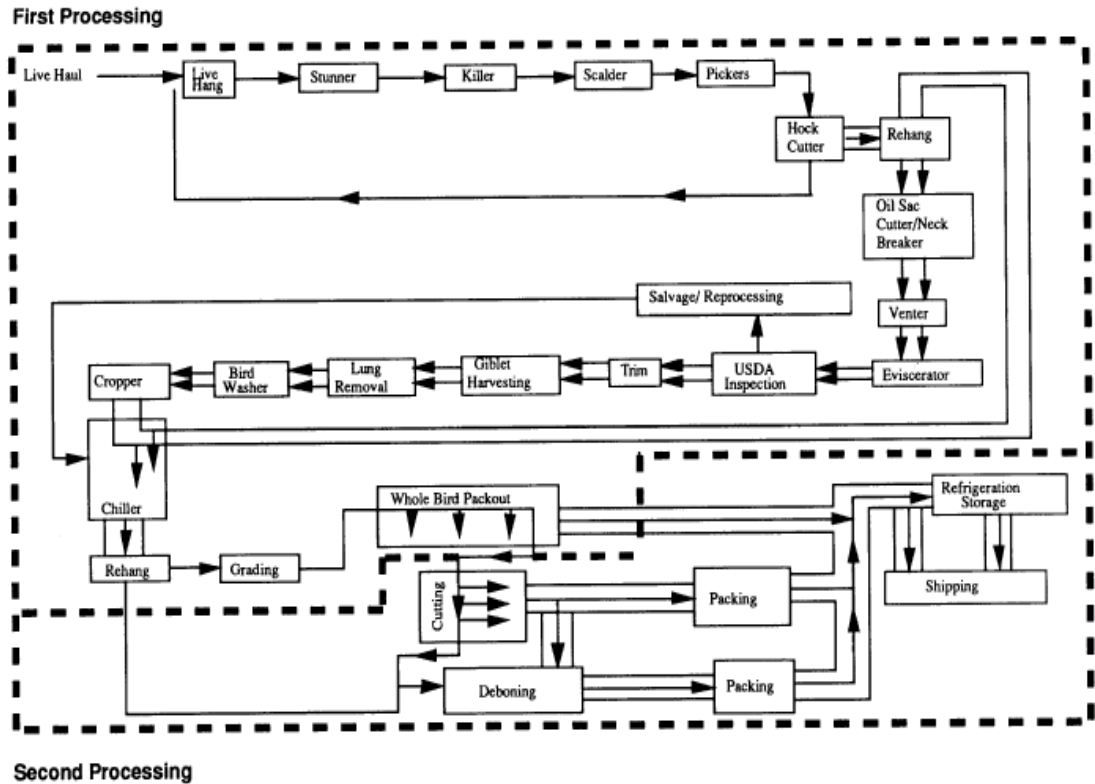


Figure 2.1: Overview of poultry processing operation.

2.2 Current WOG Hanging Process

The focus of this thesis is the WOG hanging operation that takes place near the end of first processing. It is labeled “Rehang” in Figure 2.1. At this stage of processing the feathers, feet, head, entrails and possibly the neck of the product have been removed. Prior to arriving at the hanging station the WOGs spend several hours in a water immersion chiller. Groups of WOGs are discharged onto a circulating conveyor belt at regular intervals and at temperatures of approximately 40°F (Figure 2.2). They are wet, slippery, and the cavities are sometimes partially filled with water. When discharged

onto the conveyor belt the WOGs can lay in any orientation, however they settle into a more limited set of positions after some jostling and nudging by other WOGs and the boundaries of the conveyor belt system. The WOGs generally settle lying on their backs or on their breasts. On rare occasions they can also lay stably on their sides. The WOGs are carried around in an oval path by the circulating conveyor belt system until they are picked up by workers and transferred to a moving shackle line (Figure 2.3).



Figure 2.2: WOGs discharged from the chiller.



Figure 2.3: WOGs circulating on the conveyor belt system.

Figure 2.4 shows the layout of the shackle lines and the conveyor belt system. Typically there are two shackle lines per conveyor belt system and each shackle line is loaded by a pair of workers. The shackle lines lie above the middles of the conveyor belts and travel parallel to them. WOGs are hung on the shackles by the ends of the drumsticks with the breast of the WOG facing away from the center of the conveyor belt system. The WOGs are then carried away by the shackle line for further processing. Normally all WOGs on the conveyor belt are transferred to the shackle line and all shackles passing through the WOG hang area are loaded with WOGs, however there are two noteworthy exceptions. It is possible for WOGs to be damaged prior to this stage of processing. If a WOG has been damaged in a way that makes it impossible to hang properly, if it is missing a leg for example, then the WOG is dropped down onto a secondary conveyor belt. This secondary conveyor carries the WOG away to be processed using alternate methods. It is also possible that the machines that

automatically unload the shackles will fail to completely unload a shackle. In this case a shackle will arrive with a poultry piece in it. On the right side of Figure 2.4 one of the shackles has a drumstick and thigh hanging from it. In this situation the shackle is allowed to pass without loading a WOG into it. It is assumed that the poultry piece will be unloaded the second time it passes through the automatic unloading station.



Figure 2.4: Typical conveyor belt system and shackle lines.

2.3 Quantifying the Task

In order to automate this task a detailed and quantitative description of the task must be developed. A human is able to perform the task based on the qualitative task description given above, but a robot requires specific angles, positions, weights and times. A detailed and accurate description of these quantities is needed to develop a robot that will be able to perform this task.

2.3.1 Assumptions

Before continuing with a detailed description of the task some assumptions must be made.

- 1) It is assumed that a machine vision system will be able to determine the location and orientation of the WOGs as they are presented on the conveyor belt.
- 2) It is assumed that a specialized end effector will be able to grasp those WOGs.
- 3) It is assumed that sensors will be in place to determine the velocity of the conveyor belts, and therefore the velocity of the WOGs as well, and the velocity and locations of the shackles.
- 4) It is assumed that one robot workcell will take the place of one worker.
- 5) It is assumed that the WOGs will be singulated (separated from one another on the conveyor belt).

- 6) It is assumed that the WOGs will be lying on their backs or on their breasts.
- 7) It is assumed that the WOGs will be in good enough shape to be hung.
- 8) It is assumed that the shackle will be in empty and good enough condition to receive the WOG.
- 9) It is assumed that the conveyor belt is moving in the opposite direction as the shackle line, and that a WOG occupies every second shackle.

Figure 2.5 illustrates how the robots will be positioned around the conveyor belt system. In Figure 2.5 the blue arrows indicate the direction of travel of the shackle lines and the red arrows indicate the directions of travel of the conveyor belts. Though the WOGs are not currently singulated for this task singulation equipment does exist and singulation will likely be needed by both the specialized end effector and the machine vision system. In reality only robot 2 (Figure 2.5) will operate under the conditions of assumption 9, however the other three robots will operate under less demanding conditions. A robot designed to complete the task under these conditions will have no difficulty completing the task when the conveyor belt is moving in the same direction as the shackle line and/or when all of the shackles are empty. From this point on the task discussed in this design will be the task faced by robot 2 as shown in Figure 2.5, not the general task of hanging a WOG with a robot.

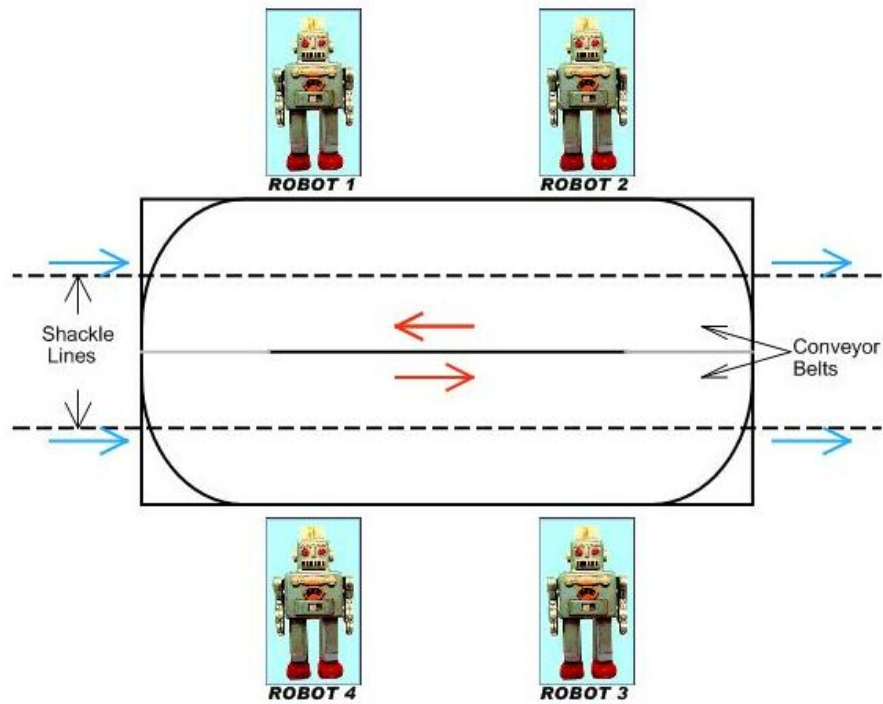


Figure 2.5: Proposed robot positions (top view).

2.3.2 Defining Coordinate Frames

Before the task of transferring WOGs from a conveyor belt to a moving shackle line can be analytically described the coordinate frames used in the description must be defined. Two coordinate frames are sufficient to describe the task in a straightforward and simple way. The first coordinate frame is the global coordinate frame. It is illustrated in Figure 2.6 and remains fixed at all times. The origin of the global coordinate frame is defined in the X and Y directions by the middle of the conveyor belt system and in the Z direction by the top of the conveyor belt surface. The second coordinate frame is the WOG coordinate frame (Figure 2.7). The origin of this

coordinate frame is at the center of mass of the WOG. There is a WOG coordinate frame rigidly attached to each of the WOGs.

The relative position of the WOG coordinate frame with respect to the global coordinate frame will be described by a position vector expressed in the global coordinate frame. The relative orientation of the WOG coordinate frame is described by the Euler angles θ, φ , and ψ using the *ZYZ* convention as illustrated in Figure 2.8. When the WOG is laying on its back with its left side pointed in the direction of travel of the shackles the Euler angles are $\theta = \varphi = \psi = 0$.

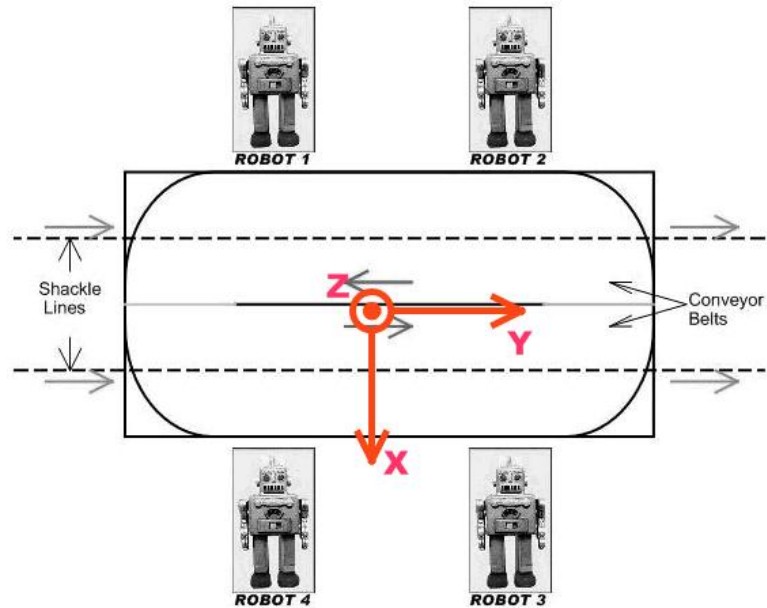


Figure 2.6: Global coordinate frame.

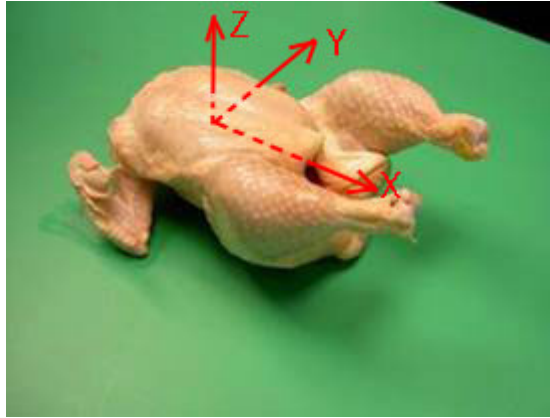


Figure 2.7: WOG coordinate frame.

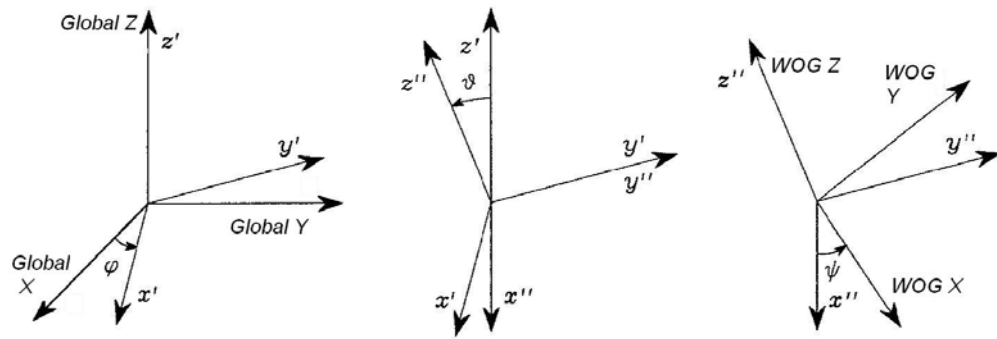


Figure 2.8: Representation of Euler angles ZYZ

2.3.3 WOG Characterization

Very little published data is available on the mass and inertial characteristics of poultry. The high variability in the size, weight and shape of WOGs, the complex shape of WOGs, and the compliance of WOGs make determining the mass and inertial properties both difficult and impractical. If precise mass and inertial properties were determined for a WOG those properties would only accurately characterize that single WOG. It would not accurately characterize the rest of the population. Simple techniques can, however, be used to estimate the worst case scenario. The highest mass and rotational inertia for any WOG the robotic workcell is likely to encounter can be estimated.

According to the Pilgrim's Pride poultry processing plant in Conyers, Georgia the target weigh for a WOG is 2.75 lbs. The variance of the WOG weights is not known so a conservative estimate of the maximum WOG weight will be used. The robot will be designed to successfully complete the WOG hanging task with WOGs that are up to double the target weight, 5.5 lb. The complex shape and compliance of a WOG prevent the rotational inertia from being estimated easily and accurately. A WOG can be modeled to an acceptable degree of accuracy however as a three dimensional ellipsoid. A group of 5 WOGs weighing close to 2.75 lbs were measured. When lying on their backs they were all found to be about 10 in long, 5.5 in wide, and 5.5 in tall. A 2.75 lb WOG will therefore be modeled as a 10 in X 5.5 in X 5.5 in ellipsoid weighing 2.75 lb. The 5.5 lb WOG can be modeled as a proportionately larger ellipsoid with the same shape and density. Such an ellipsoid would have the dimensions of 12.6 in X 6.93 in X 6.93 in or

1.05ft X 0.58 ft X 0.58 ft. Using the equations shown in Figure 2.9 the rotational inertias of this ellipsoid can be calculated as $I_{XX} = 0.185 \text{ lb}\cdot\text{ft}^2$, and $I_{YY} = I_{ZZ} = 0.396 \text{ lb}\cdot\text{ft}^2$.

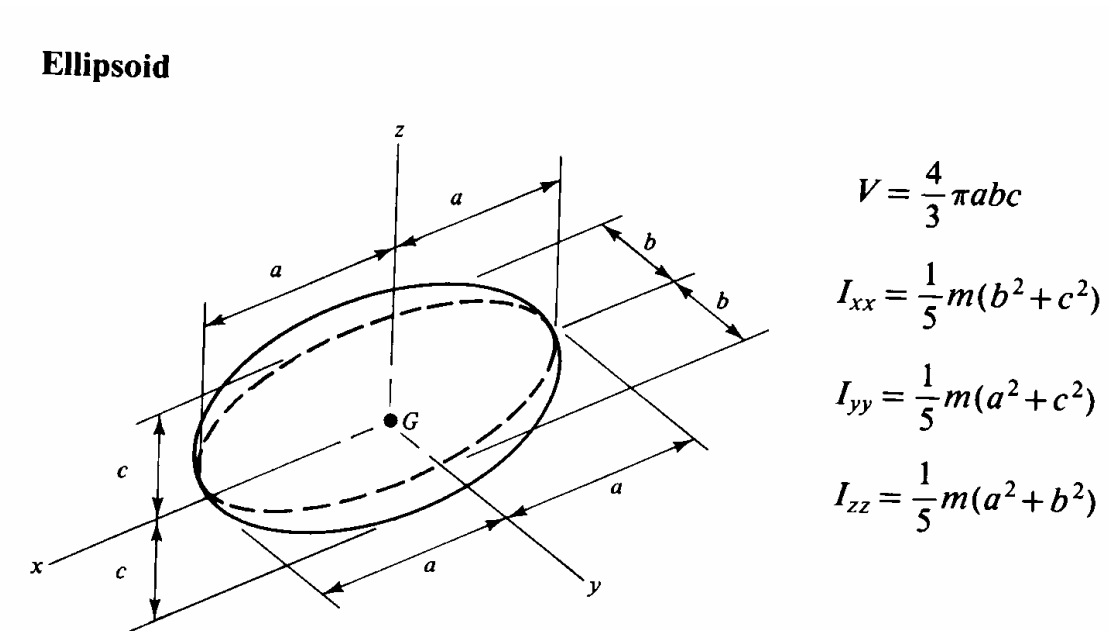


Figure 2.9: Inertial Properties of an ellipsoid

2.3.4 Constraints

Floor space, conveyor system, design and cost constraints must be defined before the robot is designed.

Floor space constraints:

Space is often at a premium in poultry processing plants. Ideally the robots should not take up more floor space than the platform the workers stand on when

transferring WOGs from the conveyor belt to the shackle line. Each worker stands on a platform that is approximately 3 ft wide and 6 ft long. To meet the floor space requirement the robot will be constrained to have a footprint of 18 square ft or less. Most poultry processing facilities can spare more than this much room for the robot to occupy, but this will provide plenty of room around the robot for ease of maintenance.

Conveyor system constraints:

The surface of the conveyor belt system is approximately 4 ft off the ground and each conveyor belt is approximately 35 in wide. The shackle lines run down the middle of the conveyor belts and the bottoms of the shackles are approximately 18 in above the surface of the conveyor belts. When a WOG is in a shackle there are approximately 8 to 10 in of clearance between the lowest point on the WOG and the conveyor belts. The robot and the specialized end effector must operate without impeding the performance of the conveyor belt or shackle lines, and must not cause or receive damage from the conveyor belts, shackle lines or WOGs.

Time constraints:

The desired throughput of a shackle hanging station is 182 WOGs per minute. This corresponds to an average rate of 45.5 WOGs per minute for each worker or an average of one WOG every 1.32 seconds. The robotic workcell must meet or exceed a WOG hanging rate of 45.5 per second for automation to be feasible. In order to achieve this time will be budgeted as follows:

- Robot transports WOG from conveyor belt to shackle: 0.4 s.
- Robot lowers WOG into shackle: 0.1 s.
- Robot waits for the end effector to release the WOG: 0.2 s.

- Robot positions end effector to grasp next WOG: 0.4 s.
- Robot waits for the end effector to grasp WOG.

Design constraints:

ANSI publishes design guidelines for poultry processing equipment as Hygiene requirements for the design of meat and poultry processing equipment [25]. These guidelines restrict the materials and parts that can be used to construct poultry processing equipment. For the purposes of conceptual design and embodiment design these detailed guidelines can be abstracted to a simpler set of guidelines. Acceptable materials are stainless steel, metals that are as corrosion resistant as austenitic stainless steel, coated metals if the base metal is non-toxic, and non-metals that don't impart flavor, color, odor, toxins, or bacteria on the product. The machinery must be easy to clean and inspect and it can not have any pits or cracks. It can not have any sharp internal angles in product contact areas. Fasteners, intrusions such as springs or perforations, bearings, and bushings should be avoided in product contact areas. Outside of product contact areas shafts must have hygienic seals and lubricated bearings must have clearance for inspection. A list of design constraints for joints can be found in Section 5.1.7 of the guidelines. In addition to meeting the ANSI guidelines the robotic workcell must be able to operate properly in a humid environment, and must be able to withstand frequent washdowns with high pressure chlorinated water. Any components that do not meet these requirements must be sealed off from this environment.

Cost constraints:

In order for the automation to be feasible the robotic workcell must have a one year payback. As discussed in Section 1.1, this allows \$60,000 for the cost of

manufacturing and implementing the workcell as well as one year's maintenance. Half of that money, \$30,000 is allotted for implementation and one years maintenance, while \$1,000 is allotted for the machine vision system (one \$4,000 vision system for four workcells), \$4,000 is allotted for the end effector and \$25,000 is allotted for the robot. This is well below the cost of any industrial robot on the market.

2.3.5 Robot Motion

The task of transferring WOGs from a conveyor belt to a shackle can now be described in terms of the relative position and orientation of the global and WOG coordinate frames. In the following paragraphs the set of possible starting WOG positions, orientations, and velocities as well as the set of all possible final WOG position, orientations and velocities are found. The results of this investigation are summarized in Table 2.1.

The set of all possible starting WOG positions, orientations, and velocities must meet the constraints of the conveyor belt system. The initial velocity of the WOG is the same as the velocity of the conveyor belt. The speed of the conveyor belt was measured as approximately 1.5 ft/s so the initial velocity of the WOG is $[\dot{X} \ \dot{Y} \ \dot{Z}] = [0 \ -1.5 \text{ ft/s} \ 0]$. Since the desired cycle time is 1.32 seconds, the average distance from one WOG to the next will be 2 ft in the Y direction. Since it will take about 0.2 seconds for the end effector to grasp the WOG, the robot will have to follow the WOG for 0.3 ft in the Y direction. The X coordinate of The WOG is constrained by the boundaries of the conveyor belt, and the Z coordinate of the WOG is

constrained by the flat surface of the conveyor belt. The desired workspace of the robot during WOG capture will be 2 ft wide in the Y direction and 2.5 ft wide in the X direction and will have no depth in the Z direction. This workspace covers all possible WOG positions in the X and Z directions. Subtracting the capture distance of 0.3 ft from the width of the workspace in the Y direction still leaves 1.7 ft to accommodate variations in WOG spacing from the average spacing of 2 ft.

The initial position and orientation of each WOG can now be expressed in terms of global $[X Y Z]$ coordinates and $[\theta \varphi \psi]$ Euler angles. The Z position of the WOG is constrained by the conveyor belt. Expressed in global coordinates, the origin of the WOG coordinate frame lies at $[X Y Z] = [X_I Y_I (height\ of\ WOG)/2]$ where X_I and Y_I are the arbitrary initial X and Y coordinates. Though there are bounds on the initial X and Y positions of the WOG coordinate frame the initial X and Y coordinates are unconstrained and arbitrary within those bounds. The WOG lays on either its back or its breast, but the orientation is otherwise unconstrained. The orientation of the WOG coordinate frame is described by the Euler angles $[\theta \varphi \psi] = [\theta_I \varphi_I \theta^\circ]$ where φ_I is either 0° (WOG lying on its back) or 180° (WOG lying on its breast) and θ_I is arbitrary. θ_I can be visualized as the direction the WOG's legs point in the horizontal plane.

There are a variety of WOG positions and orientations that will result in a successful hang. For a successful hang the positions of the WOG's feet are more important than the position of the origin of the WOG coordinate frame. The feet must be placed in a moving shackle and should end up at approximately $[X Y Z] = [-18in\ Y_F\ 20in]$ where Y_F is defined by the position of the shackle and changes over time. The position of the origin of the WOG coordinate frame depends on

the orientation and size of the WOG, but is within a few inches of the position of the feet. For a successful hang the feet must point perpendicular to the direction of travel of the shackle, the breast of the WOG must be pointing up or towards the robot and the angle between the shackle and the legs should be between 20° and 90° . The orientation of the WOG as it is being released into the shackle is described by the Euler angles $[\theta \ \varphi \ \psi] = [0^\circ \ \varphi_F \ 0^\circ]$ where φ_F is between 0° and -70° .

The final WOG velocity and the workspace that encloses all possible WOG release positions can now be defined. The required WOG velocity for a successful release is the same as the velocity of the shackle line, which was estimated at 0.76 ft/s in the Y direction. The workspace that encloses all possible final WOG positions is essentially one dimensional. All WOGs will be released at about the same X and Z coordinates. Only the Y coordinate will vary. Since it will take about 0.2 seconds for the end effector to release the WOG the robot must follow the shackle for about 0.15 ft. A WOG release workspace width of 2 ft in the Y direction (the same width as for WOG capture) is adequate. Subtracting the release distance of 0.15 ft leaves 1.85 ft. The shackles are 6 in apart, so the robot will have access to at least 3 shackles. Since every second shackle is occupied by a WOG, the robot will always have access to one or two empty shackles.

Five degrees of freedom are required to move the WOGs from their initial positions, orientations and velocities to their final positions, orientations and velocities. Two translational degrees of freedom (X and Y) are required to successfully capture an arbitrarily positioned WOG, while a third translational degree of freedom (Z) is needed to lift the WOG from the height of the conveyor belt to the height of the shackle line. Two rotational degrees of freedom are also needed. One rotational degree of freedom is

required by the arbitrary θ_I and another is required to allow WOGS with $\varphi_I = 0^\circ$ or $\varphi_I = 180^\circ$ to be rotated to the same φ_F .

Table 2.1: Summary of initial and final conditions of WOGs

	Variables Defining the Position and Orientation of the					
	X	Y	Z	θ	φ	ψ
Initial Position	Between -36 in and 0 in	Within a 24 in range	(height of WOG)/2 in	Any	0° or 180°	0°
Final Position	-18 in	Within a 24 in range	18 in	0°	Between 0° and -70°	0°
Initial Velocity	0 in/s	-18 in/s	0 in/s	$0^\circ/s$	$0^\circ/s$	$0^\circ/s$
Final Velocity	0 in/s	9 in/s	0 in/s	$0^\circ/s$	$0^\circ/s$	$0^\circ/s$

2.4 Requirement List

The final document of the planning and clarification phase of this design is a requirements list. With the task quantified and with the assumptions, the design constraints and the problem clearly defined a requirement list can be developed. The requirements list, shown in Table 2.2, is intended as a clear and concise representation of all the requirements that were realized in the planning and clarification phase. At the top of the list is a concise statement of the problem. Below is a list of requirements. All of the requirements are either demands (D) or wishes (W). An X is placed to the right of each requirement if it was addressed in the design process.

Table 2.2: Requirements list.

Requirements list		
<i>Problem Statement:</i>		
<p>The objective of this project is to design a robot that will act in coordination with a specialized end effector to pick up WOGs from a conveyor belt and hang them on a moving shackle line. The design of this robot is complicated by a maximum payback time of one year, by USDA restrictions on poultry processing equipment and by the high variability in the weight, initial position and initial orientation of the WOGs. Initially, conceptual design and evaluation will be carried out on a variety of both proven and novel robot geometries and actuation strategies. A single design will then be chosen and developed to meet the project requirements. Design of the robot will be coordinated with the concurrent design of a specialized end effector.</p>		
D W	Requirements	
	<i>Geometry</i>	
D	-Must fit in existing space	X
W	-Robot should fit in a 18 square foot patch of floor next to conveyor	X
D	-Must work with existing conveyor belt and shackle line	X
D	-Must interface with specialized end effector	X
D	-Must not be ceiling mounted	X
D	-Robot must not get in the way of the end effector picking up or releasing the WOG	X
D	-Robot must not interfere with the normal operation of the conveyor belt or shackle line	X
W	-Robot geometry should be simple and easy to manufacture	X
W	-Minimize the number of parts	X

	<i>Actuation</i>	
D	-Operates using either electrical, or pneumatic actuators	X
W	-Operates with the minimum number of actuators	X
W	-Operates with pneumatic actuators rather than electric where practical	X
D	-100 psi maximum air pressure for pneumatic actuators	X
W	-Low power consumption	
D	-Cables, hoses, and other actuator support lines can not interfere with normal operation of the end effector, robot, conveyor belt, or shackle line	X
D	-Cables, hoses and other actuator support lines can not become pinched during operation	X
D	-Actuators must be able to operate in the shackle hang environment with a reasonable life span	X
D	-Actuators must not impart any color, taste, or bacteria on WOGs under normal operating conditions	X
D	-Actuators must not impart any color, taste, or bacteria on WOGs in the event of actuator failure	X
D	-Actuators must not have any place for water or food particles to collect	X
D	-Actuators and actuator controls must not be damaged by high pressure water	X
	<i>Materials</i>	
D	-Materials must meet ANSI and USDA standards for poultry processing machinery	X
W	-Minimize the amount of material to reduce cost	X
D	-Material must have a reasonably long life span in the shackle hang environment	
	<i>Production</i>	
W	-Robot should be manufactured from standard parts and assemblies	X
W	-Robot should have a simple design to reduce production time and cost	X

	<i>Operation</i>	
D	-Robot must meet ANSI standards for sanitation	X
D	-A pair of robots must not leave any empty shackles on the shackle line	X
D	-Robot must position and orient end effector for a successful grasp regardless of initial WOG orientation	X
D	-Robot must transport WOG and end effector between the conveyor belt and a shackle	X
D	-Robot must position and orient the end effector for a successful release	X
W	-Minimum payload of 5 kg (11lb)	
D	-Robot Motion can not damage the WOG	
W	-Robot must perform its motion as quickly as possible	X
D	-Robot-end effector system must be capable of hanging more than 46 WOGs per minute	X
W	-Time to transport WOG from conveyor belt to shackle should be 0.4 s	X
W	-Time to lower WOG into shackle should be 0.1 s	
W	-Time between WOG release and beginning of next WOG capture should be 0.4 s	
D	-Choice of robot motion can not impose unreasonable demands on the performance of the specialized end effector	X
W	-Choice of robot motion should optimize the performance of the robot-end effector system	X
	<i>Maintenance</i>	
D	-Can be cleaned by periodic wash downs with high pressure water	X
W	-Maintenance must be easy to carry out	
W	-Components requiring maintenance should be easy to access	X
W	-Minimize the amount of maintenance to minimize down time and cost	
	<i>Costs</i>	
D	-Cost of construction and implementation of robot and specialized end effector should not be more than \$60,000 (1 year payback for a robot working two shifts per day)	X
W	-Cost of construction of robot should be less than \$25,000 (this allows \$5,00 for the specialized end effector, \$27,000 for implementation, and \$3,000 for maintenance)	X
	<i>Control</i>	
W	-Control system should compensate for the vibrations that are likely to occur in a robot designed to minimize the amount of material used	
W	-Control scheme should be simple and easy to implement	
D	-Control system should be robust to compensate for variation in the WOG hanging task	

CHAPTER 3

CONCEPTUAL DESIGN

In this chapter the design process for selection of the principal solution is presented. The principal solution is the solution concept deemed most likely to meet the requirements of the task. The steps outlined in Pahl and Beitz's systematic design methodology are used to help select the principal solution [10]. First the structure of the task is developed and evaluated. A large number of possible solutions to the task are then generated and evaluated to determine the principal solution.

3.1 Establishment of the Function Structure

The first step in conceptual design is the establishment of the function structure of the task. The function structure shows the relationships between the inputs and outputs of the task. It also shows the relationships between the functions and sub-functions required to complete the task of transferring WOGs from a conveyor belt to a moving shackle line. It provides an intuitive way to look at the problem. Figure 3.1 shows the overall function structure of the problem, which is the simplest form of a function structure. It consists of a simple statement of the problem, as well as a representation of the types of task inputs and outputs. The overall function structure provides little value

for determining how the task might be successfully carried out, but it provides a starting point for the expansion of the function structure into more useful forms. In the following sections two methods to expand the function structure are used. The diagrams resulting from these expansions will help develop a better understanding of what is required to successfully complete the task and will lay the foundation for development of solutions to the task.

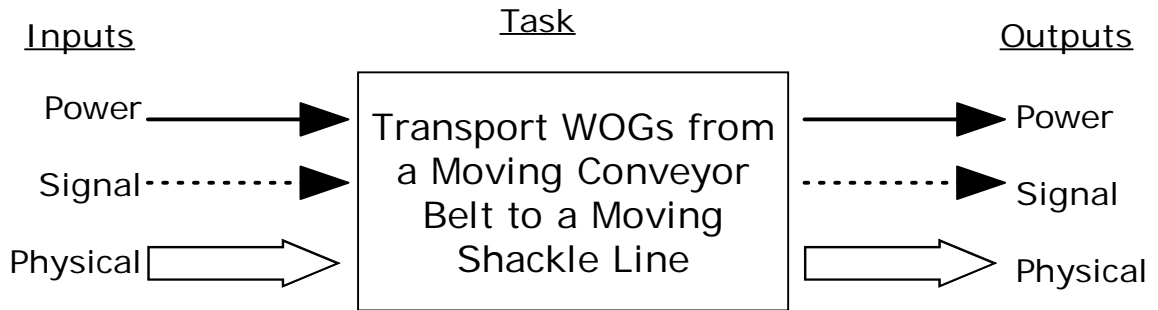


Figure 3.1: Overall function structure.

In this section the overall function structure shown in Figure 3.1 is expanded into the tree diagram shown in Figure 3.2. In a tree diagram the function is expressed as a set of sub-functions. Each of those sub-functions is then expanded further into sub-functions. This process is repeated until the overall task can be expressed as a set of simple, specific functions. A diagram is then constructed to show the hierarchy of the

functions and sub-functions required to complete the task of transporting WOGs from a moving conveyor belt to a moving shackle line.

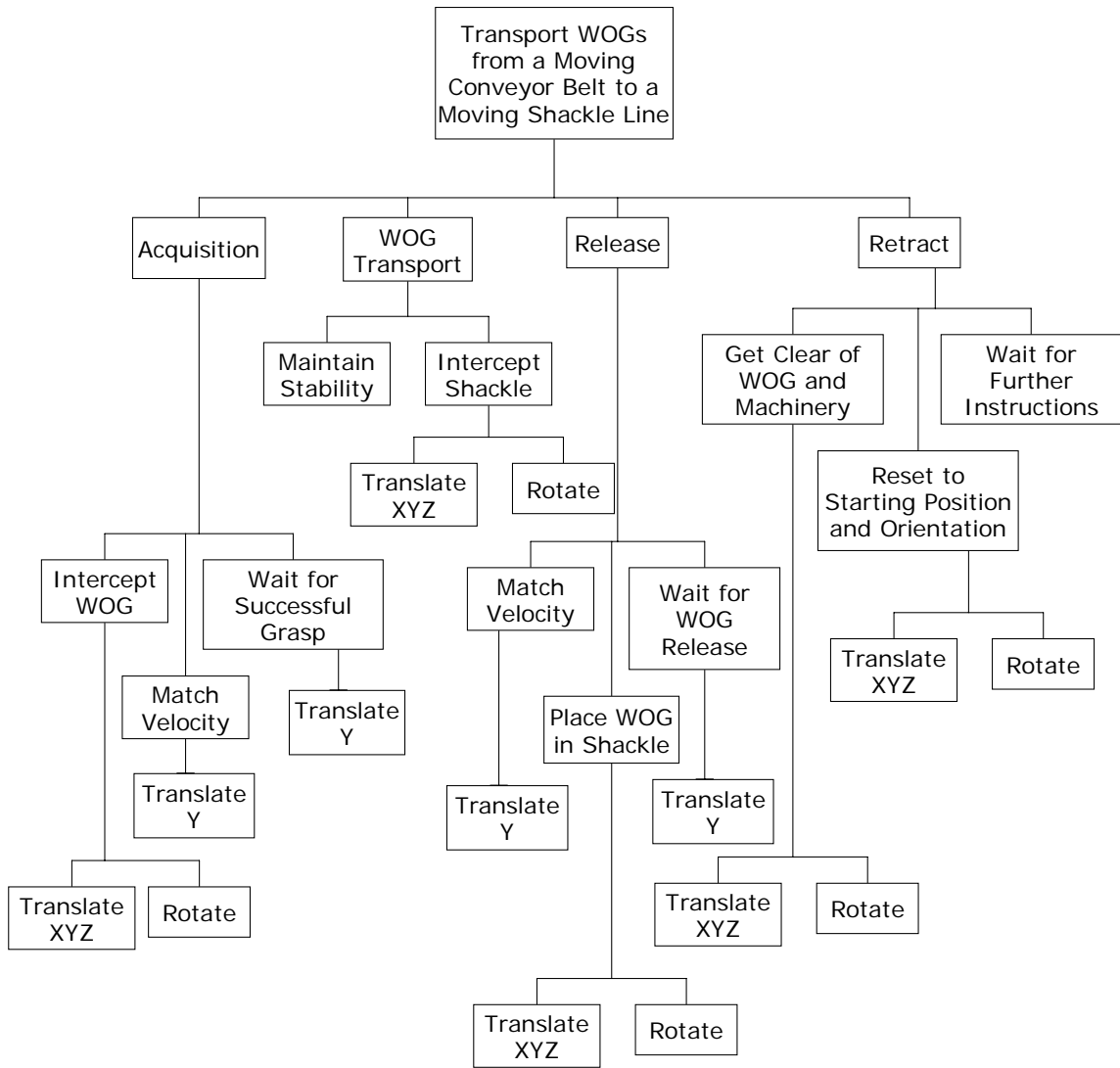


Figure 3.2: Tree diagram.

The tree diagram gives a better idea of what must be done for a robot to successfully transfer a WOG from a moving conveyor belt to a moving shackle. The

robot must acquire the WOG, transport the WOG from the conveyor belt to the shackle, release the WOG into the shackle then retract from the release point. Each of these tasks can be broken up into smaller sub-tasks. Acquisition involves intercepting the WOG, matching its velocity, and then waiting for the end effector to grasp the WOG. WOG transport involves intercepting the shackle and maintaining stability. Maintain stability could also be written as: move in a smooth and controlled manner. If the motions of the robot are too abrupt and the grasp of the end effector is not perfect then the WOG may be shaken from the grasp of the end effector. It is the responsibility of the end effector to maintain a secure grasp of the WOG, but there is no reason for the robot to make this more difficult than it needs to be. Releasing the WOG involves matching the speed of the shackle then placing the WOG into the shackle and waiting for the end effector to release the WOG. Retracting involves making sure all parts of the end effector and robot are clear of the WOG and all machinery, then resetting the robot to a pre-specified position and waiting for instructions to begin the cycle again.

The tree diagram also shows which motions are associated with each of the sub-tasks described above. Some sub-tasks are not associated with a motion while others are associated with a translation and/or a rotation of the end effector. The statement *Translate Y* in the tree diagram means that only a translation in the *Y* direction (global coordinate frame), not in the *X* or *Z* directions, is required. The statement *translate XYZ* does not necessarily mean translations will be required in all three of these directions. It simply means that translation could not be ruled out in any of these directions, and that any or all of them may be needed. Similarly, the statement *rotation* does not necessarily mean that both rotational degrees of freedom must be used.

The tree diagram provides a detailed illustration of what must be done to complete the overall task, but it does not include information about the inputs and outputs of the system, or about how material, signals, and energy flow through the system. To incorporate this information into a detailed function structure diagram a flow chart diagram is developed.

3.1.2 Flow Chart Diagram

The flow chart diagram (Figure 3.3) is another representation of the function structure. Its purpose is to show the flow of information, power, and physical influences through the task, as well as to show how the sub-tasks interact with each other. In some ways it is less detailed than the tree diagram, but it contains information that neither of the previous function structure diagrams contained. The flow chart does not show all of the sub-functions in the tree diagram. If the flow chart diagram included all of the sub-tasks shown in the tree diagram, as well as all of the information about the flow of information, power, and physical influences it would be large and complex. In order to construct a clear and informative flow chart diagram the task must be expressed as a smaller set of sub-tasks. For the sakes of clarity and simplicity a flow chart diagram should contain only one level of sub-tasks, rather than a multi-level hierarchal organization of sub-tasks as seen in the tree diagram. A set of subtasks that describe the task with detail and clarity is desired. The most detail oriented blocks in the tree diagram contain information about specific translations and rotations. A flow chart made up of these subtasks would be detailed, but would not provide a clear description of the task.

The next layer of blocks in the tree diagram provides a good combination of descriptiveness and detail. A flow chart can be based on this set of subtasks. Since the maintain stability and intercept shackle subtasks are never performed independently they are replaced by the WOG Transport sub-task as a further simplification. The resulting set of subtasks is combined with schematic representations of the flow of information, power, and physical influences to produce the flow chart diagram.

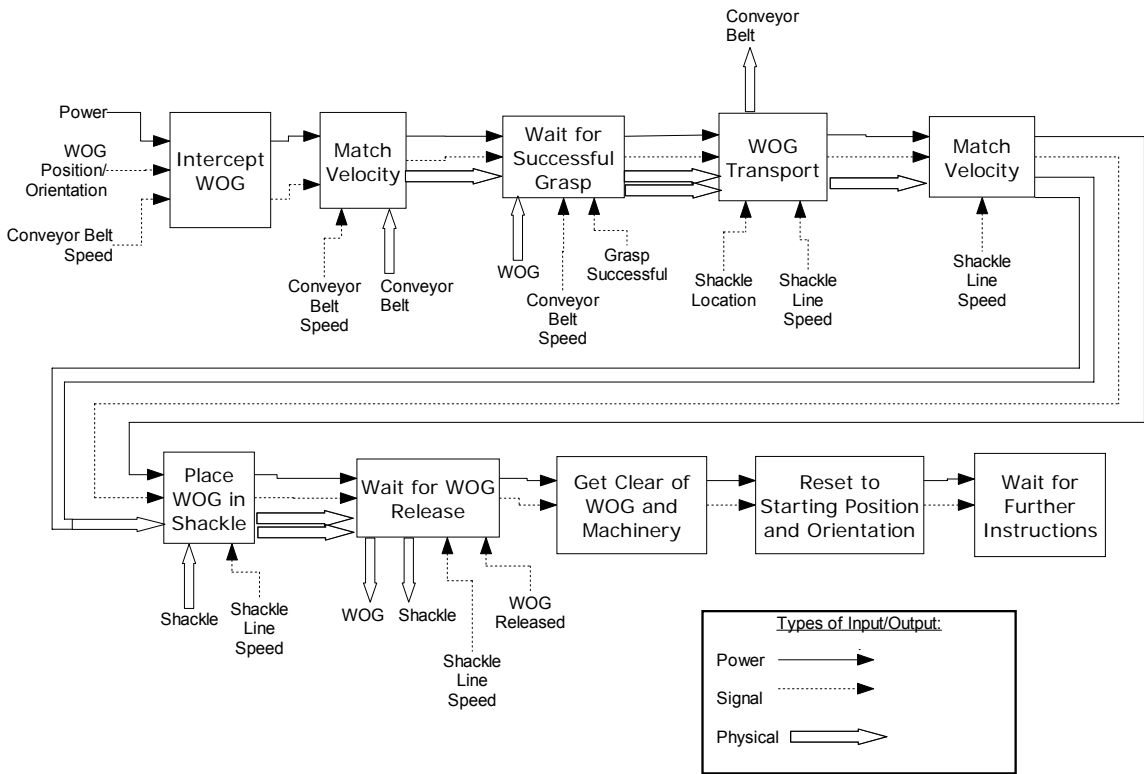


Figure 3.3: Flow chart diagram.

First the robot is provided with power, the position and orientation of the WOG, and the speed of the conveyor belt. The speed of the conveyor belt is the same as the speed of the WOG, but the speed of the conveyor belt can be obtained from a decoder on

the conveyor belt motor whereas the speed of the WOG would be more difficult to determine. The robot determines an intercept point and carries out the necessary rotations and translations to match the position and orientation of the end effector to the position and orientation of the WOG. The robot then continuously monitors and matches the speed of the conveyor belt while the end effector grasps the WOG. When the end effector has successfully grasped the WOG the robot is provided with the location of the shackle that the WOG should be placed in and the speed of the shackle line. The robot then determines an intercept point and calculates the translations and rotations required to transport the WOG from the conveyor belt to the shackle and to orient the WOG for release into the shackle. The robot carries out these translations and rotations quickly, but in a smooth and controlled manner. The robot then monitors the speed of the shackle line and matches the velocity of the shackle. While maintaining the same velocity as the shackle in the Y direction (global coordinate frame), the robot carefully lowers the WOG into the shackle and waits while the end effector releases it. After the WOG has been released the robot carefully moves away from the WOG and shackle to be sure that no part of the robot or end effector becomes caught on any WOGs or shackles. Once the robot is clear of the WOGs and the shackle line it quickly resets to its original position and waits for instructions regarding the next WOG to capture.

3.2 Concept Development

In this section a representative set of conceptual solutions is developed. Because of the complexity of the WOG hanging task, the large number of requirements and the

large number of potential solutions a systematic procedure is necessary. A systematic procedure ensures that a broad set of concepts is developed, helps in evaluating large numbers of concepts, provides guidance in the design process, and provides justification for design decisions.

The key to the concept development procedure used in this section is looking at possible solutions to the task at different levels of abstraction. First a group of potential solutions is developed and examined. These potential solutions are broken down and abstracted into their underlying fundamental ideas. These underlying ideas are then examined and they are systematically built back up into a larger more complete set of possible solutions. Finally, this large group of potential solutions is systematically distilled into a smaller, more manageable group that is representative of the full set of potential solutions.

The concept development phase of the design begins with brainstorming. Brainstorming is carried out concurrently with earlier parts of the design process. The synthesis of ideas is aided by formal brainstorming sessions, discussions with colleagues, research into previous work and contemplation of the task. Over a period of several months ideas presented themselves in a variety of ways. Some of the ideas were derived from established industrial robot technology. Some were derived from robotic technology that was not well established in industry, but had been successfully implemented experimentally. Others were derived from technology that had not been used in the field of robotics. The scope of the ideas also varied. While some ideas were for complete robotic workcells others were for smaller pieces of a system such as a mechanism to provide single degree of freedom motion, or a novel use of an actuator.

3.2.1 Decomposition of Ideas

The brainstorming process is not well suited to developing an all inclusive set of robot concepts. It can develop a wide ranging and creative set of ideas, but it leaves gaps between these ideas. When a brainstorming session leads to a new idea through a variation of an existing idea, there is a good chance that similar variations to other existing ideas would lead to more new ideas. It is difficult to fill in these gaps with more brainstorming; however robot design does lend itself to a systematic synthesis of ideas through the combination of ideas developed during brainstorming.

To synthesize a broad set of solutions from the ideas developed in the brainstorming process, these ideas must be expressed in a way that allows them to be compared and combined. Complex ideas were broken down into sets of simpler ideas. For example the idea for an electrically driven SCARA type robot with a 2 degree of freedom robotic wrist, was broken down into the ideas: SCARA + 2 DOF wrist, linear electric actuator, revolute electric actuator. Once the complex ideas were broken up it was found that all of the ideas could be sorted into four categories: conveyor geometry, robot geometry, actuation, joints. Table 3.1 lists the ideas by category and provides a brief explanation of the ideas as well as comments on advantages, disadvantages, or unanswered questions.

Table 3.1: Basic robot ideas.

Conveyor Geometry	Conveyor geometry ideas involve performing some pre-processing on the WOGs while they are still on the conveyor belt and before they reach the robot. These ideas essentially change the problem that the robot faces and are intended to make it simpler.
Basic	Leave the conveyor belt as is. Don't change anything. The advantage is low cost.
Outside	Force all WOGs to the outside part of the conveyor system. This would eliminate the need for the robot to reach under the shackle line to reach WOGs, and would result in a smaller variation in the initial WOG positions. This could probably be achieved with a passive (not actuated) device.
Single File	Force all WOGs into a straight line, <i>i.e.</i> to have the same X coordinate when they are presented to the robot. This would eliminate variation in the initial WOG position in the X direction, and would reduce the total required X positions for completion of the task to two. Can this be achieved with a passive device? Will the device have trouble dealing with variations in WOG size and orientation?
Staging	Remove WOG from conveyor belt to a stationary staging point to wait for the robot to pick it up. Greatly simplifies WOG pickup. Matching conveyor belt speed is not necessary. Device needs actuation.
WOG Flip	Flip all WOGs breast up. This would eliminate the need for the robot to flip any WOGs. The robot would need only four degrees of freedom, three translational and one rotational. Can this be achieved with a passive device?
Robot Geometry	Robot geometry ideas involve the number of and arrangement of the robot's links. These ideas do not specify materials, joint types, or actuator types. Sometimes the robot geometry necessitates that actuators be either prismatic or revolute, but these ideas do not consider the type of prismatic or revolute joints. All of these ideas assume that one of the first four conveyor geometry ideas are implemented. If WOG flip were implemented then the robot geometry ideas would be similar, but would have one fewer rotational degrees of freedom.
Cartesian + 2R	A Cartesian robot (three perpendicular prismatic actuators) with a two degree of freedom (DOF) robotic wrist. This serial geometry has been tested and proven as an industrial robot. Perpendicular directions of translation simplify control. Perpendicular actuators do not transmit loads to each other. Serial robot links tend to be large and heavy. Control of rotation and translation are de-coupled.

Cylindrical + 2R	A cylindrical robot (one revolute actuator controlling the direction from the base to the end effector, θ and two perpendicular prismatic actuators controlling the displacements in the Z and r directions) with a two DOF robotic wrist. This serial geometry has been tested and proven as an industrial robot. Control of the Z coordinate of the end effector is independent of other actuators. Perpendicular actuators do not transmit loads to each other. Serial robot links tend to be large and heavy.
Spherical + 2R	A spherical robot (two revolute actuator controlling the direction from the base to the end effector, θ and φ , and a prismatic actuator controlling the displacements in the r direction) with a two DOF robotic wrist. This serial geometry has been tested and proven as an industrial robot. Serial robot links tend to be large and heavy. Will the end effector rotation that the spherical robot produces with translation cause a problem?
Scara + 2R	A SCARA robot (two revolute actuators rotating parallel to the Z axis and controlling the X and Y position of the end effector, one prismatic actuators controlling the Z position) with a two DOF robotic wrist. This serial geometry has been tested and proven as an industrial robot, especially in pick and place operations. Control of the Z coordinate of the end effector is independent of other actuators. Revolute actuators rotating parallel to the Z axis need never support the weight of any loads against gravity. Serial robot links tend to be large and heavy.
Anthropomorphic + 2R	An anthropomorphic robot (three revolute actuators providing three degrees of translational freedom for the end effector along with some rotation) with a two DOF robotic wrist. This serial geometry has been tested and proven as an industrial robot. This geometry has high dexterity and a large workspace. Serial robot links tend to be large and heavy. Will the end effector rotation that the anthropomorphic robot produces with translation cause a problem?
TTT Parallel + 2R	Any member of the family of parallel mechanisms that produce three degrees of translation with no rotation, the Delta robot is the most famous of these, with a two DOF rotational wrist. All force loads applied to the end effector are shared by the three kinematic chains of the parallel mechanism and the corresponding actuators. No moment loads applied to the end effector are seen by the actuators of the parallel mechanism. Parallel mechanisms tend to be light weight and to have a small workspace. The delta robot has been implemented as a pick and place industrial robot. Control of translation and rotation are de-coupled.

TTR Parallel + T + R	Any member of the family of parallel mechanisms that provide two degrees of translational freedom and one degree of rotational freedom, with a prismatic actuator and a revolute actuator attached in serial. Many of the loads will be shared by the kinematic chains of the parallel mechanism and by the corresponding actuators. This robot can have a larger workspace than the TTT parallel + 2R robot in the direction of the serial prismatic actuator. The rotation available from the parallel mechanism is small ($<180^\circ$). Parallel mechanisms tend to be light weight and to have a small workspace.
TRR Parallel + 2T	Any member of the family of parallel mechanisms that provide two degrees of rotational freedom and one degree of translational freedom, with two prismatic actuators attached in serial. Moment loads and some force loads will be shared by the kinematic chains of the parallel mechanism and by the corresponding actuators. This robot can have a larger workspace than the previous two robots. The rotations available from the parallel mechanism are small ($<180^\circ$). Parallel mechanisms tend to be light weight and to have a small workspace.
Cable Driven	A robot design using a parallel mechanism that has more actuators and more kinematic chains than degrees of freedom. Cable driven robots have even more kinematic chains than non-redundant parallel robots, so the load on each chain and each actuator is even less. Having more actuators than degrees of freedom makes it possible to keep all actuators in tension. This makes it possible to use cables instead of rigid links. Cable driven robots tend to be very light weight and fast.
Curved Path	The task requires variation of the X and Z positions of the end effector, but it does not require arbitrary placement of the end effector in the XZ plane. What if a curve could be found that passed through all of the needed XZ coordinates and a robot could be designed that would allow a single actuator to move the end effector along that curve. The robot would need only two degrees of translational freedom to complete the task, and the robot would only need four actuators.
Actuator	Actuator ideas involve the ways in which power and motion can be provided to the robot.
Electric Linear	A linear (prismatic) actuator operating on electric power. It allows controlled actuation in a straight line along its full range of motion.
Electric Revolute	A revolute actuator operating on electric power. It allows controlled rotational actuation.
Pneumatic 2p Linear	A linear actuator operating on compressed air. It allows two-position actuation in a straight line. It requires a compressor if compressed air is not available. If a compressor is not needed it is cheaper than the other linear actuators.

Pneumatic 2p Revolute	A revolute actuator operating on compressed air. It allows two-position rotational actuation. It requires a compressor if compressed air is not available. If a compressor is not needed it is cheaper than the other revolute actuators.
Pneumatic (2 ⁿ)p Linear	A series of n linear pneumatic actuators with length $L \cdot 2^{i-1}$, for $n \geq i \geq 1$, connected in series. The pneumatic actuators are independently actuated to provide a range of $L \cdot (2^{n-1} - 1)$ and a resolution of L. A compressor is needed if compressed air is not available.
Pneumatic (2 ⁿ)p Revolute	A series of n revolute pneumatic actuators with range of $360^\circ / 2^{(n+1-i)}$, for $n \geq i \geq 1$, connected in series. The pneumatic actuators are independently actuated to provide a range of $360^\circ \cdot (1 - 1/2^n)$ and a resolution of $360^\circ / 2^n$. A compressor is needed if compressed air is not available.
Hydraulic Linear	A linear actuator operating on compressed fluid. It provides motion in a straight line. It is available in two-position or continuous motion control versions. It needs a hydraulic pump (one for the system, not one per actuator). The hydraulic system often leaks fluid. The main advantage of hydraulic actuators is high force output for small actuators.
Hydraulic Revolute	A revolute actuator operating on compressed fluid. It allows rotational actuation. It is available in two-position or continuous motion control versions. It needs a hydraulic pump (one for the system, not one per actuator). The hydraulic system often leaks fluid. The main advantage of hydraulic actuators is high force output for small actuators.
Cable Driven	An actuator that provides motion by extending and retracting a cable. Because of the cable this type of actuator can pull an object closer, but can not push it away. Some other device (possibly another cable driven actuator or gravity) must be used to move the object away.
Curved Actuator	An actuator that provides translation or translation and rotation along a path that is not a straight line. Imagine a linear actuator that has been bent so the actuator follows a desired curve.
Mechanism	An actuator that includes a mechanical device to transform the motion provided by a linear or revolute actuator into a more complicated motion. There are a variety of four bar linkages that turn rotational motion into complex curves.
Const. Drive Mechanism	An actuator that includes a device to transform constant rotational motion into useful intermittent motion. This would essentially provide timed repetitive motions whose timing depends on the speed of the rotational motor.
Ratchet Revolute	An actuator that provides revolute motion through a ratcheting device. The actuator would be able to provide discrete rotational positioning. A two position pneumatic actuator could be used to rotate this actuator one increment at a time.

Passive Joint	Generally, all of a serial robot's joints are actuated. Parallel robots however, have non actuated joints as well. These joints offer restricted but uncontrolled relative motion of several kinematic links. There are a variety of passive joints commercially available. Passive joint ideas are ideas for novel or unusual ways to achieve the function of a passive joint.
Flexible joint	The function of a passive joint is achieved through the use of a flexible mechanism. Often two rigid links and a joint can be replaced by a single part with two rigid sections and one flexible section. Flexible joints have the potential to reduce cost by reducing the number of parts required, reducing assembly time, and simplifying the manufacturing process. Flexible joints also have good characteristics in terms of precision, reliability, reduced wear, reduced weight and reduced maintenance. The disadvantages of flexible joints are that low cost is generally seen only when produced in high numbers, it can be difficult to model their behavior, and many of the materials well suited for flexible joints are not approved for use in a poultry plant.

3.2.2 Construction of a Morphological Matrix

The next step in the concept development is to determine which combinations of the above ideas are possible. This is done through a morphological analysis and the construction of a morphological matrix (Table 3.2). Morphology is the study of structure or form and a morphological analysis is a systematic approach to analyze the structure or form of an idea, object, device, product, system, or process [3]. To carry out the morphological analysis a morphological matrix is constructed. Ideally each type of idea would be placed along one axis of the morphological matrix, but this would lead to a four dimensional matrix. To be useful a morphological matrix must have an easy to read graphical form. The morphological matrix must therefore be reduced to a two dimensional matrix. The actuator and passive joint ideas can be placed on a single axis. These ideas concern different parts of the robot and are therefore independent of each

other. All possible combination of the conveyor geometry and robot geometry ideas are placed along the second axis. Each cell in the morphological matrix represents the combination of the ideas corresponding to the column and row of that cell. The morphological analysis is carried out by considering the combination of ideas represented by each cell in the morphological matrix. If a single example of a robot combining those ideas can be thought of then an X is placed in that cell.

Table 3.2: Morphological matrix.

Conveyor Geometry	Robot Geometry	Actuator													Passive Joint	Flexible joint
		Electric Linear	Electric Revolute	Pneumatic 2p Lin.	Pneumatic 2p Rev.	Pneumatic (2 ^o)p Lin.	Pneumatic (2 ^o)p Rev.	Hydraulic Linear	Hydraulic Revolute	Cable Driven	Curved Actuator	Mechanism Const. drive mechanism	Ratchet Revolute			
Basic	Cartesian + 2R	X	X	X	X	X	X	X					X	X		
	Cylindrical + 2R	X	X	X	X	X	X	X	X				X	X		
	Spherical + 2R	X	X		X	X	X	X	X					X		
	Scara + 2R	X	X	X	X				X				X	X		
	Anthropomorphic + 2R		X				X		X					X		
	TTT Parallel + 2R	X	X			X	X	X				X		X		X
	TTR Parallel + T + R															
	TRR Parallel + 2T															
	Cable driven		X				X				X			X		
	Curved Path	X	X			X	X	X			X	X		X		X
Outside	Cartesian + 2R	X	X	X	X	X	X	X					X	X		
	Cylindrical + 2R	X	X	X	X	X	X	X	X				X	X		
	Spherical + 2R	X	X		X	X	X	X	X					X		
	Scara + 2R	X	X	X	X	X	X		X				X	X		
	Anthropomorphic + 2R		X		X		X		X					X		
	TTT Parallel + 2R	X	X		X	X	X	X						X		X
	TTR Parallel + T + R															
	TRR Parallel + 2T															
	Cable driven		X		X		X				X			X		
	Curved Path	X	X			X	X	X			X	X		X		X
Single File	Cartesian + 2R	X	X	X	X	X	X	X					X	X		
	Cylindrical + 2R	X	X	X	X	X	X	X	X				X	X		

	Spherical + 2R	X	X		X	X	X	X	X					X	
	Scara + 2R	X	X	X	X	X	X		X					X	X
	Anthropomorphic + 2R		X		X		X		X						X
	TTT Parallel + 2R	X	X		X	X	X	X							X
	TTR Parallel + T + R														
	TRR Parallel + 2T														
	Cable driven		X		X		X			X					X
	Curved Path	X	X			X	X	X			X	X			X
Staging															
	2D-Cartesian (2T)+ 2R	X	X	X	X	X	X	X						X	X
	T + 3R	X	X		X	X	X	X	X						X
	4R		X		X		X		X						X
	TTR Parallel + R														
	TRR Parallel + T														
	Cable driven									X					
	Curved Path		X		X		X				X	X			X
WOG Flip															
	Cartesian + R	X	X	X		X	X	X						X	X
	Cylindrical + R	X	X	X		X	X	X	X					X	X
	Spherical + R	X	X			X	X	X	X						X
	Scara + R	X	X	X		X	X		X					X	X
	Anthropomorphic + R		X				X		X						X
	TTT Parallel + R	X	X			X	X	X							X
	TTR Parallel + T														
	Cable driven		X				X			X					X
	Curved Path	X	X			X	X	X			X	X			X

3.2.3 Refinement of the Morphological Matrix

The morphological analysis carried out in Section 3.3.2 serves three purposes. It yields a clear visual representation of which combinations of ideas are possible, it forces examination of the problem from a new perspective, and it forces detailed, focused thought on each of the basic robot ideas shown in Table 3.1. The morphological matrix, as well as the insight gained during its construction, allows the set of possible

combinations of basic robot ideas to be reduced and refined, which allows further design efforts to become more focused.

The morphological matrix can be used to reduce the set of design ideas. In Table 3.2 the rows corresponding to the robot geometry ideas TTR Parallel + T + R, TRR Parallel + 2T, and TTR Parallel + T have no Xs. The morphological matrix has indicated that these robot geometries will not be able to complete the task, so they will not be considered in the remainder of the design process.

The insight gained during construction of the morphological matrix can be used to reduce the set of design ideas further. It was determined during morphological analysis that hydraulic actuators are poorly suited to this task for hygienic and economic reasons. Hydraulic actuators and hoses often leak. This makes them less hygienic than electric or pneumatic actuators and complicates the design of the robot. Compressed air for pneumatic actuators is often available in poultry processing plants, but compressed liquid for hydraulic actuators rarely is. Because hydraulic actuators would require the installation of a hydraulic pump two position hydraulic actuators would be more expensive than two position pneumatic actuators and variable position hydraulic actuators would be as expensive as or more expensive than electric actuators. Hydraulic actuators are capable of producing large forces, but large forces are not necessary for this design. The maximum robot payload is about 15 lbs and the robot will be designed to be as light as possible. Hydraulic actuators will not be considered in the remainder of the design process.

It was also determined during the morphological analysis that the basic conveyor geometry would greatly complicate the task. The shackles move parallel to the conveyor

belt 18 in above the middle of the conveyor belt. When a WOG is hanging in the shackle the lowest part of the WOG is about 10 in above the conveyor belt. One of the demands of this design, as expressed in Table 2.2 is that the robot and end effector not interfere with hanging WOGs. This means the robot can only use the 10 in above the conveyor belt when reaching under the shackle line. This constraint would make it very difficult to capture and transport WOGs that begin on the inside portion of the conveyor belt. The basic conveyor geometry will not be considered in the remainder of the design process.

The remaining combinations of ideas are refined by the construction of a variation of the morphological matrix (Table 3.3). First all of the eliminated ideas discussed in the previous paragraphs are removed from the morphological matrix. For this exercise only the combinations of ideas that received an *X* in Table 3.2 are to be considered, so these cells in the new matrix are highlighted while the rest are not. For each of the highlighted cells in this refined morphological matrix a single question is asked. If a robot is designed based on the conveyor geometry and robot geometry corresponding to this row and the type of actuator corresponding to this column is preferred above all others, how many of that type of actuator will it have?

Table 3.3: Refined morphological matrix.

Conveyor Geometry	Robot Geometry	Actuator											Passive Joint			
		Electric Linear	Electric Revolute	Pneumatic 2p Lin.	Pneumatic 2p Rev.	Pneumatic (2^n)p Lin.	Pneumatic (2^n)p Rev.	Hydraulic Linear	Hydraulic Revolute	Cable Driven	Curved Actuator	Mechanism Const. drive mechanism	Ratchet Revolute	Passive Joint	Flexible joint	
Outside	Cartesian + 2R	3	2	1	1	3	2	3					1	1		
	Cylindrical + 2R	2	3	1	1	2	3	2	1				1	1		
	Spherical + 2R	1	4		1	1	4	1	2					1		
	Scara + 2R	1	4	1	1	1	4		1				1	1		
	Anthropomorphic + 2R		5		1		5		2					1		
	TTT Parallel + 2R	3	5		1	3	5	3						1		X
	Cable driven		2		1		2			4+				1		
	Curved Path	1	2			1	2	1			1	1		1		X
	Single File	Cartesian + 2R	3	2	2	1	3	2	3					2	1	
Cylindrical + 2R		2	3	1	1	2	3	2	1				1	1		
Spherical + 2R		1	4		1	1	4	1	2					1		
Scara + 2R		1	4	1	1	1	4		1				1	1		
Anthropomorphic + 2R			5		1		5		2					1		
TTT Parallel + 2R		3	5		1	3	5	3						1		X
Cable driven			2		1		2			4+				1		
Curved Path		1	2			1	2	1			1	1		1		X
Staging		2D-Cartesian (2T)+ 2R	2	2	2	1	2	2	2					2	1	
	T + 3R	1	3		1	1	3	1	1					1		
	4R		4		1		4		1					1		
	Cable driven									4+						
	Curved Path		2		1		2				1	1		1		X
	WOG Flip	Cartesian + R	3	1	1		3	1	3					1	1	
Cylindrical + R		2	2	1		2	2	2	1				1	1		
Spherical + R		1	3			1	3	1	2					1		
Scara + R		1	3	1		1	3		1				1	1		
Anthropomorphic + R			4				4		2					1		
TTT Parallel + R		3	4			3	4	3						1		X
Cable driven			1				1			4+				1		
Curved Path		1	1			1	1	1			1	1		1		X

Constructing a refined morphological matrix such as this helps in the visualization of possible solutions. It facilitates thought about how the combinations of ideas represented by each cell in the matrix can be implemented, and what the difficulties of implementation might be.

During this exercise it was determined that the staging and WOG flip conveyor geometries were possible, but were not practical. Both of these conveyor belt geometries simplify the task that the robot must perform, but they make the overall system more complicated and more expensive. All implementations of the staging conveyor geometry would require substantial modification to the conveyor belt structure, as well as additional actuators. Some ideas for simple and inexpensive implementation of the WOG flip geometry were explored, but experimentation with sample WOGs showed that such implementations were unreliable. It was determined that the center of mass of a WOG is near the center of the torso and that the WOG is almost equally stable resting on its back and on its breast. It was determined that a passive WOG flip mechanism would not work because the passive mechanism would not be able to distinguish between a WOG lying on its breast and a WOG lying on its back. A variety of flipping motions that could be achieved through simple actuated devices were also explored. It was found that the WOGs had a tendency to either roll or to not flip at all. None of the flipping motions could reliably provide a 180° flip of the WOGs.

From the insight gained in constructing Table 3.3 it is not clear if the single file conveyor geometry is feasible, but it is clear that the potential problems outweigh the potential advantages of this geometry. The single file conveyor geometry can be feasible only if a simple and passive implementation can be developed. Many challenges are

anticipated in the design of a passive mechanism that can arrange WOGs of various sizes in single file, while never getting clogged. It is anticipated that robots working with the single file conveyor geometry would not be much simpler than robots working with the outside geometry, so the robot will use the simpler to implement outside conveyor geometry. The morphological matrix can now be reduced to the final morphological matrix shown in Table 3.4. The yellow (shaded) cells represent combinations of design concepts that are feasible.

Table 3.4: Final morphological matrix.

		Actuator	Electric	Linear/revolute	Electric	Revolute	Pneumatic 2p	Lin.	Pneumatic 2p	Rev.	Pneumatic	(2 ⁿ)p Lin.	Pneumatic	(2 ⁿ)p Rev.	Cable Driven	Curved	Actuator	Mechanism	Const. drive	mechanism	Ratchet	Revolute	Passive Joint	Flexible joint	
Conveyor Geometry	Outside																								
	3T 2R																								
	Cartesian + 2R																								
	Cylindrical + 2R																								
	Spherical + 2R																								
	Scara + 2R																								
	Anthropomorphic + 2R																								
	TTT Parallel + 2R																								
	Cable driven																								
	Curved Path																								

3.2.4 Synthesis of a Representative Group of Solutions

The next step in the concept development is to develop this information into more concrete, detailed ideas for solutions to the WOG hanging task. As it will be shown in

the following paragraphs the concepts in the final morphological matrix can be combined to form a large number of solutions. This prohibits a detailed comparison of all of the solutions. To get around this problem a smaller representative group of solutions is found. This is done by splitting up the robot motion into a translation and a rotation component, then by distilling the resulting sets of solutions into smaller representative sets of solutions.

To develop the ideas in the final morphological matrix into solutions to the WOG hanging task the motions that the robot is required to perform must be examined. The robot must be able to provide translational motions in three dimensions. We will call these motions *X*, *Y*, and *Z*. The robot must also be able to provide two rotational motions. The first rotational motion is called the *Rotate* motion and is a continuous rotation about an axis that must be normal to the conveyor belt during the WOG acquisition phase of the task. The *Rotate* actuator must be able to stop at any rotational position. The second rotation is called the *Flip* motion and is a discrete rotation about an axis that must be parallel to the conveyor belt. The *Flip* actuator only needs to be able to stop at the 0° and 180°. We will call this rotation *Flip*. These motions were described in more detail in Section 2.3.4.

Next, methods for actuating the required robot motion are examined. The list of actuator and joint ideas that is at the top of the final morphological matrix is refined in an attempt to eliminate information about what type of motion the actuators produce. For example, electric linear and electric revolute are combined into electric. The flexible joint concept is combined with actuator concepts when appropriate to create new actuation concepts. For example, the flexible joint concept and the mechanism concept

are combined to form the flexible mechanism concept. For a few of the concepts, such as the curved actuator concept, it is not possible to eliminate information about the motion it provides without losing the meaning of the concept. These concepts are not altered. The new list of actuation concepts is presented and explained in Table 3.5.

Table 3.5: Actuation concepts.

Electric	An electrically powered actuator.
Pneumatic	A 2 position pneumatically powered actuator.
Multi-Position-Pneumatic	A series of actuators connected in series to provide discrete multi-position actuation.
Ratchet Pneumatic	A device that provides discrete multi-position actuation by repeatedly extending and contracting a single pneumatic actuator connected to a ratcheting device.
Constant Drive Timed Mechanism	A mechanism that transforms the motion of a revolute actuator rotating at a constant speed into a more complex repetitive motion.
Cable Driven	Actuation based on controlling the length of a flexible cable.
Curved Path Actuator	An actuator that provides motion along a curved path.
Curved Path Linkage	Actuation that uses a linkage to transform the motion of a simple linear or revolute actuator into curved path motion.
Flexible Linkage	A curved path linkage that utilizes flexible links.
Flexible Electric	An electric actuator connected to a kinematic chain that utilizes flexible links.
Flexible Multi-Position Pneumatic	A multi position pneumatic actuator connected to a kinematic chain that utilizes flexible joints.

A matrix is now formed to show how the actuation concepts listed in Table 3.5 and the robot geometries shown in the final morphological matrix (Table 3.4) can be combined to perform the 5 motions of the robot. The rows of the robotic solution matrix (Table 3.6) correspond to 8 robot geometries, while the columns of the matrix correspond

to all of the combinations of actuation that can provide the 5 required robot motions. Each of the 5 motions of the robot must be provided by one of the types of actuation in Table 3.5. Some types of actuation, such as electric actuation, can be used for any of the motions. Other types of actuation can only provide some of the motions. Two position pneumatic, for example, can not be used for the *Rotate* motion. There are 102 ways that the actuation concepts in Table 3.5 can be combined to provide the five necessary motions of the robot. Each of these combinations is referred to as an actuation strategy. Table 3.6 shows the first 12 columns of the robot solution matrix. The full robot solution matrix can be found in Appendix A in Table A.1. An “x” has been placed in every cell for which the actuation strategy and the robot geometry are compatible. This matrix yields a total of 180 robot solutions. It is simply not practical to carry out detailed comparisons of 180 solutions, so steps must be taken to reduce the number of comparisons.

There is a pattern in the robot solution matrix that allows a reduction in the number of comparisons without eliminating any of the solutions. The robot solution matrix shows that the compatibility between an actuation strategy and a robot geometry is not dictated by the choice of actuation concepts for the *Rotate* or *Flip* motions. It can be seen in Table 3.6 that the spherical +2R robot geometry is compatible with all 6 actuation strategies that use electric actuation for the *X*, *Y*, and *Z* motions, but is not compatible with any of the 6 actuation strategies that use electric actuation for the *X*, and *Y* motions but multi-position pneumatic actuation for the *Z* motion. If the combinations of actuation to be used for *Flip* and *Rotate* motions are not considered in the robot solution matrix and are instead considered separately then the number of comparisons is reduced. When the *Rotate* and *Flip* motions are not considered in the robot solution matrix it is simplified to the refined robot solution matrix shown in Table 3.7.

Table 3.7: Refined robot solution matrix.

Conveyor Geometry	Robot Geometry	Z			Y			X							
		Electric	Multi Pos Pneumatic	Multi Pos Pneumatic	Const Drive Timed Mech	Const Drive Timed Mech	Cable Driven	Curved Path Actuator	Curved Path Actuator	Curved Path Linkage	Curved Path Linkage	Flexible Linkage	Flexible Linkage	Flexible Joint Electric	Flexible Joint MP pneumatic
Outside	3T														
	Cartesian	X	X	X	X	X									
	Cylindrical	X	X	X	X	X									
	Spherical	X		X											
	Scara	X	X	X	X	X									
	Anthropomorphic	X		X											
	TTT Parallel	X		X										X	X
	Cable driven						X								
	Curved Path							X	X	X	X	X	X		

To reduce the number of comparisons further a representative group of solutions is selected from the refined robot solution matrix. Table 3.8 shows the representative group of solutions. By leaving some of the solutions from Table 3.7 out of the comparison we run the risk of leaving out the best solution. To minimize this risk the comparison of the representative group of solutions is treated as a preliminary comparison. If the results of the preliminary comparison suggest that the best solution

may not be in the representative group a secondary comparison is carried out to investigate.

Table 3.8: Representative group of robot solutions.

Conveyor Geometry	Robot Geometry	Z			Y			X						
		Electric	Multi Pos Pneumatic	Multi Pos Pneumatic	Const Drive Timed Mech	Const Drive Timed Mech	Const Drive Timed Mech	Cable Driven	Curved Path Actuator	Curved Path Actuator	Curved Path Linkage	Curved Path Linkage	Flexible Joint Electric	Flexible Joint MP pneumatic
Outside	3T													
	Cartesian	■	■	■	■	■								
	Anthropomorphic	■												
	TTT Parallel	■		■									■	■
	Cable driven							■						
	Curved Path								■	■	■	■		

3.3 Evaluation of Concepts

The next step in the design is the selection of the principal solutions, the principal solution for the *X*, *Y*, and *Z* motions and the principal solution for the *Rotate*, and *Flip*

motions. The following sections contain an evaluation process that aids in the selection of the principal solutions. The evaluation process consists of developing a set of evaluation criteria, developing weighting factors for those evaluation criteria, then using them to evaluate the solutions in Table 3.8 and the 6 possible actuation strategies for the *Flip* and *Rotate* motions.

3.3.1 Evaluation Criteria

The evaluation criteria are chosen to emphasize the wishes and demands developed in Section 2.4. There are a total of 16 evaluation criteria chosen. Some are global criteria, while others are subtask specific. The global evaluation criteria are used to evaluate properties that the robot will have at all times:

Joint/Actuator Cost – Estimated cost of joints and actuators. Electric actuators are several times the cost of pneumatic actuators. Flexible joints have the potential to be less expensive than standard joints.

Link Volume – Estimated amount of material needed to make all links of the robot. This is a good indicator of the cost of manufacturing the links.

Part Complexity – Estimation of the complexity of the parts needed to build a robot. This is also good indicator of the cost of a robot. Standard off the shelf

parts are generally cheaper than custom made parts. Simple custom made parts are generally cheaper than complex custom made parts.

Reliability/Maintenance – Estimate of the reliability of a robot and an estimate of how easy it would be to perform maintenance on the robot. Pneumatic actuators are more reliable than electric actuators. Flexible joints have the potential to have longer life than standard joints in many situations. Robots with more moving parts or more actuators tend to require more maintenance.

There are also subtask specific evaluation criteria. As shown in Figure 3.2: Tree diagram, the task of picking up a WOG from the conveyor belt and hanging it on a shackle can be accomplished by the execution of four subtasks: acquisition, WOG transport, release, and retract. Before a comparison can be carried out it is important know what each subtask entails as well as where the boundaries separating the subtasks are. The subtasks are:

Acquisition – After a WOG orientation and pick up location are determined the robot moves the end effector from its starting position to the proper orientation and location for acquisition. The robot then smoothly tracks the WOG on the conveyor belt, allowing the end effector to securely grasp the WOG.

Transport – After successful acquisition the WOG is quickly translated and rotated from the conveyor belt to the approximate location and orientation that will be required to place the WOG on the shackle.

Release – The robot smoothly tracks the shackles then lowers the legs of the WOG into the shackle. Once the legs are securely in the shackle the robot maintains the end effectors position relative to the shackle while the end effector releases the WOG.

Retract – After release the robot resets to its initial position to wait for the next WOG.

The performance of a robot in carrying out each of these subtasks is evaluated on three criteria, Ease of Control, Speed, and Robustness. The meaning of each of these criteria varies from one subtask to another. A robot characteristic that improves the Ease of Control during one of the subtasks may be a detriment to the ease of control during another subtask. Table 3.9 contains the subtask specific descriptions for ease of control, speed, and robustness. It also contains comments on what characteristics should be looked for when each of these evaluation criteria is applied.

Table 3.9: Descriptions of subtask specific evaluation criteria.

Subtask	Evaluation Criteria	Description
<u>Acquisition</u>	Ease of Control	How easy is it to control the robot during acquisition? The actuation of pneumatic actuators is simpler than the actuation of electric actuators; however it is more difficult to maintain smooth controlled motion with pneumatic actuators. The control for a prescribed motion is easier when the coordination of multiple actuators is not required.
	Speed	How quickly can the robot translate and rotate the end effector to get it into position and ready to grasp the WOG? Does the robot do anything that may require the end effector to delay in grasping the WOG?
	Robustness	How well does the robot deal with variations in the task? Does the robot lessen the end effector's ability to deal with variation in the task? If the WOGs are closer together or farther apart than expected can the robot adjust? If the initial acquisition point will not work can the robot adjust? Can the robot position the end effector in the optimal position for acquisition, or does it rely on the end effector to make a successful grasp despite only moderately accurate positioning? Will changes in operating conditions adversely affect the robot's performance? The behavior of pneumatic actuators can be sensitive to temperature.
<u>Transport</u>	Ease of Control	How easy is it to control the robot during Transport? The actuation of pneumatic actuators is simpler than the actuation of electric actuators; however it is more difficult to maintain smooth controlled motion with pneumatic actuators. The control for a prescribed motion is easier when the coordination of multiple actuators is not required.
	Speed	How quickly can the robot transport the WOG and end effector? Parallel robots tend to be faster than serial robots. Transport is faster when the path of the payload is short and direct. Robots that are lighter are generally faster.

	Robustness	How well does the robot deal with variations in the task? Does the robot lessen the end effector's ability to deal with variation in the task? If the WOG is heavier or lighter than expected will the performance of the robot be adversely affected? Parallel robots tend to be stiffer than serial robots, and therefore Parallel robots tend to be less sensitive to variations in weight. If the end effector has a poor grasp of the WOG, are the motions of the robot so abrupt that they may shake the WOG loose? Will changes in operating conditions adversely affect the robot's performance? The behavior of pneumatic actuators can be sensitive to temperature.
<u>Release</u>	Ease of Control	How easy is it to control the robot during release? The actuation of pneumatic actuators is simpler than the actuation of electric actuators; however it is more difficult to maintain smooth controlled motion with pneumatic actuators. The control for a prescribed motion is easier when the coordination of multiple actuators is not required.
	Speed	How quickly can the robot make fine adjustments to the position, velocity, and orientation of the WOG then lower it into the shackle? Does the robot do anything that may require the end effector to delay releasing the WOG? Because the translations and rotations are small for this task outright speed is not of much benefit. Time can be saved however, if the robot is able to make a smooth fluid transition from the transport phase to the release phase.
	Robustness	How well does the robot deal with variations in the task? Does the robot lessen the end effector's ability to deal with variation in the task? If the WOG is not lined up with the shackle can the robot adjust easily and quickly? Can the robot position the end effector in the optimal position for release, or does it rely on the end effector to make a successful release despite only moderately accurate positioning? Will changes in operating conditions adversely affect the robot's performance? The behavior of pneumatic actuators can be sensitive to temperature.

<u>Retract</u>	Ease of Control	How easy is it to control the robot while retracting? The actuation of pneumatic actuators is simpler than the actuation of electric actuators; however it is more difficult to maintain smooth controlled motion with pneumatic actuators. The control for a prescribed motion is easier when the coordination of multiple actuators is not required.
	Speed	How quickly can the robot retract and prepare for the next WOG? Parallel robots tend to be faster than serial robots. Retraction is usually faster when the path of the robot is simple and direct. Robots that are lighter are generally faster.
	Robustness	How well does the robot deal with variations in the task? If the release has taken longer than expected, can the robot adjust? How likely it is that part of the robot or end effector will impact something while trying to retract? How likely it is that such an occurrence will adversely affect performance or damage equipment? Will changes in operating conditions adversely affect the robot's performance? The behavior of pneumatic actuators can be sensitive to temperature.

3.3.2 Evaluation Criteria Weighting Factors

Each of the 16 evaluation criteria are important, but some are more important than others. To accurately evaluate the potential robot solutions the relative importance of the evaluation criteria must be determined. In this section the relative importance of the evaluation criteria are determined and a weighting factor is assigned to each of the evaluation criteria.

The relative importances of the evaluation criteria are determined through a binary comparison method. By this method the relative importance of the evaluation

criteria can be systematically determined by comparing pairs of evaluation criteria. A binary comparison method is easier and less susceptible to personal biases than a method based on comparing all evaluation criteria simultaneously. To facilitate the binary comparisons of the evaluation criteria a 16 x 16 Evaluation Criteria importance matrix is constructed (Table 3.10). All of the evaluation criteria are listed along the top of the matrix and along the side of the matrix. Each cell of the matrix corresponds to the question "Is the evaluation criteria corresponding to this row more important than the evaluation criteria corresponding to this column?" If yes, a four is placed in that cell. If no, a one is placed in that cell. If the row and column correspond to the same evaluation criteria the cell is left empty. The evaluation criteria weighting factors are determined by summing each row. Choosing to use ones and fours in Table 3.10 is a matter of judgment. This choice results in the most important evaluation criteria being considered four times more important than the least important evaluation criteria.

Table 3.10: Evaluation criteria importance matrix.

Subtask	Evaluation Criteria	Subtask				Subtask Specific Properties	Acquisition			Transport			Release			Retract			Weighting Factors
		Intrinsic Robot Properties					Ease of Control	Speed	Robustness										
		Joint/Actuator Cost	Link Volume	Part Complexity	Reliability/Ease of Maintenance														
Global	Joint/Actuator Cost	1	1	4		4	4	4	4	4	4	4	4	4	4	4	4	4	54
	Link Volume	4		4	4	4	4	4	4	4	4	4	4	4	4	4	4	4	60
	Part Complexity	4	1		4	4	4	4	4	4	4	4	4	4	4	4	4	4	57
	Reliability/Ease of Maintenance	1	1	1		1	1	1	4	1	1	1	4	1	4	1	4	4	27
Acquisition	Ease of Control	1	1	1	4		1	1	4	1	1	1	4	1	4	1	4	4	30
	Speed	1	1	1	4		4		1	4	1	4	4	4	4	4	1	4	42
	Robustness	1	1	1	4		4	4		4	1	4	4	4	4	4	1	4	45
Transport	Ease of Control	1	1	1	1		1	1	1		1	1	1	4	1	4	1	4	24
	Speed	1	1	1	4		4	4	4	4		4	4	4	4	4	4	4	51
	Robustness	1	1	1	4		4	1	1	4	1		4	4	1	4	1	4	36
Release	Ease of Control	1	1	1	4		4	1	1	4	1	1		4	1	4	1	4	33
	Speed	1	1	1	1		1	1	1	1	1	1		1	4	1	4	21	
	Robustness	1	1	1	4		4	1	1	4	1	4	4	4		4	1	4	39
Retract	Ease of Control	1	1	1	1		1	1	1	1	1	1	1	1		1	4	18	
	Speed	1	1	1	4		4	4	4	4	1	4	4	4	4		4	48	
	Robustness	1	1	1	1		1	1	1	1	1	1	1	1	1	1		15	

The solutions developed in Section 3.3.5 can now be evaluated. In the following section the representative group of solutions for the *X*, *Y*, and *Z* motions are evaluated. In Section 3.4.4 the solutions for the *Rotate* and *Flip* motions are evaluated.

3.3.3 Evaluation of Solutions for X , Y and Z Motions

The representative group of solutions for the X , Y and Z are evaluated based on the 16 evaluation criteria and their weighting factors. The evaluation of the representative group of solutions is done through a binary comparison method. This method begins with one of the solutions being chosen as a reference. An evaluation matrix, such as the one shown in Table 3.11, is formed with the solutions listed along the top of the matrix and the evaluation criteria listed along the side. Each cell corresponds to the evaluation of the solution at the top of its row based on the evaluation criteria at the side of its column. The evaluation of the reference is specified to be zero for all evaluation criteria. The remaining solutions are compared to the reference for each of the evaluation criteria. For a given evaluation criteria each solution that is better than the reference receives a (+1) while each solution that is worse than the reference receives a (-1). If a solution is about the same as the reference for an evaluation criterion, it receives a (0). By itself this matrix does not provide enough information to accurately evaluate the solutions. By repeating this evaluation process for all of the references in Table 3.12, and combining the resulting evaluation matrices a detailed and accurate evaluation of the solutions is obtained (Table 3.13).

Table 3.11: Evaluation matrix for X, Y, and Z motion solutions.

Subtask	Evaluation Criteria	Robot Geometry														
		Z	Y	X	Z	Y	X	Z	Y	X	Z	Y	X	Z	Y	X
<i>Intrinsic Robot Properties</i>																
Global	Joint/Actuator Cost	0	0	0	1	1	1	1	0	1	-1	1	1	1	1	1
	Link Volume	0	0	1	0	0	0	1	-1	-1	1	1	1	1	1	1
	Part Complexity	0	0	-1	0	0	0	-1	-1	-1	1	-1	-1	-1	-1	-1
	Reliability/Ease of Maintenance	0	0	-1	1	1	1	1	-1	1	-1	1	1	1	1	1
<i>Subtask Specific Properties</i>																
Acquisition	Ease of Control	1	0	-1	1	-1	-1	-1	1	-1	-1	1	-1	1	-1	-1
	Speed	0	0	1	-1	1	1	1	-1	-1	1	-1	-1	-1	1	1
	Robustness	1	0	1	1	-1	-1	-1	-1	-1	1	1	-1	1	-1	-1
Transport	Ease of Control	1	0	-1	1	1	0	-1	1	1	-1	1	1	1	-1	-1
	Speed	0	0	1	1	1	1	1	0	1	1	-1	-1	-1	1	1
	Robustness	0	0	1	-1	-1	-1	-1	0	-1	1	1	1	1	1	1
Getting Legs into Shackle	Ease of Control	1	0	-1	1	-1	-1	-1	1	-1	-1	1	-1	1	-1	-1
	Speed	0	0	0	0	0	0	0	0	0	0	1	1	1	1	0
Retract	Robustness	1	0	1	-1	-1	-1	-1	-1	-1	1	1	-1	1	-1	-1
	Ease of Control	0	0	0	1	0	0	0	1	1	-1	1	1	1	1	0
	Speed	0	0	1	1	1	1	1	-1	-1	1	-1	-1	-1	-1	1
	Robustness	1	0	1	-1	-1	-1	-1	1	-1	1	1	-1	1	-1	-1

Table 3.12: Reference geometries for evaluation of the X , Y , and Z motion solutions.

Robot Geometry	X Motion Actuation	Y Motion Actuation	Z Motion Actuation
Anthropomorphic	Electric	Electric	Electric
Cartesian	Constant Drive Timed Mechanism	Electric	Electric
Cable driven	Cable Driven	Cable Driven	Cable Driven
Curved Path	Curved Path Actuator	Curved Path Actuator	Electric
TTT Parallel	Flexible Joint Electric	Flexible Joint Electric	Flexible Joint Electric

The evaluation matrices corresponding to the five references in Table 3.12 can be found in Appendix B. Adding these matrices then multiplying the rows of the resulting matrix by the evaluation criteria weighting factors yields the matrix shown in Table 3.13. At the bottom of Table 3.13 are the total scores and normalized scores for all of the Solutions.

The total scores are obtained by summing each of the columns of the matrix. The normalized scores are obtained by the equation:

$$NS_i = \frac{TS_i - TS_{\min}}{TS_{\max} - TS_{\min}}$$

The normalized scores closest to 1 indicate the best rated solutions, while the normalized scores closest to 0 are the worst rated solutions. The highest normalized score is by definition 1 and is received by the cable driven robot that utilizes wire driven actuators. A pair of solutions using the TTT robot geometry receive scores of 0.99 and 0.97. One uses flexible joint electric actuation, while the other uses electric actuation. These results suggest that a secondary evaluation is not necessary. 14 of the solutions in Table 3.7 were left out of the representative group of solutions, but all 14 of these solutions are similar to low scoring solutions in Table 3.13.

3.3.4 Evaluation of Solutions for *Rotate* and *Flip* Motions

The solutions for the *Rotate* and *Flip* motions are evaluated based on the same 16 evaluation criteria and weighting factors. The method for evaluating this set of solutions is essentially the same method used in the previous section. Only the set of references (Table 3.14) and the set of solutions are different. The six solutions can be seen along the top of the evaluation matrix shown in Table 3.15.

Table 3.14: Reference points for evaluation of the *Flip* and *Rotate* motion solutions.

<i>Flip</i> Motion Actuation	<i>Rotate</i> Motion Actuation
Pneumatic	Electric
Pneumatic	Pneumatic Ratchet
Electric	Multi-Position Pneumatic

Three evaluation matrices, such as the one shown in Table 3.15 are created. These can be found in Appendix B. Adding them and multiplying the rows of the resulting matrix by the evaluation criteria weighting factors yields Table 3.16. It can be seen in Table 3.16 that the solution using pneumatic actuation for the *Flip* motion and Electric actuation for the *Rotate* motion has a normalized score of 1. The next highest scoring solution receives only a 0.506 normalized score.

Table 3.15: Evaluation matrix for *Flip* and *Rotate* motion solutions.

<u>Subtask</u>	<u>Evaluation Criteria</u>	<i>Flip</i>		<i>Rotate</i>				
		Electric	Pneumatic	Electric	pneumatic ratchet	pneumatic ratchet	Multi Pos Pneumatic	Multi Pos Pneumatic
<i>Intrinsic Robot Properties</i>								
All	Joint/Actuator Cost	-1	0	-1	1	-1	1	
	Link Volume	-1	0	-1	1	-1	-1	
	Part Complexity	0	0	-1	-1	-1	-1	
	Reliability/Ease of Maintenance	-1	0	-1	-1	-1	-1	
<i>Subtask Specific Properties</i>								
Acquisition	Ease of Control	0	0	1	1	-1	-1	
	Speed	0	0	-1	-1	1	1	
	Robustness	0	0	-1	-1	-1	-1	
Transport	Ease of Control	-1	0	-1	1	-1	-1	
	Speed	-1	0	-1	-1	1	1	
	Robustness	1	0	1	-1	-1	-1	
Getting Legs into Shackle	Ease of Control	-1	0	-1	1	-1	-1	
	Speed	0	0	-1	-1	0	0	
	Robustness	1	0	1	-1	-1	-1	
Retract	Ease of Control	-1	0	-1	0	-1	0	
	Speed	-1	0	-1	0	-1	0	
	Robustness	1	0	-1	-1	-1	-1	

Table 3.16: Results of evaluation of *Flip* and *Rotate* motion solutions.

<u>Subtask</u>	<u>Comparison Criteria</u>		Flip		Rotate			
	<i>Intrinsic Robot Properties</i>	Weighting Factors	Electric	Pneumatic	Electric	pneumatic ratchet	Multi Pos Pneumatic	Multi Pos Pneumatic
All	Joint/Actuator Cost	54	-162	0	-54	108	-108	54
	Link Volume	60	-60	0	-60	120	-120	-60
	Part Complexity	57	114	114	0	0	-114	-114
	Reliability/Ease of Maintenance	27	-27	54	-27	0	-54	27
<i>Subtask Specific Properties</i>								
Acquisition	Ease of Control	30	0	0	60	60	-60	-60
	Speed	42	0	0	-84	-84	84	84
	Robustness	45	90	90	-90	-90	0	0
Transport	Ease of Control	24	-24	0	-24	48	-48	-24
	Speed	51	-51	0	-153	-102	102	153
	Robustness	36	108	72	108	-72	0	-108
Getting Legs into Shackle	Ease of Control	33	-33	0	-33	66	-66	-33
	Speed	21	21	21	-63	-42	21	21
	Robustness	39	117	78	117	-78	0	-39
Retract	Ease of Control	18	-36	18	-36	18	-36	18
	Speed	48	-96	48	-96	48	-96	48
	Robustness	15	45	30	0	0	-30	-15
Total Score			6	525	-435	0	-525	-48
Normalized Score			0.506	1	0.086	0.5	0	0.454

3.4 Concept Selection

Evaluation methods such as the ones used in the previous sections are tools to help in the decision making process. They are not automatic decision mechanisms. The evaluation processes provide information to aid in choosing a primary solution and support for the decision once it is made. These evaluation processes can not account for all the factors that determine which solution is best. Some solution properties are difficult to compare from one solution to the next. Some difficulties in the implementation of a solution can not be determined at this phase of the design. In order to select the concept that has the best chance for success the results of the evaluation process must be used in cooperation with engineering judgment.

In the evaluation of the solutions for the X , Y , and Z motions three solutions scored well. The cable driven robot with wire driven actuators scored highest, while the TTT parallel robot with electric actuation and the TTT parallel robot with flexible joint electric actuation also scored well. There are several concerns about the development of a solution based on the cable driven concept. One concern is cleanliness. The wire driven actuators control the position of a moving platform by controlling the lengths of several wires connecting the moving platform to the base. All existing wire driven robots use guides for the wire to slide through, pulleys with wire in them and/or coils of wire. All of these raise concerns about the buildup of food and/or soils. Some new method of wire driven actuation would need to be developed for the poultry processing environment. There are also concerns about the robot getting in the way of the conveyor belt and shackle line. The wire driven actuators can only apply tension to the moving platform. As a result the moving platform is generally confined to remain inside the robot if high

accelerations are required. In other words, moving the moving platform from the edge of the conveyor belt to the shackle line would likely require an actuator beyond the shackle line. There are also concerns about a TTT parallel robot getting in the way of the conveyor belt, but these concerns are not a daunting. The construction of industrial Delta robots is such that the arms of the robot jut out to the sides. There are many TTT parallel robot geometries however, that do not have this property, and there are modifications that can be made to the Delta robot geometry to get around this problem. Because of the magnitude of the concerns about the cable driven robot solution it is not chosen as the primary solution.

The two solutions based on the TTT parallel geometry are different, but it is difficult and unnecessary to choose between them at this phase of the design. There are too many unknowns to determine which is better. There are concerns about both designs. For the solution using flexible joint electric actuation there are concerns about finding a material that will have the properties necessary for flexible joints and will be USDA approved. For the solution using electric actuation there are concerns about being able to buy or construct joints that will meet USDA standards. These two solutions are the same from a kinematic standpoint. Their differences lie in what materials are used and the details of how they are constructed. Material selection and construction details are not addressed in the next phase of the design, kinematic design, so these two solutions are combined into one solution. In the kinematic design a TTT parallel mechanism using electric actuation are developed to provide X , Y , and Z motion. Later in the design process, when more information is available, the type of joints are decided.

In the evaluation of solutions for the *Rotate* and *Flip* motions one solution is clearly better than the others. The primary solution is the one that uses two position pneumatic actuation for the *Flip* motion and electric actuation for the *Rotate* motion. It is not obvious from the evaluation process how these rotations should be combined with the TTT parallel mechanism chosen as the primary solution for the *X*, *Y*, and *Z* motions. Judgment must be used in this decision. There are three basic options. These actuators can be placed before the TTT parallel mechanism, after the TTT parallel mechanism, or one actuator can be placed before the TTT parallel mechanism and the other can be placed after. Placing the actuators before the TTT parallel mechanism means that the parallel mechanism will be rotated and that the *Rotate* and *Flip* actuators will not be translated. Placing rotations after the TTT parallel mechanism means that the *Flip* and *Rotate* actuators will be translated but the TTT parallel mechanism will not be rotated. Placing one rotational actuator before the TTT parallel mechanism and one after is a compromise where the TTT parallel mechanism will undergo some rotations and one of the one of the rotational actuators will be translated.

There are a couple of advantages to placing the actuators after the TTT parallel mechanism. One advantage is that the *Rotate* and *Flip* actuators can be arranged to perform rotation without also affecting translation of the end effector. Another advantage is that the moments transmitted to the TTT parallel mechanism due to the *Rotate* and *Flip* actuators would not be seen by the motors in the TTT parallel mechanism. These moments would act against the constraints of the TTT parallel geometry. If the *Rotate* and/or *Flip* actuators are before the TTT parallel mechanism many of the forces that the TTT parallel mechanism generates at the moving platform would generate moments that

the *Rotate* and *Flip* actuators would see as loads. The primary solution for the *Rotate* and *Flip* motions is to place one pneumatic (*Flip*) and one Electric (*Rotate*) actuator after the TTT parallel mechanism.

In the next chapter the design of a robot made up of an electrically actuated TTT parallel mechanism base, with a two degree of freedom robotic wrist begins. The two degree of freedom robotic wrist will be made up of a pneumatic actuator to accomplish the *Flip* motion and an electric actuator to accomplish the *Rotate* motion. It will be attached to the moving platform of the TTT parallel mechanism.

CHAPTER 4

KINEMATIC DESIGN

4.1 Introduction

This chapter details the kinematic design of a parallel-serial robot using the Embodiment Design in the Pahl and Beitz [10] methodology. The robot consists of a 3 degree of freedom translation-only parallel platform carrying two revolute actuators in series. The final concept solution from Chapter 3 is developed to the final robot structure. There are two objectives of this chapter, to develop the robot geometry and to analyze the kinematics of that geometry. The robot geometry developed in this chapter specifies the number and configuration of mechanical links making up the robot. It also specifies the types of and orientations of joints connecting these mechanical links. The kinematics study includes the development of equations to relate the positions and velocities of the end effector and actuators, and a singularity analysis of the robot geometry.

In Section 4.2 the design of the parallel mechanism is carried out. In Section 4.2.1 the basic geometry of the parallel mechanism is developed through the use of group theory. In Section 4.2.2 the reverse kinematic equations for the parallel mechanism are developed. The reverse kinematic equations allow the determination of the actuator positions if the position of the moving end of the mechanism is known. In

Section 4.2.3 the forward kinematic equations of the parallel mechanism are developed. The forward kinematic equations allow the position of the moving end of the mechanism to be determined if the positions of the actuators are known. In Section 4.2.4 the equations for the passive joint angles of the parallel mechanism are developed.

In Section 4.3 an overview of the specialized end effector developed for the task of transferring WOGs from a conveyor belt to a shackle is presented. The basic structure and operation of the end effector is discussed. The results of end effector testing on the required robot motion are also discussed.

In Section 4.4 the robotic wrist is developed and combined with the parallel mechanism designed in Section 4.2 . The robotic wrist is driven by two rotation generating actuators. In Section 4.4.1 the geometry of the robotic wrist is developed. In Section 4.4.2 the kinematic equations of the robotic wrist are developed.

In Section 4.5 the Jacobian matrix for the robot is developed and used to identify the robot singularities.

4.2 Design of Parallel Base

4.2.1 Structural Synthesis of Parallel Base Using Group Theory

In this section the structure of the parallel base is determined. The number of kinematic chains making up the parallel base is determined. The type, number and order of joints making up each kinematic chain are also determined. The method that will be

used to synthesize the structure of the robot was developed by J.M. Herve [23]. The method is based on mathematical group theory, and can be used to synthesize a large variety of parallel mechanisms capable of 3 degrees of freedom translational motion.

Consider $\{D\}$ the set of all possible displacements. In other words $\{D\}$ is a 6 dimensional group consisting of all possible combinations of translations and rotations in three dimensional space. All groups of displacements with less than 6 dimensions are subgroups of $\{D\}$. Table 4.1 lists some of the subgroups of $\{D\}$, as well as some information about each of them. The kinematic pair associated with a group generates motion within that group. The dimension of a group corresponds to the degrees of freedom of motion within that group. Some of the motion groups in Table 4.1 do not have associated kinematic pairs. These motion subgroups must be created by chains of kinematic pairs.

Table 4.1: Subgroups of $\{D\}$.

Dimensions (D.O.F.)	Notation	Description	Associated kinematic pair
1	$\{T(v)\}$	Rectilinear translation parallel to the vector v	(P) Prismatic
1	$\{R(u)\}$	Rotation about a line u	(R) Revolute
1	$\{H(u,p)\}$	Helicoidal (Screw) motion about a line u , with a pitch p	(H) Screw
2	$\{T(P)\}$	Planar translation: all translations parallel to plane P	
2	$\{C(u)\}$	Cylindrical Motion: All rotations about line u and all translations parallel to it	(C) Cylindrical
3	$\{T\}$	Spatial translation: All possible translations	
3	$\{G(P)\}$	Planar Sliding: All translations parallel to plane P and rotations about lines normal to plane P .	

3	$\{S(o)\}$	Spherical Rotation: All possible rotations about point o	(S) Ball
3	$\{Y(u,p)\}$	Y motion: All translations perpendicular to line u and helicoidal motions with pitch p and about lines parallel to line u .	
4	$\{X(w)\}$	X motion, or SCARA motion: All possible translations and all rotations about lines parallel to line w	

Motions belonging to a specific group can be generated in several ways. A group motion generator can be a single kinematic pair if there is a kinematic pair associated with the group, but group motion generators can also be created by combining motion generators for other groups. Let $\{A\}$ be an arbitrary group listed in Table 4.1. An $\{A\}$ motion generator can be constructed by connecting motion generators for subgroups of $\{A\}$ in series, or by connecting motion generators for super-groups of $\{A\}$ in parallel. When two group motion generators are connected in parallel the resulting mechanism can only generate motion that belongs to both groups. A set of motion generators for groups $\{A_1\}, \{A_2\}, \dots, \{A_n\}$ will generate $\{A\}$ motion when connected in parallel if and only if $\{A_1\} \cap \{A_2\} \cap \dots \cap \{A_n\} = \{A\}$.

We desire a mechanism that will generate $\{T\}$ motion. One way to construct a $\{T\}$ motion generator is to connect $\{T(v)\}$ generating prismatic pairs in series. If the vectors $v, v',$ and v'' are linearly independent, connecting $\{T(v)\}, \{T(v')\},$ and $\{T(v'')\}$ generating pairs in series results in a $\{T\}$ generating mechanism. A Cartesian robot is a special case of this type of $\{T\}$ generating mechanism. In a Cartesian robot $v, v',$ and v'' are chosen to be an orthogonal set of vectors. To construct a parallel mechanism that generates $\{T\}$ motion, we must look at the union of super-groups of $\{T\}$. The smallest

super group of $\{T\}$ is $\{X(w)\}$. If the constraints of $\{X(w)\}$ motion are examined it can be seen that the intersection of motion generators for $\{X(w)\}$, and $\{X(w')\}$ is $\{T\}$ as long as w is not parallel to w' .

$$\{X(w)\} \cap \{X(w')\} = \{T\} \quad w \neq w' \quad (4.1)$$

Both $\{X(w)\}$ and $\{X(w')\}$ allow all translations. $\{X(w)\}$ allows only rotations about lines parallel to w , and $\{X(w')\}$ allows only rotations about lines that are parallel to w' . Therefore $\{X(w)\} \cap \{X(w')\}$ only allows rotations that are parallel to both w and w' . As long as w and w' are not parallel to each other no rotation is allowed.

One common $\{X(w)\}$ motion chain is the RRRP chain used by the SCARA robot (Figure 4.1). The three revolute actuators provide translation of the end effector parallel to the XY plane and rotations about axes parallel to the Z axis. The prismatic actuator provides translation parallel to the Z axis. This allows the end effector three degrees of freedom in translations, and allows the end effector to rotate about axes parallel to the Z axis. Note that in this example of a $\{X(w)\}$ motion chain w is parallel to the Z axis.

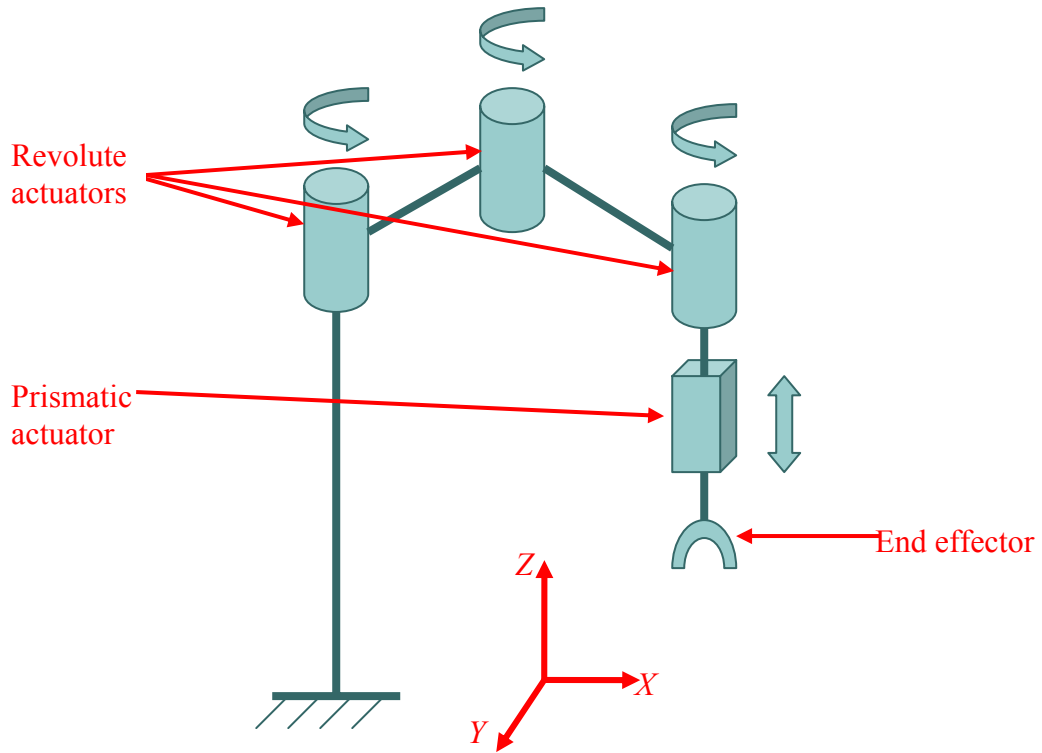


Figure 4.1: SCARA Robot

Many other $\{X(w)\}$ motion generators can be constructed by connecting in series kinematic pairs that are motion generators for subgroups of $\{X(w)\}$. We begin by only considering the single degree of freedom prismatic (P), revolute (R), and Screw (H) kinematic pairs. A $\{T(v)\}$ group is always a subgroup of $\{X(w)\}$, while $\{R(u)\}$ and $\{H(u,p)\}$ groups are subgroups of $\{X(w)\}$ if and only if u is parallel to w .

Any series of four of these kinematic pairs meeting the following two requirements is an $\{X(w)\}$ motion generator:

1. All rotation axes (u) and screw (v) axes must be parallel to w
2. There is no passive mobility in the series.

A kinematic chain has no passive mobility if and only if, when both ends of the kinematic chain are constrained all kinematic pairs in the chain remain fixed. There are many ways that kinematic pairs can be connected to allow passive mobility. A few examples are:

- Two prismatic pairs with parallel axes of motion
- Two helical pairs that share an axis of rotation and pitch
- Two revolute pairs with the same axis of rotation
- Three prismatic pairs whose axes of motion are parallel to the same plane
- Any four prismatic pairs
- Four revolute pairs whose axes of rotation are all parallel

It can be determined from the second requirement that the chain of four kinematic pairs must have three or fewer P pairs, three or fewer R pairs and four or fewer H pairs. Based on these requirements there are a total of 79 orderings of the P, R and H kinematic pairs that can form an $\{X(w)\}$ motion generator. It is worth noting that a P kinematic pair and an R kinematic pair with parallel axes and connected in series is a cylindrical motion generator. Therefore, it is also possible to construct $\{X(w)\}$ motion generators with a C pair in the place of a sequential P pair and R pair as long as the two conditions mentioned above are still met.

In practice a plane hinged parallelogram (Pa) can be used in place of a prismatic pair. As illustrated in Figure 4.2 a plane hinged parallelogram is a circular translation

connector. It allows translation without rotation along a circular path. Other curved path translation connectors could also be used in place of a prismatic pair, however the plane hinged parallelogram has been used successfully in many parallel robots while other curved path translation connectors have not. In addition, the structure of the plane hinged parallelogram is relatively simple compared to other curved path translation connectors. If $\{X(w)\}$ motion generators are allowed to consist of P, Pa, R, H, and C kinematic pairs there are a total of 287 orderings of kinematic pairs.

The number of possible orderings of kinematic pairs is overwhelming, but this number can be greatly reduced when task specific requirements are considered. Some types of kinematic pairs are not suitable for use in a translation only parallel poultry processing robot. Screws are not appropriate for use in close proximity to raw poultry. Threads are an easy place for poultry and or soil to accumulate, and USDA guidelines specifically point out threads as something to be avoided. The only way to make an H pair acceptable for this robot would be if the screw could be completely sealed off from the environment. It is anticipated that sealing the screw off from the environment while still allowing motion would be difficult or impossible. Problems are also anticipated with P and C pairs. In a translation-only parallel mechanism moments applied to the moving platform are countered by the constraints of the kinematic pairs that make up the arms of the parallel mechanism. Whenever prismatic pairs are subjected to a moment, and whenever cylindrical kinematic pairs are subjected to a moment that is not parallel to the cylindrical axis binding is a concern. These concerns are compounded by a desire to use only plain bearings. Plain bearings have the potential to be much more sanitary than other types of bearings, but they also have much higher coefficients of friction and are

more susceptible to binding. It is anticipated that all kinematic pairs will be constructed using plain bearings, so $\{X(w)\}$ motion generating kinematic chains containing P or C pairs will not be considered for this task. R and Pa pairs, shown in Figure 4.2, present fewer concerns about sanitary construction and binding. There are 14 orderings of R and Pa pairs that can generate $\{X(w)\}$ motion.

	PaPaPaR	PaPaRPa	PaRPaPa	RPaPaPa	
PaPaRR	PaRPaR	PaRRPa	RPaPaR	RPaRPa	RRPaPa
	PaRRR	RPaRR	RRPaR	RRRPa	

To choose between these 14 options the anticipated simplicity, cost and performance of each choice are considered. A simpler structure results in a lower cost $\{X(w)\}$ motion generator, and simpler kinematics. Simpler structures also have the potential to be lighter and more reliable than more complex structures. A revolute pair is less complex than a plane hinged parallelogram. The simplest and most common way to construct a plane hinged parallelogram is to connect four bars (two pairs of equal length bars) with four revolute pairs. The number of plane hinged parallelograms is therefore minimized.

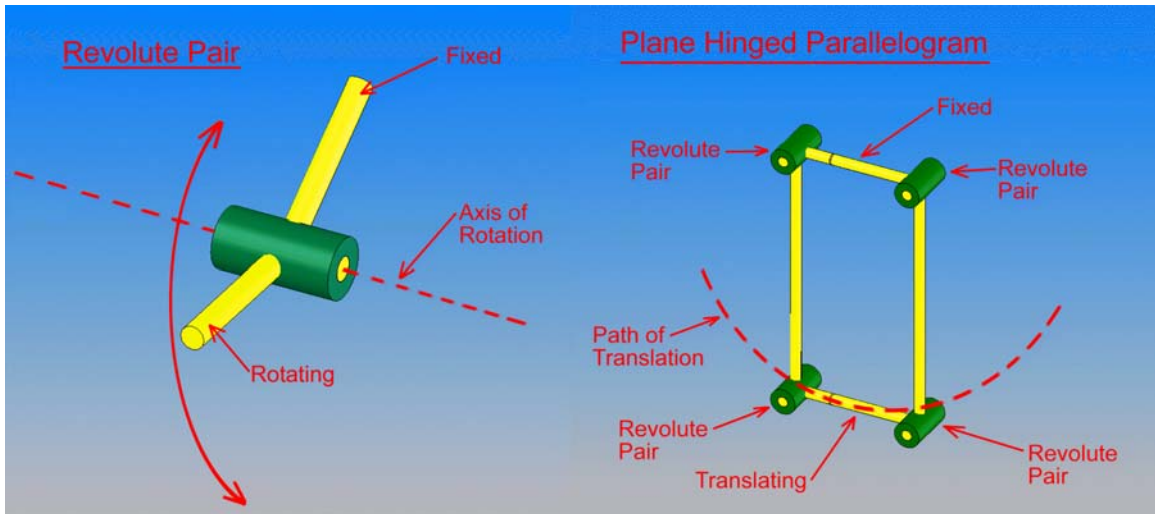


Figure 4.2: Revolute pair and plane hinged parallelogram.

There are four orderings of kinematic pairs that have only one Pa kinematic pair.

PaRRR RPaRR RRPaR RRRPa

To choose between these we look at how simple the connections between kinematic pairs can be made. Recall that the revolute pairs in an $\{X(w)\}$ motion chain must have axes of rotation parallel to w , and that the chain can have no passive mobility. To meet these requirements two revolute pairs connected in series must have a finite perpendicular distance between their axes. If an R pair is connected in series with a Pa pair the revolute pair can be connected directly to the end of the Pa pair without the chain gaining passive mobility. The kinematic orderings with the Pa pair at the ends and three R pairs in series must therefore have three link lengths, two distances between adjacent R pairs and the length of the Pa link. Kinematic chains with the Pa pair in the middle only need two link lengths, the distance between the adjacent R pairs and the length of the Pa pair. There is nothing to indicate that having more link lengths is kinematically or

dynamically beneficial to the mechanism, so the kinematic chains with fewer link lengths are preferred. Fewer link lengths results in simpler kinematics, and often leads to a lower cost lighter weight mechanism. Eliminating the kinematic orderings with Pa pairs at the ends leaves the two kinematic orderings illustrated in Figure 4.3. Note that they are the reverse of each other. The top kinematic pair is connected to the base while the bottom pair is connected to the moving platform.

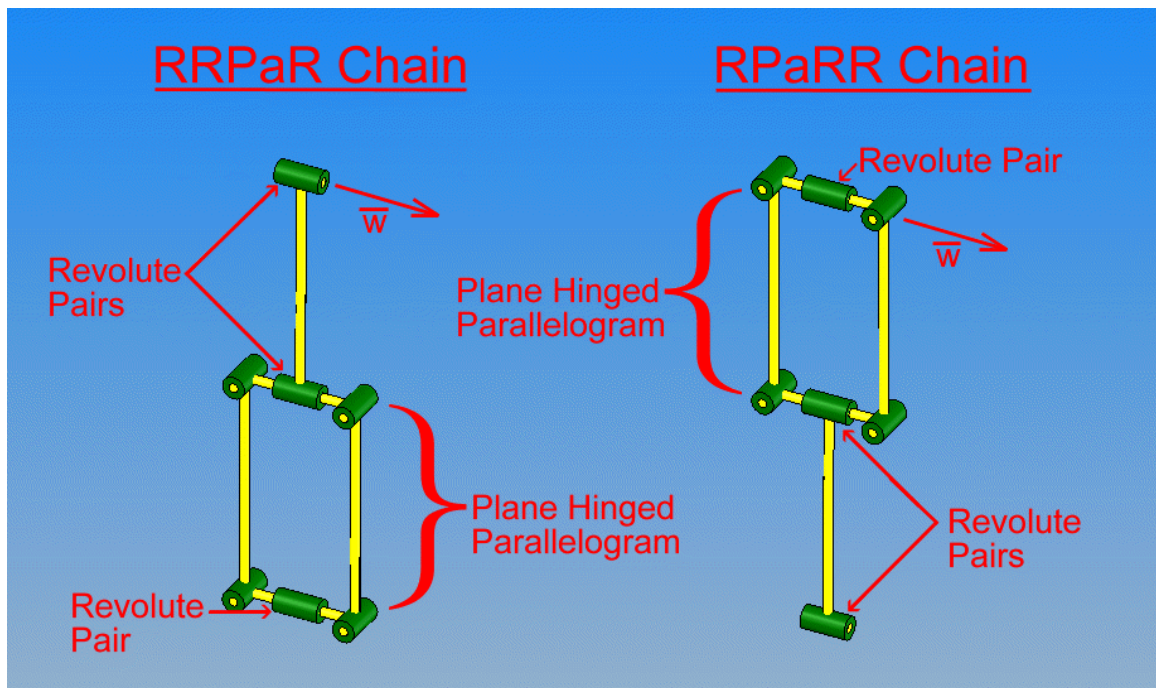


Figure 4.3: RRPaR and RPaRR kinematic chains.

The RRPaR kinematic chain is chosen for two reasons, geometric concerns and past successes of similar structures. The base of the mechanism has motors and structural elements to fix it in space, while the moving platform does not have these geometrically

constraining items. Because of the actuators and support structure that must be attached to the base it is anticipated that the geometry constraints at the base are more demanding than those at the moving platform. If the R end of the RRPaR chain is attached to the base there is less chance of the chain interfering with the rest of the robot than if the RPa end of the RPaRR chain is attached to the base. In addition, parallel robots based on the RRPaR kinematic chain, and similar kinematic chains, have been successfully implemented and have been shown to perform well.

Actuation of the parallel mechanism must now be considered. Connecting in parallel two RRPaR $\{X(w)\}$ motion generating kinematic chains results in a mechanism with three translational degrees of freedom (Figure 4.4). To control the moving platform three kinematic pairs must be actuated. Choosing the first two is easy. The revolute pairs connecting the two arms of the mechanism to the base are actuated. This choice allows the two motors to be rigidly mounted to the base. As a result, the parallel mechanism does not have to lift or move the weight of these motors.

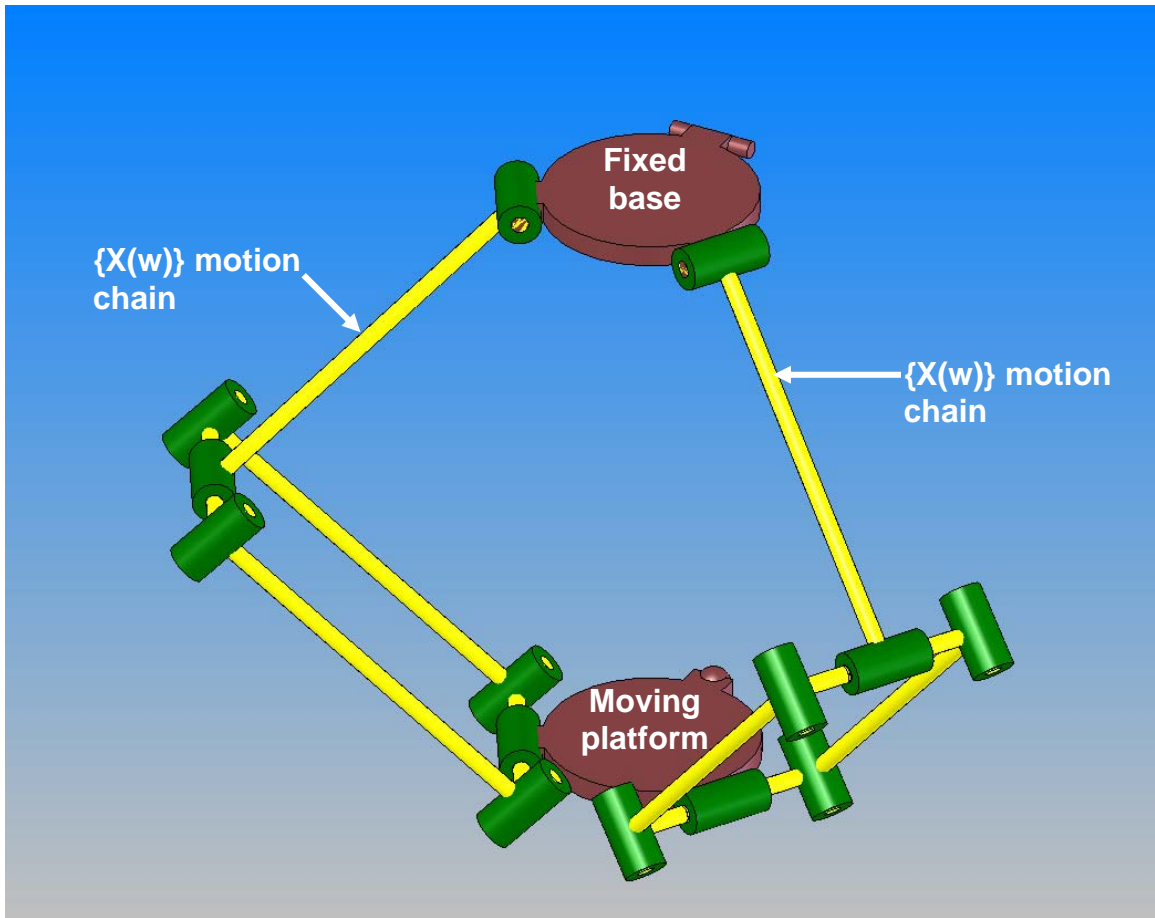


Figure 4.4: Translation-only parallel mechanism with two $\{X(w)\}$ chains.

For the last degree of freedom a third kinematic pair must be actuated. There are two ways to go about this. One of the kinematic pairs that are not adjacent to the base can be actuated, or a third kinematic chain can be added to the robot and the kinematic pair connecting that chain to the base can be actuated. The second solution has two major advantages for this application, the considerable weight of the washdown duty motor can be fixed to the base, and the structure of one of the RRPaR kinematic chains does not have to be built to accommodate the size and weight of the motor. Washdown duty motors are larger and heavier than many motors commonly used in robotics. An

investigation of washdown duty motors on the market indicates that a typical washdown duty motor and a gearbox for this robot would likely weigh between 50 lb and 100 lb, measure 7 in diameter and be 15 in to 20 in long. When only the base end of the RRPaR kinematic chains are actuated the construction of the RRPaR chain can be simple and lightweight. If the chain must be built to carry a washdown duty motor actuating one of the other kinematic pairs it is anticipated that the RRPaR chain would need to be much heavier and the construction would need to be much more complex. To allow all actuators to be attached to the base a third kinematic chain is added to the parallel mechanism.

In many translation only parallel mechanisms three identical $\{X(w)\}$ motion generating kinematic chains are used, however the third kinematic chain is unnecessary for motion constraint. The first two $\{X(w)\}$ generating kinematic chains constrain the moving platform to translate without rotating. A simpler alternative to the use of three $\{X(w)\}$ motion generating chains is the use of two $\{X(w)\}$ generating chains and a single $\{D\}$ (all displacements) generating chain (Figure 4.5 and Figure 4.6). By using a $\{D\}$ generating chain instead of an $\{X(w)\}$ generating chain the construction of the parallel mechanism is simplified and as long as all three chains have the same translational workspace the kinematic analysis is the same for each arm of the mechanism. Figure 4.5 shows a sketch of a $\{D\}$ generating chain and a $\{X(w)\}$ generating chain that have the same translational workspace. In the illustration d_1 and d_2 are unspecified distances. The $\{D\}$ generating chain is a RUS kinematic chain where U indicates a universal joint, and S indicates a ball joint. Note that the $\{D\}$ chain is structurally simpler than the $\{X(w)\}$ chain.

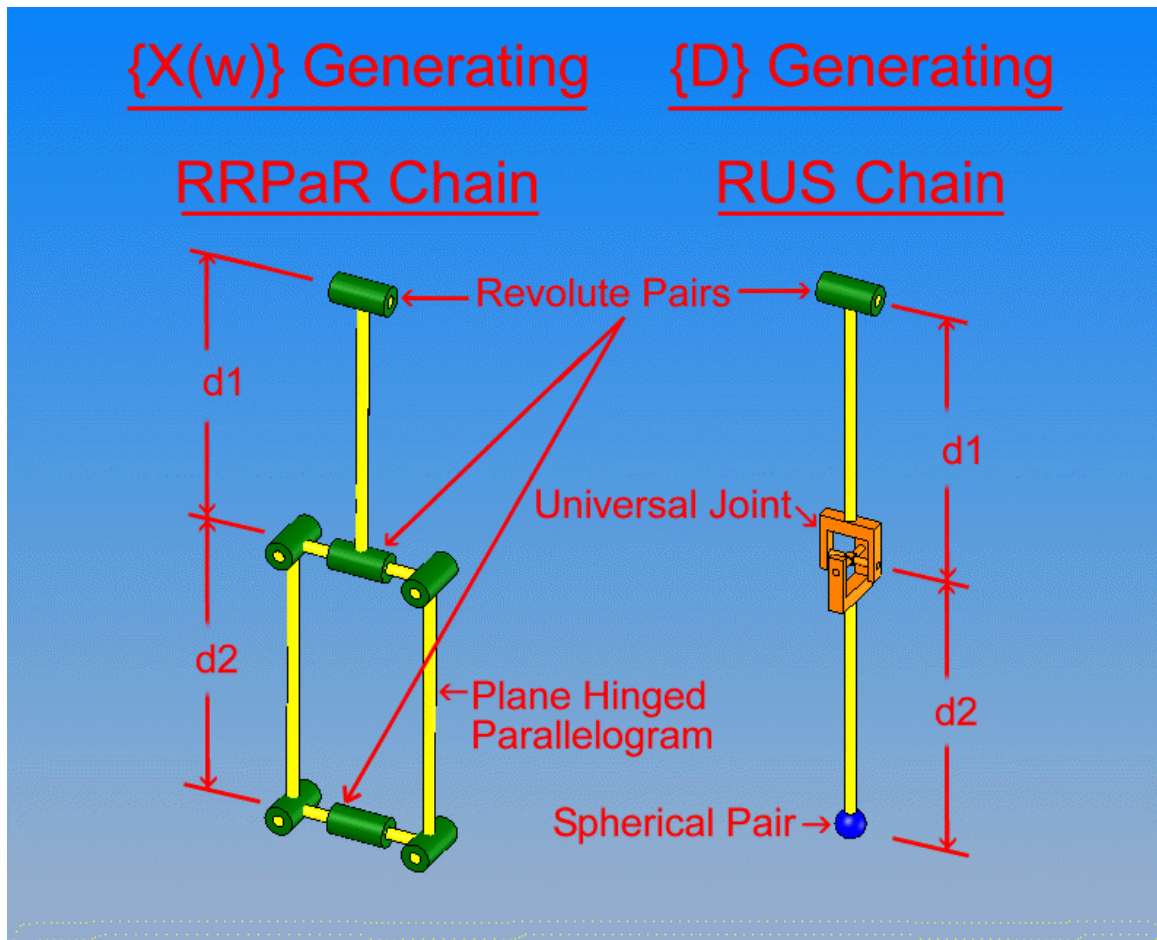


Figure 4.5: $\{X(w)\}$ and $\{D\}$ generating chains with same translational workspaces.

If the ends of these kinematic chains are constrained to prevent rotation then the chains are kinematically identical. Using a $\{D\}$ generating chain in stead of a third $\{X(w)\}$ generating chain reduces the complexity of the robot, likely reduces the cost of the robot and reduces the number of redundant constraints on the moving platform. Whenever a mechanism is constrained redundantly there is the potential for the constraining elements to be misaligned and for them to generate internal loads on the

system. These internal loads are a result of the redundant constraints resisting each other. A $\{D\}$ generating chain does not provide any rotational constraints to the moving platform. Figure 4.6 shows the translation only parallel mechanism that is used to provide the translation for the WOG hanging task. The kinematic equations of this mechanism are the same as those for the Delta robot [28] but they are derived in the following sections for completeness.

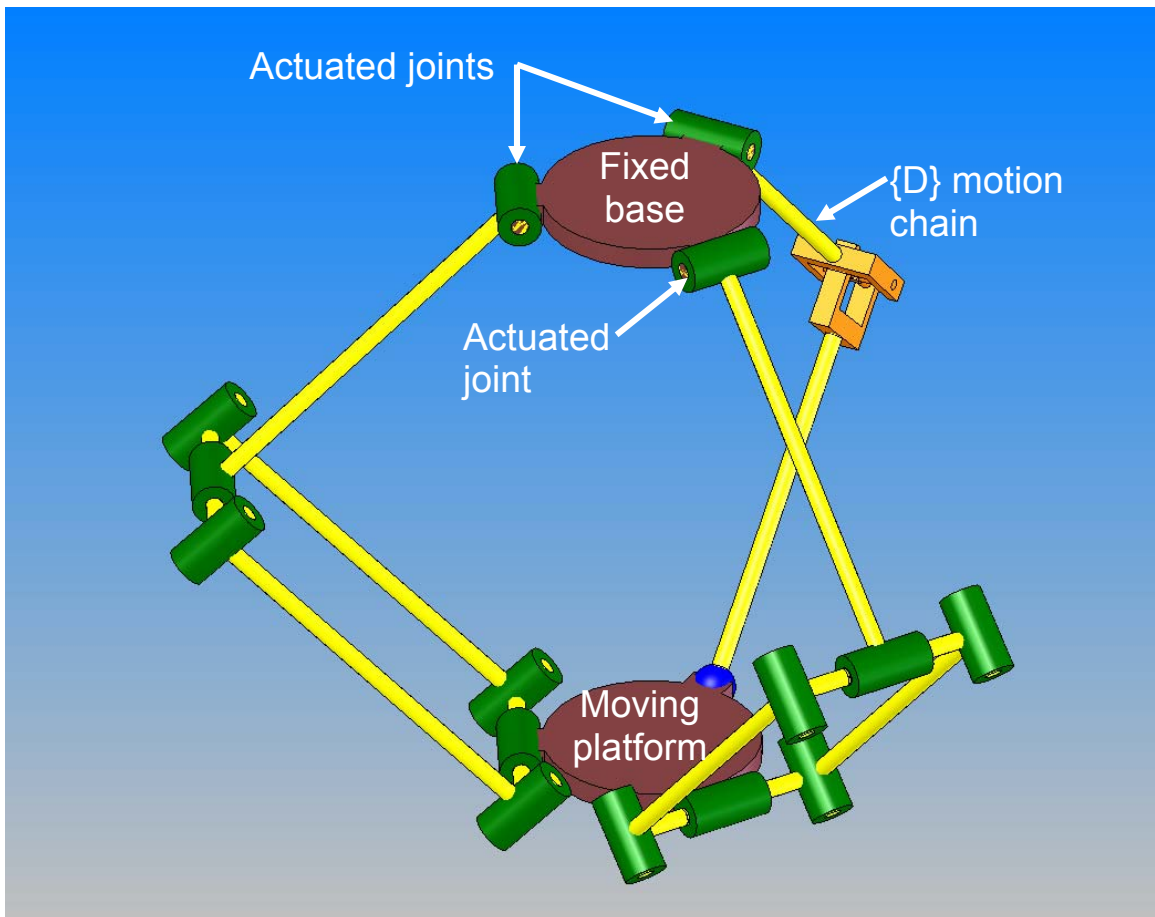


Figure 4.6: Parallel mechanism.

4.2.2 Reverse Kinematics

The reverse kinematics are the equations that map the position of the moving platform to the angles of the actuators. For this analysis the position of the moving platform is specified, and the angles of the actuated revolute joints are to be found. The inverse kinematics are generally easier to determine than the forward kinematics for a parallel mechanism because in the reverse kinematic analysis each leg of the robot can be analyzed independently. The solution to the reverse kinematic equations is generally not unique. It will be shown that for this parallel mechanism each given end effector position corresponds to two possible positions for each arm of the mechanism.

Figure 4.7 and Figure 4.8 show the i th leg of the parallel mechanism. The single leg figures in this chapter illustrate the i th leg as a RRPaR $\{X(w)\}$ chain, but the kinematic equations are the same whether the i th leg is one of the $X\{w\}$ chains or the $\{D\}$ chain. All points labeled in Figure 4.7 and Figure 4.8 are at the centers of a joint or the center of a platform. In Figure 4.7 \overline{OE} , the vector from the center of the base to the center of the moving platform, is specified and θ_{i_i} , the angle of the actuator of the i th arm of the parallel mechanism, is to be determined. To simplify the reverse kinematic equations for the i th arm of the parallel mechanism they are expressed in the local $X_{i_i}Y_{i_i}Z_{i_i}$ coordinate frame. The relationship between the global coordinate frame and the local $X_{i_i}Y_{i_i}Z_{i_i}$ coordinate frames is illustrated in Figure 4.9.

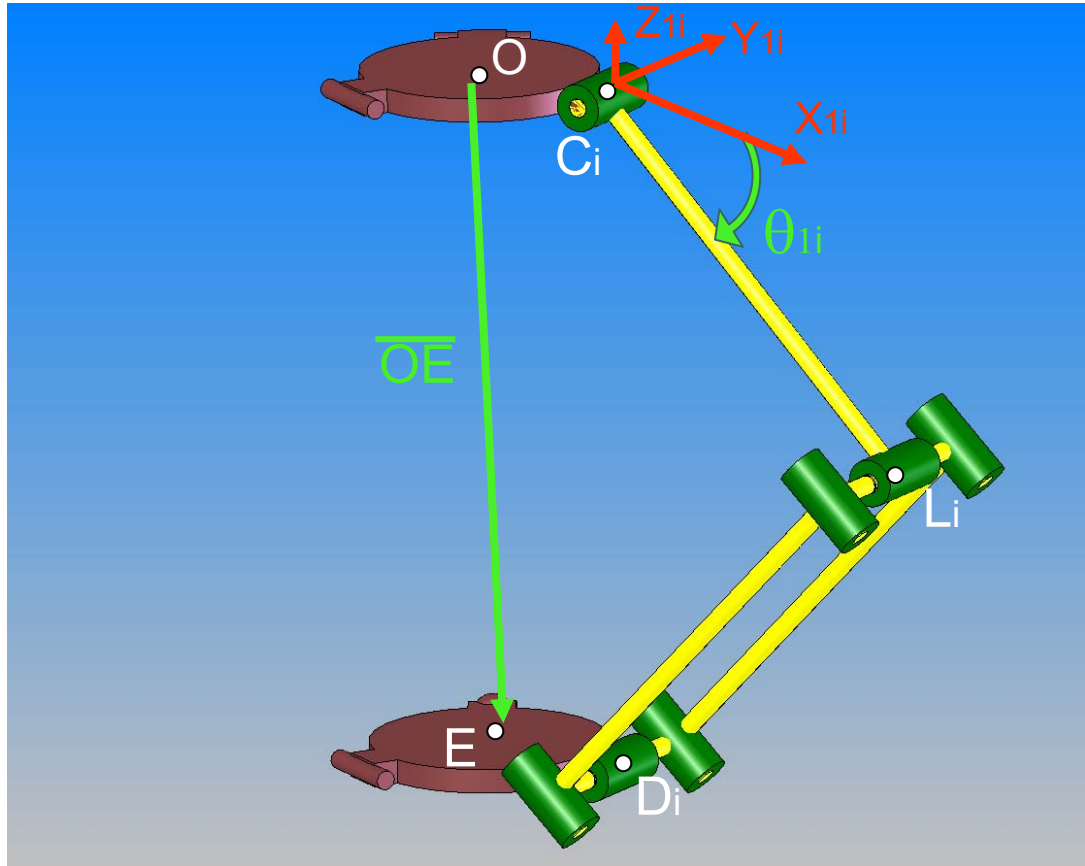


Figure 4.7: Single leg of the parallel mechanism.

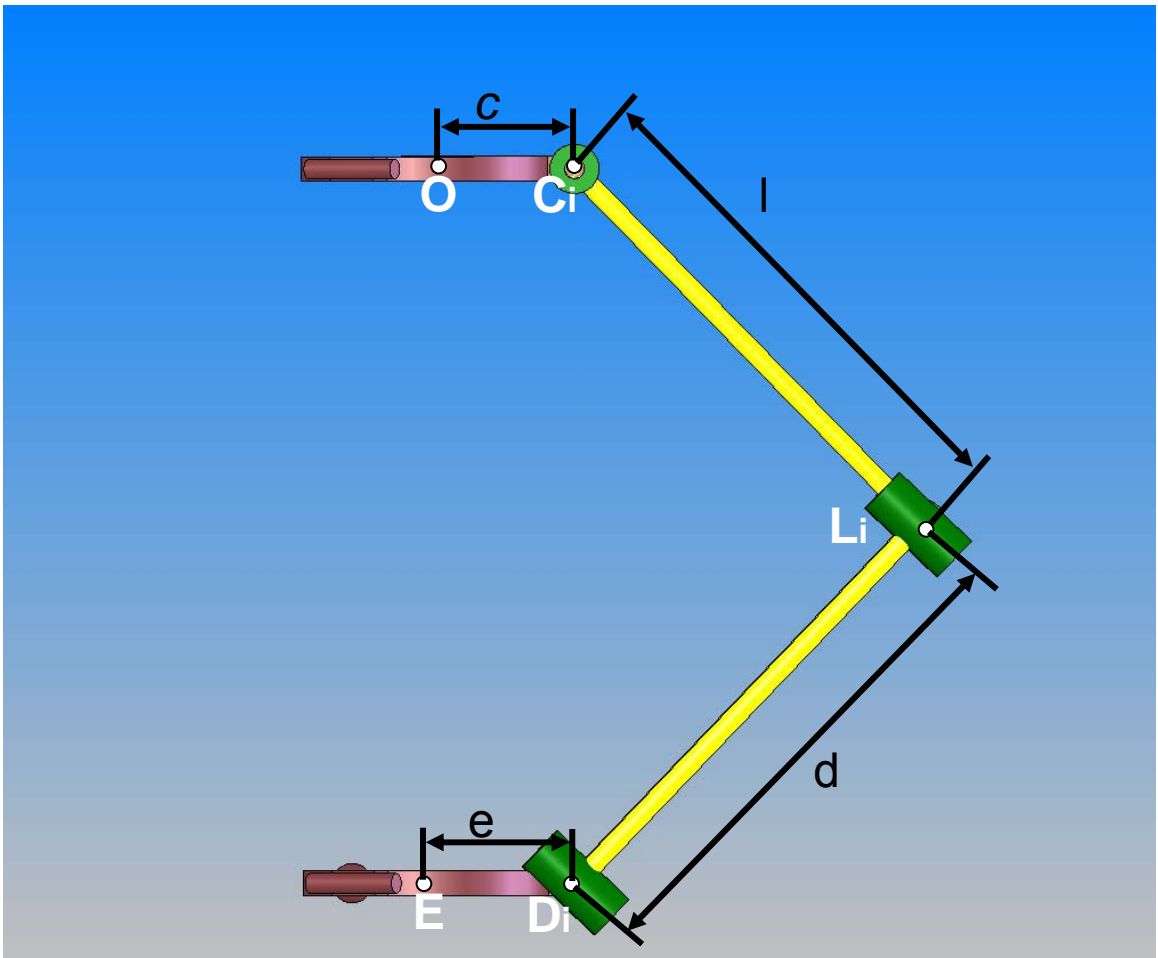


Figure 4.8: Distances between points used in the reverse kinematics.

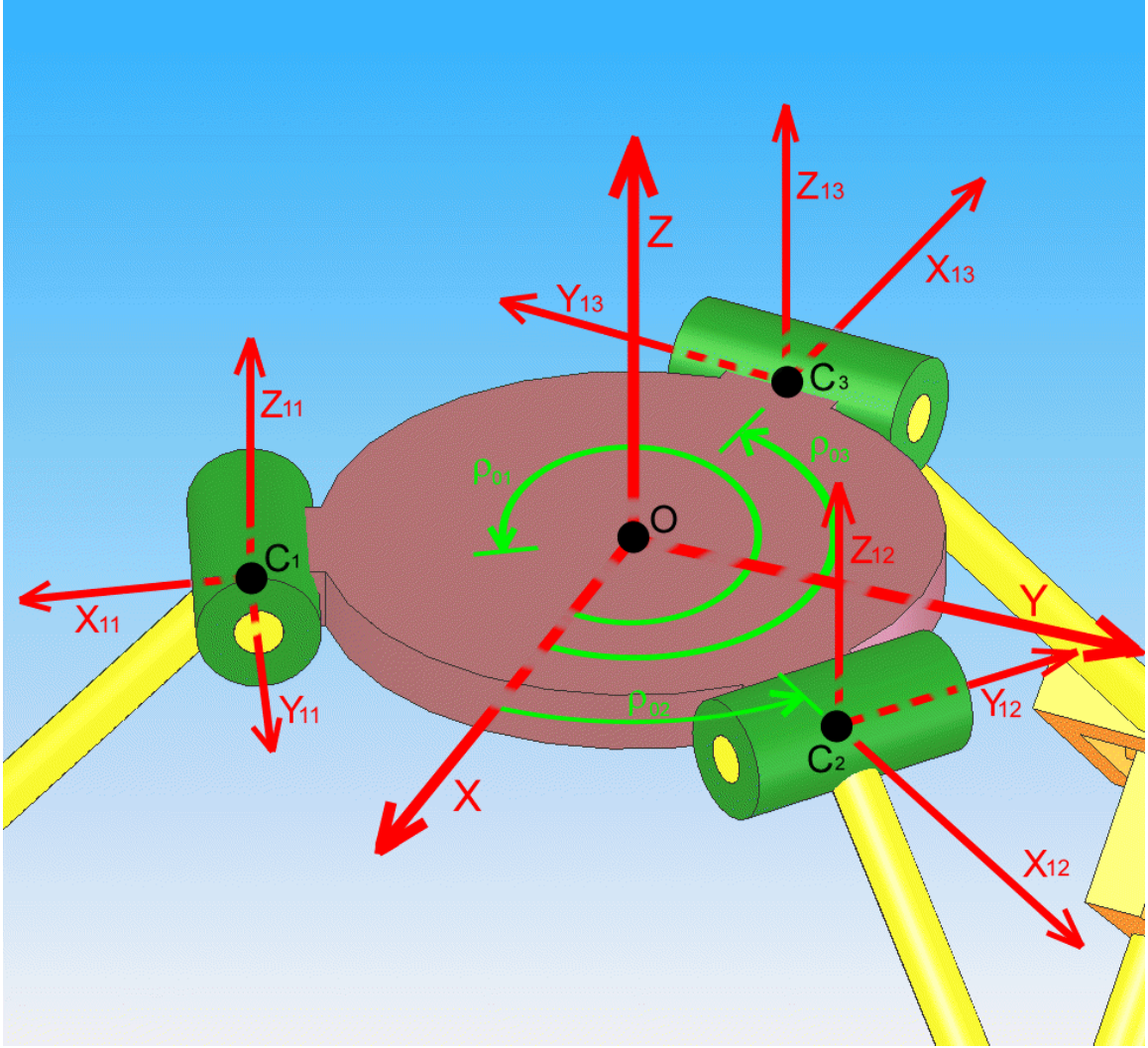


Figure 4.9: Global coordinate frame and $X_i Y_i Z_i$ coordinate frames.

Let $\overline{OE} = [ex \ ey \ ez]^T$ (expressed in the local $X_i Y_i Z_i$ coordinate frame). It is known that the vector from the center of the base to the actuated joint at the top of the i th arm is $\overline{OC_i} = [c \ 0 \ 0]^T$. Since the moving platform is constrained from rotating it is also known that the vector from the joint at the bottom of the i th arm to the center of the moving platform is $\overline{D_i E} = [-e \ 0 \ 0]^T$. The vector $\overline{L_i D_i}$ is unknown, but point L_i is constrained by the lower link of the i th arm to lie on a sphere of radius d centered at point

D_i (Figure 4.10). The vector $\overline{C_i L_i}$ is also unknown but point L_i is constrained by the upper link of the i th arm to lie on a circle of radius l lying in the $X_{1i}Z_{1i}$ plane and centered at point C_i . The two solutions to the reverse kinematics of the i th arm correspond to the two possible positions of L_i , the two intersections of the sphere and circle. Though $\overline{C_i L_i}$ is unknown it can be expressed as a function of the unknown θ_{1i} :

$$\overline{C_i L_i} = l \begin{bmatrix} \cos(\theta_{1i}) \\ 0 \\ -\sin(\theta_{1i}) \end{bmatrix} \quad (4.3)$$

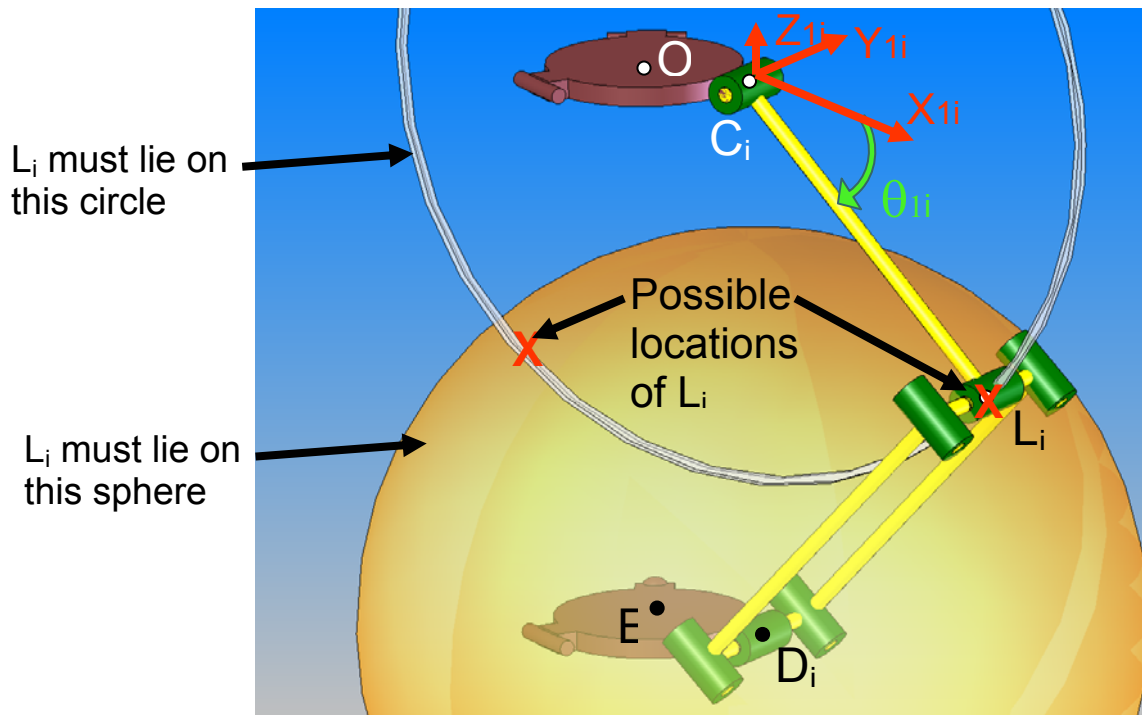


Figure 4.10: Constraints on the location of L_i .

Tracing a path from point O to point E via the i th arm it can be seen that:

$$\overline{OE} = \overline{OC}_i + \overline{C}_i\overline{L}_i + \overline{L}_i\overline{D}_i + \overline{D}_i\overline{E} \quad (4.2)$$

Solving for $\overline{L}_i\overline{D}_i$ then expressing the other vectors in terms of known quantities or θ_i yields:

$$\overline{L}_i\overline{D}_i = \begin{bmatrix} ex - c + e - l \cos(\theta_i) \\ ey \\ ez + l \sin(\theta_i) \end{bmatrix} \quad (4.3)$$

The distance from L_i to D_i is known to be d so:

$$\|\overline{LD}_i\|^2 = d^2 = -2l(ex - c + e)\cos(\theta_i) + 2lez\sin(\theta_i) + l^2 + (ex - c + e)^2 + ey^2 + ez^2 \quad (4.4)$$

Let $u = -2l(ex - c + e)$, $v = 2lez$, and $w = l^2 + (ex - c + e)^2 + ey^2 + ez^2$. Equation (4.4)

then becomes:

$$d^2 = u \cos(\theta_i) + v \sin(\theta_i) + w \quad (4.5)$$

Dividing equation (4.5) by $(u^2 + v^2)^{1/2}$ and applying the identity $\cos(\alpha - \beta) = \cos(\alpha)\cos(\beta) + \sin(\alpha)\sin(\beta)$ yields:

$$\cos(\theta_{li} - \gamma) = \frac{w}{(u^2 + v^2)^{1/2}} \quad (4.6)$$

Where:

$$\cos(\gamma) = \frac{u}{(u^2 + v^2)^{1/2}}, \quad \sin(\gamma) = \frac{v}{(u^2 + v^2)^{1/2}} \quad (4.7)$$

Since $(\cos(\theta_{li} - \gamma))^2 + (\sin(\theta_{li} - \gamma))^2 = 1$:

$$\sin(\theta_{li} - \gamma) = \pm \frac{(u^2 + v^2 - w^2)^{1/2}}{(u^2 + v^2)^{1/2}} \quad (4.8)$$

Equations (4.7) reveal angle γ to be single valued. Equations (4.6) and (4.8) reveal the quantity $(\theta_{li} - \gamma)$ to be double valued. As a result, θ_{li} must be double valued. Let θ_{li}^\pm represent the pair of possible θ_{li} angles where the upper and lower sign correspond to the upper and lower sign in equation (4.8). Once again applying the identity $\cos(\alpha - \beta) = \cos(\alpha)\cos(\beta) + \sin(\alpha)\sin(\beta)$ it can be seen that:

$$\cos(\theta_{li}^\pm) = \cos((\theta_{li}^\pm - \gamma) - (-\gamma)) = \cos(\theta_{li}^\pm - \gamma)\cos(\gamma) - \sin(\theta_{li}^\pm - \gamma)\sin(\gamma) \quad (4.9)$$

Substituting equations (4.6), (4.7) and (4.8) into equation (4.9) yields:

$$\cos(\theta_{li}^{\pm}) = \frac{uw \mp v(u^2 + v^2 - w^2)^{1/2}}{(u^2 + v^2)^{1/2}} \quad (4.10)$$

Substituting equation (4.10) into (4.5) yields:

$$\sin(\theta_{li}^{\pm}) = \frac{vw \pm u(u^2 + v^2 - w^2)^{1/2}}{(u^2 + v^2)^{1/2}} \quad (4.11)$$

The function ATAN2 can then be used to find θ_{li}^{\pm} from $\sin(\theta_{li}^{\pm})$ and $\cos(\theta_{li}^{\pm})$. The two solutions for θ_{li}^{\pm} are given by:

$$\theta_{li}^+ = \text{ATAN2}\left(\frac{vw + u(u^2 + v^2 - w^2)^{1/2}}{(u^2 + v^2)^{1/2}}, \frac{uw - v(u^2 + v^2 - w^2)^{1/2}}{(u^2 + v^2)^{1/2}}\right) \quad (4.12)$$

$$\theta_{li}^- = \text{ATAN2}\left(\frac{vw - u(u^2 + v^2 - w^2)^{1/2}}{(u^2 + v^2)^{1/2}}, \frac{uw + v(u^2 + v^2 - w^2)^{1/2}}{(u^2 + v^2)^{1/2}}\right) \quad (4.13)$$

One value of θ_{li}^{\pm} corresponds to the elbow out solution to the reverse kinematics of the i th arm while the other value of θ_{li}^{\pm} corresponds to the elbow in solution (Figure 4.11). Since there are two solutions to the reverse kinematics of each arm there are eight solutions to the reverse kinematics of the parallel mechanism.

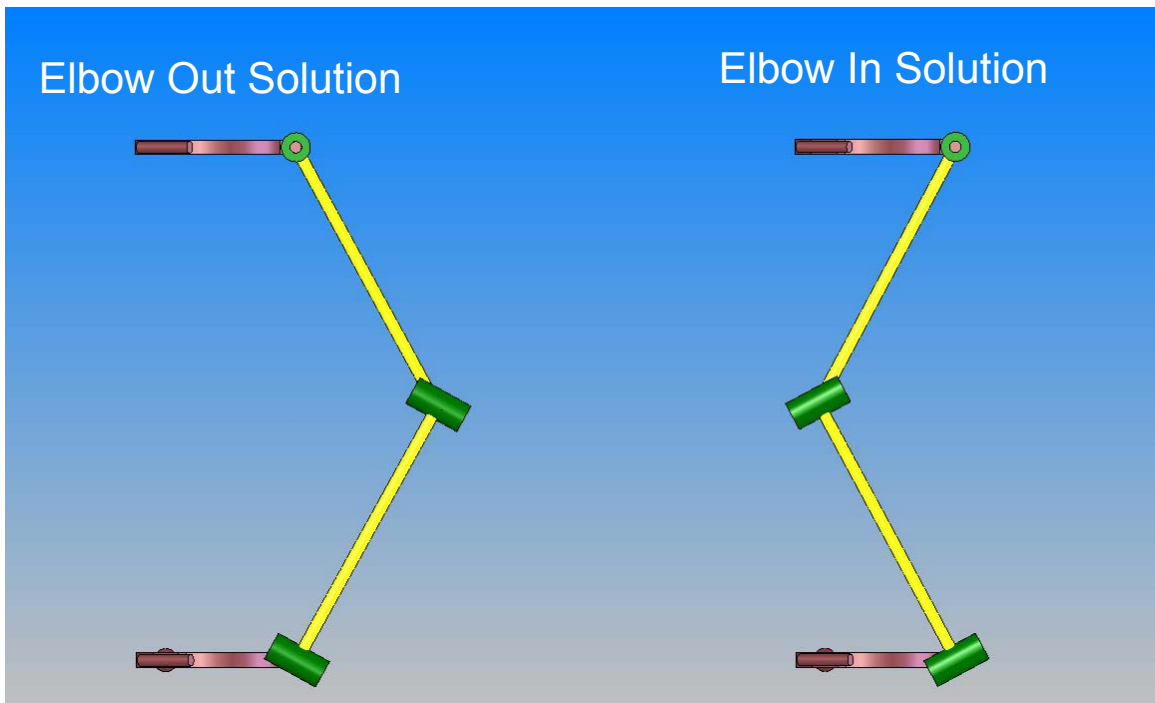


Figure 4.11: Elbow out and elbow in solutions to the reverse kinematics.

4.2.3 Forward Kinematics

The forward kinematics are the equations that map the angles of the actuated joints to the position of the moving platform. For this analysis θ_{11} , θ_{12} , and θ_{13} , the angles of the actuated revolute joints at the top of each arm of the parallel mechanism, are specified and the position of the center of the moving platform (\overline{OE}) is to be determined. Unlike serial kinematic chains the forward kinematic analysis of parallel mechanisms is generally more difficult than the reverse kinematic analysis. The forward kinematic analysis of a parallel mechanism is often very complex because the intersection of the workspaces of all of the kinematic chains must be determined. In general the solution to

the forward kinematic equations is not unique. In this case it will be shown that there are two solutions for the position of the end effector for each set of actuator positions.

Figure 4.7 and Figure 4.8 illustrate the i th arm of the parallel mechanism. The forward kinematic analysis is carried out in the global coordinate frame, not the local $X_{i_i}Y_{i_i}Z_{i_i}$ coordinate frames. Figure 4.9 shows the relationship between the global coordinate frame and the $X_{i_i}Y_{i_i}Z_{i_i}$ coordinate frames. Expressed in the global coordinate frame the vector from the center of the base to the actuated joint at the top of the i th arm is $\overline{OC}_i = [c \cos(\rho_{0i}) \quad c \sin(\rho_{0i}) \quad 0]^T$. Since the moving platform is constrained from rotating it is known that the vector from the joint at the bottom of the i th arm to the center of the moving platform is $\overline{D_iE} = [-e \cos(\rho_{0i}) \quad -e \sin(\rho_{0i}) \quad 0]^T$. The vector from the actuated joint at the top of the i th arm of the parallel mechanism to the elbow of the i th arm is $\overline{C_iL_i} = [l \cos(\theta_{ii}) \cos(\rho_{0i}) \quad l \cos(\theta_{ii}) \sin(\rho_{0i}) \quad -l \sin(\theta_{ii})]$. The vector $\overline{L_iD_i}$ is unknown but the lower link of the i th arm of the parallel mechanism constrains point D_i to lie on a sphere of radius d centered at point L_i (Figure 4.12). Since point E is offset from D_i by the constant vector $\overline{D_iE}$ point E is also constrained to lie on a sphere of radius d . This second sphere is offset from the first by $\overline{D_iE}$ and is therefore centered at point V_i , where V_i is the point offset from L_i by $\overline{D_iE}$ (Figure 4.13). The vector from the center of the base to V_i is:

$$\overline{OV}_i = \overline{OC}_i + \overline{C_iL_i} + \overline{D_iE} = \begin{bmatrix} (c + l \cos(\theta_{ii}) - e) \cos(\rho_{0i}) \\ (c + l \cos(\theta_{ii}) - e) \sin(\rho_{0i}) \\ -l \sin(\theta_{ii}) \end{bmatrix} \quad (4.14)$$

To simplify the forward kinematic equations let this vector be expressed as

$$\overline{OV}_i = [vx_i \quad vy_i \quad vz_i]^T.$$

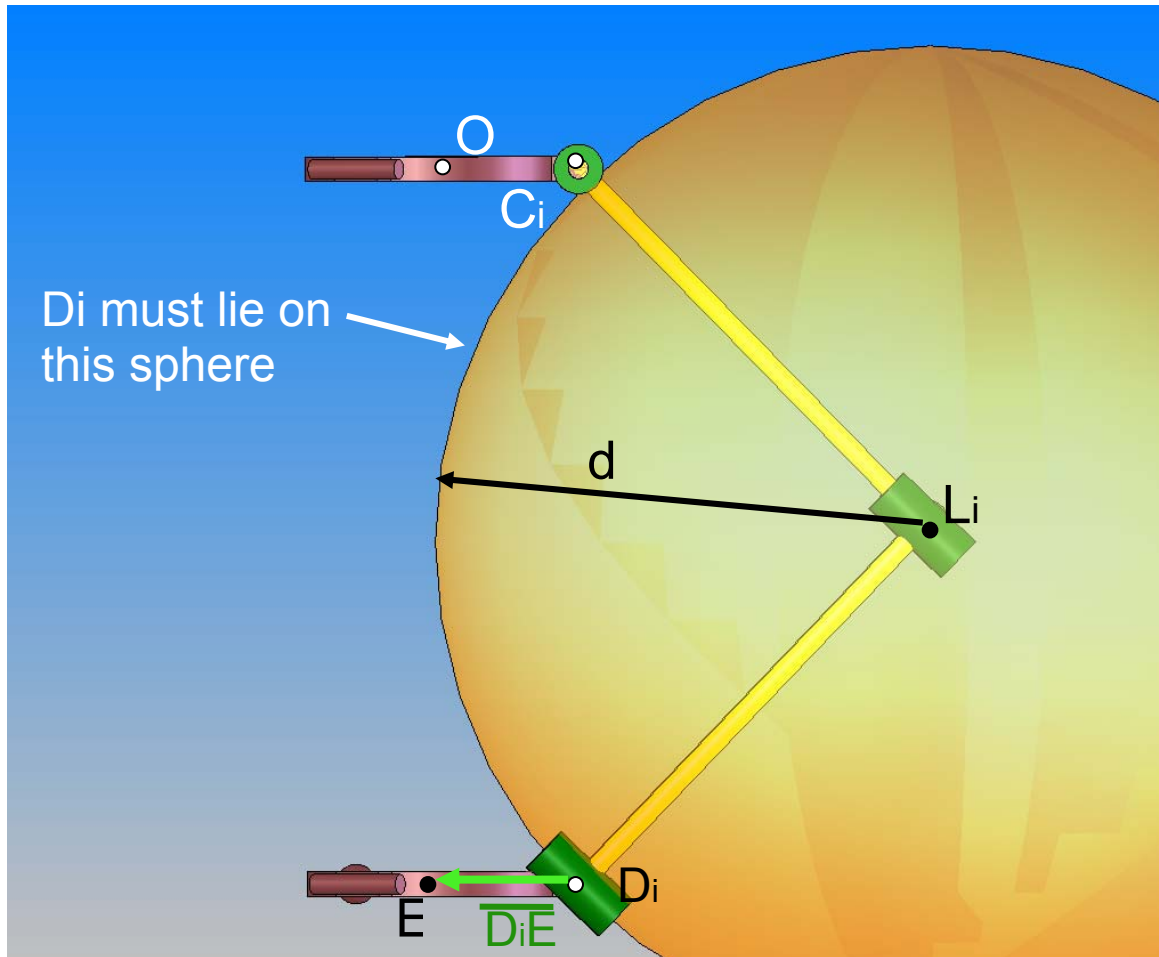


Figure 4.12: Constraint on the position of D_i .

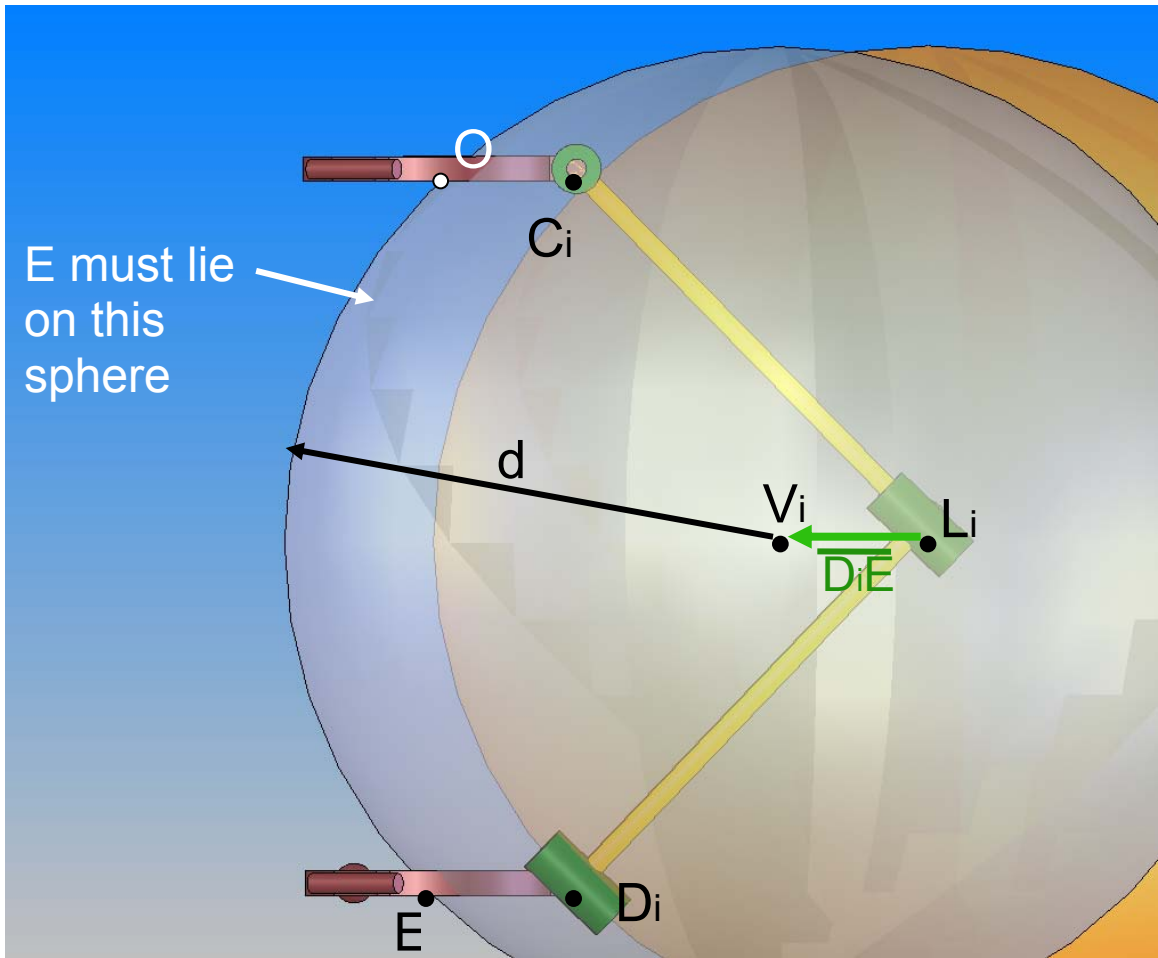


Figure 4.13: Constraint on the position of E .

Let the unknown vector from the center of the base to the center of the moving platform be $\overline{OE} = [E_x \ E_y \ E_z]^T$ (expressed in the global coordinate frame). For point E to lie on a sphere of radius d centered at V_i the following equation must be satisfied:

$$d^2 = (E_x - vx_i)^2 + (E_y - vy_i)^2 + (E_z - vz_i)^2 \quad (4.15)$$

Since the parallel mechanism has three arms E is simultaneously constrained to lie on three spheres of radius d centered at V_1 , V_2 , and V_3 . The following set of equations must therefore be satisfied.

$$d^2 = (Ex - vx_1)^2 + (Ey - vy_1)^2 + (Ez - vz_1)^2 \quad (4.16)$$

$$d^2 = (Ex - vx_2)^2 + (Ey - vy_2)^2 + (Ez - vz_2)^2 \quad (4.17)$$

$$d^2 = (Ex - vx_3)^2 + (Ey - vy_3)^2 + (Ez - vz_3)^2 \quad (4.18)$$

This is a set of three second order equations in three unknowns, x , y and z . This set of equations cannot be solved directly in its current form. If (4.17) is subtracted from (4.16) and (4.18) is subtracted from (4.16) the resulting set of two equations are first order.

$$0 = Ex(vx_1 - vx_2) + Ey(vy_1 - vy_2) + Ez(vz_1 - vz_2) + \frac{vx_2^2 + vy_2^2 + vz_2^2 - vx_1^2 - vy_1^2 - vz_1^2}{2} \quad (4.19)$$

$$0 = Ex(vx_1 - vx_3) + Ey(vy_1 - vy_3) + Ez(vz_1 - vz_3) + \frac{vx_3^2 + vy_3^2 + vz_3^2 - vx_1^2 - vy_1^2 - vz_1^2}{2} \quad (4.19)$$

Solving (4.14) and (4.15) for Ex and Ey it is found that:

$$Ey = Ez * w1 + w2 + vy_1 \quad (4.20)$$

$$Ex = Ez * w3 + w4 + vx_1 \quad (4.21)$$

Where:

$$w1 = \frac{(vz_1 - vz_3)(vx_1 - vx_2) - (vz_1 - vz_2)(vx_1 - vx_3)}{(vy_1 - vy_2)(vx_1 - vx_3) - (vy_1 - vy_3)(vx_1 - vx_2)} \quad (4.22)$$

$$w2 = \frac{(vx_3^2 + vy_3^2 + vz_3^2 - vx_1^2 - vy_1^2 - vz_1^2)(vx_1 - vx_2) - (vx_2 + vy_2 + vz_2 - vx_1 - vy_1 - vz_1)(vx_1 - vx_3)}{(vy_1 - vy_2)(vx_1 - vx_3) - (vy_1 - vy_3)(vx_1 - vx_2)} - vy_1 \quad (4.23)$$

$$w3 = \frac{(vz_1 - vz_3)(vy_1 - vy_2) - (vz_1 - vz_2)(vy_1 - vy_3)}{(vx_1 - vx_2)(vy_1 - vy_3) - (vx_1 - vx_3)(vy_1 - vy_2)} \quad (4.24)$$

$$w4 = \frac{(vx_3^2 + vy_3^2 + vz_3^2 - vx_1^2 - vy_1^2 - vz_1^2)(vy_1 - vy_2) - (vx_2 + vy_2 + vz_2 - vx_1 - vy_1 - vz_1)(vy_1 - vy_3)}{(vx_1 - vx_2)(vy_1 - vy_3) - (vx_1 - vx_3)(vy_1 - vy_2)} - vx_1 \quad (4.25)$$

Substituting (4.20) and (4.21) into (4.16) leads to

$$0 = Ez^2(1 + w1^2 + w3^2) + Ez * 2(w1 * w2 + w3 * w4 + vz1) + w2^2 + w4^2 + vz1^2 \quad (4.26)$$

Solving for Ez it is found that

$$Ez = \frac{vz_1 - w1 * w2 - w3 * w4 \pm \sqrt{(w1 * w2 + w3 * w4 - vz_1)^2 - (1 + w1^2 + w3^2)(w2^2 + w4^2 + vz_1^2)}}{1 + w1^2 + w3^2} \quad (4.27)$$

Once Ez is determined it is substituted into (4.20) and (4.21) to determine Ex and Ey . Note that there are two solutions for Ez . Geometrically this corresponds to the two intersection points of the three spheres (Figure 4.14). The two solutions to the forward kinematic equations can be thought of as the platform-up solution and the platform down solution. These solutions are illustrated in Figure 4.15. The higher solution shown in

Figure 4.15 corresponds to the Ez value found by adding the quantity under the square root in (4.18).

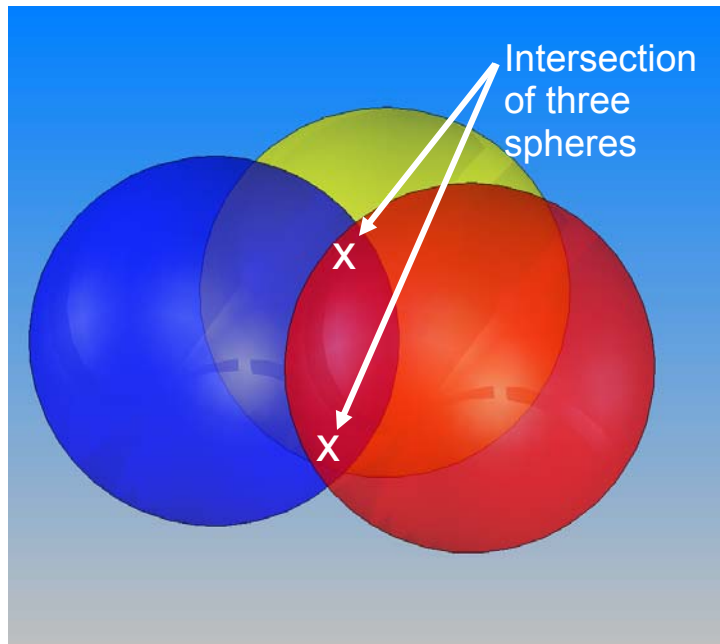


Figure 4.14: Intersection of three spheres.

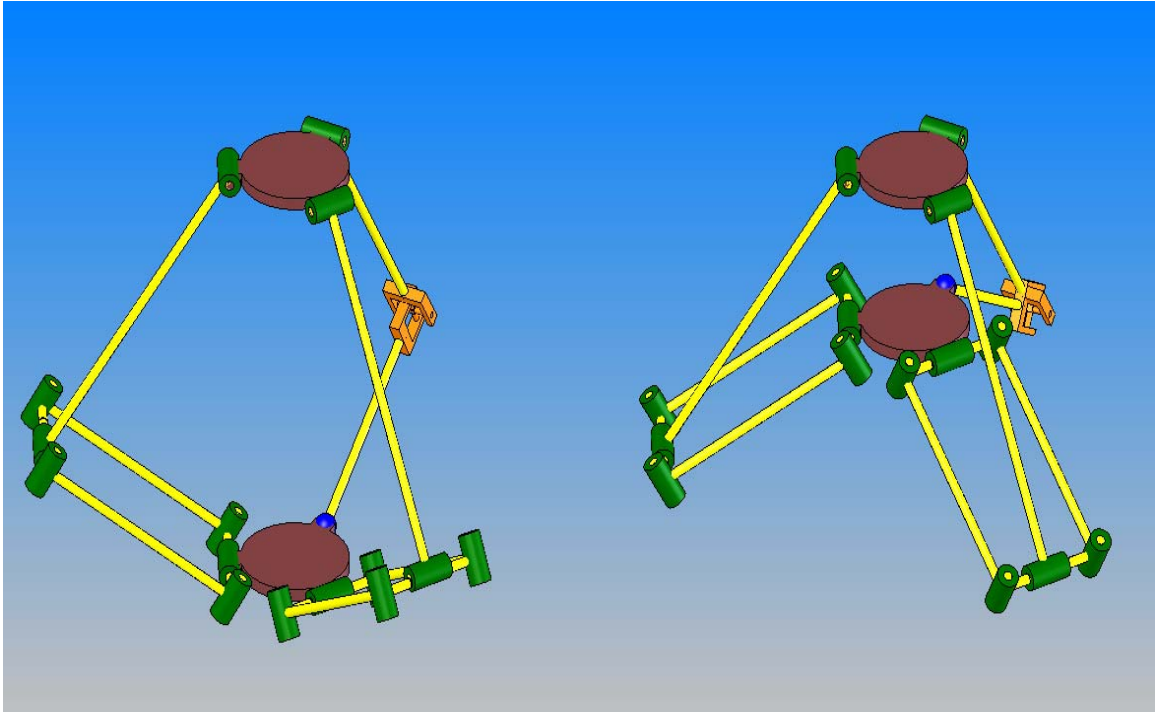


Figure 4.15: Platform up and platform down solutions to the forward kinematics.

4.2.4 Angles of Passive Joints of the Parallel Mechanism

In this section the equations for the angles of the passive joints of the parallel mechanism are determined. The joint angles of the i th arm are shown in Figure 4.16 and Figure 4.17. All angles except θ_{1i} correspond to passive joints. The angles θ_{1i} , θ_{2i} , and θ_{4i} are about axes parallel to the Y_{1i} axis, while ρ_{3i} is about the Z_{3i} axis. If either the set of actuator angles (θ_{11} , θ_{12} , and θ_{13}) or the position of the moving platform \overline{OE} are known the kinematic equations of the parallel mechanism can be used to determine the other. Once both are known the passive joint angles can be determined.

Figure 4.7 shows the points on the i th leg of the parallel mechanism that will be referred to in this analysis. Figure 4.8 shows the distance between these points. Expressed in the local $X_{i_i}Y_{i_i}Z_{i_i}$ coordinate frame the vector from the center of the base to the actuated joint at the top of the i th arm is $\overline{OC}_i = [c \ 0 \ 0]^T$, the vector from that joint to the elbow of the i th arm is $\overline{C}_iL_i = [l \cos(\theta_{1_i}) \ 0 \ -l \sin(\theta_{1_i})]^T$, the vector from there to the joint at the bottom of the i th arm is $\overline{L}_iD_i = [d \cos(\theta_{1_i} + \theta_{2_i}) \cos(\rho_{3_i}) \ d \sin(\rho_{3_i}) \ -d \sin(\theta_{1_i} + \theta_{2_i}) \cos(\rho_{3_i})]^T$, and the vector from there to the center of the moving platform is $\overline{D}_iE = [-e \ 0 \ 0]^T$. Let $\overline{OE} = [ex \ ey \ ez]^T$ (expressed in the local $X_{i_i}Y_{i_i}Z_{i_i}$ coordinate frame). Substituting into the loop equation:

$$\overline{OE} = \overline{OC}_i + \overline{C}_iL_i + \overline{L}_iD_i + \overline{D}_iE \quad (4.28)$$

It can be seen that:

$$\overline{OE} = \begin{bmatrix} ex \\ ey \\ ez \end{bmatrix} = \begin{bmatrix} c + l \cos(\theta_{1_i}) + d \cos(\theta_{1_i} + \theta_{2_i}) \cos(\rho_{3_i}) - e \\ d \sin(\rho_{3_i}) \\ -l \sin(\theta_{1_i}) - d \sin(\theta_{1_i} + \theta_{2_i}) \cos(\rho_{3_i}) \end{bmatrix} \quad (4.29)$$

Solving the second row of (4.29) for ρ_{3_i} :

$$\rho_{3_i} = \arcsin(ey / d) \quad (4.30)$$

Solving the first and third rows for $d \cos(\rho_{3i}) \cos(\theta_{1i} + \theta_{2i})$ and $d \cos(\rho_{3i}) \sin(\theta_{1i} + \theta_{2i})$ respectively:

$$d \cos(\rho_{3i}) \cos(\theta_{1i} + \theta_{2i}) = ex - c - l \cos(\theta_{1i}) + e \quad (4.31)$$

$$d \cos(\rho_{3i}) \sin(\theta_{1i} + \theta_{2i}) = ez + l \sin(\theta_{1i}) \quad (4.32)$$

The ATAN2 function can then be used to solve for $(\theta_{1i} + \theta_{2i})$:

$$(\theta_{1i} + \theta_{2i}) = \text{ATAN2}(ez + l \sin(\theta_{1i}), ex - c - l \cos(\theta_{1i}) + e) \quad (4.33)$$

and θ_{2i} is given by:

$$\theta_{2i} = \text{ATAN2}(ez + l \sin(\theta_{1i}), ex - c - l \cos(\theta_{1i}) + e) - \theta_{1i} \quad (4.34)$$

Since the moving platform is parallel to the base the following equation must be satisfied:

$$\theta_{1i} + \theta_{2i} + \theta_{4i} = 180^\circ \quad (4.35)$$

so θ_{4i} is given by:

$$\theta_{4i} = 180^\circ - \theta_{1i} - \theta_{2i} \quad (4.36)$$

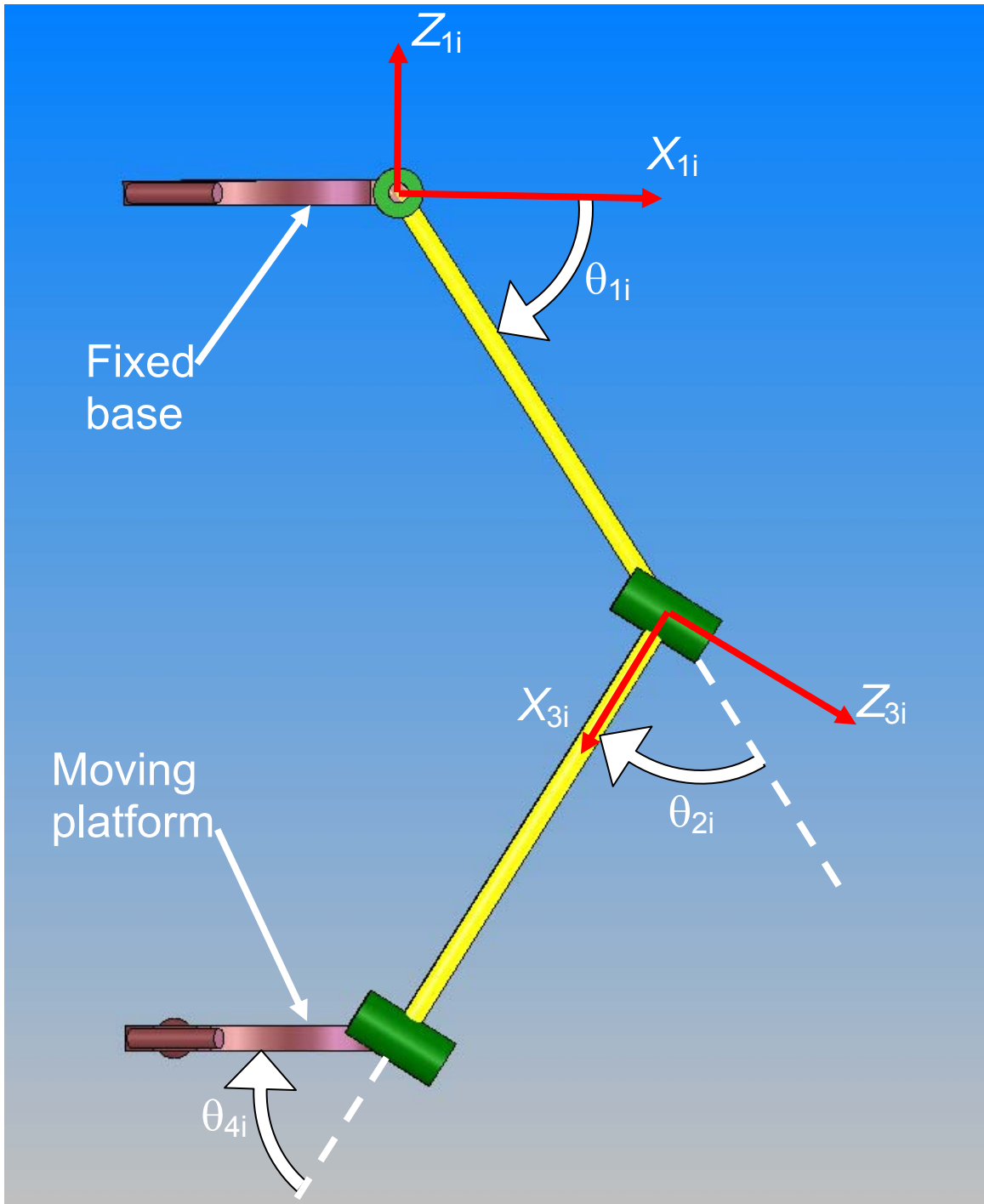


Figure 4.16: Angles of the joints of the i th leg (viewed along Y_{1i})

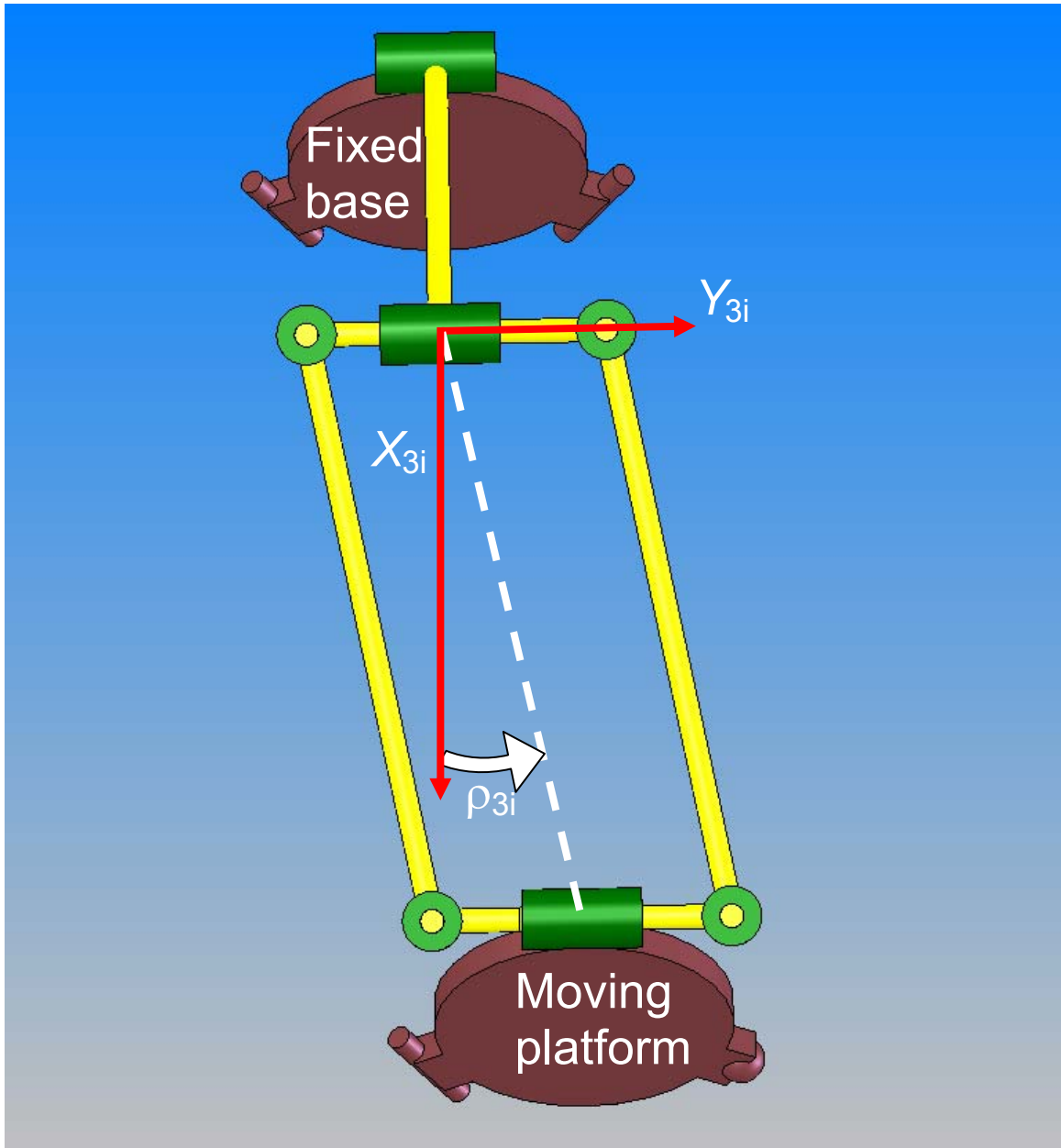


Figure 4.17: Angles of the joints of the i th leg (viewed along Z_{3i})

4.3 Overview of Specialized End Effector Design

At this point the design of the robot must be coordinated with the specialized end effector. Figure 4.18 is a CAD rendering of the specialized end effector that was developed by Christoph Coquemond [26] and Olivier Celton [27] for picking up WOGs, securely transporting them and releasing them onto shackles. Figure 4.19 shows the specialized end effector in operation. It has successfully grasped a WOG lying in the breast-up position and is transferring the WOG to the stationary shackle in the upper right hand corner of the figure. The end effector is actuated by a linear pneumatic actuator, which can be seen cut away near the top of Figure 4.18. The pneumatic actuator causes the arms on both sides of the end effector to rotate about the pivot pins. To capture a WOG the pneumatic cylinder pulls in on the tops of the arms, forcing the lower parts of the arms to rotate outward. The end effector is then positioned such that the upright is between the legs of the WOG and the arms are near the points where the legs of the WOG are connected to the torso. The pneumatic cylinder then pushes out on the tops of the arms, which causes the lower parts of the arms to rotate inward and grasp the WOG.

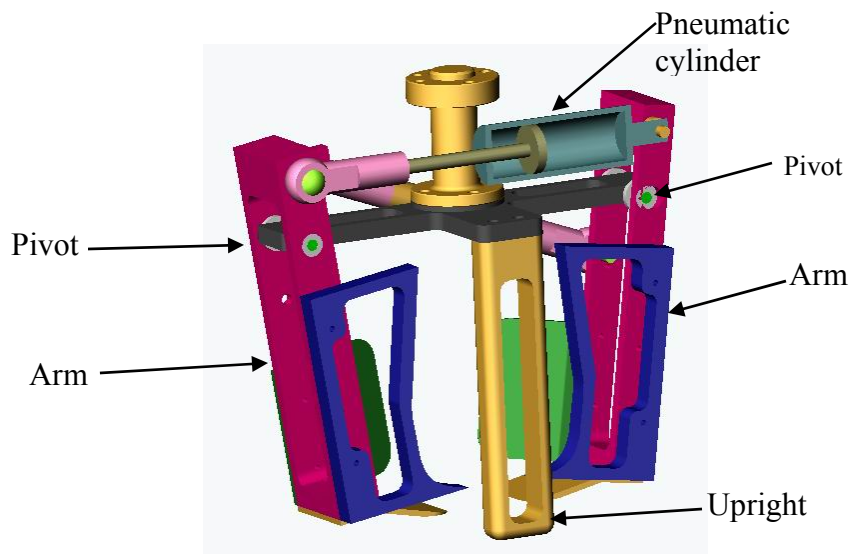


Figure 4.18: CAD rendering of specialized end effector.

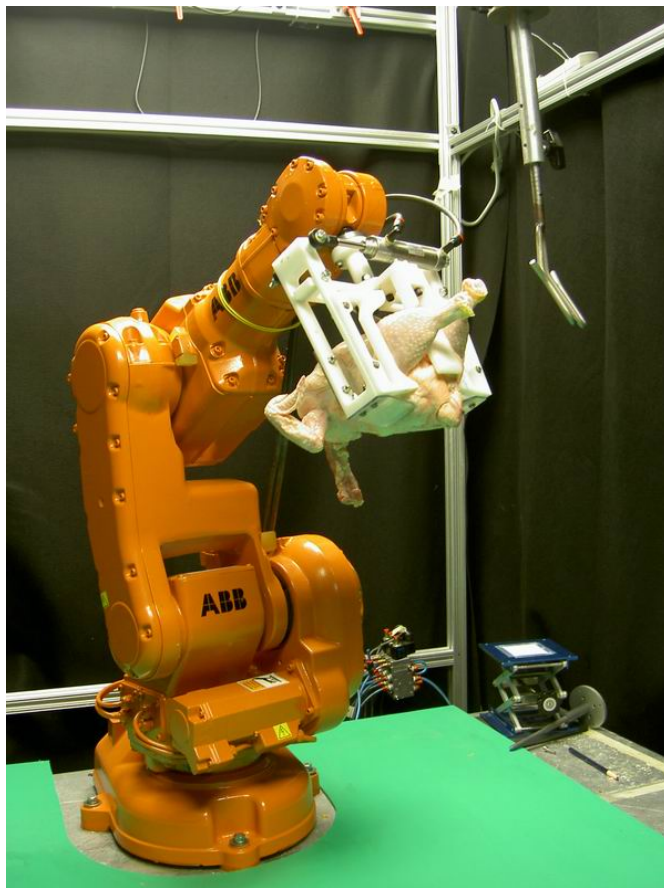


Figure 4.19: Specialized end effector in operation.

Testing showed this end effector can grasp and secure WOGs of various sizes in both the breast up position and the breast down position [26] [27]. When the WOGs are acquired in the breast up position they can be successfully released into the shackles by placing the ends of the legs of the WOG into the shackles, then opening the end effector (Figure 4.20). The body of the WOG simply falls out of the end effector. When a WOG is acquired in the breast down position it must be flipped over before the legs of the WOG can be placed in the shackle. As a result, the end effector and part of the robot are beneath the WOG (Figure 4.21). In this case the WOG can be successfully released if the end effector is opened, then the end effector is rotated down and towards the shackle about a fixed axis parallel to the shackle line.

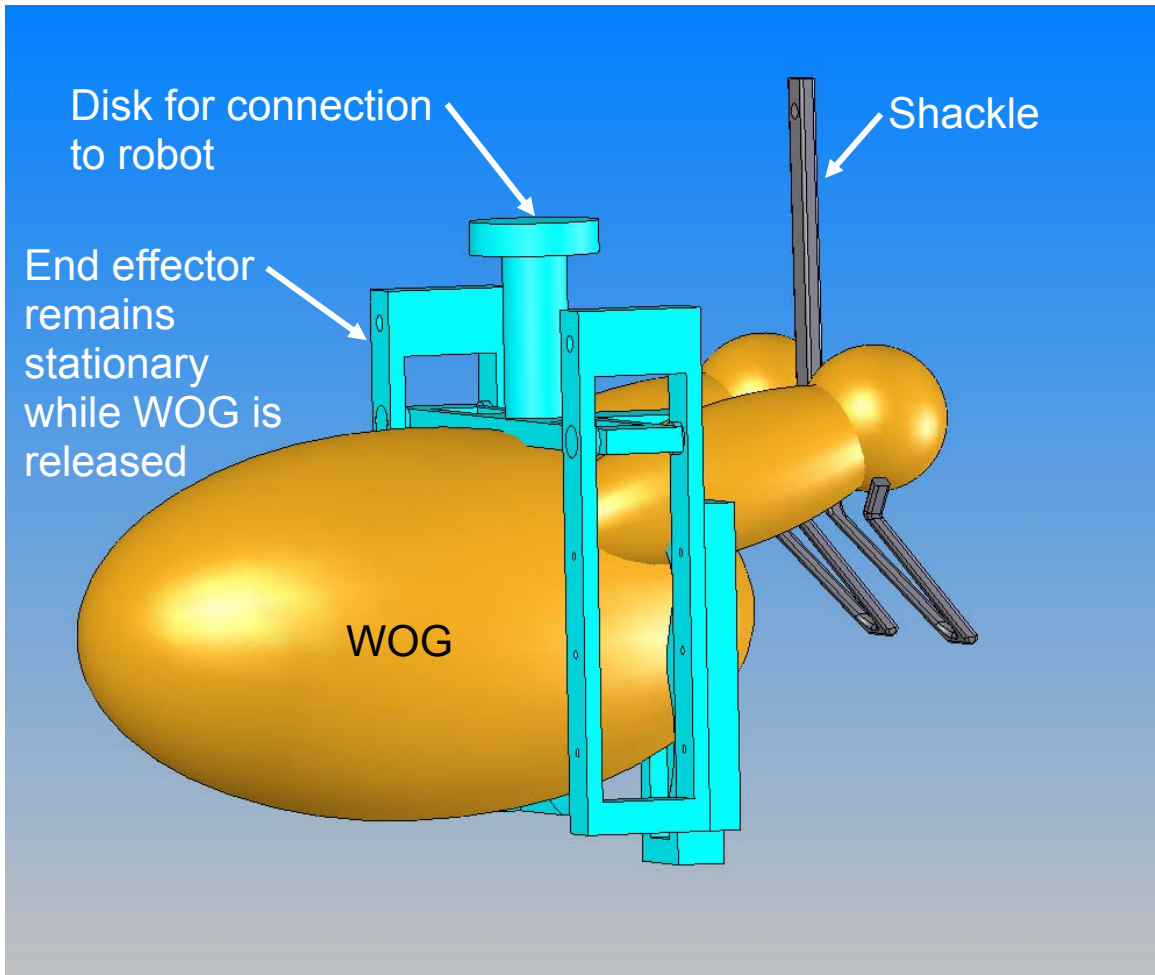


Figure 4.20: Release method when WOG is acquired breast up.

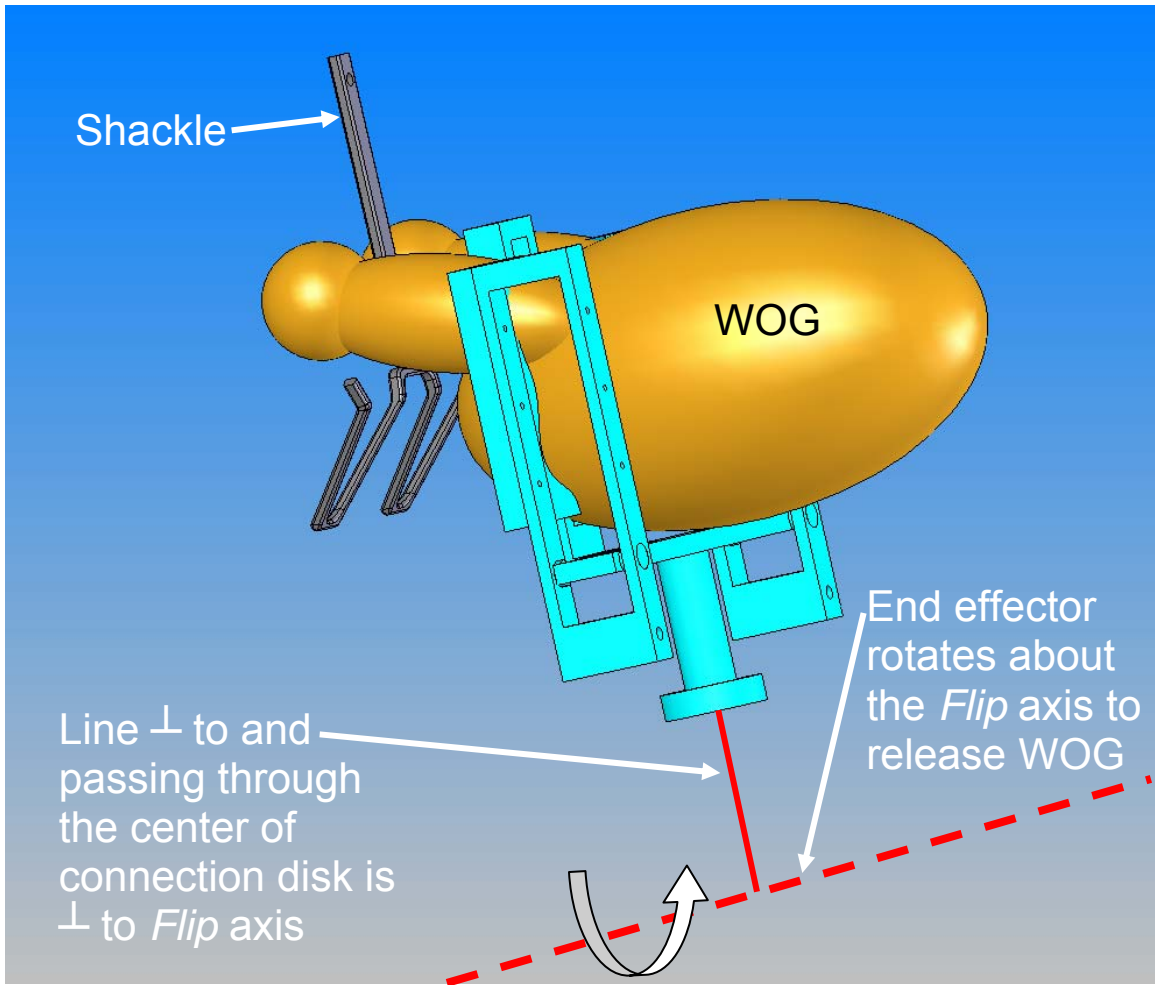


Figure 4.21: Release method when WOG is acquired breast down.

4.4 Design and Integration of Robotic Wrist

4.4.1 General Design

There are two fundamentally different ways to design the 2 DOF wrist. The wrist can be designed to perform the *Flip* motion then the *Rotate* motion, or vice versa .

To aid in the design of the wrist several guidelines are developed:

- *Rotate* axis must be perpendicular to the conveyor belt surface during WOG acquisition.
- End effector should lie on *Rotate* axis during WOG acquisition.
- *Flip* axis must be perpendicular to *Rotate* axis.
- *Flip* motion used in some WOG release scenarios should be similar to *Flip* motion used in the design and testing of the end effector.
- Wrist structure should be simple.
- Minimize the weight of the wrist.
- Place heavier objects closer to the parallel mechanism.

The *Rotate* axis must be perpendicular to the conveyor belt for the end effector to grasp WOGs in all of their possible initial orientations. When the end effector lies on the *Rotate* axis the *Rotate* motion does not affect the position of the end effector. This simplifies control of the robot. If the *Flip* axis and *Rotate* axis are perpendicular to each other the actuator loads from one actuator will not be transmitted to the other. If the WOG is captured in a breast down position the *Flip* motion is used during WOG release.

Figure 4.21 illustrates the *Flip* motion used in the design and testing of the end effector. Different *Flip* motions might also result in a successful WOG hang, but this motion is known to work so the wrist should be designed to perform a similar motion. The wrist design should be as simple as possible. Simpler designs generally cost less. The weight of the wrist should be minimized to reduce the loads on the actuators of the robot. Heavier objects should be placed kinematically closer to the parallel mechanism to reduce the rotating mass of the wrist. The more heavy things are rotated the larger the loads on the wrist actuators will be.

An evaluation of several *Rotate* first then *Flip* wrist designs revealed that this ordering of kinematic pairs has one significant advantage over the alternative, but also has some disadvantages. The advantage of the *Rotate* first then *Flip* wrist is that it places the heaviest actuator closer to the parallel mechanism. It was decided in Chapter 3 that a pneumatic actuator would be used for the *Flip* motion while an electric motor would be used for the *Rotate* motion. A review of available pneumatic actuators reveals that a linear pneumatic actuator with a rack and pinion or a revolute pneumatic actuator with an integral gearbox would likely weigh 2 lb to 5 lb. A washdown proof servo motor for the *Rotate* motion would likely weigh 10 lb to 20 lb but depending on the loads required from the actuator it could weigh much more. The disadvantages of *Rotate* then *Flip* wrists are that all of the desirable *Flip* and *Rotate* motion characteristics can not be achieved, and that their structures tend to be more complex. Figure 4.22 and Figure 4.23 illustrate two possible designs for a *Rotate* then *Flip* wrist. The wrist in Figure 4.22 provides a *Flip* motion similar to the one used in the design and testing of the end effector, but the end effector is not on the *Rotate* axis. For the wrist shown in Figure 4.23

the end effector is on the Rotate axis during WOG acquisition, but the wrist does not provide a *Flip* motion similar in the one used in the design and testing of the end effector.

The *Flip* then *Rotate* wrist shown in Figure 4.24 provides a *Flip* motion similar to the one used in the design and testing of the end effector and the end effector is on the Rotate axis. It is also anticipated that this design can have a simpler structure than any of the *Rotate* then *Flip* wrists. This assessment of structural simplicity is based on knowledge of mechanical design and considering many ways that the potential wrist designs could be built. The wrist is chosen to have a *Flip* first then *Rotate* geometry such as the one shown in Figure 4.24. The *Flip* motion is actuated by a two position pneumatic actuator that provides rotation about an axis that is parallel to the *Y* axis of the global coordinate frame. The *Rotate* motion is actuated by a washdown proof electric motor. The axis of rotation of the electric motor is parallel to the global *Z* axis during WOG acquisition.

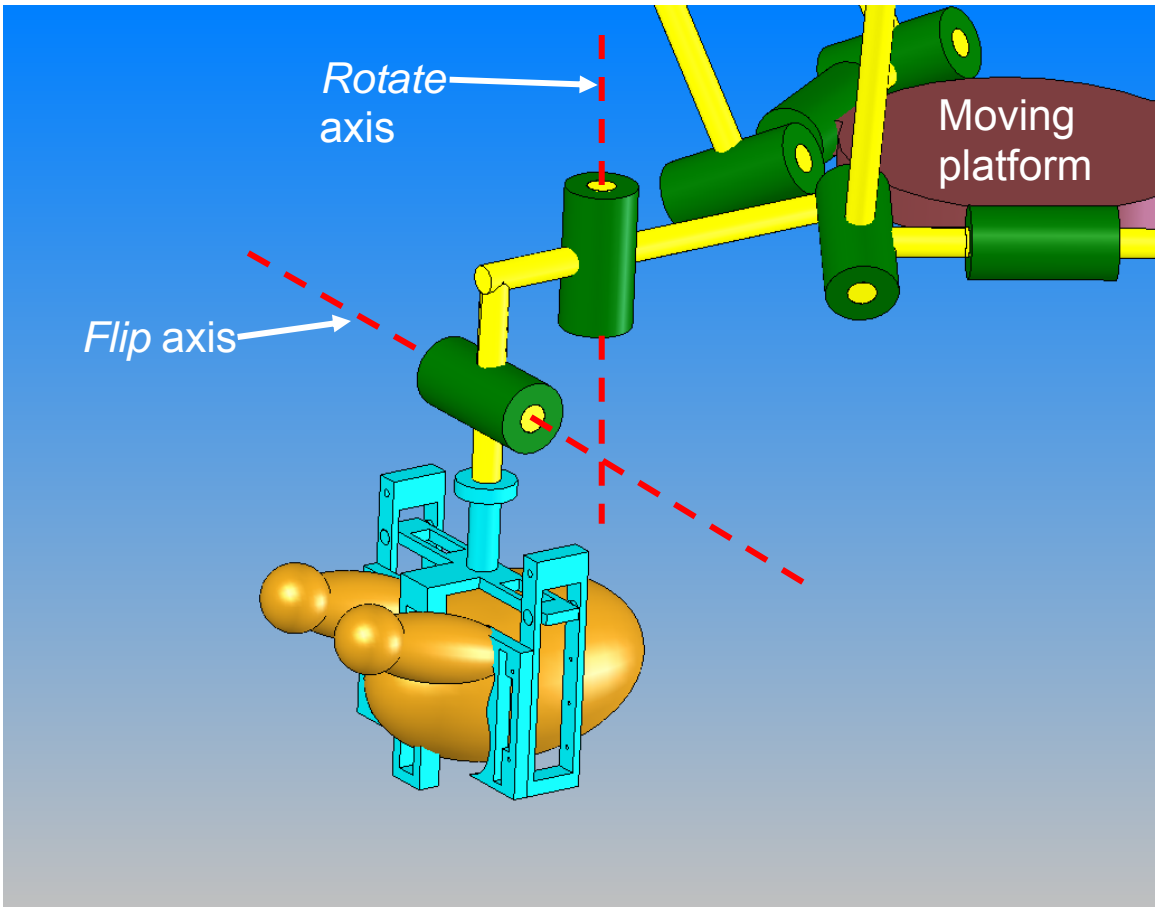


Figure 4.22: First example of a *Rotate* then *Flip* wrist.

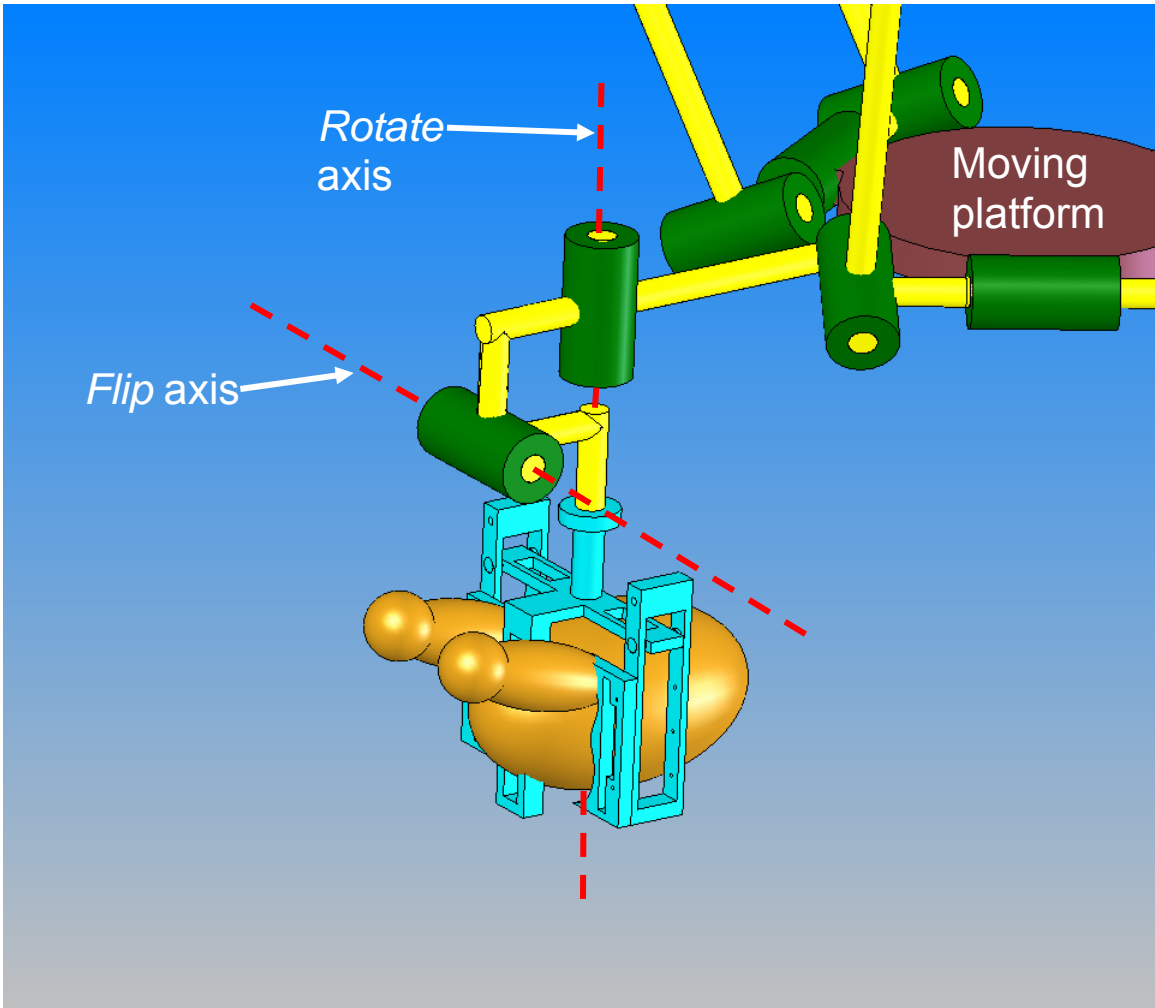


Figure 4.23: Second example of a *Rotate* then *Flip* wrist.

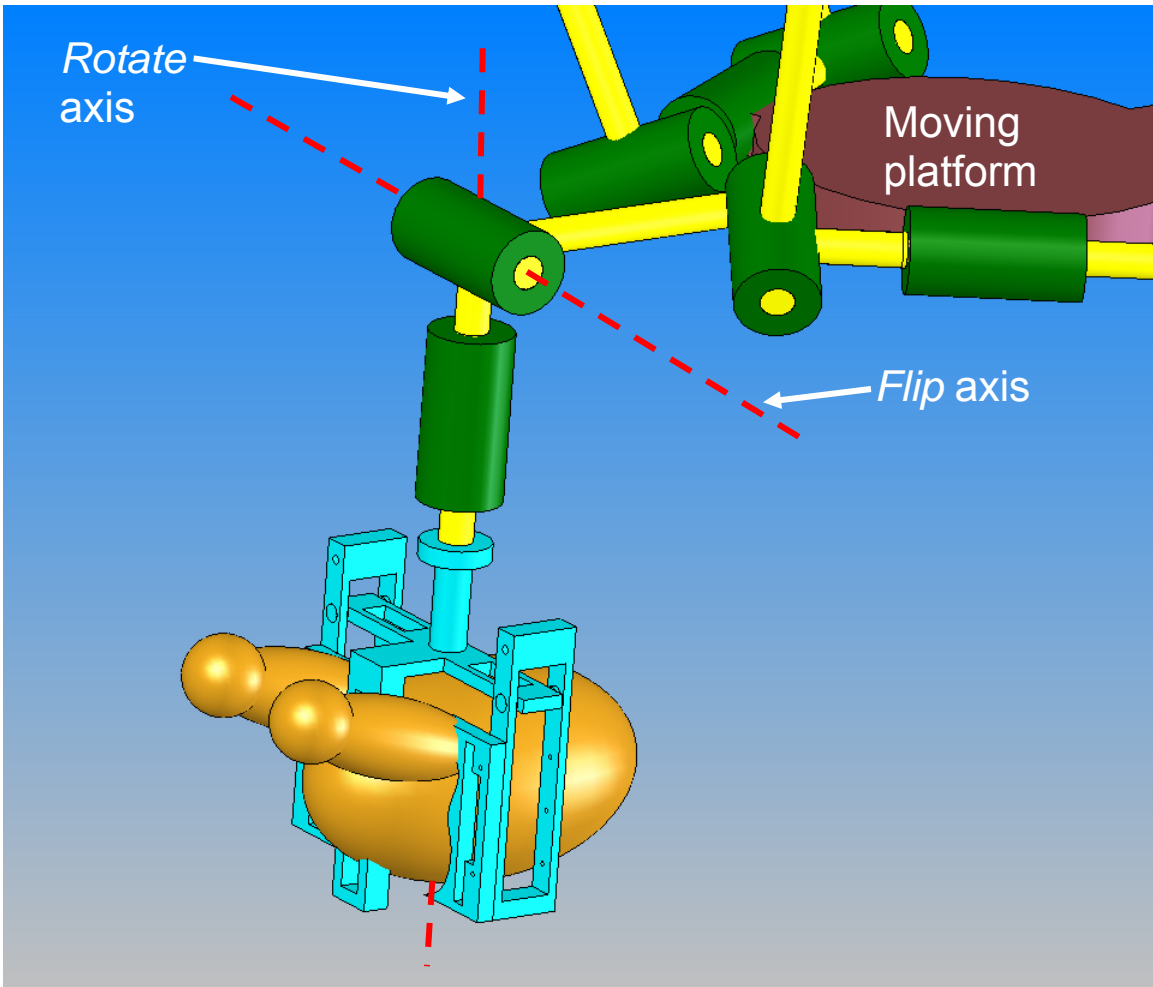


Figure 4.24: One possible *Flip* then *Rotate* wrist.

4.4.2 Kinematics of the Wrist

In this section the kinematics of the 2 DOF wrist are developed. In Figure 4.25 it can be seen that point F is the center of the wrist and point G is the point where the end effector is connected to the robot. The orientation of the $X_g Y_g Z_g$ coordinate frame is specified by the angles of the pneumatic *Flip* (θ_w) and electric *Rotate* (ρ_w) actuators. The location of the center of the wrist with respect to the center of the moving platform is

given by the constant vector \overline{EF} . Expressed in the global coordinate frame, the location of point G with respect to the center of the wrist is $\overline{FG} = \|\overline{FG}\| [\sin(\theta_w) \ 0 \ \cos(\theta_w)]^T$ where $\|\overline{FG}\|$ is a fixed property of the robot. The location of point G with respect to the center of the moving platform is then:

$$\overline{EG} = \overline{EF} + \|\overline{FG}\| [\sin(\theta_w) \ 0 \ \cos(\theta_w)]^T \quad (4.37)$$

The position of point G with respect to the center of the base of the parallel mechanism (O) is the sum of the vectors from the center of the base to the center of the moving platform (\overline{OE}) and from the center of the moving platform to G (\overline{EG}).

$$\overline{OG} = \overline{OE} + \overline{EG} \quad (4.38)$$

Equations (4.28) and (4.29) can be used with the forward kinematic equations of the parallel mechanism to determine the location of point G with respect to the base of the parallel mechanism from the positions of the robot actuators: θ_{11} , θ_{12} , θ_{13} , θ_w , and ρ_w . They can also be used with the reverse kinematic equations of the parallel mechanism to find the positions of the actuators of the parallel mechanism (θ_{11} , θ_{12} , and θ_{13}) from the position of G with respect to the center of the base (\overline{OG}) and the angles of the wrist actuators (θ_w , and ρ_w).

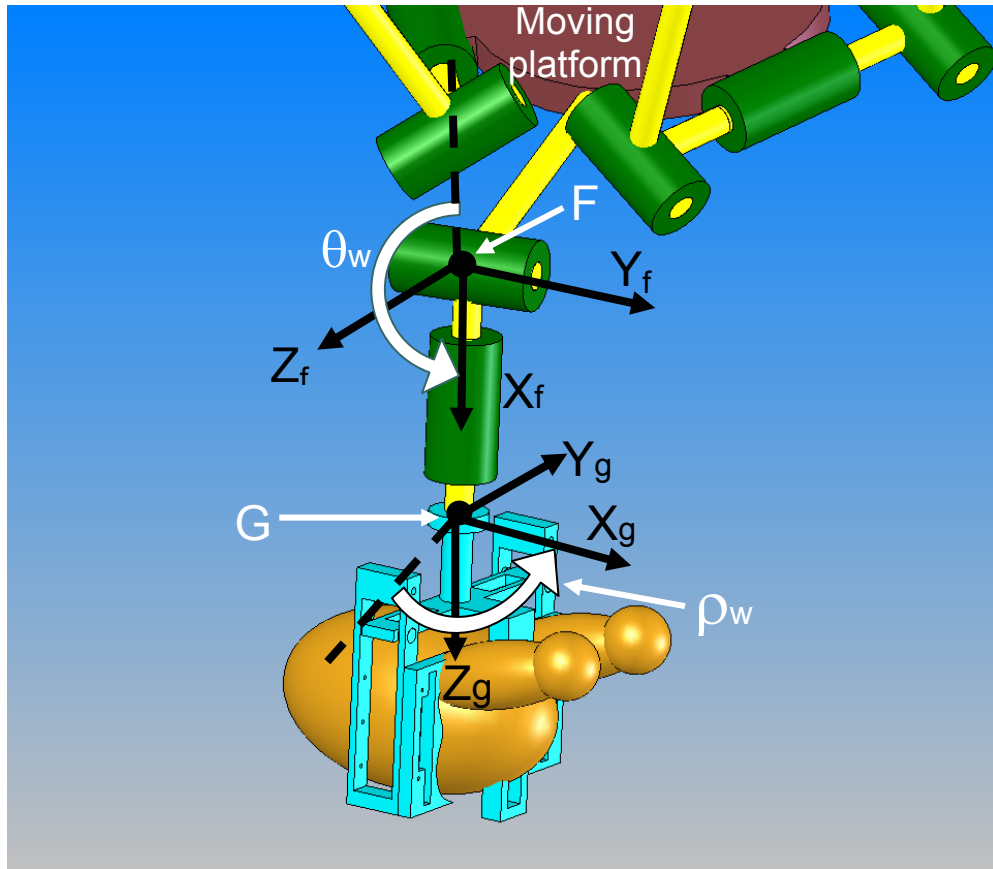


Figure 4.25: 2 DOF wrist.

4.5 Jacobian and Singularity analysis of the Parallel Mechanism

In this section the Jacobian of the parallel mechanism is developed and a singularity analysis of the parallel mechanism is carried out. The Jacobian of the parallel platform relates the velocity of the moving platform in the global coordinate frame to the angular velocities of the parallel mechanism actuators. Let the vector expressing the velocity of the moving platform with respect to the base be \overline{OE} and let angular velocities

of the parallel mechanism actuators be given by the vector $\dot{\Theta} = [\dot{\theta}_{11} \quad \dot{\theta}_{12} \quad \dot{\theta}_{13}]^T$. The Jacobian derived in this section will be a two part Jacobian and will relate \dot{OE} and $\dot{\Theta}$ as:

$$J_1 \dot{OE} = J_2 \dot{\Theta} \quad (4.39)$$

Where J_1 and J_2 are 3 x 3 matrices. The advantage of deriving the two part Jacobian instead of the more common single matrix Jacobian is that it will allow two different types of parallel mechanism singularity to be identified separately.

Kinematic singularities are mechanism configurations that increase or decrease the degrees of freedom of the end of the mechanism. Let a mechanism have the proper number of actuators to fully, but not redundantly, control the end of the mechanism. If the end of the mechanism gains degrees of freedom it can be moved while all of the actuators are fixed. If the end of the mechanism loses degrees of freedom at least one of the actuators can be moved while the end of the mechanism is fixed.

The analysis in this section does not include the wrist. Including the wrist in the Jacobian derivation and singularity analysis complicates the equations and makes the analysis much harder to follow without providing much insight. The relationship between the velocity provided by the wrist and the angular velocities of the wrist actuators can be found by taking the derivative of (4.28). It is unnecessary to include the wrist in the singularity analysis because the wrist can not cause a singular configuration. A change in the angle of either wrist actuator always results in a change in the orientation and/or position of the end effector. The singularities of the parallel mechanism are then the singularities of the robot.

4.5.1 Two Part Jacobian of Parallel Mechanism

The derivation of the two part Jacobian begins with the differentiation of equation (4.29), a loop equation relating the vector that goes directly from the center of the base to the center of the moving platform ($\overline{OE} = [ex \ ey \ ez]^T$) to the summation of vectors that go from the center of the base to the center of the moving platform via the i th arm, with respect to time. All quantities in equation (4.40) are expressed in the local $X_{1i}Y_{1i}Z_{1i}$ coordinate frame.

$$\frac{\partial}{\partial t} \begin{bmatrix} ex \\ ey \\ ez \end{bmatrix} = \frac{\partial}{\partial t} \begin{bmatrix} c + l \cos(\theta_{1i}) + d \cos(\theta_{1i} + \theta_{2i}) \cos(\rho_{3i}) - e \\ d \sin(\rho_{3i}) \\ -l \sin(\theta_{1i}) - d \sin(\theta_{1i} + \theta_{2i}) \cos(\rho_{3i}) \end{bmatrix} \quad (4.40)$$

which leads to:

$$\begin{bmatrix} \dot{ex} \\ \dot{ey} \\ \dot{ez} \end{bmatrix} = \begin{bmatrix} \dot{\theta}_{1i}(-l \sin(\theta_{1i}) - d \sin(\theta_{1i} + \theta_{2i}) \cos(\rho_{3i})) + \dot{\theta}_{2i}(-d \sin(\theta_{1i} + \theta_{2i}) \cos(\rho_{3i})) + \dot{\rho}_{3i}(-d \cos(\theta_{1i} + \theta_{2i}) \sin(\rho_{3i})) \\ \dot{\rho}_{3i} d \cos(\rho_{3i}) \\ \dot{\theta}_{1i}(-l \cos(\theta_{1i}) - d \cos(\theta_{1i} + \theta_{2i}) \cos(\rho_{3i})) + \dot{\theta}_{2i}(-d \cos(\theta_{1i} + \theta_{2i}) \cos(\rho_{3i})) + \dot{\rho}_{3i}(d \sin(\theta_{1i} + \theta_{2i}) \sin(\rho_{3i})) \end{bmatrix} \quad (4.40)$$

This can be considered a set of three equations in three unknowns (θ_{1i} , θ_{2i} , and ρ_{3i}).

Solving the set of equations to eliminate θ_{2i} , and ρ_{3i} then simplifying yields:

$$\dot{\theta}_{1i} l \sin(\theta_{2i}) \cos(\rho_{3i}) = \dot{ex} \cos(\theta_{1i} + \theta_{2i}) \cos(\rho_{3i}) + \dot{ey} \sin(\rho_{3i}) - \dot{ez} \sin(\theta_{1i} + \theta_{2i}) \cos(\rho_{3i}) \quad (4.41)$$

Equation (4.41) relates the velocity of the moving platform in the local $X_{1i}Y_{1i}Z_{1i}$ coordinate frame ($\overline{OE} = \begin{bmatrix} \dot{ex} & \dot{ey} & \dot{ez} \end{bmatrix}^T$) to the angular velocity of the actuator at the top of the i th arm of the parallel mechanism. The relation given in Equation (4.42) is used with Equation (4.41) to yield Equation (4.43), which relates the velocity of the moving platform in the global coordinate frame ($\overline{OE} = \begin{bmatrix} \dot{Ex} & \dot{Ey} & \dot{Ez} \end{bmatrix}^T$) to the angular velocity of the actuator at the top of the i th arm of the parallel mechanism. The angle ρ_{0i} is shown in Figure 4.9.

$$\begin{bmatrix} \dot{ex} \\ \dot{ey} \\ \dot{ez} \end{bmatrix} = \begin{bmatrix} \cos(\rho_{0i}) & \sin(\rho_{0i}) & 0 \\ -\sin(\rho_{0i}) & \cos(\rho_{0i}) & 0 \\ 0 & 0 & 1 \end{bmatrix} \begin{bmatrix} \dot{Ex} \\ \dot{Ey} \\ \dot{Ez} \end{bmatrix} \quad (4.42)$$

$$\begin{aligned} \dot{\theta}_{1i} l \sin(\theta_{2i}) \cos(\rho_{3i}) &= \dot{Ex} (\cos(\rho_{0i}) \cos(\theta_{1i} + \theta_{2i}) \cos(\rho_{3i}) - \sin(\rho_{0i}) \sin(\rho_{3i})) + \\ &\dot{Ey} (\sin(\rho_{0i}) \cos(\theta_{1i} + \theta_{2i}) \cos(\rho_{3i}) + \cos(\rho_{0i}) \sin(\rho_{3i})) - \dot{Ez} \sin(\theta_{1i} + \theta_{2i}) \cos(\rho_{3i}) \end{aligned} \quad (4.43)$$

Since there are three arms there are three versions of Equation (4.43). Combining them and arranging them in the form of equation (4.39) yields the split Jacobian equation:

$$J_1 \begin{bmatrix} \dot{Ex} \\ \dot{Ey} \\ \dot{Ez} \end{bmatrix} = J_2 \begin{bmatrix} \dot{\theta}_{11} \\ \dot{\theta}_{12} \\ \dot{\theta}_{13} \end{bmatrix} \quad (4.44)$$

Where:

$$J_1 = \begin{bmatrix} j_{11} & j_{12} & j_{13} \\ j_{21} & j_{22} & j_{23} \\ j_{31} & j_{32} & j_{33} \end{bmatrix} \quad (4.45)$$

$$J_2 = \begin{bmatrix} l \sin(\theta_{21}) \cos(\rho_{31}) & 0 & 0 \\ 0 & l \sin(\theta_{22}) \cos(\rho_{32}) & 0 \\ 0 & 0 & l \sin(\theta_{23}) \cos(\rho_{33}) \end{bmatrix} \quad (4.46)$$

and

$$J_{i1} = \cos(\rho_{0i}) \cos(\theta_{1i} + \theta_{2i}) \cos(\rho_{3i}) - \sin(\rho_{0i}) \sin(\rho_{3i}) \quad (4.47)$$

$$J_{i2} = \sin(\rho_{0i}) \cos(\theta_{1i} + \theta_{2i}) \cos(\rho_{3i}) + \cos(\rho_{0i}) \sin(\rho_{3i}) \quad (4.48)$$

$$J_{i3} = \sin(\theta_{1i} + \theta_{2i}) \cos(\rho_{3i}) \quad (4.49)$$

4.5.2 Singularity Analysis

There are two types of singularity for this mechanism, platform singularities and arm singularities. Platform singularities result in the platform gaining degrees of freedom. The platform is able to move even if all actuators are fixed. Arm singularities result in the platform losing degrees of freedom, but result in one or more arms gaining degrees of freedom. One or more actuators can move even if the platform is fixed.

Platform singularities occur when there are wrenches that can not be resisted by the parallel mechanism. In other words, the platform gains degrees of freedom when the wrenches that can be applied to the moving platform by the three arms of the mechanism do not span all wrenches. The arms of the parallel mechanism constrain the platform from rotating. It follows that the wrenches that can be applied by the arms of the parallel mechanism span all moments. The only forces the arms of the parallel mechanism can apply to the moving platform are along the $\overline{L_i D_i}$ vectors, which specify the length and orientation of the lower links of the arms of the parallel mechanism. The forces from the three legs of the parallel mechanism can span all forces if and only if the $\overline{L_i D_i}$ vectors span 3 dimensional space. If two or more $\overline{L_i D_i}$ vectors are parallel to each other (Figure 4.26) or if all three $\overline{L_i D_i}$ vectors lie in the same plane (Figure 4.27) or in parallel planes the mobility of the parallel mechanism is increased and fixing the actuators is not sufficient to fix the position of the moving platform.

These singularities correspond to mechanism configurations that cause J_1 to be singular. If transposed, the rows of J_1 are unit vectors that point in the directions of the $\overline{L_i D_i}$ vectors. When the three $\overline{L_i D_i}$ vectors do not span three dimensional space the three rows of J_1 are not linearly independent.

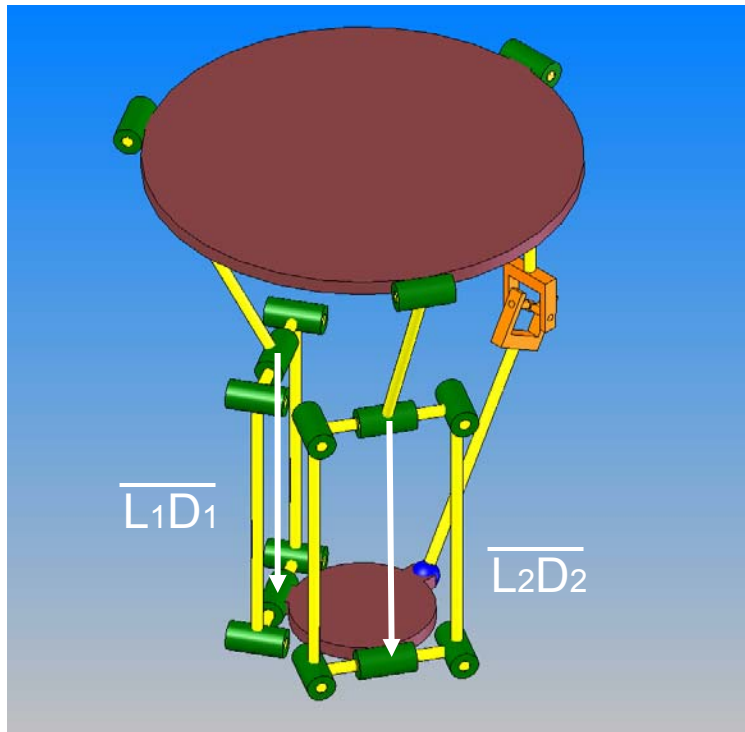


Figure 4.26: Platform singularity due to two parallel $\overline{L_iD_i}$ vectors.

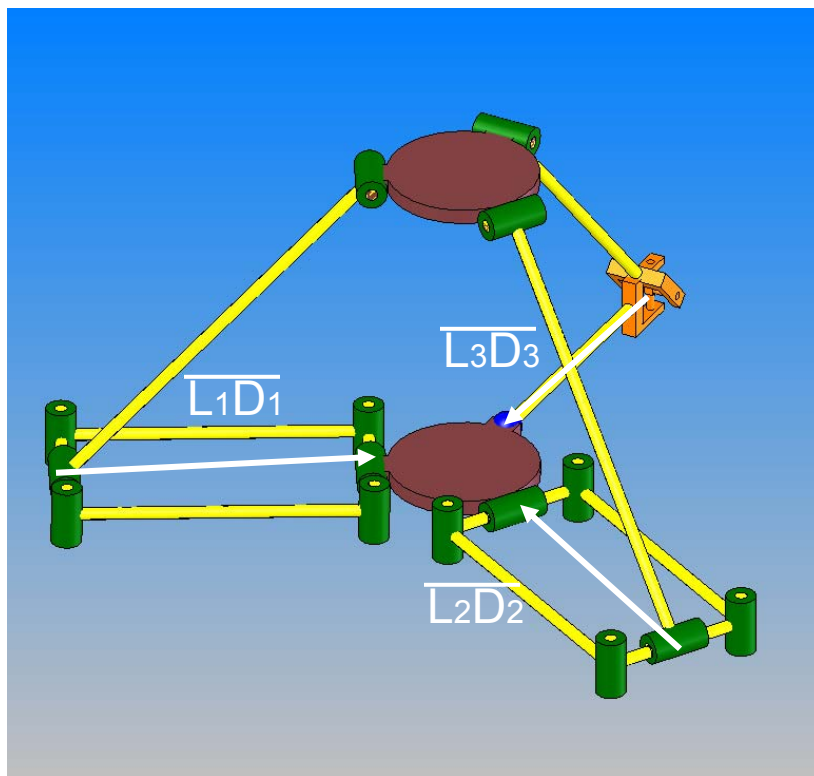


Figure 4.27: Platform singularity due to three co-planar $\overline{L_iD_i}$ vectors.

Arm singularities occur when an infinitesimal change in the position of an actuator causes no change in the position of the moving platform. These singularities correspond to mechanism configurations that cause J_2 to be singular. It can be seen from Equation 4.46 that if θ_{2i} is 0° or 180° , or if ρ_{3i} is $\pm 90^\circ$ ($i = 1,2,3$) the i th diagonal of J_2 becomes 0 and J_2 becomes singular. These singularities are shown in Figure 4.28, Figure 4.29, and Figure 4.30.

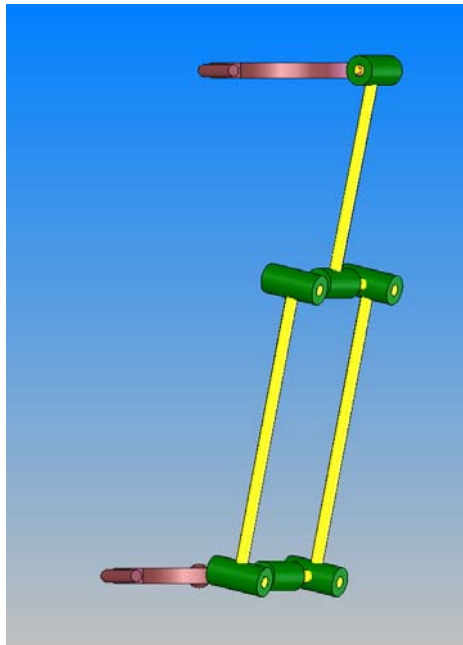


Figure 4.28: $\theta_{2i} = 180^\circ$ arm singularity.

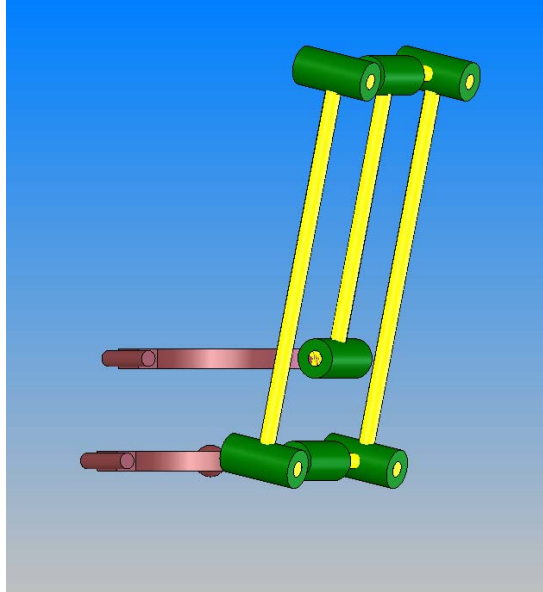


Figure 4.29: $\theta_{2i} = 0^\circ$ arm singularity.

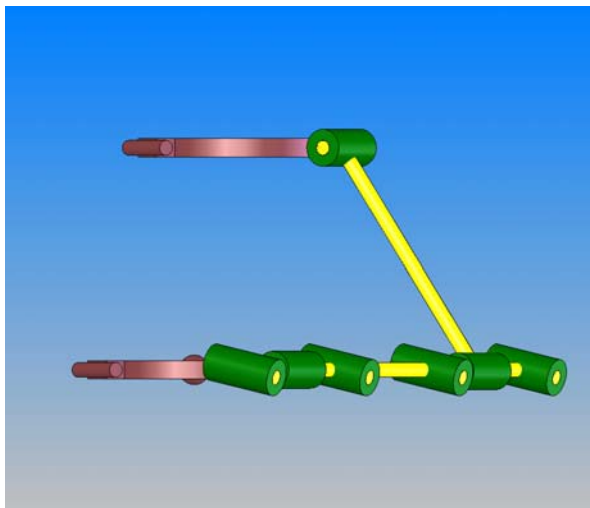


Figure 4.30: $\rho_{3i} = -90^\circ$ arm singularity.

CHAPTER 5

OPTIMIZATION OF ROBOT PARAMETERS

In this chapter the robot dimensions are determined. Section 5.1 presents a set of parameters that define the size and shape of the robot. In Section 5.2 the required robot workspace is determined. In Section 5.3 the robot parameters are varied and a visual method is used to gain insight into the effects of the variations. The insight gained in Sections 5.2 and 5.3 is then used to focus the optimization problem. In Section 5.4 variations in the ratios of the link lengths of the robot are considered. For each ratio of links the parallel portion of the robot is scaled until the workspace of the robot can encompass the required robot process. In Section 5.6 the position of the wrist is determined with respect to the position of the moving platform of the parallel mechanism and the position of the connection point of the end effector is determined with respect to the wrist.

5.1 Characterization of Parameters

The angles ρ_{01} , ρ_{02} , and ρ_{03} specify the orientations of the parallel mechanism arms and partially define where they are attached to the fixed base (Figure 5.1) and the moving platform. The link lengths of the arms of the parallel mechanism c , l , d , and e are

shown in Figure 5.2. The vector from the center of the moving platform to the center of the wrist (\overline{EF}) and the vector from the center of the wrist to the connection point of the end effector (\overline{FG}) are illustrated in (Figure 5.3). The parameters ρ_{01} , ρ_{02} , ρ_{03} , c , l , d , and e are determined in Sections 5.3 and 5.4 while the vectors \overline{EF} and \overline{FG} are determined in Section 5.6.

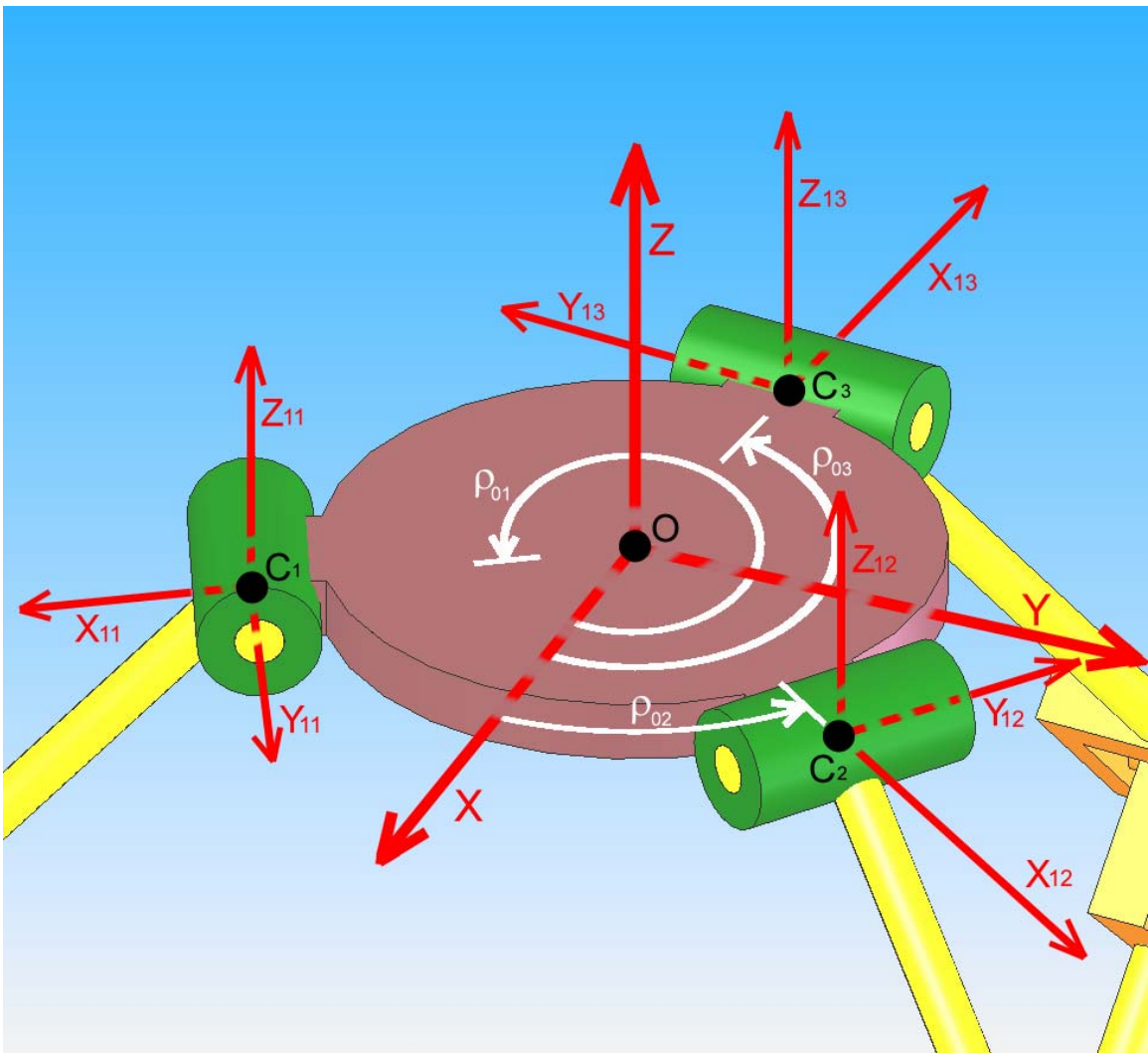


Figure 5.1: Illustration of ρ_{0i} angles.

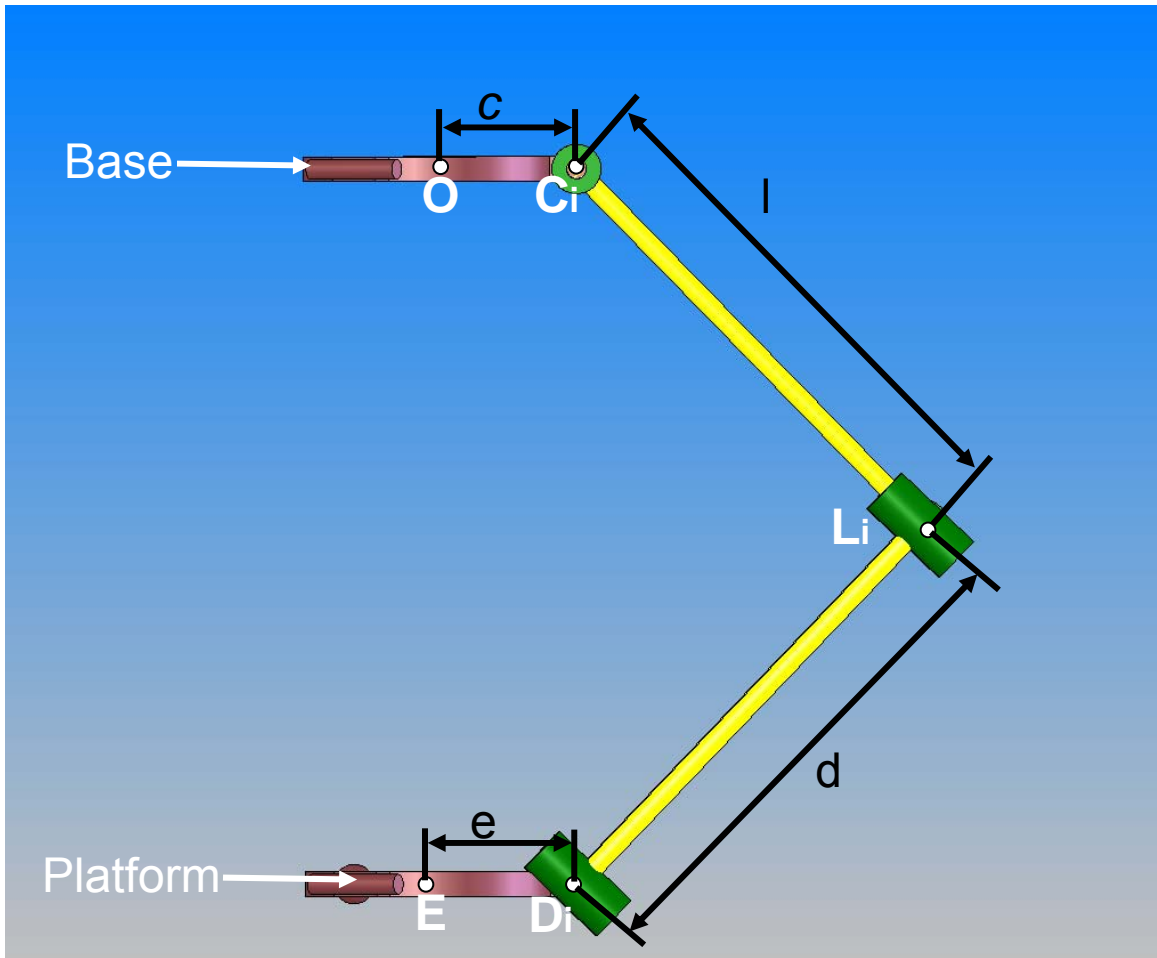


Figure 5.2: Link lengths of the i th arm of the parallel mechanism.

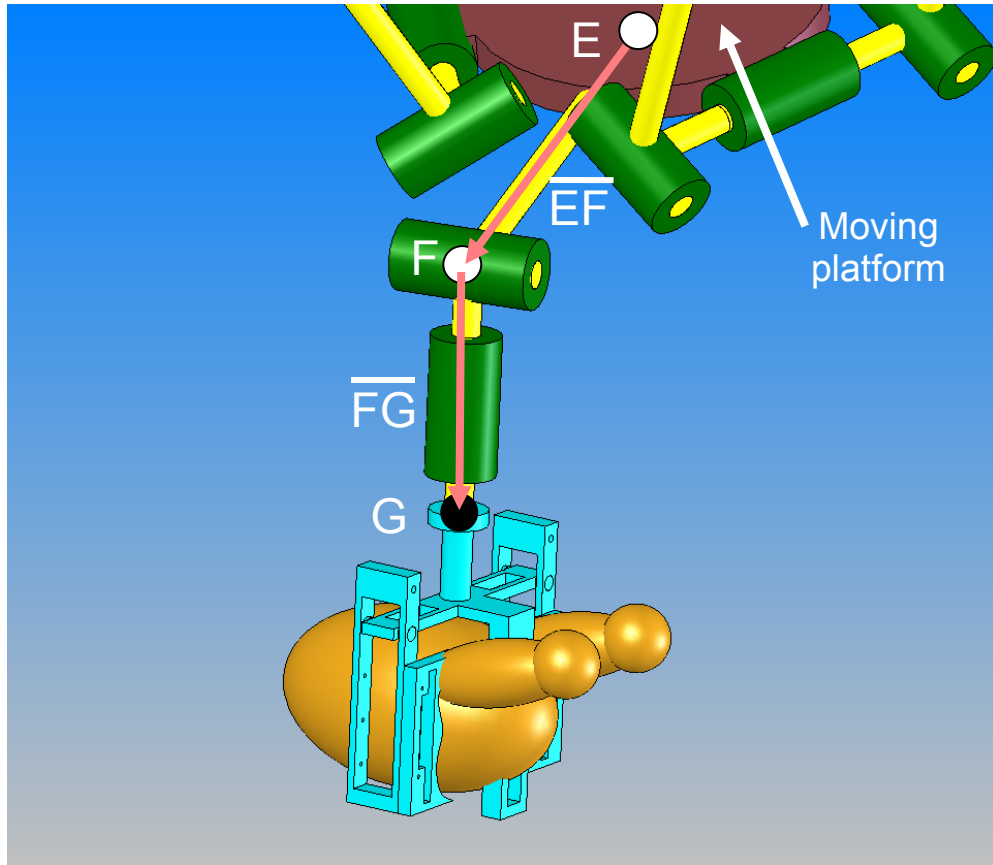


Figure 5.3: vectors \overline{EF} and \overline{FG} .

5.2 Characterization of Workspace

Before the robot parameters are optimized the required robot workspace must be determined. The initial estimate of the required translational workspace calls for a rectangular workspace measuring 2.5 ft x 2 ft x 2 ft in the global X , Y and Z directions respectively (Section 2.3.4). However, forcing the WOGs to lie on the outside of the conveyor belt, as suggested in Section 3.3.3, cuts the X dimension of this workspace in

half. Applying a safety factor of 1.25 to this workspace yields a workspace measuring 1.875ft x 2.5 ft x 2.5 ft.

If the WOG is acquired in the breast down position it is flipped over while being transferred to the shackle. In this case the *Flip* motion of the wrist provides some of the necessary translation of the WOG in the *Z* direction. If the WOG is acquired in the breast up position the parallel mechanism provides all of the translation. The parallel mechanism must therefore accommodate a 1.875 ft x 2.5 ft x 2.5 ft workspace.

5.3 Qualitative Work Space Study

The parameters ρ_{01} , ρ_{02} , ρ_{03} , c , l , d , and e all affect the workspace of the parallel mechanism. Since the workspace of the parallel mechanism is the intersection of the workspaces of three kinematic chains, it is difficult to visualize how each of these parameters affects the workspace. The point of this section is to visualize the affect of varying these parameters, and to draw conclusions about which parameter values might provide the ideal workspace.

To isolate the affect of parameter variation, a reference is chosen: $\rho_{01} = 30^\circ$, $\rho_{02} = 150^\circ$, $\rho_{03} = 270^\circ$, and $c = l = d = e = 1$. Figure 5.4 is the workspace plot for these reference parameters. By systematically varying these parameters away from the reference values and comparing the resulting workspace plots, insight into the affect of each parameter can be gained

The workspace of the parallel mechanism is visualized with the help of MATLAB and equations (4.8), (4.9), and (4.10), the reverse kinematic equations of the parallel mechanism. The MATLAB programs in Section C.1 vary the parameters and produce four plots, such as the ones shown in Figure 5.4, for each set of parameters. These plots are cross sections of the workspace of the parallel mechanism with the origin at the center of the robot base. They show the intersections of mechanism workspace with the planes given by the equations: $Z = -0.5$, $Z = -1$, $Z = -1.5$, and $X = 0$.

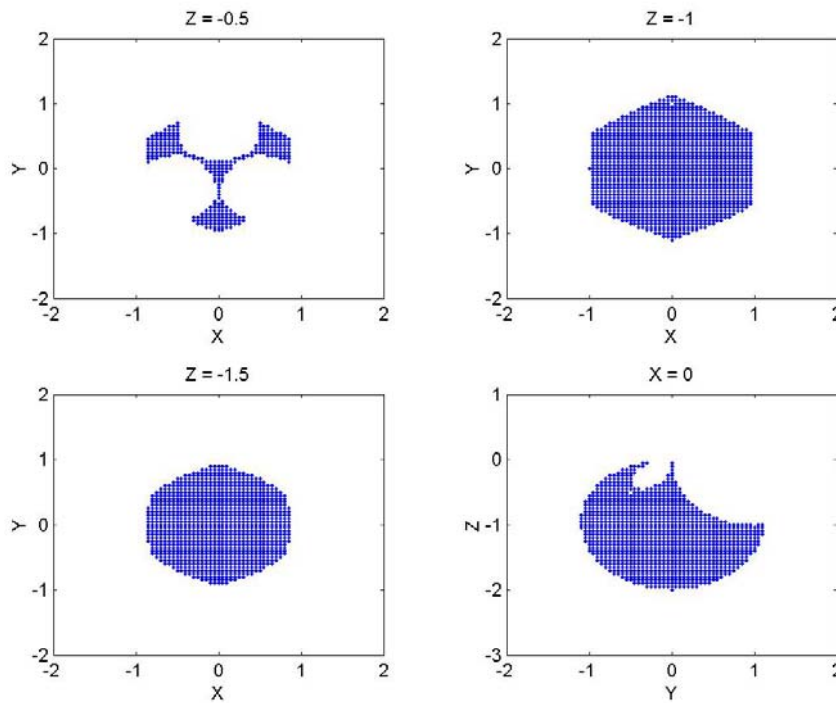


Figure 5.4: Workspace plot for $\rho_{0i} = 30^\circ, 150^\circ, 270^\circ, l = 1, d = 1, c = 1, e = 1$.

For the first workspace study one, two, or three parameters are varied. The c , l , d , and e parameters are varied over the values 0.5, 1, 1.5, and 2. ρ_{01} , ρ_{02} , and ρ_{03} are varied over the values $[\rho_{01} \ \rho_{02} \ \rho_{03}] = [15^\circ \ 165^\circ \ 270^\circ]$, $[30^\circ \ 150^\circ \ 270^\circ]$, $[45^\circ \ 135^\circ \ 270^\circ]$, and $[60^\circ \ 120^\circ \ 270^\circ]$. Parameters not being varied are set at the reference values. Plots for a total of 60 robot configurations are presented in Appendix D (Figure D.1 through Figure D.15). Four workspace plots correspond to the variation of ρ_{01} , ρ_{02} , and ρ_{03} , while 56 correspond to the single double and triple parameter variations of c , l , d , and e . An examination of these plots for trends reveals two important facts. The parameters c and e are not independent parameters. The workspace of the robot is affected by the difference ($c-e$), not the values of c or e . In other words the mechanism workspace depends on the difference between the size of the base and the size of the moving platform. The workspace is largest and most appropriately shaped when ρ_{01} , ρ_{02} , and ρ_{03} are evenly spaced, such as $\rho_{01} = 30^\circ$, $\rho_{02} = 150^\circ$, and $\rho_{03} = 270^\circ$. Varying the arm connection points away from an even spacing, had little positive affect. As the arm connection point spacing gets more asymmetrical the workspace gets narrower in one horizontal direction, while the width in the perpendicular horizontal direction and the height remain about the same.

Based on the results from the first round of workspace plots the robot parameters are redefined to be l , d , and ($c-e$) and another set of plots is produced. l , and d must be positive but ($c-e$) can be positive or negative so two references are chosen for this round of workspace plots. The reference values for the parameters are $l = d = 1$, and ($c-e$) = ± 0.5 . Two sets of workspace plots were created one set for positive ($c-e$) and one for negative ($c-e$). l and d are varied over the values 0.5, 1, 1.5, and 2 while the magnitude of

$(c-e)$ is varied over the values 0.25, 0.5, 0.75 and 1. Parameters not being varied were set to the appropriate reference values. Carrying out single and double parameter variations gives plots for 48 robot configurations (appendix D, Figure D.16 through Figure D.27). The trends observed for each variation are presented in the following tables.

Table 5.1: Single parameter variation for $(c-e) > 0$.

Varied Parameter	Observations
$(c-e)$	The size and shape of the workspace in the X and Y direction remains pretty constant, but the height of the workspace gets smaller as $(c-e)$ increases.
l	For $l \geq 1$ the workspace is shifted downward and gets flatter, but does not really change size. When $l = 0.5$ the workspace is smaller.
d	The workspace gets larger, flatter and lower as d is increased.

Table 5.2: Two parameter variation for $(c-e) > 0$.

Varied Parameters	Observations
$(c-e) \& l$	The workspace gets lower and flatter as the parameters are increased. The size of the workspace is not significantly increased.
$(c-e) \& d$	The workspace gets larger as the parameters are increased. The increase in size in the X and Y directions is not as much as when only d is increased, but the increase in size in the Z direction is greater. The shape changes as the parameters are varied, but not that much.
$l \& d$	The workspace gets larger and lower as the parameters are increased. The increase is more than was seen for any other sets of parameters, and is very uniform. The shape changes as the parameters are varied, but only slightly.

Table 5.3: Single parameter variation for $(c-e) < 0$.

Varied Parameter	Observations
$(c-e)$	As $(c-e)$ is made more negative, the workspace becomes more compact, but, seems to become a little smaller. The shape of the workspace looks pretty good when $(c-e) = 0.75$
l	The workspace is shifted lower as l is increased. The workspace seems to get smaller and flatter as l moves away from 1
d	The workspace increases in size as d increases. The size in the X and Y directions always increases, and the height increases up to $d = 1.5$, but the height actually decreases when d goes to 2.

Table 5.4: Two parameter variation for $(c-e) < 0$.

Varied Parameters	Observations
$(c-e) \& l$	The workspace is shifted lower as the parameters increase. The lower part of the workspace seems to remain about the same, but the upper part of the workspace seems to get thinner and taller. The middle two parameter settings yield the most useable workspace.
$(c-e) \& d$	The workspaces here are very similar to the workspaces when only d is varied
$l \& d$	As these parameters are increased the workspace is shifted downward and is scaled up in size. There is some change in the shape of the workspace, but the change is very small among the last three sets of parameters.

From these observations it appears that the robot with the best workspace will likely have a $(c-e)$ value that is negative and close to zero, and will have a d value that is significantly larger than the l value.

5.4 Quantitative Work Space Study

The shape of the workspace is determined by the relative proportions of the parameters l , d , and $(c-e)$. The size of the workspace is determined by the scaling of these parameters. The preliminary workspace study carried out in the previous section used unitless robot parameters. Any set of parameters from the range studied in Section 5.3 can be scaled to accommodate the required mechanism workspace determined in Section 5.2. In this section sets of parameters are defined as ratios with respect to l . Sets of robot parameters having d values significantly larger than l and $(c-e)$ values near 0 are scaled to accommodate the 1.875 ft x 2.5 ft x 2.5 ft required mechanism workspace. The scaled parameters are examined to determine the best set.

Before the optimum parameters can be determined the contextual meaning of optimum must be specified. For the parameters l and d smaller is better since decreasing one of these parameters while holding the other parameters constant generally decreases the size, weight and cost of the robot. Decreasing l also decreases the length of the moment arms driven by the electric actuators at the base which decreases the required torques. For c and e smaller is also better to some extent. Decreasing e makes the moving platform of the parallel mechanism smaller, lighter and generally makes it cheaper, however e must be large enough to connect the wrist to the moving platform. The optimum c is determined mainly by the size of the parallel mechanism actuators. The smallest c that accommodates the actuators and allows enough room for easy maintenance access is optimum. The optimum c is larger than the optimum e so larger values of the parameter $(c-e)$ are better as long as $(c-e)$ is not too large. Engineering judgment can be used to determine when $(c-e)$ is too large.

It is not always possible to optimize all the parameters. A desirable change in one parameter may cause an undesirable change in one or both of the other parameters. To estimate the overall desirability of a set of parameters, the equivalent length of that set of parameters is determined. The equivalent length (L_E) is calculated by Equation (5.1) and is a weighted summation of the parameters l , d , and the absolute value of the quantity ($CE_{opt} - (c-e)$), where CE_{opt} is the optimum value for how much c should be larger than e . At this phase of the design the value of CE_{opt} is a judgment call, since the construction details of the base and moving platform can not be determined. For the qualitative workspace study in Section 5.4.2 CE_{opt} is chosen to be 6 in. A good approximation of the optimum parallel mechanism dimensions can be determined by minimizing the equivalent length while maintaining one constraint. The set of parameters must correspond to a parallel mechanism workspace capable of accommodating the required mechanism workspace.

$$L_E = 3l + d + |CE_{opt} - (c - e)| \quad (5.1)$$

5.4.1 Concerns About Singular and Near-Singular Configurations

When optimizing the parameters care must be taken to exclude singular and near-singular configurations from the robot workspace. Singular and near-singular configurations cause control problems. As discussed in Section 4.5.2 there are two types of singularities for the parallel mechanism, arm singularities and platform singularities.

Arm singularities occur when an arm of the parallel mechanism is fully extended (Figure 4.28), when an arm of the mechanism is folded back on itself (Figure 4.29), and

when one of the parallelogram links is completely skewed (Figure 4.30). To stay away from singularities of this type two constraints are imposed:

$$5^\circ < \theta_{2i} < 175^\circ$$

$$-90^\circ < \rho_{3i} < 90^\circ$$

The angles θ_{2i} and ρ_{3i} are illustrated in Figure 4.16 and Figure 4.17.

Platform singularities occur when two or more of the lower links of the arms of the parallel mechanism ($\overline{L_i D_i}$ for $i = 1, 2, 3$) are parallel (Figure 4.26) or when all three of those links are co-planar (Figure 4.27). To stay away from the first type of platform singularity the angle the $\overline{L_i D_i}$ vector makes with the $\overline{L_j D_j}$ vector is constrained to be between 5° and 175° for $i = 1, 2, 3, j = 1, 2, 3$ but $i \neq j$. To avoid the second type of platform singularity each of the $\overline{L_i D_i}$ vectors are constrained point at least 5° out of the plane spanned by the other two $\overline{L_i D_i}$ vectors ($i = 1, 2, 3$).

5.4.2 Study Procedure and Results

To find the dimensions of a parallel mechanism that can accommodate the required workspace the dimensionless parameters are scaled. This is done with MATLAB and equations (4.8), (4.9), and (4.10), the reverse kinematic equations of the parallel mechanism. In this study the robot parameters d , and $(c-e)$, are specified as ratios of l . The MATLAB programs in Section C.2 take S_i the initial scaling factor and a range of d , and $(c-e)$ values as inputs. The parameters l , d , and $(c-e)$ are scaled by S_i . If the

required workspace fits in the workspace of the scaled parallel mechanism the scaling factor is systematically reduced to find the closest fit.

To determine if the required workspace fits inside the parallel mechanism workspace MATLAB checks fixed points on the required workspace against points in the parallel mechanism workspace. It can be seen in the results of the preliminary workspace study that the boundaries of all of the mechanism workspaces are characterized by smooth curves on the bottom portion of the workspace and generally more complex curves on the top portion of the workspace (Figure 5.4 and Figure D.1 through Figure D.27). From an examination of these workspace plots it is determined that if the top and bottom faces of the required workspace are within the parallel mechanism workspace the entire required workspace is within the parallel mechanism workspace.

Nine points on each the top and bottom plane of the required workspace (Figure 5.5) are checked against the parallel mechanism workspace. If all 18 points can simultaneously be within the parallel mechanism workspace MATLAB considers the parallel mechanism big enough to accommodate the required workspace. In some rare cases it is possible for the 9 test points on the top face of the required workspace to be within the parallel mechanism workspace without the entire top face of the required workspace being within the parallel mechanism workspace. Dramatically increasing the number of test points could eliminate this possibility, but the resulting increase in computation time is prohibitive. To guard against this potential problem, and to provide a double check of the output a plot of the intersection of the parallel mechanism workspace and the top face and bottom face of the required workspace is produced and visually inspected.

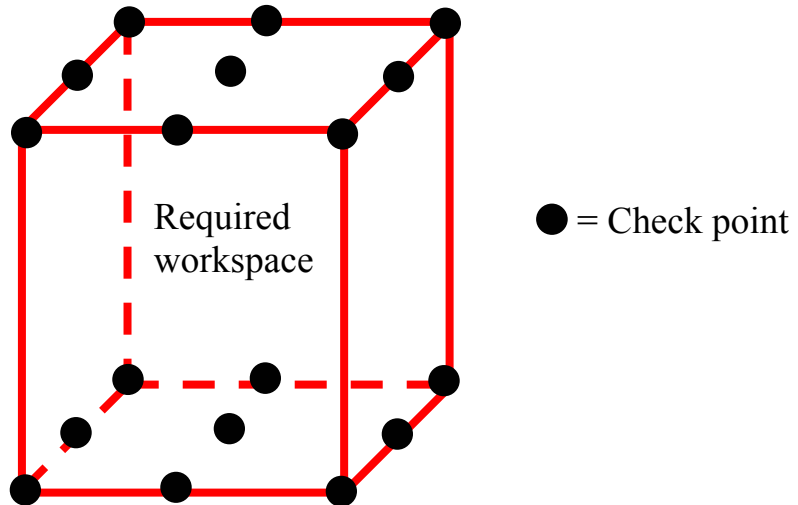


Figure 5.5: Check points on the top and bottom face of the required workspace.

The qualitative workspace study shows that parallel mechanisms with d larger than l and $(c-e)$ near 0 have the most promising workspace shapes. For the first round of the quantitative workspace study a wide range of parameter values with these properties are examined. Calculations of the optimum scaling factor, the resulting dimensioned parameters, and the equivalent length are carried out for the parameter values $l = 1, d = 1, 1.5, \text{ or } 2$, and $(c-e) = 0.75, 0.5, 0.25, 0, -0.25, -0.5, \text{ or } -0.75$. The results are shown in Table 5.5.

Table 5.5: First set of results for secondary workspace study.

Unscaled Dimensions			Scaling Factor (in)	Scaled Dimensions (in)			Equivalent Length
l	$(c-e)$	d		l	$(c-e)$	d	
1	0.75	1	48	48	36	48	222
1	0.75	1.5	30	30	22.5	45	151.5
1	0.75	2	21.6	21.6	16.2	43.2	118.2
1	0.5	1	42	42	21	42	183
1	0.5	1.5	26.4	26.4	13.2	39.6	126
1	0.5	2	19.2	19.2	9.6	38.4	99.6
1	0.25	1	37.2	37.2	9.3	37.2	152.1
1	0.25	1.5	24	24	6	36	108
1	0.25	2	19.2	19.2	4.8	38.4	97.2
1	0	1	33.6	33.6	0	33.6	140.4
1	0	1.5	21.6	21.6	0	32.4	103.2
1	0	2	19.2	19.2	0	38.4	102
1	-0.25	1	32.4	32.4	-8.1	32.4	143.7
1	-0.25	1.5	20.4	20.4	-5.1	30.6	102.9
1	-0.25	2	19.2	19.2	-4.8	38.4	106.8
1	-0.5	1	30	30	-15	30	141
1	-0.5	1.5	22.8	22.8	-11.4	34.2	120
1	-0.5	2	22.8	22.8	-11.4	45.6	131.4
1	-0.75	1	28.8	28.8	-21.6	28.8	142.8
1	-0.75	1.5	26.4	26.4	-19.8	39.6	144.6
1	-0.75	2	24	24	-18	48	144

In Table 5.5 the three lowest equivalent lengths are highlighted. All three of these equivalent lengths correspond to sets of unitless parameters with $l = 1$ and $d = 2$. They have $(c-e)$ values of 0.5, 0.25 and 0. The second round of the quantitative workspace study focuses on unitless parameter values near these. Calculations of the optimum scaling factor, the resulting dimensioned parameters, and the equivalent length are carried out for the parameter values $l = 1$, $d = 1.75, 2$, or 2.25 , and $(c-e) = 0.1, 0.2, 0.3, 0.4, 0.5$, or 0.6 . The results are shown in Table 5.6.

Table 5.6: Results from round two of quantitative workspace study.

Unscaled Parameters			Scaling Factor (in)	Scaled Dimensions (in)			Equivalent Length (in)
l	$(c-e)$	d		l	$(c-e)$	d	
1	0.6	1.75	22.8	22.8	13.7	39.9	116.0
1	0.6	2	20.4	20.4	12.2	40.8	108.2
1	0.6	2.25	19.8	19.8	11.9	44.55	109.8
1	0.5	1.75	21.6	21.6	10.8	37.8	107.4
1	0.5	2	19.2	19.2	9.6	38.4	99.6
1	0.5	2.25	19.8	19.8	9.9	44.55	107.9
1	0.4	1.75	21	21	8.4	36.75	102.2
1	0.4	2	19.2	19.2	7.7	38.4	97.7
1	0.4	2.25	18.6	18.6	7.4	41.85	99.1
1	0.3	1.75	19.8	19.8	5.9	34.65	94.1
1	0.3	2	18.6	18.6	5.6	37.2	93.4
1	0.3	2.25	19.2	19.2	5.8	43.2	101.0
1	0.2	1.75	19.8	19.8	4.0	34.65	96.1
1	0.2	2	18.6	18.6	3.7	37.2	95.3
1	0.2	2.25	18.6	18.6	3.7	41.85	99.9
1	0.1	1.75	19.2	19.2	1.9	33.6	95.3
1	0.1	2	18.6	18.6	1.9	37.2	97.1
1	0.1	2.25	18.6	18.6	1.9	41.85	101.8
1	0	1.75	19.2	19.2	0.0	33.6	97.2
1	0	2	18.6	18.6	0.0	37.2	99.0
1	0	2.25	18.6	18.6	0.0	41.85	103.7
1	-0.1	1.75	19.2	19.2	-1.9	33.6	99.1
1	-0.1	2	19.2	19.2	-1.9	38.4	103.9
1	-0.1	2.25	18.6	18.6	-1.9	41.85	105.5

In Table 5.6 the four lowest equivalent length scores are highlighted. There are many other equivalent length scores however, that are not much higher than these scores. When the equivalent length scores are this close it is difficult to determine which set of parameters is best. Some of the scaled parameters in Table 5.6 are specified to 0.01 in. The MATLAB programs written for this study are not capable of accurately determining the optimum scaled dimensions with this precision. To simplify the specification of robot parameters and to reduce the effect of the resolution of the MATLAB programs on the optimization process all scaled parameters are rounded and the equivalent lengths are

recalculated. Each parameter is rounded in the direction that increases the volume of the parallel mechanism workspace. It is know from the qualitative workspace study that this will occur when l and d are rounded up, while $(c-e)$ is rounded down. Rounding the scaled parameters from Table 5.6 and re-calculating the equivalent lengths leads to Table 5.7

Table 5.7: Rounded results from round two of quantitative workspace study.

Unscaled Parameters			Scaling Factor (in)	Scaled & Rounded Parameters (in)			Equivalent Length (in)
l	$(c-e)$	d		l	$(c-e)$	d	
1	0.6	1.75	22.8	23	13	40	116
1	0.6	2	20.4	21	12	41	110
1	0.6	2.25	19.8	20	11	45	110
1	0.5	1.75	21.6	22	10	38	108
1	0.5	2	19.2	20	9	39	102
1	0.5	2.25	19.8	20	9	45	108
1	0.4	1.75	21	21	8	37	102
1	0.4	2	19.2	20	7	39	100
1	0.4	2.25	18.6	19	7	42	100
1	0.3	1.75	19.8	20	5	35	96
1	0.3	2	18.6	19	5	38	96
1	0.3	2.25	19.2	20	5	44	105
1	0.2	1.75	19.8	20	3	35	98
1	0.2	2	18.6	19	3	38	98
1	0.2	2.25	18.6	19	3	42	102
1	0.1	1.75	19.2	20	1	34	99
1	0.1	2	18.6	19	1	38	100
1	0.1	2.25	18.6	19	1	42	104
1	0	1.75	19.2	20	0	34	100
1	0	2	18.6	19	0	38	101
1	0	2.25	18.6	19	0	42	105
1	-0.1	1.75	19.2	20	-1	34	101
1	-0.1	2	18.6	19	-1	38	102
1	-0.1	2.25	18.6	19	-1	42	106

In Table 5.7 two sets of unscaled parameters are tied for the lowest equivalent length. Both of these sets of unitless parameters have $l = 1$ and $(c-e) = 0.3$. One of them has $d = 1.75$, while the other has $d = 2$. The next lowest equivalent length score is shared by two sets of unscaled parameters with $l = 1$ and $(c-e) = 0.2$. One of them has $d = 1.75$, while the other has $d = 2$. The third and final round of the quantitative workspace study focuses on unscaled parameter values near these. Calculations of the optimum scaling factor, the resulting dimensioned and rounded parameters, and the equivalent length are carried out for the parameter values $l = 1$, $d = 1.6, 1.7, 1.8, 1.9, 2$ or 2.1 , and $(c-e) = 0.2$ or 0.3 . The results are shown in Table 5.8. Two sets of parameters tied for the lowest equivalent length score. Both provide good proportions for the robot, but the set of parameters with $l = 19$ in, $(c-e) = 3$ in and $d = 34$ in is chosen for the parallel mechanism because a reduction in d from 36 in to 34 in is deemed more important than an increase in $(c-e)$ from 3 in to 5 in.

Table 5.8: results of final round of quantitative workspace study.

Unscaled Parameters			Scaling Factor (in)	Rounded & Scaled Parameters (in)			Equivalent Length (in)
l	$(c-e)$	d		l	$(c-e)$	d	
1	0.2	1.6	0.146667	22	4	34	96
1	0.2	1.7	0.138333	20	3	34	91
1	0.2	1.8	0.1275	19	3	34	88
1	0.2	1.9	0.126667	19	3	35	89
1	0.2	2	0.126667	19	3	37	91
1	0.2	2.1	0.125833	19	3	39	93
1	0.3	1.6	0.1525	22	6	36	96
1	0.3	1.7	0.140833	21	6	35	92
1	0.3	1.8	0.133333	20	5	35	90
1	0.3	1.9	0.13	19	5	36	88
1	0.3	2	0.129167	19	5	38	90
1	0.3	2.1	0.126667	19	5	39	91

5.5 Range of Motion

In this section the range of motion of the moving platform and range of motion of the joints of the parallel mechanism are presented. The range of motion required by each joint dictates how each joint and each link of the parallel mechanism can be constructed. The range of motion of the moving platform dictates how the wrist should be attached to the moving platform and where the fixed portion of the parallel mechanism should be mounted with respect to the conveyor belt and shackle line.

The range of motion of the moving platform is given as an output of the MATLAB programs used in the previous section and is given in Table 5.9 where the origin is at the center of the base.

Table 5.9: Location and range of mechanism workspace.

	X Direction	Y Direction	Z Direction
Max \overline{OE}	-9 in	-15 in	-46 in
Min \overline{OE}	9 in	15 in	-16 in

The range of joint angles experienced by the arms of a parallel mechanism with $l = 19$ in, $(c-e) = 3$ in, $d = 34$ in are determined by the MATLAB program JointRange.m. The program examines a large number of points within the range of motion of the moving platform. For each of these points it calculates the θ_{1i} , θ_{2i} , ρ_{3i} , and θ_{4i} values of each arm (Figure 4.16 and Figure 4.17). The range of values observed for each of these angles is presented in Table 5.10.

Table 5.10: Range of joint angles for parallel mechanism.

	θ_{1i}	θ_{2i}	ρ_{3i}	θ_{4i}
Max Angle	94°	168°	31°	103°
Min. Angle	-71°	25°	-31°	2°
Δ Angle	165°	113°	62°	101°

5.6 Wrist Vectors \overline{FG} and \overline{EF}

Figure 5.6 shows the two vectors that are specified in this section.

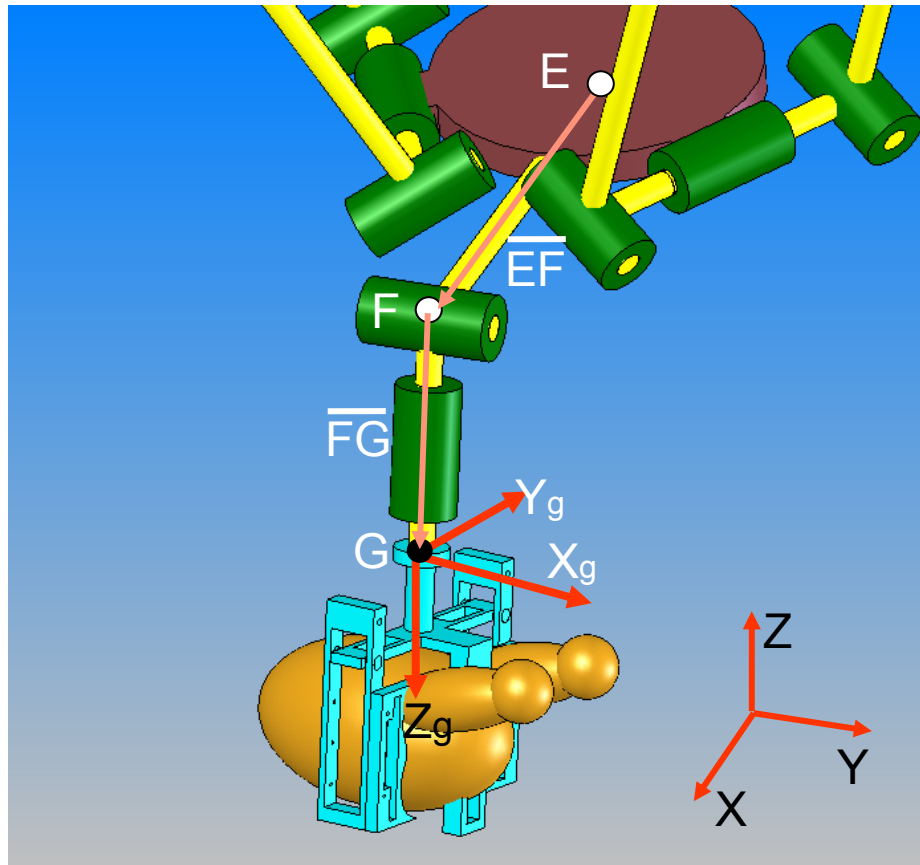


Figure 5.6: Wrist vectors.

The vector \overline{FG} is tentatively selected to be $\overline{FG} = [0 \quad 0 \quad 1.5 \text{ in}]^T$ in the $X_g Y_g Z_g$ coordinate frame. The specialized end effector testing carried out by Coquemond [26] and Celton [27] shows that WOGs can be successfully hung if $\overline{FG} = [0 \quad 0 \quad 3 \text{ in}]^T$, but it is believed that $\overline{FG} = [0 \quad 0 \quad 1.5 \text{ in}]^T$ also acceptable. If $\overline{FG} = [0 \quad 0 \quad 1.5 \text{ in}]^T$ works, it is preferable to $\overline{FG} = [0 \quad 0 \quad 3 \text{ in}]^T$ in two ways. It appears that if $\overline{FG} = [0 \quad 0 \quad 3 \text{ in}]^T$ the end effector may hit the conveyor belt during some WOG release scenarios. With $\overline{FG} = [0 \quad 0 \quad 1.5 \text{ in}]^T$ this is not a concern. In addition, the moments required of the *Flip* motion generating actuator are decreased with the decrease in the length of \overline{FG} . This tentative selection of vector \overline{FG} is tested in the following chapter.

The vector \overline{EF} must be chosen such that the robot does not interfere with the shackle line or conveyor belt, and should be chosen to have as small a length as is practical. It is sufficient for vector \overline{EF} to have no components in the global Y and Z directions. There are no external constraints on the motion of the robot in the Y direction and the only external constraints on the motion of the robot in the Z direction is the conveyor belt and the short wall that surrounds the conveyor belt (about 5 in tall). when \overline{EF} has no component in the Z direction all parts of the parallel mechanism are at or above the level of the center of the wrist. Since the end effector is about 9 in tall and \overline{FG} is 1.5 inches in the Z_g direction the center of the wrist is 10.5 in above the conveyor belt during WOG acquisition. During WOG release the center of the wrist is about 13 in above the conveyor belt for the case when the WOG is acquired in a breast down position (Figure 4.21) and is about 26 in above the conveyor belt for the case when the WOG is

acquired in a breast up position (Figure 4.20). Therefore, the robot always has adequate clearance to avoid the conveyor belt and the short wall surrounding it.

The component of vector \overline{EF} in the global X direction must be non-zero. The elbows of the arms of the parallel mechanism jut out beyond the base and moving platform (Figure 5.7). These elbows limit how close the robot base can be placed to the shackle line. The center of the wrist must therefore be offset in the global X direction from the center of the moving platform to achieve the required workspace. The X component of \overline{EF} is chosen such that the center of the wrist is above the center of the required workspace when the moving platform is in the center of the parallel mechanism workspace.

Figure 5.7 is a top view of the parallel mechanism when all $\theta_{1i} = 0^\circ$. To simplify the illustration the lower links of the parallel mechanism are not shown. To keep the arms of the parallel mechanism away from the shackle line the centers of the elbows (L_i) are constrained to be at least 6 in away from the vertical plane passing through the shackle line. It is assumed that the arms of the robot will be operated in the elbows-out configuration, and that the ρ_{0i} parameters are $\rho_{01} = -60^\circ$, $\rho_{02} = 60^\circ$, and $\rho_{03} = 180^\circ$. The arms of the parallel mechanism come closest to the shackle line when $\theta_{11} = 0^\circ$, or when $\theta_{12} = 0^\circ$. Examining arm one in Figure 5.7 it can be seen that for L_1 to be 6 in from the shackle line when $\theta_{11} = 0^\circ$ the center of the base (Point O) must be 6 in + $(c+l)\cos(\rho_{01})$ from the shackle line in the X direction (Figure 5.8).

Recall that the required workspace is 18 in wide in the X direction and is bounded by the shackle line and the edge of the conveyor belt. The center of the required

workspace in the X direction is then 9 in from the shackle line as labeled in Figure 5.7. The center of the parallel mechanism workspace is directly beneath the center of the base so the X component of \overline{EF} must be the difference between the X coordinates of the center of the required workspace and the center of the base:

$$\overline{EF} = [(c+l)\cos(\rho_{01}) - 3 \text{ in} \quad 0 \quad 0]^T \quad (5.2)$$

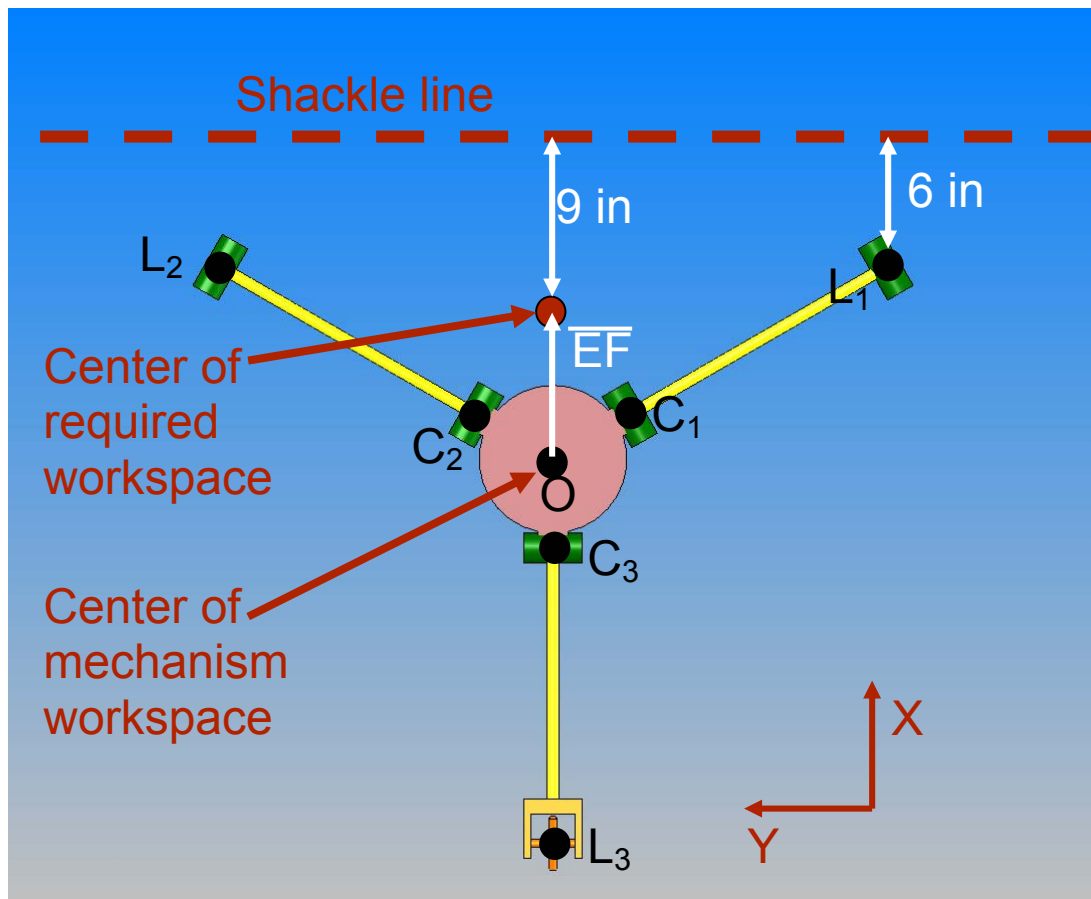


Figure 5.7: Top view schematic of parallel mechanism and shackle line for $\theta_{11} = \theta_{12} = \theta_{13} = 0^\circ$ (lower links not shown).

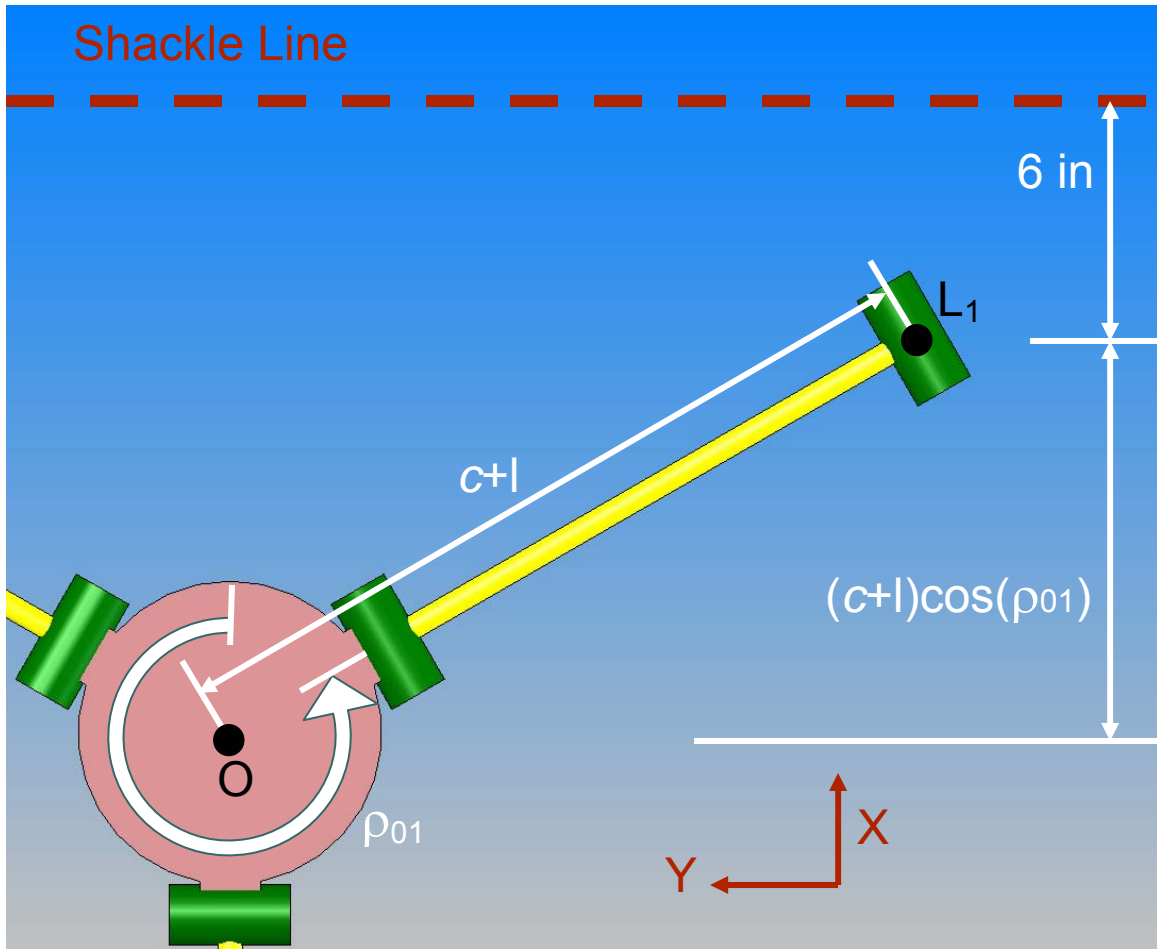


Figure 5.8: Top view of arm one and shackle line for $\theta_{11} = 0^\circ$ (lower links not shown).

5.7 Conclusion

In this chapter many of the robot parameters are determined. Based on a 1.875 ft x 2.5 ft x 2.5 ft required translational workspace the parallel mechanism parameters are chosen to be $\rho_{01} = -60^\circ$, $\rho_{02} = 60^\circ$, $\rho_{03} = 270^\circ$ (Figure 5.1), $(c-e) = 3$ in, $l = 19$ in and $d = 34$ in (Figure 5.2). Based on the motion used in the testing and design of a specialized end effector for picking up WOGs, the vector from the center of the wrist to the connection point of the end effector is chosen to be $\overline{FG} = [0 \quad 0 \quad 1.5 \text{ in}]^T$ in the

$X_g Y_g Z_g$ coordinate frame (Figure 5.6). To keep the arms of the parallel mechanism from interfering with the shackle line the center of the wrist is offset from the center of the moving platform by the vector $\overline{EF} = [(c + l) \cos(\rho_{01}) - 3 \text{ in} \quad 0 \quad 0]^T$ (global coordinate frame). This concludes the embodiment design. In the following chapter the detail design begins. The robot is modeled and many details of the design are determined.

CHAPTER 6

MODELING AND DETAIL DESIGN

6.1 Introduction

In this chapter the robot is modeled and details of the design are determined. In the previous chapters the dimensions, workspace, and joint types used in the robot are determined. This chapter focuses on realizing the robot in a way that is practical, inexpensive and USDA Compliant. In this chapter a series of design prototypes are generated and analyzed. The prototypes serve two purposes: i) they will show the developed concept and solution are feasible and ii) they identify constructability issues and solutions.

In Section 6.2 the generation of a proof of concept mockup is documented. The mockup is full size, non-actuated, and constructed of wood. It demonstrates the workspace, demonstrates the motion of the wrist, and reveals constructability issues. Section 6.2.1 presents several constructability and the resulting design decisions. Section 6.2.2 presents the testing and analysis of the mockup.

In Section 6.3 the primary construction materials and joint construction guidelines are presented.

In Section 6.4 a dynamic model of the robot is developed in two parts. In Section 6.4.1 the dynamic model of the wrist is developed. The dynamic model of the parallel mechanism is developed in 6.4.2 .

In Section 6.5 the dynamic model used to simulate the performance of a series of design prototypes. These are used to improve the design until a feasible prototype is developed. Sections 6.5.1 and 6.5.2 define the simulation tasks using two simple motion planning strategies. Section 6.5.3 explains the procedure for generating a CAD model and determining the mass and rotational inertia of the prototype components. Prototypes are generated, tested and analyzed in Sections 6.5.4 , 6.5.5 , and 6.5.6 .

Section 6.6 presents preliminary actuator selections while Section 6.7 presents a simple cost analysis of the final prototype.

6.2 Proof of Concept Mockup

The proof of concept mockup has realistic kinematics but is not built to have the required materials, actuation, strength, reliability, or compliance with USDA regulations. The mockup serves two purposes. It confirms the predicted robot behavior and it identifies constructability issues.

For simple and inexpensive construction the mockup is built primarily out of wood. The radius of the base and moving platform are chosen to be $c = 9$ in and $e = 6$ in. As determined in Section 5.4.2 $l = 19$ in and $d = 34$ in and as determined in Section 5.6 $\|\overline{FG}\| = 1.5$ in. From equation (5.2) $\overline{EF} = [11 \text{ in} \quad 0 \quad 0]^T$. These vectors and

lengths are illustrated in Figure 4.7 and Figure 5.6. Where possible, pre-fabricated hinges are used for revolute kinematic pairs.

6.2.1 Constructability Issues

The proof of concept model reveals two significant constructability issues: i) the availability of an acceptable spherical (S) kinematic pair, ii) attaching the arms of the parallel mechanism to maintain the kinematic symmetry of the parallel mechanism.

A review of available stainless steel spherical joints reveals that they have insufficient range of motion for use at point D_3 of the robot (Figure 6.1). They provide 360° of rotation about one axis but no more than 33° normal to this axis. As shown in Table 5.10, the required rotations are 101° of rotation about one axis and 62° normal to this. A spherical motion generator with a larger range of motion is constructed by connecting a universal joint in series with a revolute whose axis passes through the universal joint center (Figure 6.2). This provides full rotation about the revolute joint and nearly 180 (deg) of rotation about all axes perpendicular to it. The spherical motion is about the point at which all three axes, shown as black dashed lines, of the device intersect, the center of the universal joint. This device is used at point D_3 .

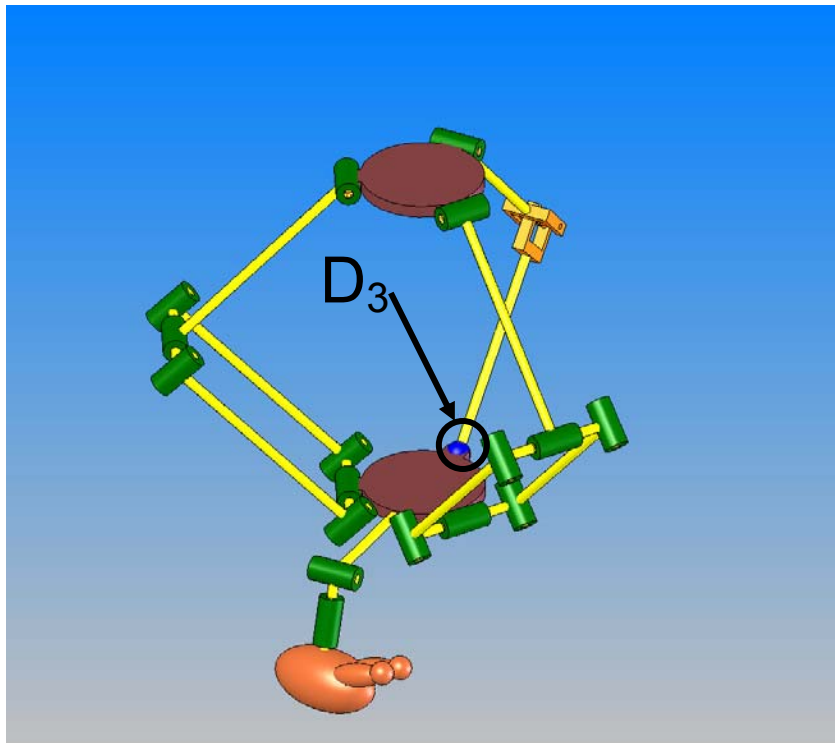


Figure 6.1: Spherical joint at point D_3

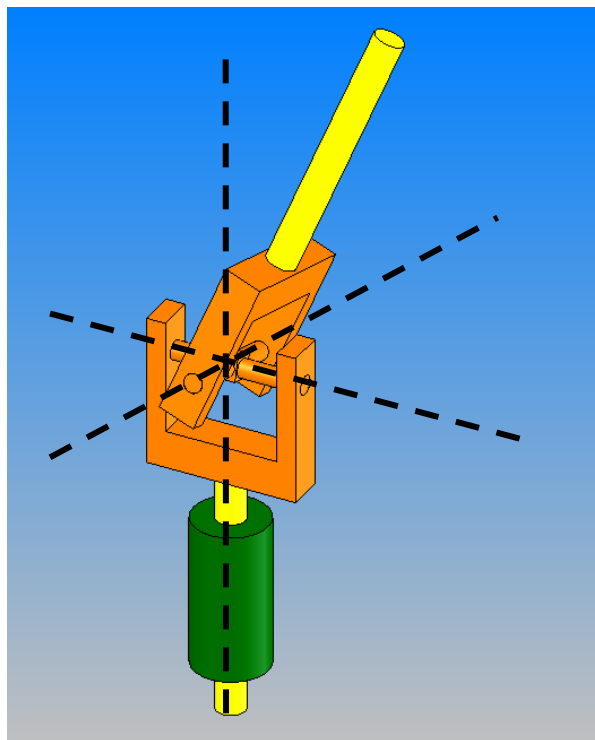


Figure 6.2: Spherical motion generator made from a revolute pair and a universal joint.

In the kinematic design it is assumed that the {D} generating arm is attached to the moving platform with the center of the spherical motion generator at point D_3 , a point on the moving platform that is $\overline{ED_3} = e[\cos(\rho_{03}) \quad \sin(\rho_{03}) \quad 0]^T$ (global coordinate frame) from the center of the moving platform, where e is illustrated in Figure 5.2 and ρ_{03} is illustrated in Figure 5.1. In practice there is some difficulty connecting the spherical motion generator shown in Figure 6.2 such that the center of motion is at D_3 .

Connecting the {D} generating arm to the moving platform is simple if the center of spherical motion is shifted up and inward from D_3 . Figure 6.3 shows how the arms of the proof of concept mockup are connected to the moving platform. To preserve the behavior of the {D} generating arm and to preserve the kinematic symmetry of the parallel mechanism the connection of the top of the {D} generating arm to the base must be shifted the same way. Figure 6.4 shows a regular arm of the parallel mechanism and an arm that has been shifted by the vector \overline{shift} . For the regular arm, tracing a path from the center of the base to the center of the platform via the arm yields the loop equation:

$$\overline{OE} = \overline{OC_i} + \overline{C_iL_i} + \overline{L_iD_i} + \overline{D_iE} \quad (6.1)$$

For the shifted arm the loop equation is:

$$\overline{OE} = \overline{OC_i} + \overline{shift} + \overline{C_iL_i} + \overline{L_iD_i} - \overline{shift} + \overline{D_iE} \quad (6.2)$$

The shifts do not affect the arm because they cancel each other out:

$$\overline{OE} = \overline{OC_i} + \overline{C_iL_i} + \overline{L_iD_i} + \overline{D_iE} + (\overline{shift} - \overline{shift}) \quad (6.3)$$

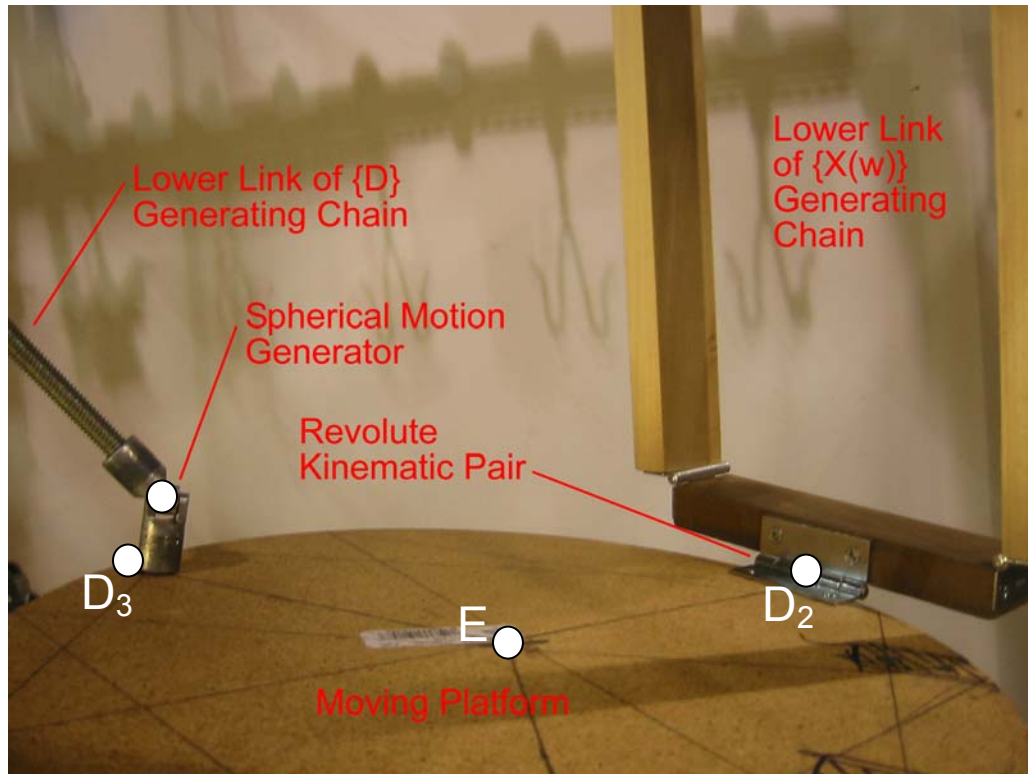


Figure 6.3: Connections of arms and moving platform of the parallel mechanism.

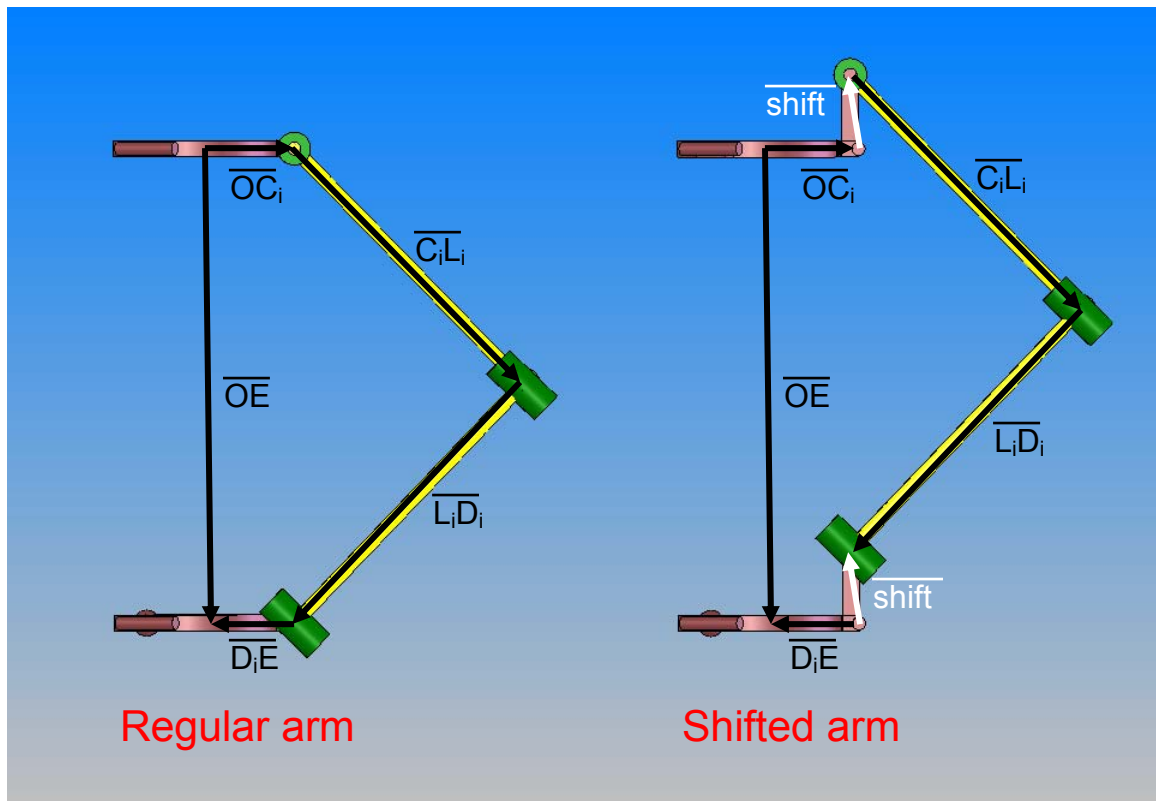


Figure 6.4: Regular arm and shifted arm.

6.2.2 Confirmation of Robot Behavior

Figure 6.5 shows the proof of concept mockup. First the mockup is moved through the required workspace to make sure it is entirely contained in the robot workspace without singularities. The specialized end effector developed by Coquemond [26] and Celton [27] is then used to pick up WOGs and transfer them to a shackle, confirming that this robot geometry will work for all possible starting WOG positions identified in Chapter 2. Figure 6.6 shows the proof of concept model and specialized end effector placing a WOG in a shackle during one of the tests.

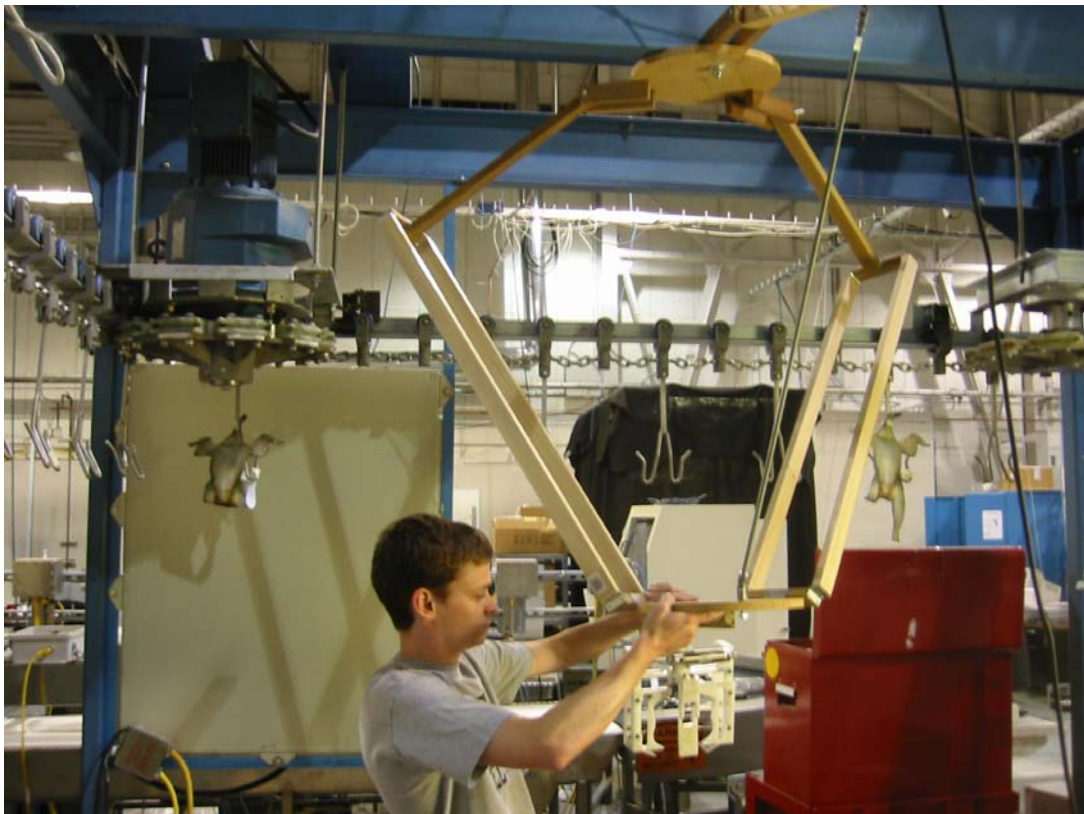


Figure 6.5: Proof of concept model.



Figure 6.6: Proof of concept model and end effector placing a WOG in a shackle.

The proof of concept mockup does not perform as predicted when moments are applied to the moving platform. It does not remain perfectly parallel to the base. The moving platform rotates approximately 5° to 10° from horizontal due to play in the revolute joints of the {X(w)} motion generating arms. This is attributed to loose tolerances and flexing of wood components. This will be eliminated in the final robot by using more rigid materials and tighter tolerances.

6.3 Comments on Materials and Joint Construction

The USDA has strict guidelines about the materials that are appropriate for use in a poultry processing plant. Acceptable metals include 300 series stainless steel, any metal that is at least as corrosion resistant as 300 series stainless steel, and a few types of coated metals. Acceptable non-metals include some types of Delrin, Acetal, high density polyethelene, and Rulon. Certain types of rubber and food grade lubrication are acceptable in some situations, but should be avoided when possible. These non-metals are usually specified as USDA compliant if they are acceptable for use in a meat handling robot. The primary structural materials for the robot are Delrin and 300 series stainless steel. An attempt will be made to use plain bearings, which are more sanitary than other types of bearings because they can be used without lubrication. They are USDA compliant if they are made of high density polyethelene or Rulon 641.

Conventional revolute joints are more appropriate than flexible joints. Flexible joints are susceptible to twisting as well as bending and allow small amounts of rotation

perpendicular to the intended axis of rotation which results in rotations of the moving platform.

The USDA [25] defines a product contact surface as “all surfaces:

- a. Exposed to the product, or
- b. Exposed to the surfaces of the packaging materials which touch the product, or
- c. That touch the surfaces of the packaging materials which touch the product, or
- d. From which liquids or other materials may drain, drop, diffuse or be drawn into the product, or
- e. From which liquids or other materials may drain, drop, diffuse or be drawn onto the surfaces that touch or are exposed to the surfaces of the packaging materials which touch the product.”

Parts in product contact areas must not have sharp internal angles. Soils and product can collect in sharp internal angles and can be difficult to clean during washdown. If any component of the robot has an internal angle of less than 135° it must be rounded to a radius of 1/8 in or larger (Figure 6.7).

Acceptable

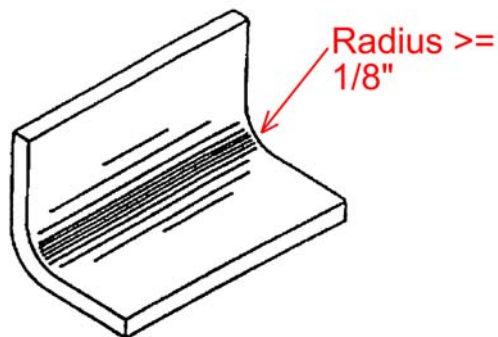


Figure 6.7: Acceptable construction for a part with an internal angle $<135^\circ$.

All shafts in product contact areas must be constructed with grooves to allow easy cleaning as in Figure 6.8.

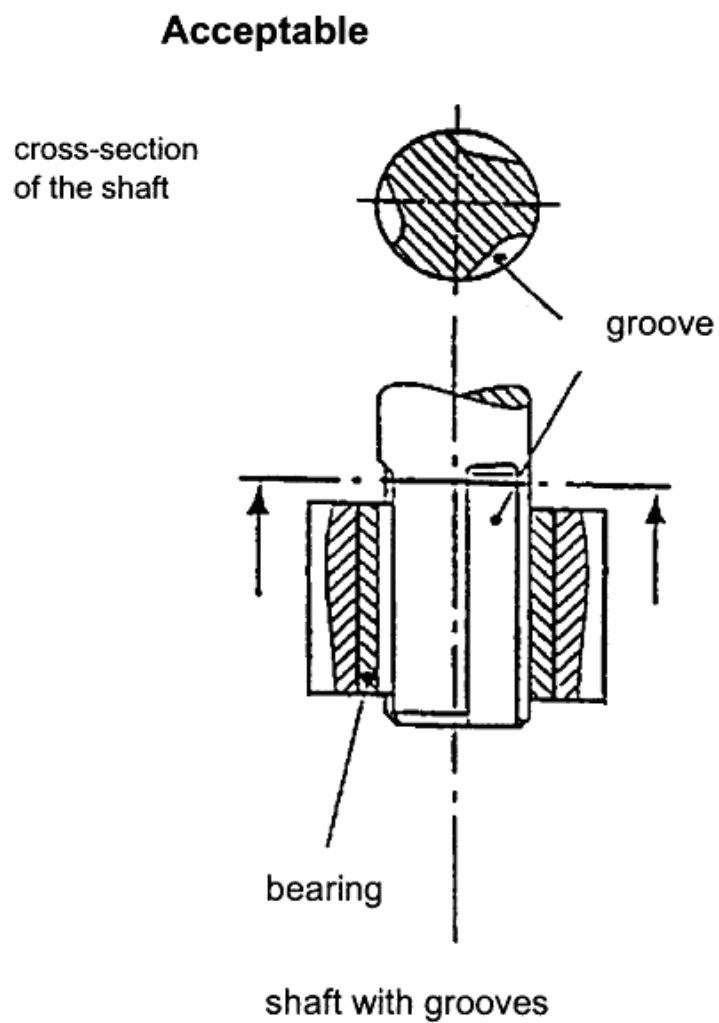


Figure 6.8: Acceptable construction for a shaft in a product contact area.

6.4 Dynamic Model

In this section a dynamic model of the robot is developed. The inputs are the dimensions of the robot, the masses of the robot components, the rotational inertias of the robot components, and a required robot motion. The output of the dynamic model is the moments the actuators must generate to achieve the specified robot motion.

The dynamic model has two parts, a dynamic model of the robot wrist and a dynamic model of the parallel mechanism. The required robot motion is specified as wrist actuator rotations and a required translation of the platform. If the required position \overline{OE} of the moving platform is known as a function of time the angles θ_{li} of the actuators of the parallel mechanism can be determined as a function of time. The angular velocity $\dot{\theta}_{li}$ and angular acceleration $\ddot{\theta}_{li}$ of these actuators can then be found by differentiation of θ_{li} . The quantities that are considered known are: the position \overline{OE} , velocity \bar{v}_E , and acceleration \bar{a}_E of the moving platform of the parallel mechanism; the angular positions θ_{li} , velocities $\dot{\theta}_{li}$, and accelerations $\ddot{\theta}_{li}$ of the parallel mechanism actuators; and the angular positions θ_w, ρ_w , velocities $\dot{\theta}_w, \dot{\rho}_w$, and accelerations $\ddot{\theta}_w, \ddot{\rho}_w$ of the wrist actuators.

6.4.1 Dynamic Wrist Model

The first step in the dynamic analysis is to determine the forces and moments required at the center of the wrist (point F) due to all of the rotating objects connected at

or after the wrist (Figure 6.9). These objects include objects being carried by the robot, such as a WOG, and parts of the robot, such as the *Rotate* actuator. For each of the objects that rotate with the wrist four things must be known: the mass of the object, the position of the center of mass of the object with respect to the center of the wrist (point F), the 3x3 rotational inertia matrix of the object expressed at the center of mass of the object, and whether the object is attached such that it will undergo both the *Flip* (given by θ_w) and the *Rotate* (given by ρ_w) motions, or whether it is attached such that it will only undergo the *Flip* motion. For simplicity, this model assumes the joints are frictionless.

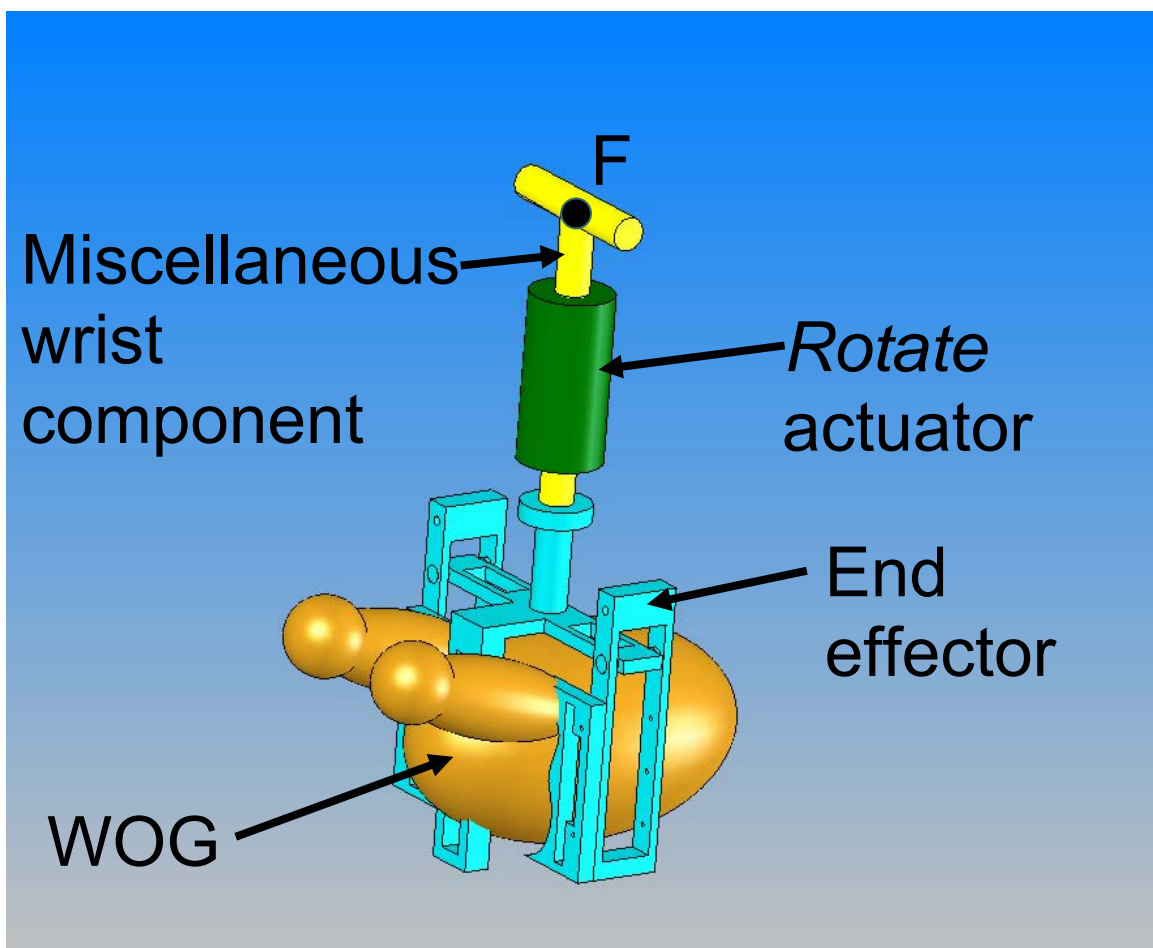


Figure 6.9: Objects rotating with the wrist.

Figure 6.10 shows two coordinate frames that rotate with the wrist. The $X_f Y_f Z_f$ coordinate frame undergoes only the *Flip* motion while the $X_g Y_g Z_g$ coordinate frame undergoes both the *Flip* and *Rotate* motions. The Y_f axis is always parallel to the global Y axis, while the X_f and Z_f axes are aligned with the global X and Z axes only when $\theta_w = 0$. The Z_g axis is always parallel to the Z_f axis, while the X_g and Y_g axes are aligned with the X_f and Z_f axes only when $\rho_w = 0$. The *Flip* motion is a positive rotation of θ_w about the Y_f axis and the *Rotate* motion is a positive rotation of ρ_w about the Z_g axis.

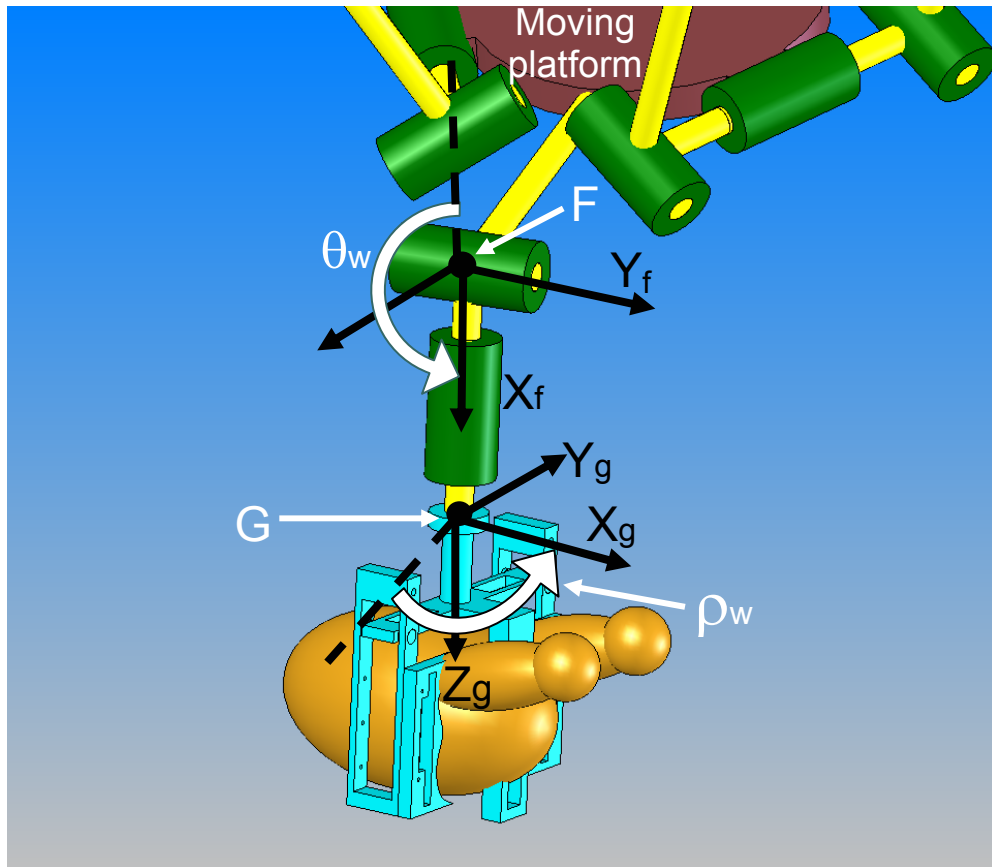


Figure 6.10: Wrist coordinate frames.

If the object is attached to the wrist such that it only undergoes the *Flip* motion the angular velocity ($\bar{\omega}_o$) and angular ($\bar{\alpha}_o$) acceleration are given by

$$\bar{\omega}_o = \dot{\theta}_w \bar{Y}_f \quad (6.4a)$$

$$\bar{\alpha}_o = \ddot{\theta}_w \bar{Y}_f \quad (6.5a)$$

If the object is attached to the wrist such that it undergoes both the *Flip* and *Rotate* motions the angular velocity and angular acceleration are given by

$$\bar{\omega}_o = \dot{\theta}_w \bar{Y}_f + \dot{\rho}_w \bar{Z}_f \quad (6.4b)$$

$$\bar{\alpha}_o = \dot{\theta}_w \dot{\rho}_w \bar{X}_f + \ddot{\theta}_w \bar{Y}_f + \ddot{\rho}_w \bar{Z}_f \quad (6.5b)$$

The forces and moments that the wrist must produce to achieve the required rotation are determined by independently examining each object that rotates with the wrist. Each object undergoes either the *Flip* motion or both the *Flip* and *Rotate* motions of the wrist. For each object the moments and forces required to achieve that motion are calculated. The forces and moments that the wrist must produce are calculated by summing the forces and moments required by the individual objects.

The motion of each object (Figure 6.11) is governed by the force and moment balance equations expressed below.

$$\Sigma \bar{F}_o = m_o \bar{\alpha}_o \quad (6.6)$$

$$\Sigma \bar{M}_o = I_o \bar{\alpha}_o + \bar{\omega}_o \times I_o \bar{\omega}_o \quad (6.7)$$

where $\Sigma \bar{F}_O$ is the sum of the forces exerted on the object, m_o is the mass, \bar{a}_o is the acceleration of the center of mass, $\Sigma \bar{M}_O$ is the sum of the moments exerted on the object at the center of mass, and I_o is the three by three rotational inertia matrix.

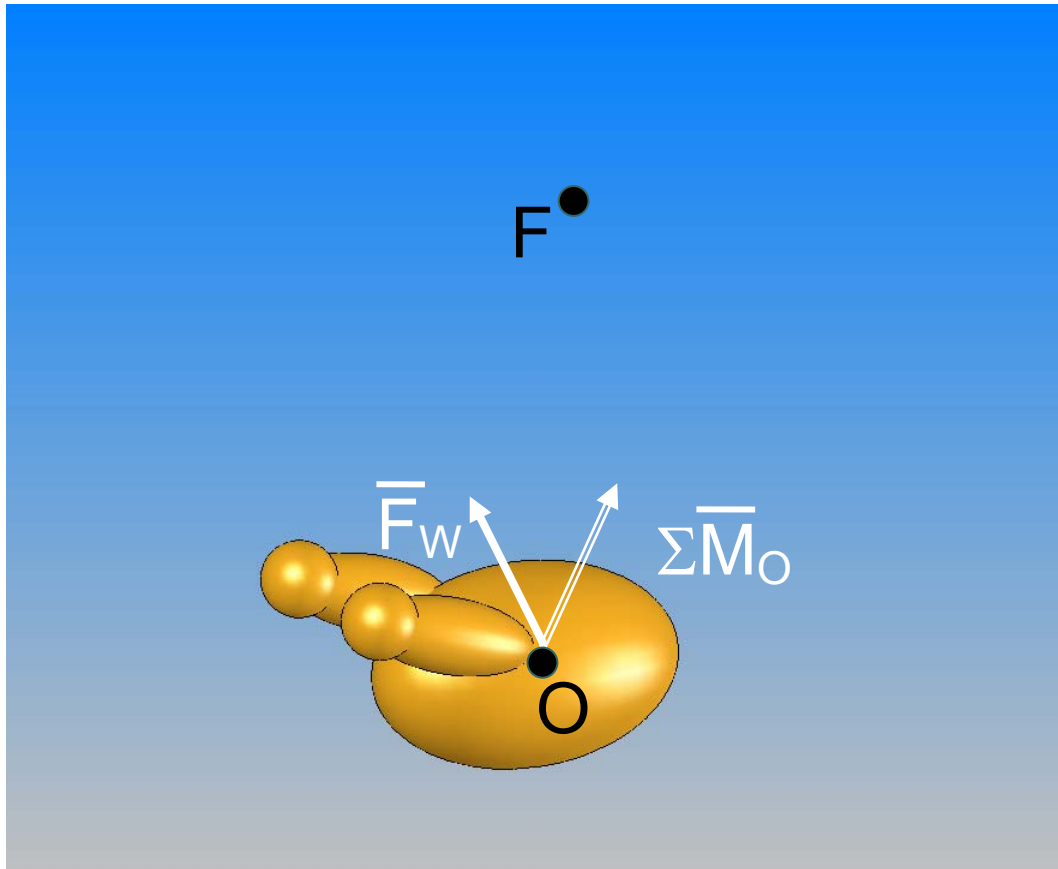


Figure 6.11: One moving object, required moment and force at center of mass.

The required wrist force is found by breaking $\Sigma \bar{F}_O$ up into the forces provided by the wrist and the force exerted by gravity.

$$\bar{F}_w = m_o \bar{a}_o - m_o \bar{g} \quad (6.8)$$

The acceleration of the center of mass of the object is given by

$$\bar{a}_o = \bar{a}_F + \bar{\alpha}_O \times \bar{r}_{FO} + \bar{\omega}_O \times (\bar{\omega}_O \times \bar{r}_{FO}) \quad (6.9)$$

In this equation \bar{a}_F is the acceleration of point F, which is the same as the acceleration of the moving platform (\bar{a}_E). \bar{r}_{FO} is the vector from point F to the center of mass of the object. The required wrist force is therefore:

$$\bar{F}_w = m_o(\bar{a}_F + \bar{\alpha}_o \times \bar{r}_{FO} + \bar{\omega}_o \times (\bar{\omega}_o \times \bar{r}_{FO}) - \bar{g}) \quad (6.10)$$

The required moment at the center of mass of the object is given by equation (6.7). The equivalent moment at the center of the wrist is (Figure 6.13):

$$\bar{M}_w = \Sigma \bar{M}_o + \bar{r}_{FO} \times \Sigma \bar{F}_o = I_o \bar{\alpha}_o + \bar{\omega}_o \times I_o \bar{\omega}_o + \bar{r}_{FO} \times \Sigma \bar{F}_o \quad (6.11)$$

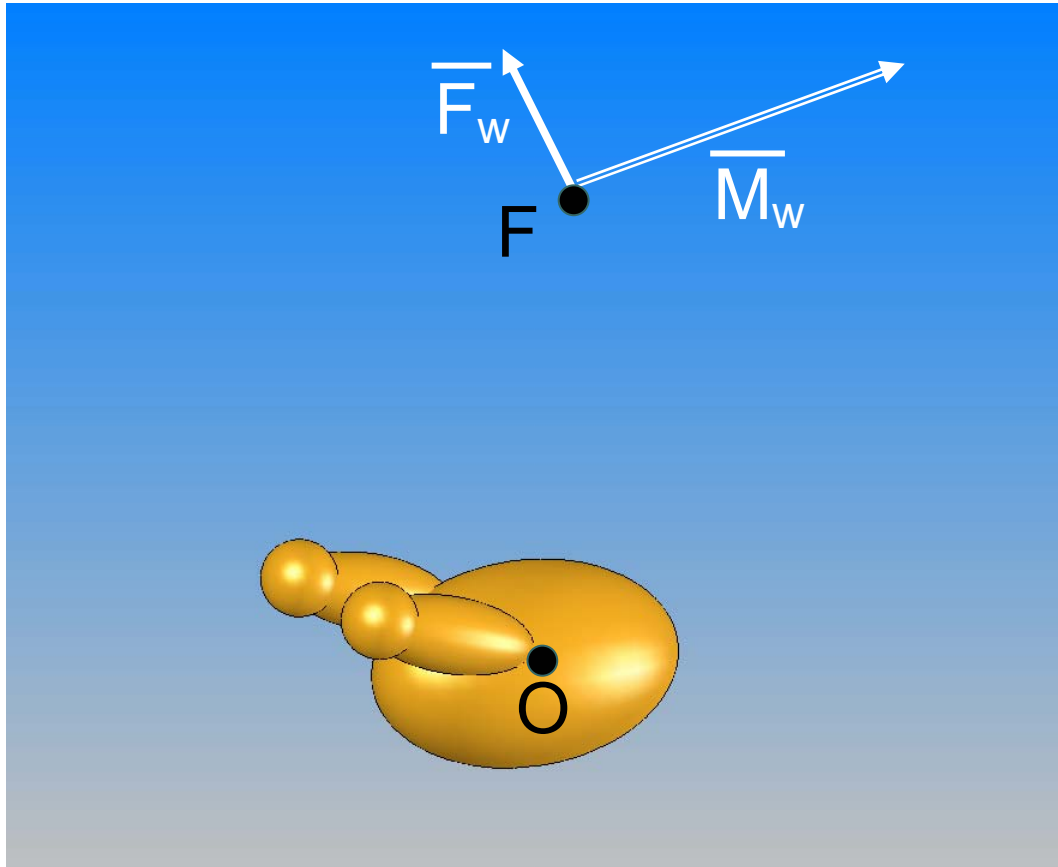


Figure 6.12: One moving object, required moment and force at center of wrist.

At point F the forces and moments required by each object are:

$$\bar{F}_F = \Sigma \bar{F}_w \quad (6.12)$$

$$\bar{M}_F = \Sigma \bar{M}_w \quad (6.13)$$

The moments that the *Flip* and *Rotate* motion generators are required to produce are the components of \bar{M}_F that are along their respective axes. In the following equations M_{θ_w} is the moment provided by the *Flip* motion generator and M_{ρ_w} is the moment provided by the *Rotate* motion generator. The component of \bar{M}_F perpendicular to the axes of the *Flip* and *Rotate* motion generators is provided by the constraints of the wrist.

$$M_{\theta_w} = \bar{M}_F \cdot \bar{Y}_f \quad (6.14)$$

$$M_{\rho_w} = \bar{M}_F \cdot \bar{Z}_f \quad (6.15)$$

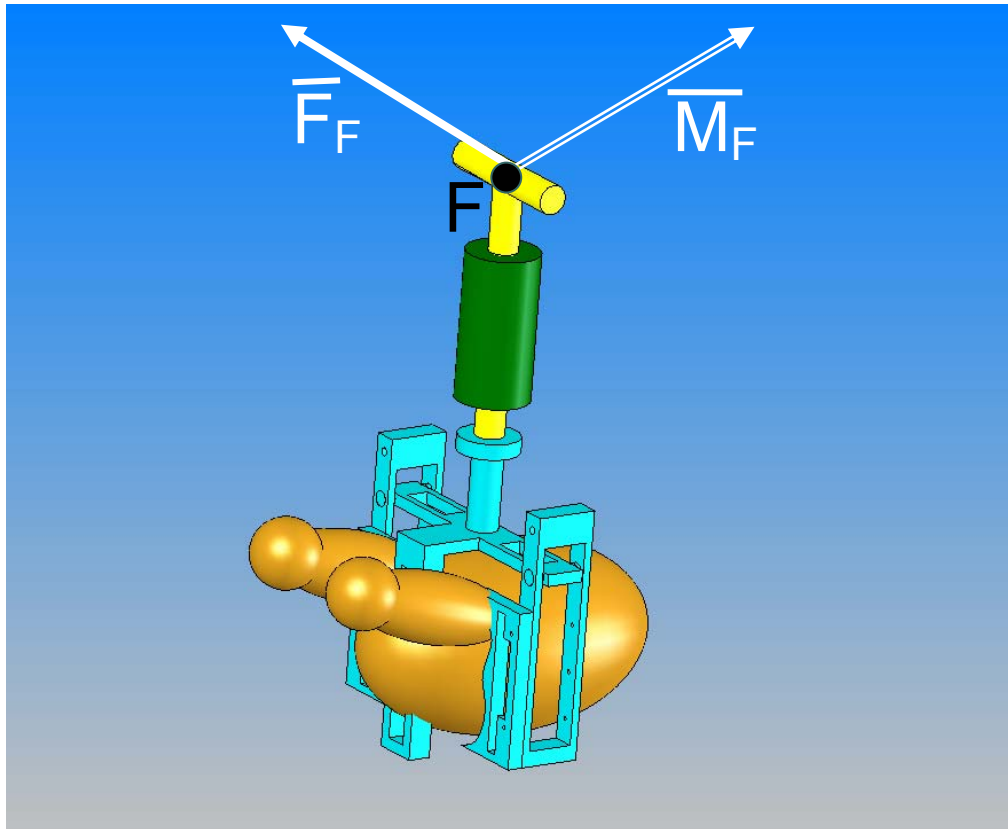


Figure 6.13: Required force and moment at the wrist.

6.4.2 Dynamic Parallel Mechanism Model

To simplify the dynamic model of the parallel mechanism two assumptions are made. First it is assumed that the joints are frictionless. Second, it is assumed that for each arm the mass of the linkage connecting point L_i to point D_i is concentrated at the ends of the linkage. In other words half the mass of the components linking L_i with D_i is assumed to be concentrated at L_i , the elbow of the i th arm, while the other half of the mass is concentrated at D_i , the connection point of the arm and the moving platform. This assumption yields conservative estimates of rotational inertia. As a consequence of the second assumption the forces transmitted by the linkage connecting point L_i to point D_i are along the vector $\overline{L_i D_i}$. Pierrot et al. [24] have used these assumptions to model similar robots.

Motion of the platform and the objects rigidly attached to it (Figure 6.15) is governed by the same force balance equation given in equation (6.6). The acceleration of the moving platform \bar{a}_E is an input of the dynamic model. The forces acting on the moving platform are due to the wrist, the three arms of the parallel mechanism, and gravity (Figure 6.14). The motion of the platform is therefore governed by the following equation.

$$m_E \bar{a}_E = \lambda_1 \overline{LD}_1 + \lambda_2 \overline{LD}_2 + \lambda_3 \overline{LD}_3 - \bar{F}_H + m_E \bar{g} \quad (6.16)$$

In this equation m_E is the summation of the mass of the moving platform, the mass of all objects that are rigidly fixed to the moving platform, and half the masses of the three linkages connecting the L_i points to the D_i points. \overline{LD}_1 , \overline{LD}_2 , and \overline{LD}_3 can be easily found from the known position of the moving platform and the solution to the reverse

kinematic equations while λ_1 , λ_2 , and λ_3 are unknown scaling factors. Solving for λ_1 , λ_2 , and λ_3 leads to the following equation.

$$[\lambda_1 \quad \lambda_2 \quad \lambda_3]^T = [\overline{LD}_1 \quad \overline{LD}_2 \quad \overline{LD}_3]^{-1} (m_E \overline{a}_E + \overline{F}_H - m_E \overline{g}) \quad (6.17)$$

The force that the i th arm of the parallel mechanism must exert at point D_i is then given by the following equation.

$$\overline{F}_i = \lambda_i \overline{LD}_i \quad (6.18)$$

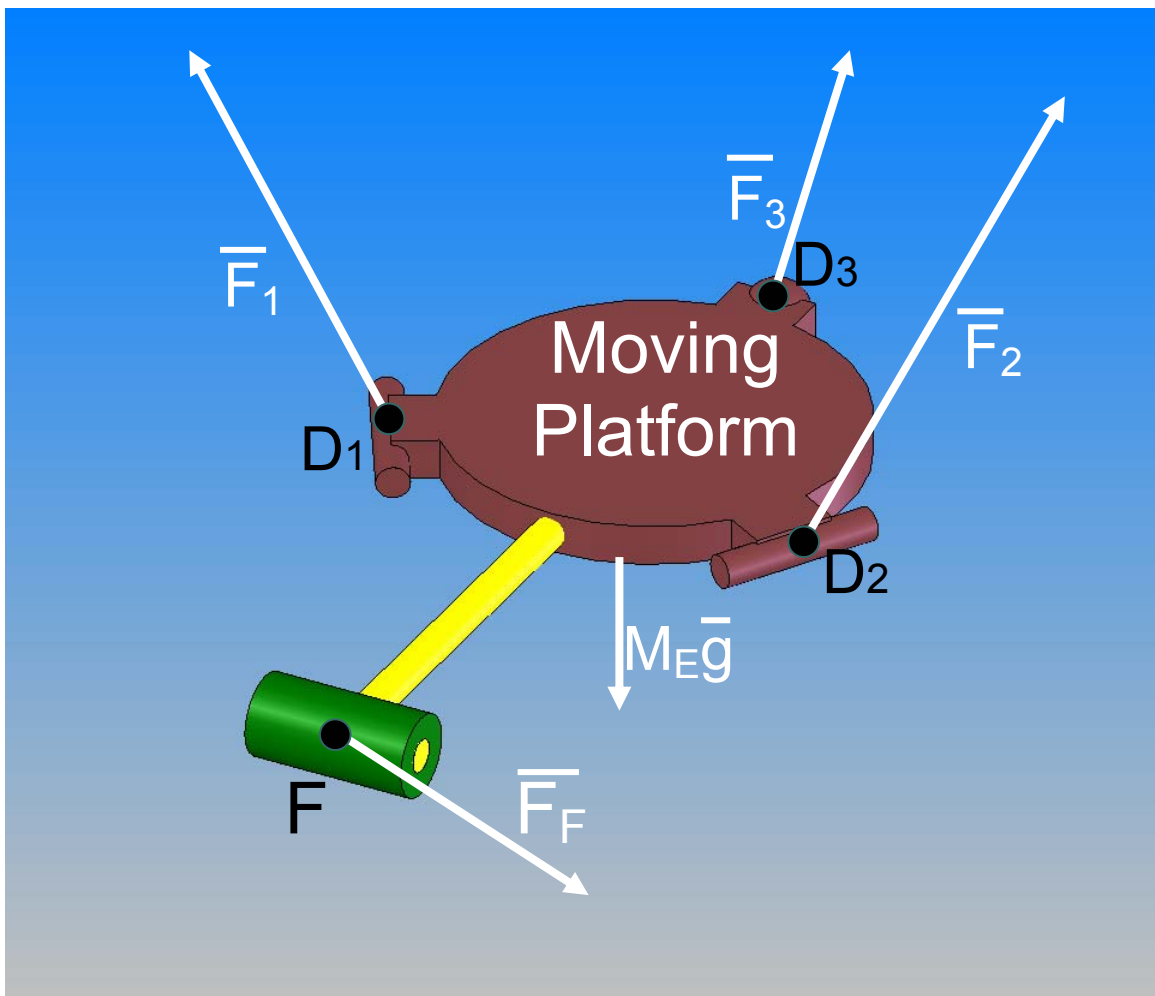


Figure 6.14: Forces acting on the moving platform.

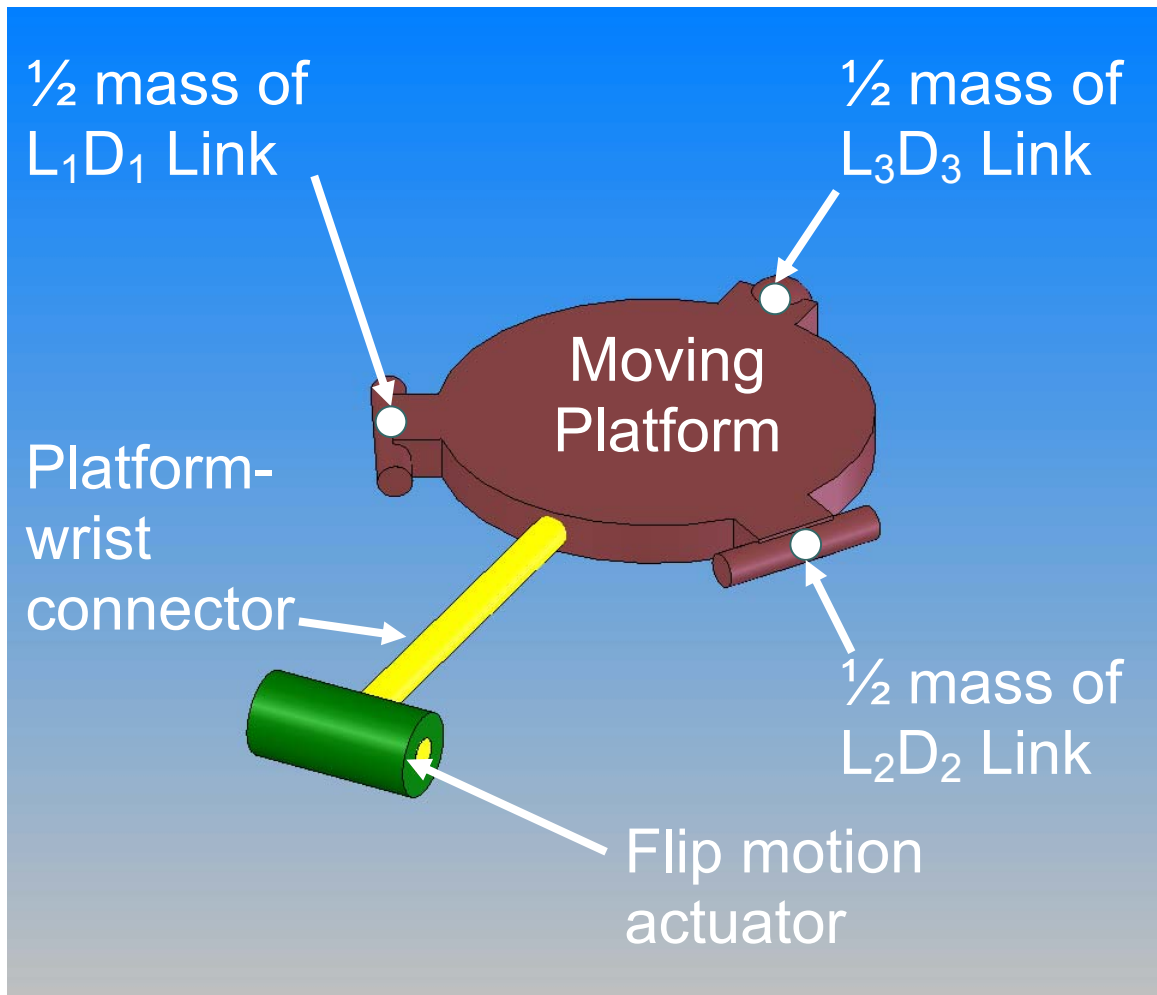


Figure 6.15: Objects included in the platform force balance.

Once \bar{F}_i is determined a moment balance of the upper link of the i th arm can be used to determine the moment required from the actuator at the top of the i th arm (Figure 6.16).

The upper link of the i th arm is the link from point C_i , the center of the actuated joint connecting the i th arm to the base of the parallel mechanism, to point L_i . The motion of the upper link of the i th arm is governed by equation (6.7). Summing the moments about point C_i leads to the following equation.

$$\Sigma \bar{M} = \bar{M}_{C_i} + \bar{C}L_i \times (-\bar{F}_i) = I_{C_i} \bar{\alpha}_{C_i} + W I_{C_i} \bar{\omega}_{C_i} \quad (6.19)$$

Expressing all quantities in the $X_{l_i}Y_{l_i}Z_{l_i}$ coordinate frame and solving for \bar{M}_{C_i} yields

$$\bar{M}_{C_i} = I_{C_i} \begin{bmatrix} 0 \\ \ddot{\theta}_{l_i} \\ 0 \end{bmatrix} + \begin{bmatrix} 0 & 0 & \dot{\theta}_{l_i} \\ 0 & 0 & 0 \\ -\dot{\theta}_{l_i} & 0 & 0 \end{bmatrix} I_{C_i} \begin{bmatrix} 0 \\ \dot{\theta}_{l_i} \\ 0 \end{bmatrix} - \begin{bmatrix} l \\ 0 \\ 0 \end{bmatrix} \times (-\bar{F}_i) \quad (6.20)$$

where

$$I_{C_i} = I_{C_{L_i}} + \frac{m_{L_{D_i}}}{2} \begin{bmatrix} 0 & 0 & 0 \\ 0 & l^2 & 0 \\ 0 & 0 & l^2 \end{bmatrix} \quad (6.21)$$

\bar{M}_{C_i} is the required moment at point C_i . $I_{C_{L_i}}$ is the rotational inertia of the upper link of the i th arm and is expressed at point C_i in the $X_{l_i}Y_{l_i}Z_{l_i}$ coordinate frame. The other quantity on the right hand side of equation (6.21) accounts for the rotational inertia of the point mass that is assumed to be at point L_i . $m_{L_{D_i}}$ is the mass of the linkage connecting point L_i to point D_i . The moment the actuator is required to generate can be found by taking the dot product of \bar{M}_{C_i} and the axis of rotation of the actuator, the Y_{l_i} axis.

$$M_{\theta_{l_i}} = \left(I_{C_i} \begin{bmatrix} 0 \\ \ddot{\theta}_{l_i} \\ 0 \end{bmatrix} + \begin{bmatrix} 0 & 0 & \dot{\theta}_{l_i} \\ 0 & 0 & 0 \\ -\dot{\theta}_{l_i} & 0 & 0 \end{bmatrix} I_{C_i} \begin{bmatrix} 0 \\ \dot{\theta}_{l_i} \\ 0 \end{bmatrix} - \begin{bmatrix} l \\ 0 \\ 0 \end{bmatrix} \times (-\bar{F}_i) \right) \cdot \begin{bmatrix} 0 \\ 1 \\ 0 \end{bmatrix} \quad (6.22)$$

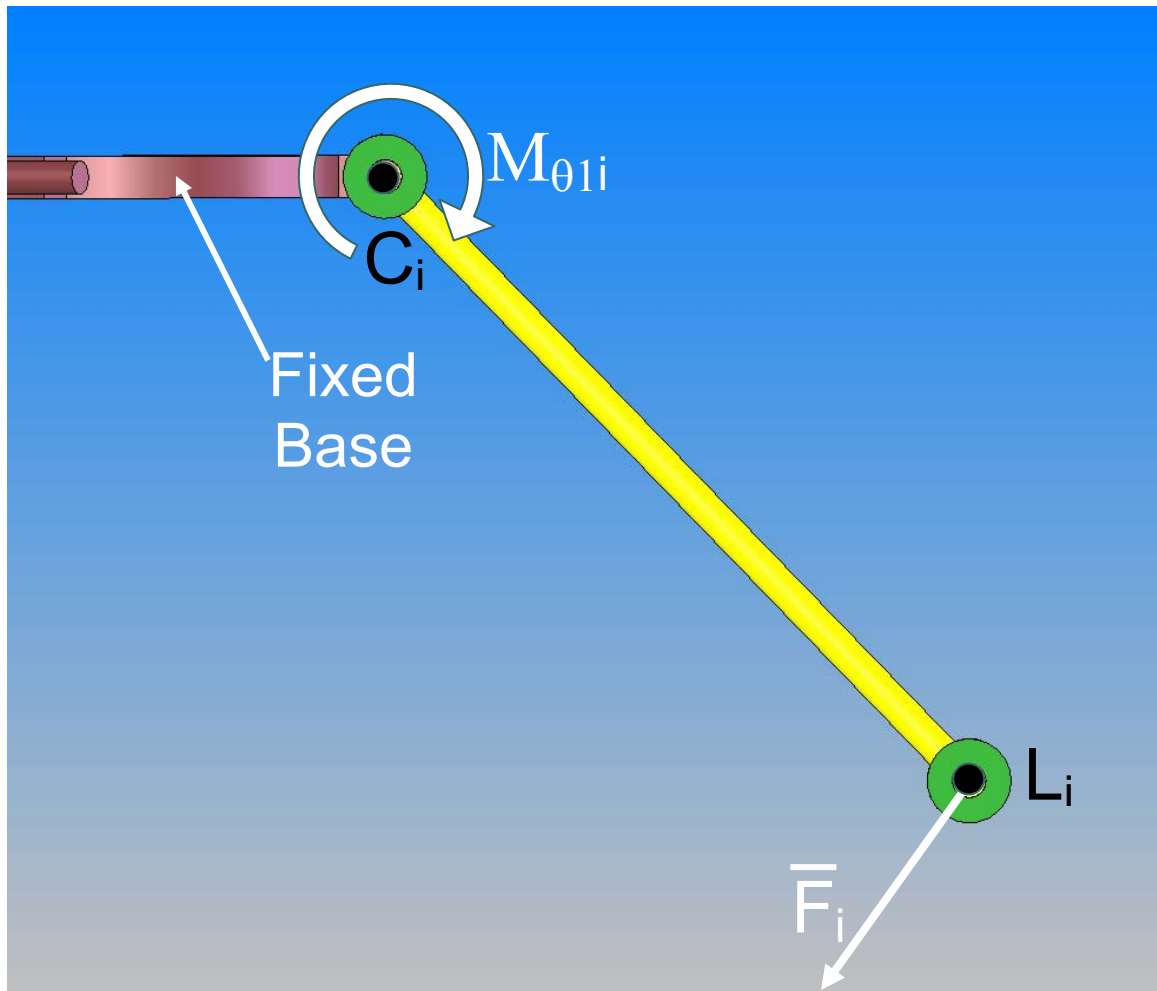


Figure 6.16: Upper link of i th arm.

6.5 Dynamic Analysis

In this section the dynamic analysis of a series of prototype robots is carried out. First the groundwork for the dynamic analysis is laid out. In the following three sections the tasks to be simulated are defined, the motion planning strategy for the robot is described, and the generation of CAD prototypes is described. A series of prototypes are then analyzed to determine the demands that will be placed on the actuators of the robot.

The results of each dynamic analysis are used to improve the design of each successive prototype until an acceptable prototype is developed.

6.5.1 Defining the Tasks

The goal of the dynamic analysis of a robot prototype is to estimate the maximum loads and speeds that will be required by the actuators of the prototype. To do this the most demanding sub-task must be simulated, the transport of a WOG from the conveyor belt to an empty shackle. This sub-task is most demanding when the WOG acquisition point and the WOG release point are as far away from each other as is allowed (Figure 6.17 and Figure 6.18). In the global X and Y directions the most demanding WOG transport requires translations of 18 in and 24 in respectively. In the global Z direction the translation depends on whether the WOG is acquired breast up or breast down. The specialized end effector is 9 in tall. At the end of WOG transport the legs of the WOG should be about an inch above the top of the opening in the shackle or about 22 in above the conveyor belt. When the WOG is acquired in the breast up position the legs are about 4 in above the conveyor belt. After a translation of 18 in in the Z direction they are 22 in above the conveyor belt. When the WOG is acquired in the breast down position the feet of the WOG are about 2 in above the conveyor belt or about 8.5 in below point F, the center of the wrist. After the WOG is flipped over it is 8.5 in above point F. If the moving platform is translated 3 in in the Z direction the feet of the WOG are 22 in above the conveyor belt. As discussed in Chapter 2 the task of transferring WOGs from the conveyor belt to a shackle must have a cycle time of less than 1.32 seconds. Further, 0.4

seconds are allowed for the WOG transport. If 0.2 seconds are allowed for the end effector to grasp the WOG, 0.1 seconds are allowed to lower the WOG into the shackle, 0.2 seconds are allowed for the end effector to release the WOG and 0.4 seconds are allowed to position the end effector for the next WOG capture the cycle time is 1.3 seconds. The initial and final conditions for each task are presented in Table 6.1 and Table 6.2.

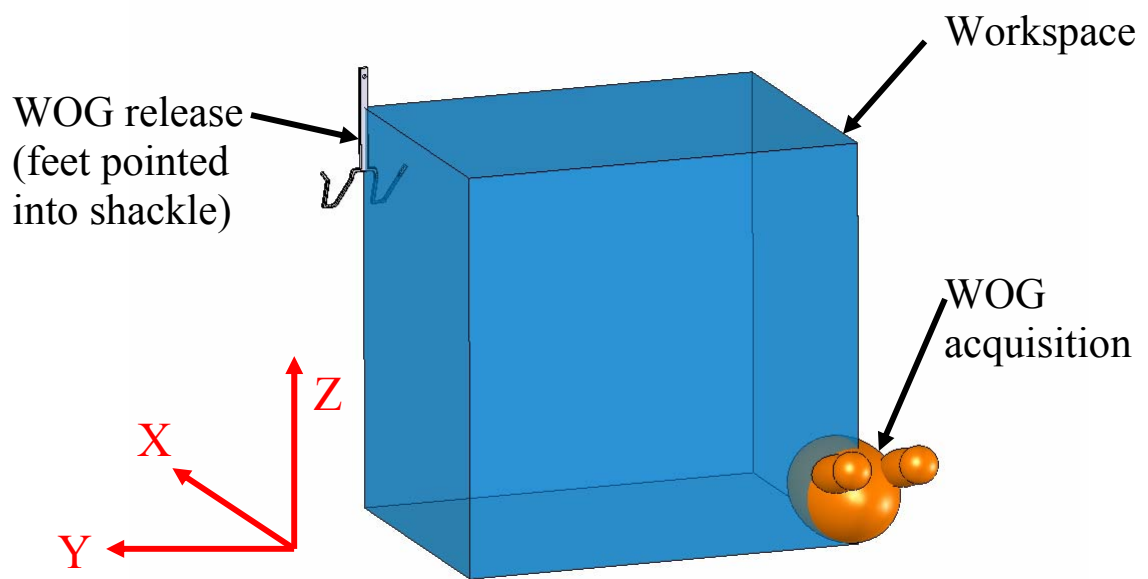


Figure 6.17: Most demanding WOG transport for breast up WOG acquisition.

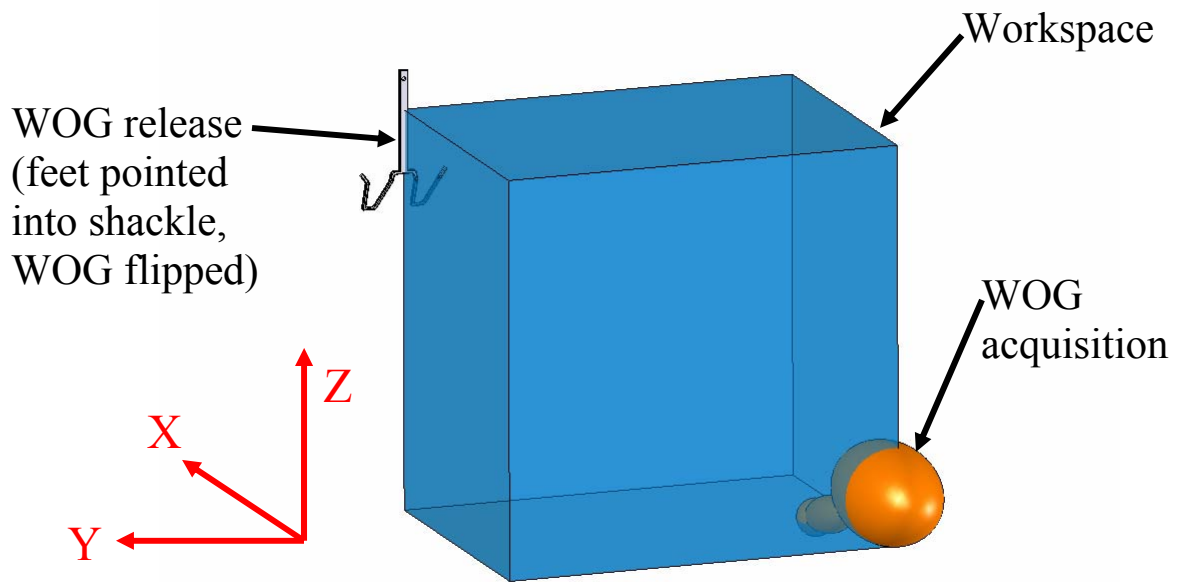


Figure 6.18: Most demanding WOG transport for breast down WOG acquisition.

Table 6.1: Task definition for breast up WOG capture.

	Wrist Variables		Moving Platform Variables			Time
	θ_w	ρ_w	X	Y	Z	t
Initial Position	180°	180°	-9 in	-12 in	-39	0
Final Position	180°	360°	9 in	12 in	-21	0.4
Change	0°	180°	18 in	24 in	18	0.4
Initial Velocity	0°/s	0°	0	-1.517	0	NA
Final Velocity	0°/s	NA	0	0.758	0	NA
Change	0°/s	NA	0	-2.275	0	NA

Table 6.2: Task definition for breast down WOG capture.

	Wrist Variables		Moving Platform Variables			Time
	θ_w	ρ_w	X	Y	Z	t
Initial Position	180°	0°	-9 in	-12 in	-39	0
Final Position	0°	180°	9 in	12 in	-36	0.4
Change	-180°	180°	18 in	24 in	3 in	0.4
Initial Velocity	0°/s	0°	0	-1.517	0	NA
Final Velocity	0°/s	NA	0	0.758	0	NA
Change	0°/s	NA	0	-2.275	0	NA

6.5.2 Motion Planning

The position of the moving platform and the position of the wrist actuator corresponding to the *Rotate* motion are specified by fitting 3rd order polynomials to the constraints specified in Table 6.1 and Table 6.2. As can be seen in Figure 6.19 fitting a 3rd order polynomial to a position variable provides a linear acceleration profile, a parabolic velocity profile and a smooth 3rd order curve position profile. The 3rd order curve can be fully defined by constraints on the initial position, initial velocity, final position and final velocity. Let q represent one of the four variables X , Y , Z and ρ_w . q , \dot{q} , and \ddot{q} are specified by the following equations.

$$q = a_3 t^3 + a_2 t^2 + a_1 t + a_0 \quad (6.23)$$

$$\dot{q} = a_3 t^2 + a_2 t + a_1 \quad (6.24)$$

$$\ddot{q} = a_3 t + a_2 \quad (6.25)$$

The coefficients of the third order polynomial a_0 , a_1 , a_2 , and a_3 are now determined. This is done by matching the initial and final conditions to equations (6.23) and (6.24) and by solving the resulting set of four equations shown below. In the

following set of equations the subscript i indicates the initial value of a variable while the subscript f indicates the final value of a variable.

$$q_i = a_0 \quad (6.26)$$

$$\dot{q}_i = a_1 \quad (6.27)$$

$$q_f = a_3 t_f^3 + a_2 t_f^2 + a_1 t_f + a_0 \quad (6.28)$$

$$\dot{q}_f = a_3 t_f^2 + a_2 t_f + a_1 \quad (6.29)$$

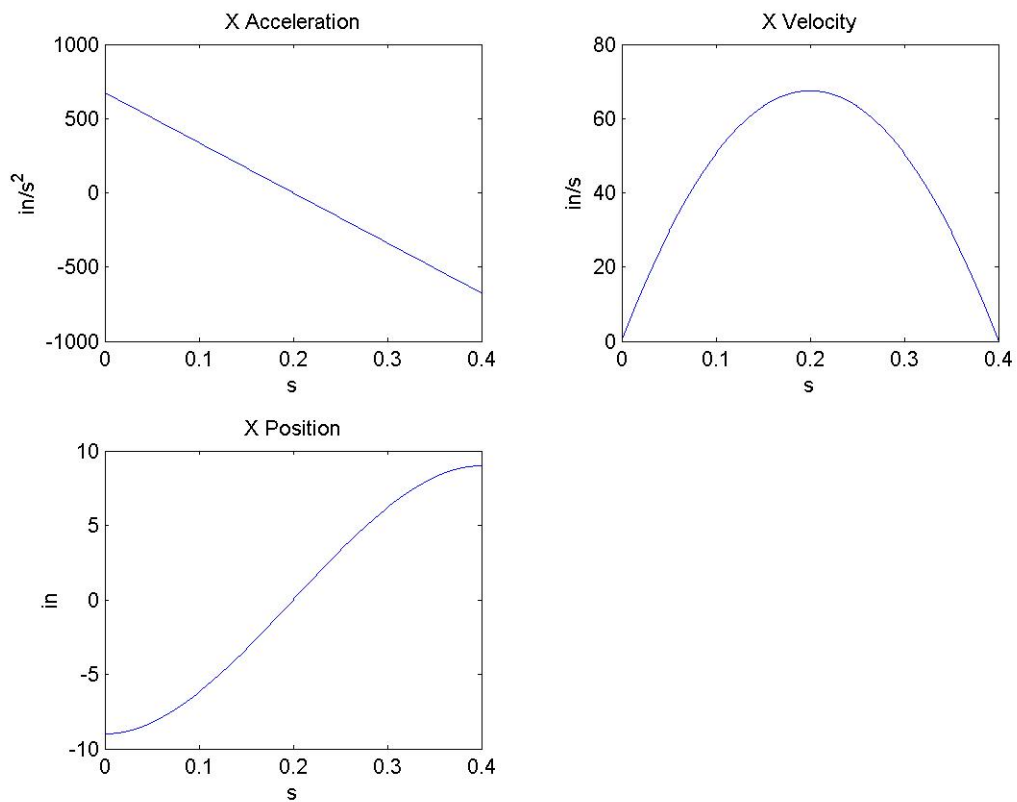


Figure 6.19: Results of fitting a 3rd order polynomial to the X position of the moving platform.

The wrist actuator associated with the *Flip* motion is pneumatic and is not capable of the kind of position control described in the previous paragraphs. Double acting pneumatic actuators are either off or on. When they are on they provide a relatively constant force or moment. When they are off they provide a force or moment that is roughly equal and opposite to the force or moment they provide when on. The dynamic model of the robot does not allow force to be specified as an input, so the pneumatic actuator is modeled as having a constant acceleration. The acceleration of the *Flip* motion generating actuator is given by:

$$\ddot{\theta}_w = 2(\theta_{wf} - \theta_{wi})/t_f^2 \quad (6.30)$$

The position and velocity of the variable θ_w are then given by equations (6.31) and (6.32).

$$\dot{\theta}_w = (2(\theta_{wf} - \theta_{wi})/t_f^2)t \quad (6.31)$$

$$\theta_w = \theta_{wi} + ((\theta_{wf} - \theta_{wi})/t_f^2)t^2 \quad (6.32)$$

Note that $\dot{\theta}_w$ is not 0 at t_f . This is acceptable because a mechanical stop, not the actuator will be used to halt the *Flip* motion. The stop uses little time to halt the motion and will be ignored in the dynamic modeling carried out below.

6.5.3 Generating CAD Prototypes

Each prototype begins with the generation of a 3D CAD model in Solid Works, and a corresponding dynamic model in COSMOS Motion. These models aid in the

collection of the inertial properties of prototype components and provide visual verification of the construction and behavior of the prototype. They provide a visual verification that all the component dimensions are correct and that all of the components fit together properly. Once the density of a part is specified SolidWorks/COSMOS Motion can provide the mass and rotational inertia matrix of the part as well as the location of the center of mass of the part and the principal axes of the part. The prototype can also be animated to visually verify that the specified actuator motions provide the desired end effector motion.

COSMOS Motion has dynamic analysis capabilities, but has trouble modeling this robot. The results often claim that large spikes in the actuator moments are needed though these spikes can not be explained by the configuration or motion of the robot. Sometimes the results claim the actuators need to produce large moments that oscillate about zero with high frequencies.

For each of the dynamic analyses carried out below a picture of the CAD prototype is presented. The first such picture is Figure 6.20. Each of these prototypes follows a color code and each picture views the prototype from about the same angle. All components shown in grey or gold are stainless steel, while all components shown in blue or white are delrin. The fixed base of the robot is light green, while the bright green rectangular object in the foreground of the picture is a washdown proof servo motor with a USDA approved epoxy coating. The yellow ellipsoid is modeling a 5.5 lb WOG. The details of the design of the base are not dealt with in this thesis. The base shown in these prototypes is designed only as a means of mounting all of the actuators of the parallel mechanism in the correct relative positions.

Attached to the base are the three motors that actuate the parallel mechanism. Attached to these three motors are the three arms of the parallel mechanism. The two foremost arms in the picture are the $\{X(w)\}$ generating kinematic chains, while the arm at the back of the picture is the $\{D\}$ motion generating kinematic chain.

6.5.4 First Dynamic Prototype

Figure 6.20 is a picture of the first prototype. For this prototype $c = 10$ in, $l = 19$ in, $d = 34$ in, $e = 7$ in, $\|\overline{EF}\| = 11.5$ in, and $\|\overline{FG}\| = 1.5$ in (Figure 5.2 and Figure 5.3).

The prototype is constructed primarily out of rectangular stainless steel tubing with a 0.1 in wall thickness. There are solid stainless steel rods used to construct the lower link of the $\{D\}$ motion generating arm of the parallel mechanism and the upper and lower bars of the parallelogram links of the $\{X(w)\}$ motion generating arms. The moving platform is constructed of delrin, while the wrist is constructed of delrin and stainless steel. In this prototype the *Rotate* motion generating servo motor weighs 10 lb, while the *Flip* motion generating stainless steel air motor weighs 3 lb, the WOG weighs 5.5 lb and the end effector weighs 2.5 lb. All other component weights are determined by SolidWorks from the density of the construction materials. The combined weight of all the moving components of the robot (all items shown in Figure 6.20 excluding the robot base, the actuators of the parallel mechanism, the WOG and the End Effector) is 52.5 lb.

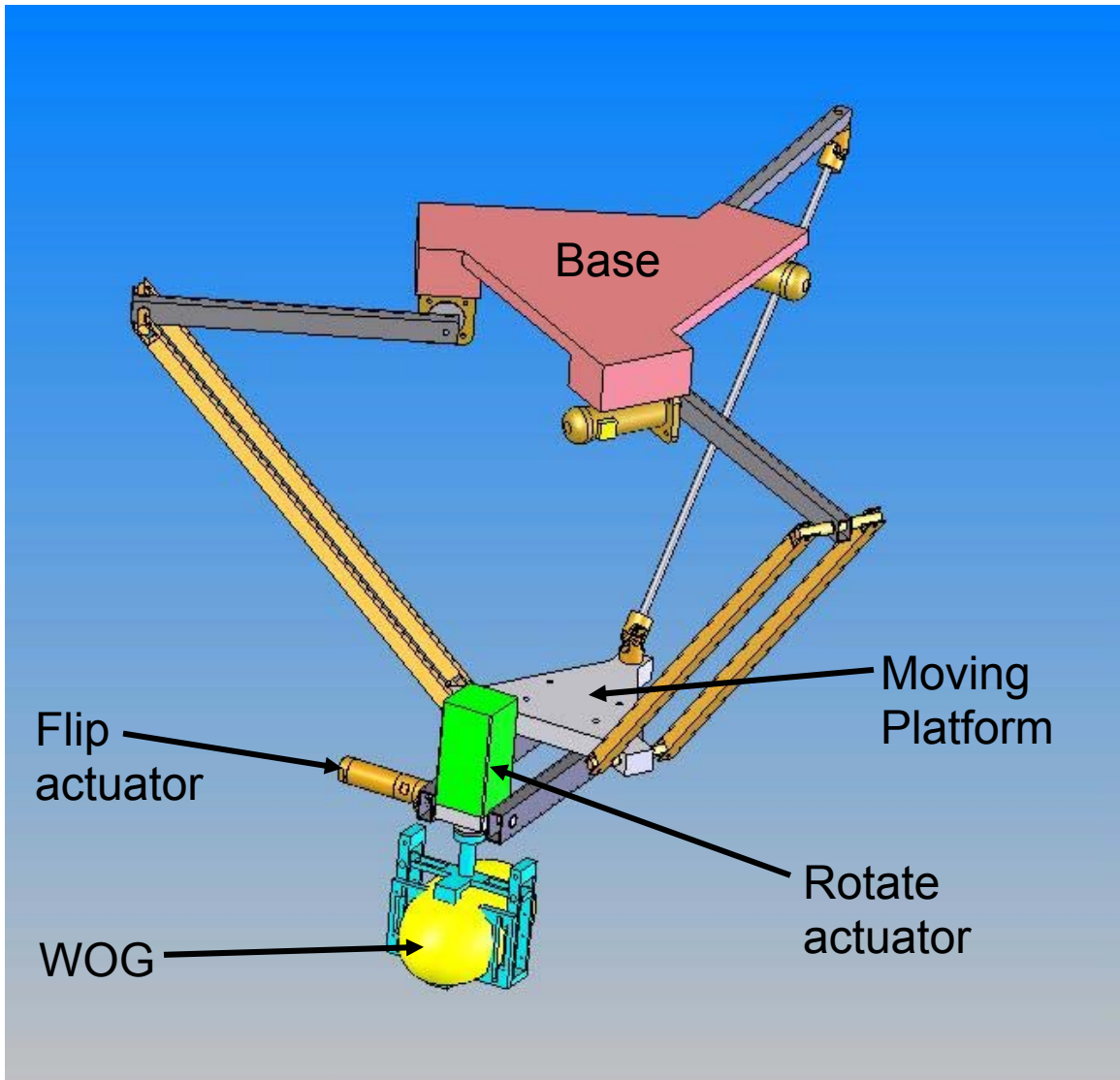


Figure 6.20: 3-D CAD model of first dynamic prototype.

The full results of the dynamic analyses of the prototypes are in Appendix E (Figure E.1 through Figure E.48). For each of the two tasks outlined in Section 6.5.1 the results include plots of the position, velocity, and acceleration of the moving platform in the X , Y , and Z directions as well as the angular position, velocity, and acceleration of all the actuated joints of the robot. The results also include the moments that each actuator

must produce to achieve the specified motion. None of the actuated joints required high speeds, so the required moments are the most limiting factor. The actuator moments required to complete the task outlined in Table 6.1 are shown in Figure 6.21, while the actuator moments required to complete the task outlined in Table 6.2 are shown in Figure 6.22. In these figures thw indicates the stainless steel air motor that provides the *Flip* (or θ_w) motion of the wrist, and pw indicates the servo motor that provides the *Rotate* (or ρ_w) motion of the wrist. $th11$, $th12$, and $th13$ indicate the motors that actuate the parallel mechanism.

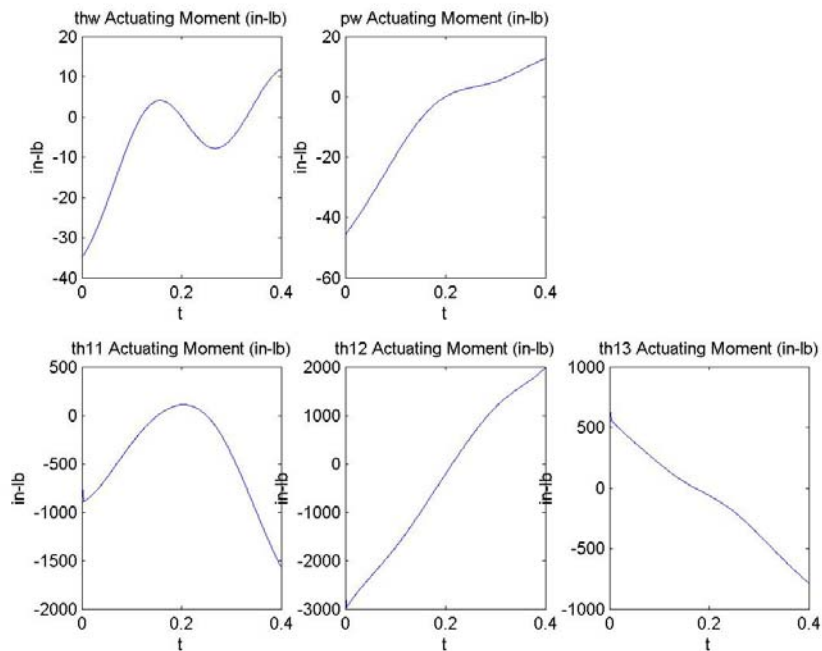


Figure 6.21: Actuator moments for the first prototype when the WOG begins breast up.

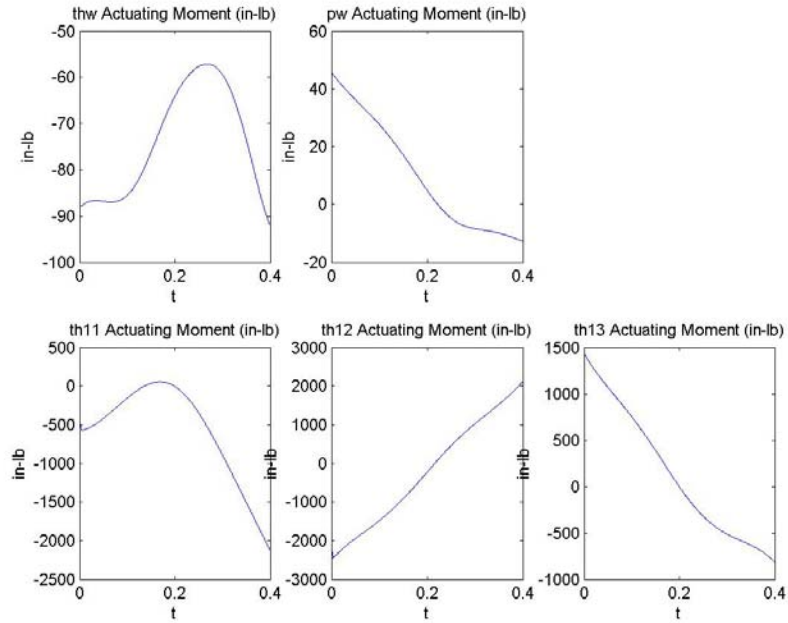


Figure 6.22: Actuator moments for the first prototype when the WOG begins breast down.

The moments required of the parallel mechanism actuators are simply too large. For the case where the WOG is acquired in the breast up position one of the actuators of the parallel mechanism is required to produce nearly 3000 in-lb.

6.5.5 Second Dynamic Prototype

In an effort to reduce the loads on the actuators of the parallel mechanism the second prototype is designed with an emphasis on reducing the weight of the moving components. For the most part the weight of the robot is reduced by replacing simple stainless steel and delrin parts with delrin parts that are machined to remove excess

material. The sides of the parallelogram links in the two $\{X(w)\}$ motion generating chains are constructed of delrin instead of stainless steel, a large amount of excess material has been removed from the moving platform of the parallel mechanism, and the two bars connecting the moving platform to the wrist are constructed of delrin instead of steel. These changes reduce the combined weight of the moving components of the robot from 52.5 lb to 37.6 lb .

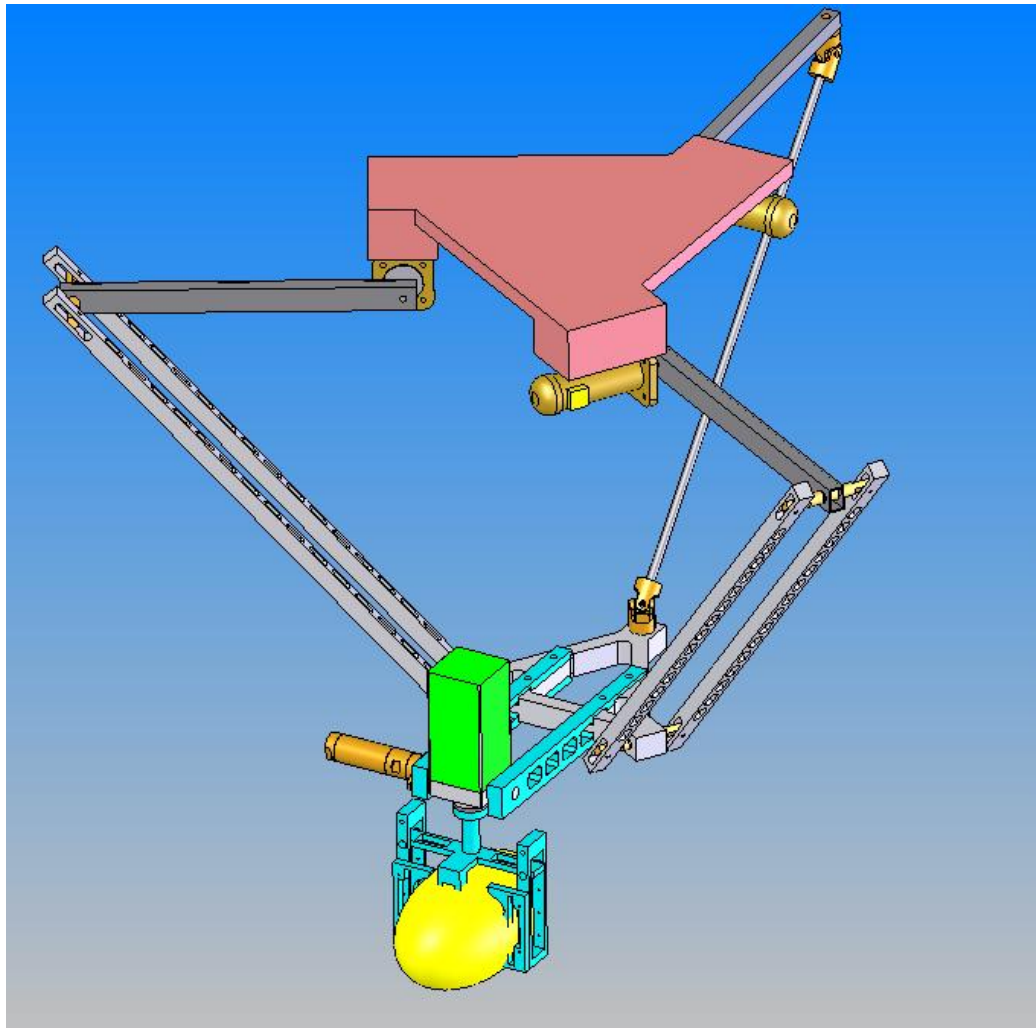


Figure 6.23: 3D CAD model of second dynamic prototype.

The actuator moments required to complete the task outlined in Table 6.1 are shown in Figure 6.24, while the actuator moments required to complete the task outlined in Table 6.2 are shown in Figure 6.25. The moments required of the parallel mechanism's actuators have decreased significantly but they are still too high. In Figure 6.24 it can be seen that one of the actuators requires over 2100 in-lb for the case when the WOG begins breast up.

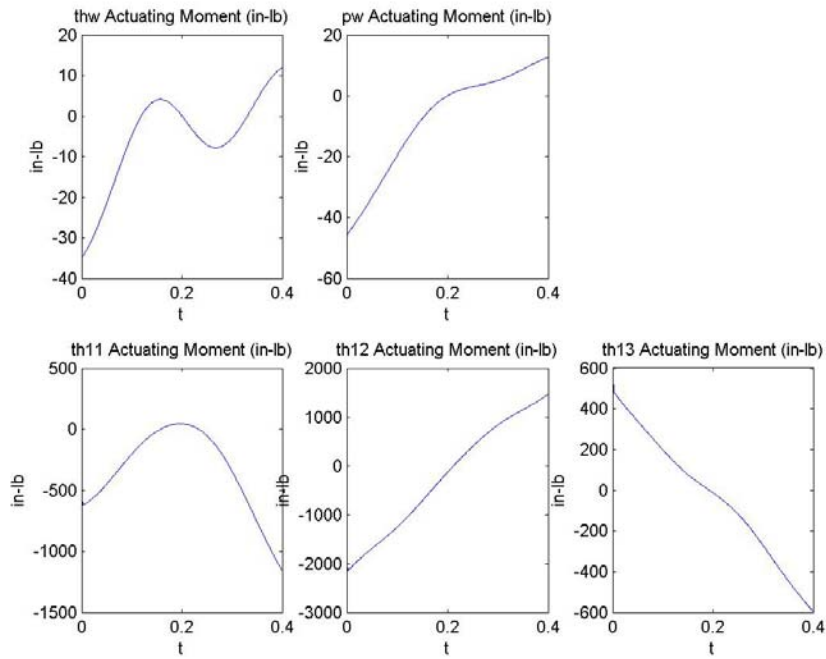


Figure 6.24: Actuator moments for second prototype when the WOG begins breast up.

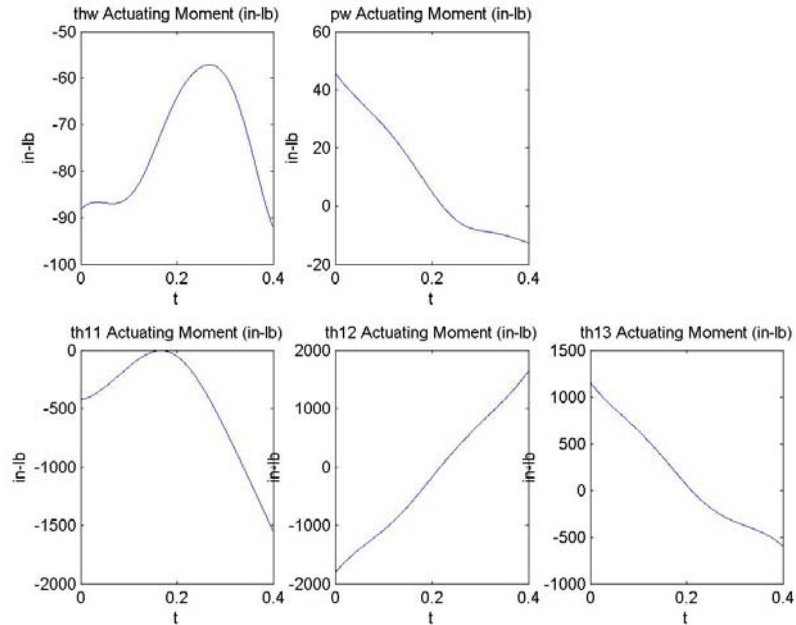


Figure 6.25: Actuator moments for the second prototype when the WOG begins breast down.

6.5.6 Third Dynamic Prototype

To reduce the required moments further the dimensions of the robot are reduced. The first two prototypes are designed to accommodate a workspace that is larger than necessary for this task. This gives them more adaptability and may allow them to perform other tasks where a larger workspace is required. Unfortunately, as shown above, the moments required from their parallel mechanism actuators are simply too high. The first two prototypes are designed to accommodate a rectangular workspace 1.875 ft x 2.5 ft x 2.5 ft in the X , Y and Z directions respectively. For the third prototype the parallel mechanism is dimensioned to accommodate a 1.5 ft x 2 ft x 2 ft workspace. As discussed previously the moments seen by the actuators of the parallel mechanism generally increase as the dimension l , the length of the upper links of the arms of the

parallel mechanism, increases. Scaling down the parallel mechanism both decreases the dimension l and decreases the weight of many components of the robot. In the development of this prototype a preliminary selections of the wrist actuators are made and the weights of the wrist actuators are updated accordingly. In this prototype the electric servo motor providing the *Rotate* motion (shown in bright green) weighs 6.4 lb while the pneumatic air motor providing the *Flip* motion weighs 2.7 lb. The combined weight of the moving components of this prototype is 30 lb.

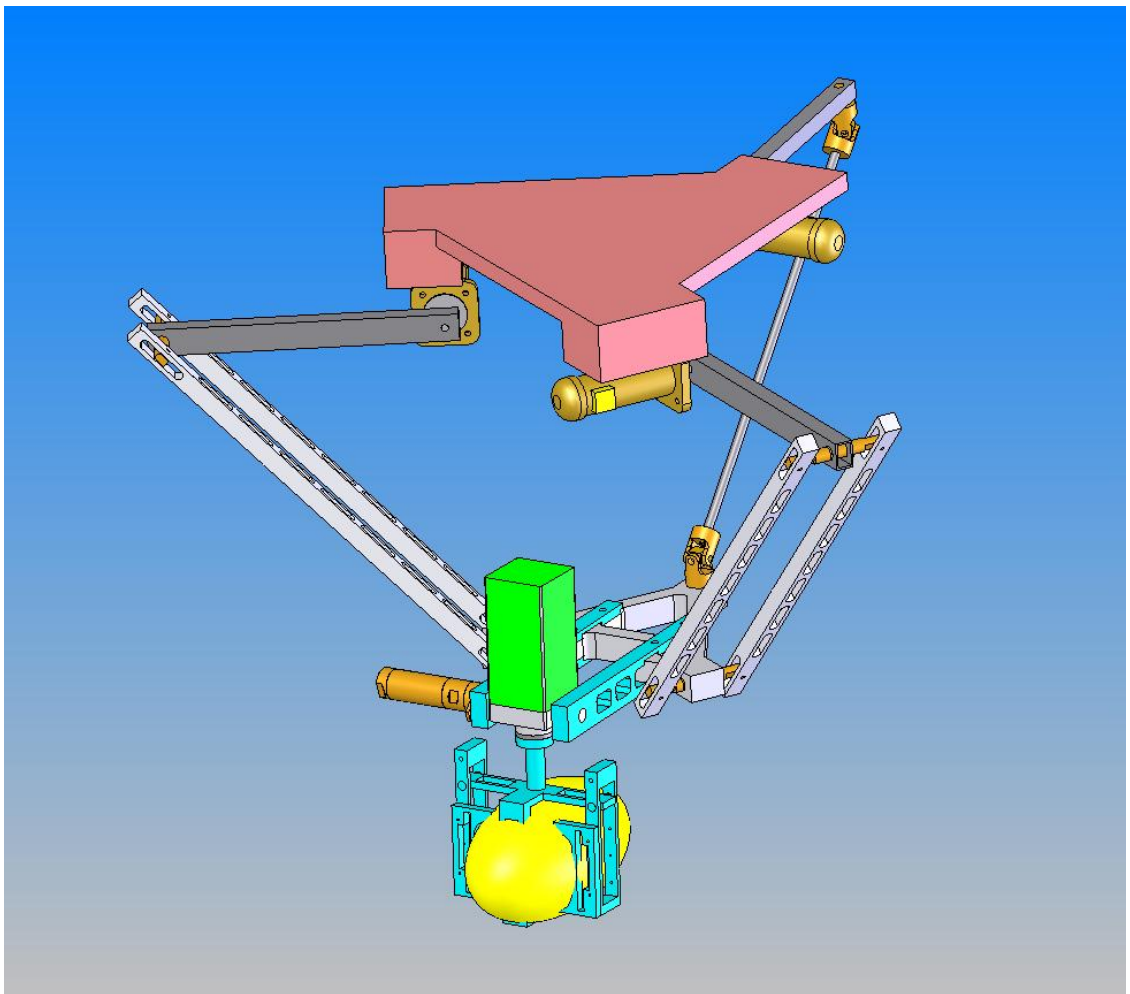


Figure 6.26: 3D CAD model of third dynamic prototype.

The third prototype has $c = 9$ in, $l = 15$ in, $d = 25$ in, $e = 7$ in and $\|\overline{FG}\| = 1.5$ in.

Because c and l have been reduced the bars connecting the moving platform of the parallel mechanism to the wrist can also be shortened, leaving $\|\overline{EF}\| = 9$ in. Scaling down the parallel mechanism causes the workspace of the robot to get smaller and shift upward. As a result, the tasks defined in Table 6.1 and Table 6.2 must be redefined for this prototype. The redefined tasks are presented in Table 6.3 and Table 6.4.

Table 6.3: Revised task definition for breast up WOG capture.

	Wrist Variables		Moving Platform Variables			Time
	θ_w	ρ_w	X	Y	Z	t
Initial Position	180°	180°	-9 in	-12 in	-33	0
Final Position	180°	360°	9 in	12 in	-15	0.4
Change	0°	180°	18 in	24 in	18	0.4
Initial Velocity	0°/s	0°	0	-1.517	0	NA
Final Velocity	0°/s	NA	0	0.758	0	NA
Change	0°/s	NA	0	-2.275	0	NA

Table 6.4: Revised task definition for breast down WOG capture.

	Wrist Variables		Moving Platform Variables			Time
	θ_w	ρ_w	X	Y	Z	t
Initial Position	180°	0°	-9 in	-12 in	-33	0
Final Position	0°	180°	9 in	12 in	-30	0.4
Change	-180°	180°	18 in	24 in	3 in	0.4
Initial Velocity	0°/s	0°	0	-1.517	0	NA
Final Velocity	0°/s	NA	0	0.758	0	NA
Change	0°/s	NA	0	-2.275	0	NA

The moments required to complete these tasks are shown below. The maximum moment required from an actuator of the parallel mechanism is now 1010 in-lb. This is less than half of the maximum moment required for the second prototype, and is an acceptable value for the maximum required moment.

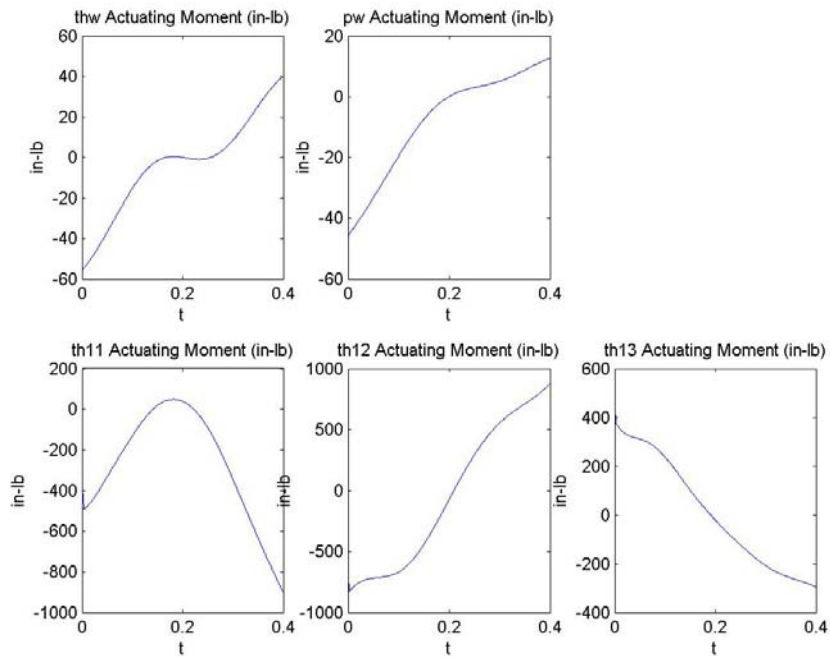


Figure 6.27: Actuator moments for third prototype when the WOG begins breast up.

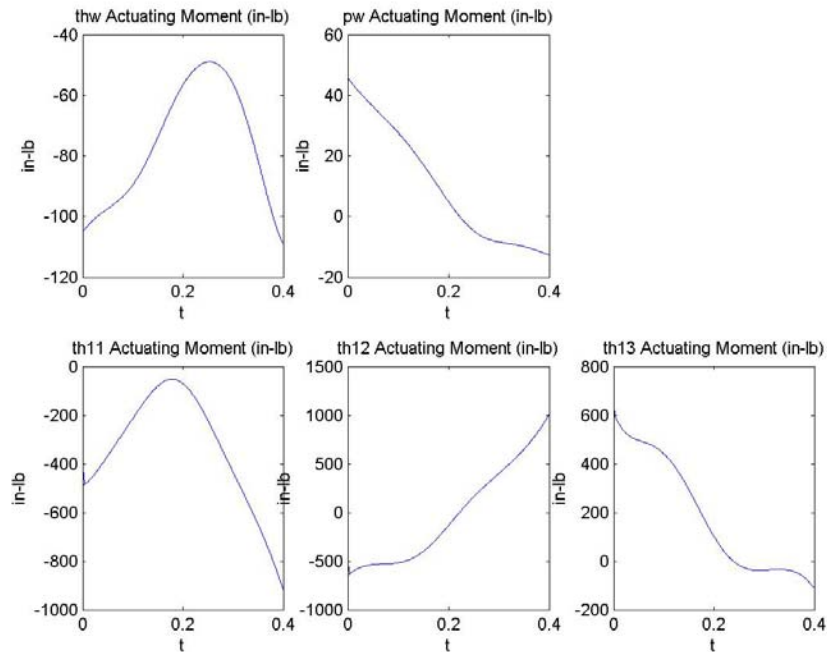


Figure 6.28: Actuator moments for third prototype when the WOG begins breast down.

Notice that the highest moment required of any of the parallel mechanism actuators is required by the *th12* actuator when the WOG is acquired breast down (Figure 6.28). This is surprising because the moving platform travels a shorter distance when the WOG is acquired breast down and because the other prototypes required greater moments from the parallel mechanism actuators when the WOG was acquired breast up. This suggests that for the task where the WOG is acquired breast down the arms of the parallel mechanism on the third prototype might not be cooperating as best they can. It also suggests that there is potential to lower the required actuating moments of the parallel mechanism. A more sophisticated motion planning strategy may be able lower the moments required for this task.

6.6 Motor Selection

In this section preliminary actuator selections are made to demonstrate that the requirements are reasonable. The final motor selections should not be made until all the details of the construction of the robot are worked out and coordinated with a final dynamic analysis. Time constraints have left these tasks outside the scope of this thesis. Cutsheets for all of the preliminary actuator selections are included in appendix F.

The same actuator is chosen for all three arms of the parallel mechanism based on the maximum loads and speeds required of the third prototype. A 1 hp washdown vector motor paired with a 60:1 washdown gear reducer is selected. Specifically, the Baldor ZDWNM3546T vector motor and WDFG6032AG gear reducer are selected. The motor and gearbox have a combined weight of 115 lb, are washdown proof and are coated with a USDA approved epoxy. The maximum moment available from the selected actuator during continuous operation is 1467 in-lb and the maximum speed is 100 rpm, while the maximum moment required by the dynamic analysis is 1010 in-lb and the maximum speed is 70 rpm. These two quantities don't tell the whole story however because the maximum torque provided by the selected actuator is not constant over the whole range of speeds. The actuator can provide approximately 1467 in-lb between 0 and 29 rpm (positive or negative velocity), and can provide approximately constant power from 29 to 100 rpm. This means that the actuator can provide about 734 in-lb at 58 rpm and about 489 in-lb at 87 rpm. In the dynamic analysis there is not a simple relationship between actuator speed and required moment but generally speaking the highest moments are required at low speeds. Table 6.5 compares the maximum moments required at several actuator speeds to the maximum continuous moment that the selected actuator can

provide. The chosen actuator can provide higher moments for small periods of time. Based on these results the actuator can provide the required moments over the whole range of necessary speeds.

Table 6.5: Analysis of selected parallel mechanism actuator.

	Actuator Speed (rpm)					
	~0	15	30	45	60	70
Selected Actuator Moment (in-lb)	1467	1467	1467	978	794	629
Maximum Required Moment (in-lb)	1010	750	700	675	600	250
Safety Factor (Ratio of Moments)	1.45	1.96	2.10	1.45	1.32	2.5

For the electric *Rotate* actuator a Pacific Scientific PMA23 servo motor is selected. The PMA23 is specified with IP67 protection, which allows it to withstand washdowns. The weight of this motor is 6.4 lb. The continuous stall torque is 17.7 in-lb. The peak torque is 63.7 in-lb and the rated speed is 3600 rpm. The maximum required speed according to the dynamic analysis is about 110 rpm. Since the maximum required speed is 1/32 the rated speed it can be assumed that over the range of required motion the actuator motion can provide 63.7 in-lb of peak torque. The highest moment required in the dynamic analyses is 47 in-lb. As a result there is a 1.36 safety factor for the peak moment of the *Rotate* motion. To prevent overheating, the rms actuator torque must be below the continuous stall torque. For the situations simulated in the dynamic analysis of the third prototype the rms torques are larger than the continuous stall torque. For the breast down scenario the rms torque is 21.3 in-lb and for the breast up scenario the rms

torque is 18.4 in-lb. Over longer periods of time the rms torque is expected to be well below the continuous stall torque. The situations simulated in the dynamic analysis represent the most demanding 0.4 second periods of time that the actuator is ever likely to encounter. During each cycle there are also 0.3 seconds where no *Rotate* motion is needed and 0.4 seconds where the *Rotate* motion is carried out without a WOG. Even other WOG transport tasks are expected to be less demanding than those simulated in the dynamic analysis. In reality the WOGs will usually weigh much less than 5.5 lb and the required rotation is usually less than 180°. This actuator has plenty of speed and peak torque. The dynamic analysis revealed that for a fraction of a second the rms torque may be higher than the maximum rms torque. This is not a problem though because over longer periods of time, such as a full cycle of the WOG hang task (1.3 seconds), the rms torque will be acceptable.

For the pneumatic *Flip* actuator an Atlas Copco LZB 34RL AR004 air motor is selected. The air motor is stainless steel, is lubrication free and weighs 2.6 lb. According to the dynamic analysis the maximum speed required of this actuator is about 150 rpm and the maximum load required is 109 in-lb. The moment provided by the actuator varies as a function of speed. Operating at 91 psi the torque varies linearly from 192 in-lb at 0 rpm to 120 in-lb at 150 rpm. Table 6.6 shows a comparison of the required moments called for by the dynamic analysis and the moment that would be provided by the selected air motor. In this table the selected actuator moment is estimated based on the speed stated in the dynamic analysis. At the end of the *Flip* task the safety factor is only 1.1, however the safety factors are so large during the rest of the task that the

selected actuator will have no problem completing the *Flip* motion in less than the allowed 0.4 seconds.

Table 6.6: Analysis of Selected *Flip* motion Actuator.

	Time (s)				
	0	0.1	0.2	0.3	0.4
Actuator Speed (rpm)	0	37.5	75	112.5	150
Selected Actuator Moment (in-lb)	192	174	156	138	120
Required Moment (in-lb)	105	95	57	60	109
Safety Factor (Ratio of Moments)	1.83	1.83	2.74	2.30	1.10

6.7 Cost Analysis

To further evaluate the feasibility of the robot a cost estimate is produced (Table 6.7).

Table 6.7: Robot cost estimate.

	Number	Estimated Cost per unit (\$)	Estimated Cost (\$)	Notes
Structural Components				
Stainless Steel Component	9	600	5400	1
Delrin Component	8	200	1600	1
Stainless Steel U-Joint	2	100	200	2
Stainless Steel Enclosure for Electronics	1	1000	1000	3
Stainless Steel Frame/Base	1	5000	5000	3

Miscellaneous Plain Bearings and Connectors	1	500	500	2
Parallel Mechanism Actuators				
1 hp washdown Vector Drive	3	1693	5079	4
60: 1 Stainless Steel Washdown Gearbox	3	961	2883	4
Cables	3	400	1200	3
Industrial Hardened Amplifier/Controller	3	2200	6600	3, 6
Wrist Actuators				
Stainless Steel Air Motor	1	1000	1000	7
Solenoid Valve	2	82.63	165.26	3
Solenoid Coil	2	12.82	25.64	3
Solenoid Cables	2	13.88	27.76	3
Manifold	1	74.25	74.25	3
Filter Regulator	1	78.89	78.89	3
Startup Valve	1	39.72	39.72	3
Feet of Tubing	50	0.85	42.5	3
Washdown Servo Motor	1	658.35	658.35	5
Industrial Hardened Servo Controller	1	950	950	5, 6
Cables	1	400	400	5

Total:	\$ 32,924
---------------	------------------

Notes:

- 1) Estimate based on rule of thumb used by GTRI to estimate machined part costs
- 2) Estimate based on prices from www.mcmastercar.com
- 3) Estimate based on quotes obtained by GTRI for similar products
- 4) Estimate based on prices from www.baldor.com
- 5) Estimate based on price quote from Cornerstone Technical Group, Atlanta, GA
- 6) Industrial hardened controllers are devices that have all of the necessary controller and amplifier components assembled in a single enclosure with simple inputs and outputs
- 7) Estimate based on Atlas Copco air motor supplier

In the requirements list developed in Chapter 2 it is demanded that the cost of construction and implementation of the robot and specialized end effector not be more

than \$60,000. This amount represents a one year payback. This budget contains \$4,000 for the specialized end effector, \$1000 for the vision system, \$3,000 for maintenance, \$27,000 for implementation of the system, and \$25,000 for the robot. The robot cost estimate presented in Table 6.7 indicates that the robot is \$7,924.37 over budget. If this is accurate and the other parts of the budget remain the same the robotic workcell will have a 1.13 year payback.

CHAPTER 7

CLOSURE

This chapter has a summary of the thesis, a critical review of the robot design, comments on relevant contributions and recommendations for further work.

7.1 Summary

In this thesis a low cost, high speed robot for poultry processing is designed. The robot is aimed at making it feasible to automate the transfer of WOGs from a moving conveyor belt to a moving shackle. Chapter 1 explains the goals of the thesis and the reasons for wanting to automate the transfer of WOGs from a conveyor belt to a moving shackle. It also gives an overview of previous work in the automation of poultry processing tasks and an overview of robotics.

Chapter 2 plans and clarifies the task. It provides a thorough evaluation of the problem and generates the specifications that are used for the rest of the design process. First an overview of the poultry processing environment and the current WOG hanging procedure are given. The task is then quantified and a requirements list is generated.

In Chapter 3, Conceptual Design, the principal solution is generated. First the structure of the task is developed and evaluated. A large number of possible solutions to

the task are then generated and evaluated. Finally a robot consisting of a 2 DOF robotic wrist and a 3 DOF translation only parallel mechanism is chosen as the principal solution.

In Chapter 4 the kinematic design of the robot is carried out. The structure of the robot is developed, including the number of, ordering of, and orientation of joints. The equations governing the position and motion of the robot is then derived and evaluated.

In Chapter 5 the dimensions of the robot are optimized. First the workspace required by the task is determined. The optimum robot dimensions to meet these requirements are then determined.

In Chapter 6 robot prototypes are generated and used to finalize many of the details of the design. Both physical and CAD models are generated and used to simulate the performance of the robot. Preliminary actuator selections and a preliminary cost analysis are also carried out.

7.2 Critical Review of Design

In this thesis a problem is identified in the automation of a poultry processing task with high variability. The feasibility of solving the problem with robotic automation is then explored. In two related projects a specialized end effector for grasping WOGs is developed, and a vision system for identifying the positions and orientations of WOGs is developed. These two related projects make transferring WOGs from a conveyor belt to a moving shackle possible, but the robot developed in this thesis makes the automation of the task practical. The robot developed in this task makes it possible to transfer WOGs from a conveyor belt to a moving shackle line with human level performance. It can

withstand the hostile environment of a poultry processing plant, and meet USDA design guidelines. Preliminary cost estimates indicate that a robot workcell would have a 1.13 year payback, but it may be possible to achieve a one year payback with modifications to the design.

To completely address the problem of automating the WOG hanging task the robot must meet all of the demands stated in the requirements list. The robot developed in this thesis has not met all of the demands of the requirements list, but it has met as many demands as it can meet at this phase of the design. The remaining demands require additional work, testing, and a level of design detail that is outside of the scope of this thesis. Some demands cannot be considered met or unmet until all the details of the robot design have been completed. Even though further work is required before such a robot can be built, the work in this thesis has shown it is feasible and a large amount of the design has been completed.

7.3 Future Work

The main area of future work to be done on this project can be considered a continuation of the work done in this thesis. There are many design details that must be worked out before a fully functional USDA compliant robot can be built. Reductions in the weight of the robot are still possible, as well as reductions in the cost of the robot and in the size, weight and power of the actuators.

Next the robot must be incorporated into a workcell that transfers WOGs from a moving conveyor belt to a moving shackle. This work allows the robot, the specialized

end effector and the vision system to cooperate to complete the task. Work must also be done on optimizing the control of that workcell. The motion planning used to perform the dynamic analysis of the robot is simple. With a more sophisticated motion planning strategy there may be potential to lower the demands placed on the actuators or improve the performance of the robot.

Once a fully functional USDA compliant prototype has been constructed and incorporated into a robotic workcell it must be tested. The tests and simulations carried out in this thesis provide useful insight into the behavior of the robot, but they consider only very limited situations and often rely on simplified models that ignore real world effects such as friction. There is no substitute for testing a fully functional prototype under real world conditions.

Work must also be done on modifications to the conveyor belt system that will prepare the WOG for a successful capture by the robotic workcell. As discussed earlier in the thesis a device that will force all the WOGs to the outside of the conveyor belt must be developed. The means of singulating the WOGs must also be determined.

There is also work that can be done adapting the robot to other tasks. One aspect of transferring WOGs from a conveyor belt to a moving shackle that was not considered in this thesis, but must be considered eventually is the possibility of encountering a damaged WOG. Currently, when a WOG is too damaged to be hung on a shackle human workers remove the WOG from the conveyor belt. The robot will likely have to do something similar. The robot might also be suitable for automating totally different food processing tasks. One likely candidate is picking up gas stunned WOGs in the early stages of poultry processing and hanging them in shackles

APPENDIX A

COMPLETE ROBOT SOLUTION MATRIX

The following pages contain the complete robot solution matrix discussed in Section 3.2.4.

X	Electric	Electric	Curved Path Actuator	Curved Path Actuator	Curved Path Actuator	Electric
X	Pneumatic	Electric	Curved Path Actuator	Curved Path Actuator	Curved Path Actuator	Electric
X	Electric	pneumatic ratchet	Curved Path Actuator	Curved Path Actuator	Curved Path Actuator	Electric
X	Pneumatic	pneumatic ratchet	Curved Path Actuator	Curved Path Actuator	Curved Path Actuator	Electric
X	Electric	Multi Pos Pneumatic	Curved Path Actuator	Curved Path Actuator	Curved Path Actuator	Electric
X	Pneumatic	Multi Pos Pneumatic	Curved Path Actuator	Curved Path Actuator	Curved Path Actuator	Electric
X	Electric	Electric	Curved Path Actuator	Curved Path Actuator	Curved Path Actuator	Multi Pos Pneumatic
X	Pneumatic	Electric	Curved Path Actuator	Curved Path Actuator	Curved Path Actuator	Multi Pos Pneumatic
X	Electric	pneumatic ratchet	Curved Path Actuator	Curved Path Actuator	Curved Path Actuator	Multi Pos Pneumatic
X	Pneumatic	pneumatic ratchet	Curved Path Actuator	Curved Path Actuator	Curved Path Actuator	Multi Pos Pneumatic
X	Electric	Multi Pos Pneumatic	Curved Path Actuator	Curved Path Actuator	Curved Path Actuator	Multi Pos Pneumatic
X	Pneumatic	Multi Pos Pneumatic	Curved Path Actuator	Curved Path Actuator	Curved Path Actuator	Multi Pos Pneumatic
X	Electric	Electric	Curved Path Linkage	Curved Path Linkage	Curved Path Linkage	Electric
X	Pneumatic	Electric	Curved Path Linkage	Curved Path Linkage	Curved Path Linkage	Electric
X	Electric	pneumatic ratchet	Curved Path Linkage	Curved Path Linkage	Curved Path Linkage	Electric
X	Pneumatic	pneumatic ratchet	Curved Path Linkage	Curved Path Linkage	Curved Path Linkage	Electric
X	Electric	Multi Pos Pneumatic	Curved Path Linkage	Curved Path Linkage	Curved Path Linkage	Electric
X	Pneumatic	Multi Pos Pneumatic	Curved Path Linkage	Curved Path Linkage	Curved Path Linkage	Electric
X	Electric	Electric	Curved Path Linkage	Curved Path Linkage	Curved Path Linkage	Multi Pos Pneumatic
X	Pneumatic	Electric	Curved Path Linkage	Curved Path Linkage	Curved Path Linkage	Multi Pos Pneumatic
X	Electric	pneumatic ratchet	Curved Path Linkage	Curved Path Linkage	Curved Path Linkage	Multi Pos Pneumatic

APPENDIX B

SOLUTION EVALUATION MATRICES

In Section 3.3.3 a representative set of 16 solutions for providing the X , Y , and Z translations of the end effector are evaluated based on 16 evaluation criteria and weighting factors for those weighting factors. The resulting evaluation matrices are presented in Section B.1 of this appendix. In Section 3.2.4 a set of 6 solutions for the *Flip* and *Rotate* motions are evaluated based on the same evaluation criteria and weighting factors. The resulting evaluation matrices are presented in Section B.2 of this appendix.

B.1 Evaluation of Solutions for the X, Y, and Z Motions

Table B.1: First evaluation matrix for X, Y, and Z motion solutions.

Subtask	Comparison Criteria	Robot Geometry															
		Z			Y			X			Z			Y			X
		Cartesian + 2R	Anthropomorphic + 2R	TTT Parallel + 2R	Cartesian + 2R	Cartesian + 2R	Anthropomorphic + 2R	TTT Parallel + 2R	Cartesian + 2R	Cartesian + 2R	Cable driven	Curved Path	Curved Path	Curved Path	Curved Path	TTT Parallel + 2R	TTT Parallel + 2R
		Electric	Electric	Electric	Multi Pos Pneumatic	Multi Pos Pneumatic	Multi Pos Pneumatic	Multi Pos Pneumatic	Const Drive Timed Mech	Const Drive Timed Mech	Cable Driven	Curved Path Actuator	Curved Path Actuator	Curved Path Linkage	Curved Path Linkage	Flexible Joint Electric	Flexible Joint MP pneumatic
		Electric	Electric	Electric	Multi Pos Pneumatic	Multi Pos Pneumatic	Multi Pos Pneumatic	Multi Pos Pneumatic	Electric	Multi Pos Pneumatic	Cable Driven	Curved Path Actuator	Curved Path Actuator	Curved Path Linkage	Curved Path Linkage	Flexible Joint Electric	Flexible Joint MP pneumatic
		Electric	Electric	Electric	Multi Pos Pneumatic	Multi Pos Pneumatic	Multi Pos Pneumatic	Multi Pos Pneumatic	Electric	Multi Pos Pneumatic	Cable Driven	Curved Path Actuator	Curved Path Actuator	Curved Path Linkage	Curved Path Linkage	Flexible Joint Electric	Flexible Joint MP pneumatic
All	Joint/Actuator Cost	0	0	0	1	1	1	1	0	1	-1	1	1	1	1	1	1
	Link Volume	0	0	1	0	0	0	1	-1	-1	1	1	1	1	1	1	1
	Part Complexity	0	0	-1	0	0	0	-1	-1	-1	1	-1	-1	-1	-1	-1	-1
	Reliability/Ease of Maintenance	0	0	-1	1	1	1	1	-1	1	-1	1	1	1	1	-1	1
Subtask Specific Properties																	
Acquisition	Ease of Control	1	0	-1	1	-1	-1	-1	1	-1	-1	1	-1	1	-1	-1	-1
	Speed	0	0	1	-1	1	1	1	-1	-1	1	-1	-1	-1	-1	1	1
	Robustness	1	0	1	1	-1	-1	-1	-1	-1	1	1	-1	1	-1	1	-1
Transport	Ease of Control	1	0	-1	1	1	0	-1	1	1	-1	1	1	1	1	-1	-1
	Speed	0	0	1	1	1	1	1	0	1	1	-1	-1	-1	-1	1	1
	Robustness	0	0	1	-1	-1	-1	-1	0	-1	1	1	1	1	1	1	1
Getting Legs into Shackle	Ease of Control	1	0	-1	1	-1	-1	-1	1	-1	-1	1	-1	1	-1	-1	-1
	Speed	0	0	0	0	0	0	0	0	0	0	1	1	1	1	0	0
	Robustness	1	0	1	-1	-1	-1	-1	-1	-1	1	1	-1	1	-1	1	-1
Retract	Ease of Control	0	0	0	1	0	0	0	1	1	-1	1	1	1	1	0	0
	Speed	0	0	1	1	1	1	1	-1	-1	1	-1	-1	-1	-1	1	1
	Robustness	1	0	1	-1	-1	-1	-1	1	-1	1	1	-1	1	-1	1	-1

Table B.2: Second evaluation matrix for X, Y, and Z motion solutions.

Subtask		Robot Geometry															
		Z				Y				X							
Comparison Criteria		Cartesian + 2R	Anthropomorphic + 2R	TTT Parallel + 2R	Cartesian + 2R	Cartesian + 2R	Anthropomorphic + 2R	TTT Parallel + 2R	Cartesian + 2R	Cartesian + 2R	Cartesian + 2R	Cable driven	Curved Path	Curved Path	Curved Path	Curved Path	
Intrinsic Robot Properties		Electric	Electric	Electric	Multi Pos Pneumatic	Multi Pos Pneumatic	Multi Pos Pneumatic	Multi Pos Pneumatic	Multi Pos Pneumatic	Multi Pos Pneumatic	Multi Pos Pneumatic	Const Drive Timed Mech	Const Drive Timed Mech	Cable Driven	Curved Path Actuator	Curved Path Actuator	
Subtask Specific Properties		Electric	Electric	Electric	Multi Pos Pneumatic	Multi Pos Pneumatic	Multi Pos Pneumatic	Multi Pos Pneumatic	Multi Pos Pneumatic	Multi Pos Pneumatic	Multi Pos Pneumatic	Electric	Electric	Cable Driven	Curved Path Actuator	Curved Path Actuator	
All	Joint/Actuator Cost	0	0	0	1	1	1	1	0	1	-1	1	1	1	1	1	1
	Link Volume	1	1	1	1	1	1	1	0	0	1	1	1	1	1	1	1
	Part Complexity	1	1	1	1	1	1	1	0	0	1	-1	-1	-1	-1	-1	-1
	Reliability/Ease of Maintenance	1	1	1	1	1	1	1	0	1	-1	1	1	1	1	1	1
Acquisition	Ease of Control	0	-1	-1	0	-1	-1	-1	0	-1	-1	0	-1	0	-1	-1	-1
	Speed	1	1	1	1	1	1	1	0	0	1	1	1	1	1	1	1
	Robustness	1	1	1	1	-1	-1	-1	0	-1	1	1	-1	1	-1	1	-1
Transport	Ease of Control	-1	-1	-1	-1	-1	-1	-1	0	-1	-1	-1	-1	-1	-1	-1	-1
	Speed	0	0	1	1	1	1	1	0	1	1	-1	-1	-1	-1	1	1
	Robustness	0	0	1	-1	-1	-1	-1	0	-1	1	1	1	1	1	1	1
Getting Legs into Shackle	Ease of Control	-1	-1	-1	-1	-1	-1	-1	0	-1	-1	-1	-1	-1	-1	-1	-1
	Speed	0	0	0	0	0	0	0	0	0	0	1	1	1	1	0	0
	Robustness	1	1	1	1	1	1	1	0	1	1	1	1	1	1	1	1
Retract	Ease of Control	-1	-1	-1	-1	-1	-1	-1	0	1	-1	0	1	0	1	-1	-1
	Speed	1	1	1	1	1	1	1	0	0	1	1	1	1	1	1	1
	Robustness	1	-1	1	-1	-1	-1	-1	0	-1	1	1	-1	1	-1	1	-1

Table B.3: Third evaluation matrix for X, Y, and Z motion solutions.

Subtask	Comparison Criteria	Robot Geometry																
		Z			Y			X			Z			Y			X	
All	Joint/Actuator Cost	1	1	1	1	1	1	1	1	1	0	1	1	1	1	1	1	1
	Link Volume	-1	-1	-1	-1	-1	-1	-1	-1	-1	0	-1	-1	-1	-1	-1	-1	-1
	Part Complexity	-1	-1	-1	-1	-1	-1	-1	-1	-1	0	-1	-1	-1	-1	-1	-1	-1
	Reliability/Ease of Maintenance	1	1	1	1	1	1	1	1	1	1	0	1	1	1	1	1	1
Subtask Specific Properties																		
Acquisition	Ease of Control	1	1	1	1	-1	-1	-1	1	-1	0	1	-1	1	-1	1	-1	-1
	Speed	-1	-1	-1	-1	-1	-1	-1	-1	-1	0	-1	-1	-1	-1	-1	-1	-1
	Robustness	-1	-1	0	-1	-1	-1	-1	-1	-1	0	-1	-1	-1	-1	0	-1	-1
Transport	Ease of Control	1	1	1	1	1	1	1	1	1	0	1	1	1	1	1	1	1
	Speed	-1	-1	-1	-1	-1	-1	-1	-1	-1	0	-1	-1	-1	-1	-1	-1	-1
	Robustness	-1	-1	1	-1	-1	-1	1	-1	-1	0	1	1	1	1	1	1	1
Getting Legs into Shackle	Ease of Control	1	1	1	1	-1	-1	-1	1	-1	0	1	-1	1	-1	1	-1	-1
	Speed	0	0	0	0	0	0	0	0	0	0	1	1	1	1	0	0	0
	Robustness	-1	-1	0	-1	-1	-1	-1	-1	-1	0	0	-1	0	-1	0	-1	-1
Retract	Ease of Control	1	1	1	1	1	1	1	1	1	0	1	1	1	1	1	1	1
	Speed	-1	-1	-1	-1	-1	-1	-1	-1	-1	0	-1	-1	-1	-1	-1	-1	-1
	Robustness	0	-1	0	-1	-1	-1	-1	-1	-1	0	1	-1	1	-1	0	-1	-1

Table B.4: Fourth evaluation matrix for X, Y, and Z motion solutions.

Subtask		Robot Geometry															
		Z					Y					X					
Comparison Criteria		Cartesian + 2R	Anthropomorphic + 2R	TTT Parallel + 2R	Cartesian + 2R	Cartesian + 2R	Anthropomorphic + 2R	TTT Parallel + 2R	Cartesian + 2R	Cartesian + 2R	Cable driven	Curved Path	Curved Path	Curved Path	Curved Path	TTT Parallel + 2R	TTT Parallel + 2R
Intrinsic Robot Properties		Electric	Electric	Electric	Multi Pos Pneumatic	Multi Pos Pneumatic	Multi Pos Pneumatic	Multi Pos Pneumatic	Multi Pos Pneumatic	Multi Pos Pneumatic	Multi Pos Pneumatic	Multi Pos Pneumatic	Multi Pos Pneumatic	Multi Pos Pneumatic	Multi Pos Pneumatic	Multi Pos Pneumatic	Multi Pos Pneumatic
Subtask Specific Properties		Electric	Electric	Electric	Multi Pos Pneumatic	Multi Pos Pneumatic	Multi Pos Pneumatic	Const Drive Timed Mech	Const Drive Timed Mech	Cable Driven	Cable Driven	Curved Path Actuator	Curved Path Actuator	Curved Path Linkage	Curved Path Linkage	Curved Path Linkage	Curved Path Linkage
All	Joint/Actuator Cost	-1	-1	-1	-1	-1	-1	-1	-1	-1	-1	-1	0	-1	0	-1	-1
	Link Volume	-1	-1	1	-1	-1	-1	1	-1	-1	1	0	0	-1	-1	1	1
	Part Complexity	1	1	1	1	1	1	1	-1	-1	1	0	0	1	1	-1	-1
	Reliability/Ease of Maintenance	-1	-1	-1	-1	-1	-1	-1	-1	-1	-1	-1	0	-1	1	-1	-1
Acquisition	Ease of Control	1	1	1	1	-1	-1	-1	1	-1	1	1	0	1	-1	1	-1
	Speed	1	1	1	1	1	1	1	-1	-1	1	-1	0	-1	0	1	1
	Robustness	1	1	1	1	-1	-1	-1	1	-1	1	1	0	1	-1	1	-1
Transport	Ease of Control	1	-1	-1	1	-1	-1	-1	1	-1	-1	1	0	1	-1	-1	-1
	Speed	1	1	1	1	1	1	1	1	1	1	0	0	0	0	1	1
	Robustness	-1	-1	1	-1	-1	-1	-1	-1	-1	-1	1	0	1	0	1	-1
Getting Legs into Shackle	Ease of Control	1	1	1	1	-1	-1	-1	1	-1	1	1	0	1	0	1	-1
	Speed	-1	-1	-1	-1	-1	-1	-1	-1	-1	-1	0	0	0	0	-1	-1
	Robustness	1	1	1	-1	-1	-1	-1	-1	-1	1	1	0	1	0	1	-1
Retract	Ease of Control	-1	-1	-1	-1	-1	-1	-1	-1	-1	-1	-1	0	-1	0	-1	-1
	Speed	1	1	1	1	1	1	1	-1	-1	1	0	0	0	0	1	1
	Robustness	1	1	1	1	-1	-1	-1	1	-1	1	1	0	1	0	1	-1

Table B.6: Weighted and summed evaluation matrix for X, Y, and Z motion solutions.

Subtask	Evaluation Criteria	Robot Geometry																
		X		Y		Z		Cartesian + 2R		Anthropomorphic + 2R		TTT Parallel + 2R		Cartesian + 2R		TTT Parallel + 2R		
		Electric	Electric	Electric	Electric	Multi Pos Pneumatic	Multi Pos Pneumatic	Multi Pos Pneumatic	Electric	Multi Pos Pneumatic	Cable Driven	Electric	Multi Pos Pneumatic	Electric	Multi Pos Pneumatic	Flexible Joint Electric	Flexible Joint MP pneumatic	
Global	Joint/Actuator Cost	54	-54	-54	-54	162	162	162	162	-54	54	-216	162	216	162	216	108	162
	Link Volume	60	-120	-120	120	-120	-120	-120	120	-240	-240	240	0	0	-60	-60	120	120
	Part Complexity	57	114	114	57	114	114	57	-114	-114	228	-114	-114	-57	-57	-228	-228	
	Reliability/Ease of Maintenance	27	54	54	-27	81	81	81	81	-54	81	-108	81	108	81	135	0	81
Acquisition	Ease of Control	30	120	60	30	120	-150	-150	-150	60	-150	-60	120	-120	120	-150	0	-150
	Speed	42	0	0	84	-42	42	42	126	-168	-168	168	-126	-84	-126	-84	84	126
	Robustness	45	45	0	135	45	-225	-225	-225	-90	-225	135	45	-180	45	-225	135	-225
Transport	Ease of Control	24	72	0	-48	72	24	0	-48	96	24	-96	72	48	72	24	-48	-48
	Speed	51	-51	-51	51	51	51	51	153	-51	51	204	-204	-204	-204	-204	102	153
	Robustness	36	-108	-108	108	-180	-180	-180	-108	-108	-180	0	108	72	108	72	144	36
Getting into Shackle	Ease of Control	33	99	66	0	99	-165	-165	-165	132	-165	-66	99	-132	99	-132	0	-165
	Speed	21	-21	-21	-21	-21	-21	-21	-21	-21	-21	-21	84	84	84	84	-21	-21
	Robustness	39	39	0	117	-117	-117	-117	-117	-156	-117	117	117	-78	117	-78	117	-117
Retract	Ease of Control	18	-18	-18	-18	18	-18	-18	-18	36	54	-72	36	72	36	72	-18	-18
	Speed	48	0	0	96	48	48	48	144	-192	-192	192	-96	-96	-96	-96	96	144
	Robustness	15	45	-30	45	-45	-75	-75	-75	0	-75	45	75	-60	75	-60	45	-75
Totals		216	-108	675	285	-549	-573	-84	-924	-1383	690	459	-468	456	-543	636	-225	
Normalized Score		0.771	0.61505065	0.99	0.8046	0.4023	0.39073806	0.62663	0.221	0	1	0.889	0.441	0.89	0.4052	0.974	0.5586	

B.2 Evaluation of Solutions for the *Flip* and *Rotate* Motions

Table B.7: First evaluation matrix for *Flip* and *Rotate* motion solutions.

<u>Subtask</u>	<u>Comparison Criteria</u>	Flip		Rotate					
		Electric	Pneumatic	Electric	Electric	pneumatic ratchet	pneumatic ratchet	Multi Pos Pneumatic	Multi Pos Pneumatic
<i>Intrinsic Robot Properties</i>									
All	Joint/Actuator Cost	-1	0	-1	1	-1	1		
	Link Volume	-1	0	-1	1	-1	-1		
	Part Complexity	0	0	-1	-1	-1	-1		
	Reliability/Ease of Maintenance	-1	0	-1	-1	-1	-1		
<i>Subtask Specific Properties</i>									
Acquisition	Ease of Control	0	0	1	1	-1	-1		
	Speed	0	0	-1	-1	1	1		
	Robustness	0	0	-1	-1	-1	-1		
Transport	Ease of Control	-1	0	-1	1	-1	-1		
	Speed	-1	0	-1	-1	1	1		
	Robustness	1	0	1	-1	-1	-1		
Getting Legs into Shackle	Ease of Control	-1	0	-1	1	-1	-1		
	Speed	0	0	-1	-1	0	0		
	Robustness	1	0	1	-1	-1	-1		
Retract	Ease of Control	-1	0	-1	0	-1	0		
	Speed	-1	0	-1	0	-1	0		
	Robustness	1	0	-1	-1	-1	-1		

Table B.8: Second evaluation matrix for *Flip* and *Rotate* motion solutions.

<u>Subtask</u>	<u>Comparison Criteria</u>	Flip		Rotate				
		Electric	Pneumatic	Electric	pneumatic ratchet	pneumatic ratchet	Multi Pos Pneumatic	Multi Pos Pneumatic
<i>Intrinsic Robot Properties</i>								
All	Joint/Actuator Cost	-1	-1	-1	0	-1	-1	
	Mechanism Volume	-1	-1	-1	0	-1	-1	
	Part Complexity	1	1	0	0	-1	-1	
	Reliability/Ease of Maintenance	-1	1	-1	0	-1	1	
<i>Subtask Specific Properties</i>								
Acquisition	Ease of Control	-1	-1	0	0	-1	-1	
	Speed	1	1	0	0	1	1	
	Robustness	1	1	0	0	1	1	
Transport	Ease of Control	-1	-1	-1	0	-1	-1	
	Speed	1	1	-1	0	1	1	
	Robustness	1	1	1	0	1	-1	
Getting Legs into Shackle	Ease of Control	-1	-1	-1	0	-1	-1	
	Speed	1	1	-1	0	1	1	
	Robustness	1	1	1	0	1	1	
Retract	Ease of Control	-1	0	-1	0	-1	0	
	Speed	-1	0	-1	0	-1	0	
	Robustness	1	1	0	0	-1	-1	

Table B.9: Third evaluation matrix for *Flip* and *Rotate* motion solutions.

<u>Subtask</u>	<u>Comparison Criteria</u>	Flip		Rotate			
		Electric	Pneumatic	Electric	pneumatic ratchet	Multi Pos Pneumatic	Multi Pos Pneumatic
<i>Intrinsic Robot Properties</i>							
All	Joint/Actuator Cost	-1	1	1	1	0	1
	Mechanism Volume	1	1	1	1	0	1
	Part Complexity	1	1	1	1	0	0
	Reliability/Ease of Maintenance	1	1	1	1	0	1
<i>Subtask Specific Properties</i>							
Acquisition	Ease of Control	1	1	1	1	0	0
	Speed	-1	-1	-1	-1	0	0
	Robustness	1	1	-1	-1	0	0
Transport	Ease of Control	1	1	1	1	0	1
	Speed	-1	-1	-1	-1	0	1
	Robustness	1	1	1	-1	0	-1
Getting Legs into Shackle	Ease of Control	1	1	1	1	0	1
	Speed	0	0	-1	-1	0	0
	Robustness	1	1	1	-1	0	-1
Retract	Ease of Control	0	1	0	1	0	1
	Speed	0	1	0	1	0	1
	Robustness	1	1	1	1	0	1

Table B.10: Weighted and summed evaluation matrix for *Flip* and *Rotate* motion solutions.

<u>Subtask</u>	<u>Comparison Criteria</u>	Weighting Factors	Flip		Rotate			
			Electric	Pneumatic	Electric	pneumatic ratchet	Multi Pos Pneumatic	Multi Pos Pneumatic
All	Joint/Actuator Cost	54	-162	0	-54	108	-108	54
	Link Volume	60	-60	0	-60	120	-120	-60
	Part Complexity	57	114	114	0	0	-114	-114
	Reliability/Ease of Maintenance	27	-27	54	-27	0	-54	27
<i>Subtask Specific Properties</i>								
Acquisition	Ease of Control	30	0	0	60	60	-60	-60
	Speed	42	0	0	-84	-84	84	84
	Robustness	45	90	90	-90	-90	0	0
Transport	Ease of Control	24	-24	0	-24	48	-48	-24
	Speed	51	-51	0	-153	102	102	153
	Robustness	36	108	72	108	-72	0	-108
Getting Legs into Shackle	Ease of Control	33	-33	0	-33	66	-66	-33
	Speed	21	21	21	-63	-42	21	21
	Robustness	39	117	78	117	-78	0	-39
Retract	Ease of Control	18	-36	18	-36	18	-36	18
	Speed	48	-96	48	-96	48	-96	48
	Robustness	15	45	30	0	0	-30	-15
Totals			6	525	-435	0	-525	-48
Normalized Score			0.506	1	0.086	0.5	0	0.454

APPENDIX C

MATLAB CODE

Matlab is used four times in this thesis. It is used in Section 5.3 to generate a series of plots illustrating the size and shape of the parallel mechanism for a wide variety of robot parameters. These plots are included in Appendix D and the Matlab code used to generate them is presented in Section C.1. Matlab is then used in the quantitative workspace study (Section 5.4) to scale sets of robot parameters such that the required workspace fits in the parallel mechanism workspace without inducing any singular or near singular configurations. The Matlab code used in the qualitative workspace study is presented in Section C.2. Once a set of robot parameters is chosen the Matlab code in Section C.3 is used to determine the range of angles the joints of the parallel mechanism experience within the required workspace. The Matlab code in Section C.4 is used to carry out the dynamic prototype analyses discussed in Section 6.4. The results of these analyses are included in Appendix E.

C.1 Matlab Code for Qualitative Workspace Study

The generation of workspace plots for the qualitative workspace study begins with RotDeltVar.m for the first round of the study and RotDeltVar2.m for the second round of the study. These programs vary the robot parameters as required by the qualitative workspace study, call the function RDeltWSRKin.m to generate workspace plots for each set of parameters, then saves the results. RDeltWSRKin.m scans through the $Z = -0.5$, $Z = -1$, $Z = -1.5$, and $X = 0$ planes. It uses the function RKinRot.m, an implementation of the reverse kinematic equations, and a set of geometric checks to determine where the planes and the workspace of the parallel mechanism coincide. RDeltWSRKin.m then calls WSplotRKin.m to plot the results.

C.1.1 RotDeltVar.m

```
function RotDeltVar

global l e d thl the pho anglelimit th c
resetvaluesftwsm
k=0;
for i = 1:4
    cc=.5*i;
    c=[cc cc cc];
    file = ['Ac' num2str(i) '.jpg'];
    [WSyz,WSz,h]=RDeltWSRKin(c,l,e,d,th);
    saveas(h,file);
end
resetvaluesftwsm
for i = 1:4
    ll = .5*i;
    l = [ll ll ll];
    file = ['Al' num2str(i) '.jpg'];
    [WSyz,WSz,h]=RDELTWSRKin(c,l,e,d,th);
    saveas(h,file);
end
resetvaluesftwsm
```

```

for i = 1:4
    ee = .5*i;
    e = [ee ee ee];
    file = ['Ae' num2str(i) '.jpg'];
    [WSyz,WSz,h]=RDELTWSRKin(c,l,e,d,th);
    saveas(h,file);
end
resetvaluesftwsm
for i = 1:4
    dd=.5*i;
    d=[dd dd dd];
    file = ['Ad' num2str(i) '.jpg'];
    [WSyz,WSz,h]=RDELTWSRKin(c,l,e,d,th);
    saveas(h,file);
end
resetvaluesftwsm
for i = 1:4
    cc=.5*i;
    c=[cc cc cc];
    l=c;
    file = ['Acl' num2str(i) '.jpg'];
    [WSyz,WSz,h]=RDeltWSRKin(c,l,e,d,th);
    saveas(h,file);
end
resetvaluesftwsm
for i = 1:4
    cc=.5*i;
    c=[cc cc cc];
    e=c;
    file = ['Ace' num2str(i) '.jpg'];
    [WSyz,WSz,h]=RDeltWSRKin(c,l,e,d,th);
    saveas(h,file);
end
resetvaluesftwsm
for i = 1:4
    cc=.5*i;
    c=[cc cc cc];
    d=c;
    file = ['Acd' num2str(i) '.jpg'];
    [WSyz,WSz,h]=RDeltWSRKin(c,l,e,d,th);
    saveas(h,file);
end
resetvaluesftwsm
for i = 1:4
    ll=.5*i;
    l=[ll ll ll];
    e=l;
    file = ['Ale' num2str(i) '.jpg'];
    [WSyz,WSz,h]=RDeltWSRKin(c,l,e,d,th);
    saveas(h,file);
end
resetvaluesftwsm
for i = 1:4
    ll=.5*i;
    l=[ll ll ll];
    d=l;
    file = ['Ald' num2str(i) '.jpg'];

```

```

        [WSyz,WSz,h]=RDeltWSRKin(c,l,e,d,th);
        saveas(h,file);
    end
    resetvaluesftwsm
    for i = 1:4
        ee=.5*i;
        e=[ee ee ee];
        d=e;
        file = ['Aed' num2str(i) '.jpg'];
        [WSyz,WSz,h]=RDeltWSRKin(c,l,e,d,th);
        saveas(h,file);
    end
    resetvaluesftwsm
    for i = 1:4
        cc=.5*i;
        c=[cc cc cc];
        l=c;
        e=c;
        file = ['Acle' num2str(i) '.jpg'];
        [WSyz,WSz,h]=RDeltWSRKin(c,l,e,d,th);
        saveas(h,file);
    end
    resetvaluesftwsm
    for i = 1:4
        cc=.5*i;
        c=[cc cc cc];
        l=c;
        d=c;
        file = ['Acld' num2str(i) '.jpg'];
        [WSyz,WSz,h]=RDeltWSRKin(c,l,e,d,th);
        saveas(h,file);
    end
    resetvaluesftwsm
    for i = 1:4
        cc=.5*i;
        c=[cc cc cc];
        d=c;
        e=c;
        file = ['Aced' num2str(i) '.jpg'];
        [WSyz,WSz,h]=RDeltWSRKin(c,l,e,d,th);
        saveas(h,file);
    end
    resetvaluesftwsm
    for i = 1:4
        ll=.5*i;
        l=[ll ll ll];
        e=l;
        d=l;
        file = ['Alde' num2str(i) '.jpg'];
        [WSyz,WSz,h]=RDeltWSRKin(c,l,e,d,th);
        saveas(h,file);
    end
    resetvaluesftwsm
    for i = 1:4
        t=i*(pi/12)
        th = [t (pi-t) (3/2)*pi];
        file = ['Ath' num2str(i) '.jpg'];
    end

```

```

    [WSyz,WSz,h]=RDeltWSRKin(c,l,e,d,th);
    saveas(h,file);
end

function resetvaluesftwsm
global l e d th c
c = ones(1,3);
l = ones(1,3);
e = ones(1,3);
d = ones(1,3);
th = [pi/6 (5/6)*pi (3/2)*pi];

```

C.1.2 RotDeltVar2.m

```

function RotDeltVar

global l e d th c
%%%%%%%%%%%%%%%%%%%%%%%%%%%%%%%%%%%%%%%%%%%%%%%%%%%%%%%%%%%%%%%%%%%%%%%%
%%Parameter variations when (c-e) is positive
%%%%%%%%%%%%%%%%%%%%%%%%%%%%%%%%%%%%%%%%%%%%%%%%%%%%%%%%%%%%%%%%%%%%%%%%
resetvaluesftwsm
k=0;
for i = 1:4
    cc=.25*i;
    c=1+[cc cc cc];
    file = ['pce' num2str(i) '.jpg'];
    [WSyz,WSz,h]=RDeltWSRKin(c,l,e,d,th);
    saveas(h,file);
end
resetvaluesftwsm
c=1.5*c;
for i = 1:4
    ll = .5*i;
    l = [ll ll ll];
    file = ['pl' num2str(i) '.jpg'];
    [WSyz,WSz,h]=RDELTWSRKin(c,l,e,d,th);
    saveas(h,file);
end
resetvaluesftwsm
c=1.5*c;
for i = 1:4
    dd=.5*i;
    d=[dd dd dd];
    file = ['pd' num2str(i) '.jpg'];
    [WSyz,WSz,h]=RDELTWSRKin(c,l,e,d,th);
    saveas(h,file);
end
resetvaluesftwsm
for i = 1:4
    cc=.25*i;
    c=1+[cc cc cc];
    l=2*[cc cc cc];

```

```

        file = ['pcel' num2str(i) '.jpg'];
        [WSyz,WSz,h]=RDeltWSRKin(c,l,e,d,th);
        saveas(h,file);
    end
    resetvaluesftwsm
    for i = 1:4
        cc=.25*i;
        c=1+[cc cc cc];
        d=2*[cc cc cc];
        file = ['pced' num2str(i) '.jpg'];
        [WSyz,WSz,h]=RDeltWSRKin(c,l,e,d,th);
        saveas(h,file);
    end
    resetvaluesftwsm
    c=1.5*c;
    for i = 1:4
        ll=.5*i;
        l=[ll ll ll];
        d=l;
        file = ['pld' num2str(i) '.jpg'];
        [WSyz,WSz,h]=RDeltWSRKin(c,l,e,d,th);
        saveas(h,file);
    end
    %%%%%%%%%%%%%%%%%%%%%%%%%%%%%%%%%%%%%%%%%%%%%%%%%%%%%%%%%%%%%%%%%%%%%%%%%%%
    %%Parameter variations when (c-e) is negative
    %%%%%%%%%%%%%%%%%%%%%%%%%%%%%%%%%%%%%%%%%%%%%%%%%%%%%%%%%%%%%%%%%%%%%%%%%%%
    resetvaluesftwsm
    k=0;
    for i = 1:4
        ee=.25*i;
        e=1+[ee ee ee];
        file = ['nce' num2str(i) '.jpg'];
        [WSyz,WSz,h]=RDeltWSRKin(c,l,e,d,th);
        saveas(h,file);
    end
    resetvaluesftwsm
    e=1.5*e;
    for i = 1:4
        ll = .5*i;
        l = [ll ll ll];
        file = ['nl' num2str(i) '.jpg'];
        [WSyz,WSz,h]=RDELTWSRKin(c,l,e,d,th);
        saveas(h,file);
    end
    resetvaluesftwsm
    e=1.5*e;
    for i = 1:4
        dd=.5*i;
        d=[dd dd dd];
        file = ['nd' num2str(i) '.jpg'];
        [WSyz,WSz,h]=RDELTWSRKin(c,l,e,d,th);
        saveas(h,file);
    end
    resetvaluesftwsm

    for i = 1:4
        ee=.25*i;

```

```

        e=1+[ee ee ee];
        l=2*[ee ee ee];
        file = ['ncel' num2str(i) '.jpg'];
        [WSyz,WSz,h]=RDeltWSRKin(c,l,e,d,th);
        saveas(h,file);
    end
    resetvaluesftwsm
    for i = 1:4
        ee=.25*i;
        e=1+[ee ee ee];
        d=2*[ee ee ee];
        file = ['nced' num2str(i) '.jpg'];
        [WSyz,WSz,h]=RDeltWSRKin(c,l,e,d,th);
        saveas(h,file);
    end
    resetvaluesftwsm
    e=1.5*e;
    for i = 1:4
        ll=.5*i;
        l=[ll ll ll];
        d=l;
        file = ['nld' num2str(i) '.jpg'];
        [WSyz,WSz,h]=RDeltWSRKin(c,l,e,d,th);
        saveas(h,file);
    end
end

```

```

function resetvaluesftwsm
global l e d th c
c = ones(1,3);
l = ones(1,3);
e = ones(1,3);
d = ones(1,3);
th = [pi/6 (5/6)*pi (3/2)*pi];

```

C.1.3 RDeltWSRKin.m

```

function [WSyz,WSz,f]=RDeltWSRKin(c,l,e,d,th);

E = zeros(3);
E(1,:) = -e.*cos(th);
E(2,:) = -e.*sin(th);
C=zeros(3);
C(1,:) =c.*cos(th);
C(2,:) =c.*sin(th);
C2=[C C];
E2=[E E];
m=0;
for i=-3:0.2:3;
    for j=-6:0.2:0;

```

```

        ee=[0 0 0;i i i;j j j];
        [ph,LD]=rKinRot(ee,C,E,l,d,th);
        if imag(ph)==0
            AllLimb=[0 0 0];
            LD2=[LD LD];
            L(1,:)=[l.*cos(ph(1,:,1)).*cos(th)
l.*cos(ph(1,:,2)).*cos(th)];
            L(2,:)=[l.*cos(ph(1,:,1)).*sin(th)
l.*cos(ph(1,:,2)).*sin(th)];
            L(3,:)=[-l.*sin(ph(1,:,1)) -l.*sin(ph(1,:,2))];
            D=LD2-L;
            CxLD=cross(C2,LD2,1);
            LxD=cross(L,D,1);
            DxE=cross(D,E2,1);
            d1=dot(CxLD,LxD);
            d2=dot(CxLD,DxE);
            for k=0:1
                for a=1:3
                    if d1(a+3*k)>0
                        if d2(a+3*k)>0
                            AllLimb(a)=1;
                        end
                    end
                end
            end
            if AllLimb==1
                m=m+1;
                WSyz(m,:)=[ee(:,1)',ph(1,:,k)];
            end
        end
    end
end
WSz=zeros(3,12,3);
for k=1:3
    m=0;
    for i=-3:0.2:3
        for j=-3:0.2:3
            ee=[i;j;-0.5*k];
            ee=[ee ee ee];
            [ph,LD]=rKinRot(ee,C,E,l,d,th);
            if imag(ph)==0
                AllLimb=[0 0 0];
                LD2=[LD LD];
                L(1,:)=[l.*cos(ph(1,:,1)).*cos(th)
l.*cos(ph(1,:,2)).*cos(th)];
                L(2,:)=[l.*cos(ph(1,:,1)).*sin(th)
l.*cos(ph(1,:,2)).*sin(th)];
                L(3,:)=[-l.*sin(ph(1,:,1)) -l.*sin(ph(1,:,2))];
                D=LD2-L;
                CxLD=cross(C2,LD2,1);
                LxD=cross(L,D,1);
                DxE=cross(D,E2,1);
                d1=dot(CxLD,LxD);
                d2=dot(CxLD,DxE);
                for n=0:1
                    for a=1:3
                        if d1(a+3*n)>0

```

```

                                if d2(a+3*n)>0
                                    AllLimb(a)=1;
                                end
                            end
                        end
                    end
                if AllLimb==1
                    m=m+1;
                    WSz(m, :, k)=[ee(:, 1)', ph(1, :, n)];
                end
            end
        end
    end
end

f=WSPlotRKin(WSyZ, WSz);

```

C.1.4 rKinRot.m

```

function [ph,CD] = rKinRot(ee,C,E,l,d,th)

CD = ee-E-C;
X1=zeros(3);
Y1=zeros(3);
X1(1, :)=cos(th);
X1(2, :)=sin(th);
Y1(3, :)=[-1 -1 -1];
CDX=dot(CD,X1,1);
CDY=dot(CD,Y1,1);
a=2*l.*CDX+l.^2-d.^2+dot(CD,CD,1);
b=-4*l.*CDY;
c=-2*l.*CDX+l.^2-d.^2+dot(CD,CD,1);
if a~=0
    t1=(-b+sqrt(b.^2-4*a.*c))./(2*a);
    t2=(-b-sqrt(b.^2-4*a.*c))./(2*a);
    ph(1, :, 1)=2*atan(t1);
    ph(1, :, 2)=2*atan(t2);
    CDi=[CD(1, :).*cos(th)+CD(2, :).*sin(th);-
CD(1, :).*sin(th)+CD(2, :, :).*cos(th);CD(3, :)];
else
    ph(1, :, 1)=[i i i];
    ph(1, :, 2)=[i i i];
end

```

C.1.5 WSplotRKin.m

```
function f = WSplotRKin(WSyZ,WSz)

Subplot(2,2,1);
plot(WSz(:,1,1),WSz(:,2,1),'.');
Xlabel('X');
ylabel('Y');
title('Z = -0.5');
axis([-3 3 -3 3]);
Subplot(2,2,2);
if size(WSz,3)>1
    plot(WSz(:,1,2),WSz(:,2,2),'.');
end
Xlabel('X');
ylabel('Y');
title('Z = -1');
axis([-3 3 -3 3]);
Subplot(2,2,3);
if size(WSz,3)==3
    plot(WSz(:,1,3),WSz(:,2,3),'.');
end
Xlabel('X');
ylabel('Y');
title('Z = -1.5');
axis([-3 3 -3 3]);
Subplot(2,2,4);
plot(WSyZ(:,2),WSyZ(:,3),'.');
Xlabel('Y');
ylabel('Z');
title('X = 0');
axis([-3 3 -6 0]);
f=figure(1);
```

C.2 Matlab Code for Quantitative Workspace Study

The Matlab code for the Quantitative workspace study begins with LinkVar.m. It varies the robot parameters as specified in each round of the quantitative workspace study. It specifies a maximum scaling factor then calls robotscale3.m to calculate the minimum scaling factor that will allow the required workspace to fit inside the scaled parallel mechanism workspace. robotscale3.m systematically reduces the scaling factor and compares the required workspace to the workspace of the scaled parallel mechanism

until the required workspace will no longer fit. To determine if the required workspace will fit in the scaled parallel mechanism workspace it calls FaceInWS2.m to determine if the top and bottom faces of the required workspace fit in the scaled parallel mechanism workspace. FaceInWS2.m checks whether each face is in the parallel mechanism workspace by calling inWS2.m to check 9 strategically chosen points on the face. When the minimum scaling factor has been determined robotscale3.m calls RDeltWSRKin2 to produce a workspace plot similar to those produced in the qualitative workspace study, and WSBoundary2.m to produce a plot showing the intersections of the top and bottom faces of the required workspace with the workspace of the parallel mechanism.

C.2.1 LinkVar.m

```
clear Results
count=1;
sf=3;

l=1;
%%First round of quantitative workspace study
% for c=0.75:-0.25:-0.75
%   for d=1:0.5:2
%%Second round of quantitative workspace study
% for c=0.6:-0.1:-0.1
%   for d=1:0.5:2
%%Third round of quantitative workspace study
for c=0.2:0.1:0.3
    for d=1.6:0.1:2.1
%%%%%%%%%%%%%%%%%%%%%%%%%%%%%%%%%%%%%%%%%%%%%%%%%%%%%%%%%%%%%%%%%%%%%%%%
        co = c*ones(1,3);
        lo = l*ones(1,3);
        eo = 1*ones(1,3);
        do = d*ones(1,3);
        ce=c-1;
        ans =robotscale3(co,lo,eo,do,sf,count);
        Results(count,:)= [l ce d ans];
        count=count+1;
    end
end
Results
```

C.2.2 robotscale3.m

```
function ans =robotscale3(co,lo,eo,do,sf, count)

% Given a set of robot link lengths and a required robot workspace
% this program will determine woy much the robot link lengths must
% be scaled up or down to achieve the smallest robot with a workspace
% that will fit the required workspace with a safety factor.
WS=[2.5 1.875 2.5];
th = [pi/6 (5/6)*pi (3/2)*pi];
Eo = zeros(3);
Eo(1,:) = -eo.*cos(th);
Eo(2,:) = -eo.*sin(th);
Co=zeros(3);
Co(1,:) =co.*cos(th);
Co(2,:) =co.*sin(th);
maxmino=[1.5 1.5 0;-1.5 -1.5 -3];
incriment=1/12;
yes=1;
a=0.1; %Scaling factor step incriment
while yes
    sf=sf-a
    C=sf*Co;
    E=sf*Eo;
    l=sf*lo;
    d=sf*do;
    maxmin=maxmino*sf;
    maxmin(1,:)=maxmin(1,)-WS;
    clear ang;
    yes=0;
    for k=maxmin(2,3):incriment:maxmin(1,3)
        i=-WS(1)/2;
        j=-WS(2)/2;
%bottom face
        [y,ang1]=FaceInWS2(WS,i,j,k,C,E,l,d,th);
        if y
%top face
            [y,ang2]=FaceInWS2(WS,i,j,k+WS(3),C,E,l,d(1),th);
            if y
                yes=1;
                coord=[i j k];
            end
        end
    end
    if yes
        break
    end
end
end
sf=sf+a;
```

```

ans=[sf coord];
c=co*sf;
l=lo*sf;
e=eo*sf;
C=sf*Co;
E=sf*Eo;
l=sf*lo;
d=sf*do;
figure((count*2)-1);
WSBoundry2(C,l,E,d,th,WS,coord);
figure(count*2);
[WSyz,WSz]=RDeltWSRKin2(c,l,e,d,th);

```

C.2.3 FaceinWS2.m

```

function [yes,ang]=FaceInWS2(WS,i,j,k,C,E,l,d,th)

yes =0;
ang=zeros(1,12);
WS2=WS./2;
%first corner
ee=[i j k];
ee=[ee' ee' ee'];
[in,ang(1,:)]=inWS2(ee,C,E,l,d,th);
if in
%second corner
    ee=[i+WS(1) j+WS(2) k];
    ee=[ee' ee' ee'];
    [in,ang(2,:)]=inWS2(ee,C,E,l,d,th);
    if in
%third corner
        ee=[i j+WS(2) k];
        ee=[ee' ee' ee'];
        [in,ang(3,:)]=inWS2(ee,C,E,l,d,th);
        if in
%fourth corner
            ee=[i+WS(1) j k];
            ee=[ee' ee' ee'];
            [in,ang(4,:)]=inWS2(ee,C,E,l,d,th);

            if in
%center of face
                ee=[i+WS2(1) j+WS2(2) k];
                ee=[ee' ee' ee'];
                [in,ang(5,:)]=inWS2(ee,C,E,l,d,th);
                if in
%first side
                    ee=[i+WS2(1) j+WS(2) k];
                    ee=[ee' ee' ee'];
                    [in,ang(6,:)]=inWS2(ee,C,E,l,d,th);
                    if in

```



```

m=0;
for i=border(1,2):0.2:border(2,2);
    for j=border(1,3):0.2:border(2,3);
        ee=[0 0 0;i i i;j j j];
        [in,ang(3,:)]=inWS2(ee,C,E,l,d,th);
        if in
            m=m+1;
            WSyz(m,:)=ee(:,1)';
        end
    end
end
end
WSz=zeros(3,3,3);
for k=1:2
    m=0;
    for i=border(1,1):0.2:border(2,1);
        for j=border(1,2):0.2:border(2,2);
            ee=[i;j;z(k)];
            ee=[ee ee ee];
            [in,ang(3,:)]=inWS2(ee,C,E,l,d,th);
            if in
                m=m+1;
                WSz(m,:,k)=ee(:,1)';
            end
        end
    end
end
end
Subplot(2,2,1);
plot(WSyz(:,2),WSyz(:,3),'.');
xlabel('Y');
ylabel('Z');
title('X = 0');
axis([border(1,2) border(2,2) border(1,3) border(2,3)]);
Subplot(2,2,3);
plot(WSz(:,1,1),WSz(:,2,1),'.');
xlabel('X');
ylabel('Y');
z1=num2str(z(1));
z1=['Z = ' z1];
title(z1);
axis([border(1,1) border(2,1) border(1,2) border(2,2)]);
Subplot(2,2,4);
plot(WSz(:,1,2),WSz(:,2,2),'.');
xlabel('X');
ylabel('Y');
z2=num2str(z(2));
z2=['Z = ' z2];
title(z2);
axis([border(1,1) border(2,1) border(1,2) border(2,2)]);

```

C.2.6 RDeltWSRKin2.m

```
function [WSyz,WSz]=RDeltWSRKin2(c,l,e,d,th);

E = zeros(3);
E(1,:) = -e.*cos(th);
E(2,:) = -e.*sin(th);
C=zeros(3);
C(1,:) =c.*cos(th);
C(2,:) =c.*sin(th);
C2=[C C];
E2=[E E];
m=0;
o=0;
for i=-4:0.2:4;
    for j=-8:0.25:0;
        ee=[0 0 0;i i i;j j j];
        [in,ang(3,:)]=inWS2(ee,C,E,l,d,th);
        if in
            m=m+1;
            WSyz(m,:)=ee(:,1)';
        end
    end
end
WSz=zeros(1,3,3);
for k=1:3
    m=0;
    for i=-4:0.25:4
        for j=-4:0.25:4
            ee=[i;j;-1.5*k];
            ee=[ee ee ee];
            [in,ang(3,:)]=inWS2(ee,C,E,l,d,th);
            if in
                m=m+1;
                WSz(m,:,k)=ee(:,1)';
            end
        end
    end
end
f=WSPlotRKin(WSyz,WSz);
```

C.3 Matlab Code for Calculating Range of Joint Angles

The Matlab code shown below estimates the range of joint angles experienced by the joints of the parallel mechanism. It examines 1331 points within the required

workspace and determines what all of the actuated and non- actuated joint angles of the parallel mechanism are at each position. The maximum and minimum values calculated for each joint angle give the range of angles each joint experiences.

C.3.1 JointRange.m

```
function JointRange

% This function determines the joint angles of the non-actuated joints
of the
% parallel mechanism. From this information it determines the range of
motion
% of the non-actuated joints.
c = ((12+3)/12)*ones(1,3);
l = (19/12)*ones(1,3);
e = 1*ones(1,3);
d = (34/12)*ones(1,3);
th = [-(1/3)*pi (1/3)*pi (3/2)*pi];
E = zeros(3);
E(1,:) = -e.*cos(th);
E(2,:) = -e.*sin(th);
C=zeros(3);
C(1,:) = c.*cos(th);
C(2,:) = c.*sin(th);
WS=[1.875 2.5 2.5];
coord=[-WS(1)/2 -WS(2)/2 -(46/12)];
h=0;
for i=0:.1:1
    for j=0:.1:1
        for k=0:.1:1
            h=h+1;
            point(h,:)=coord+WS.*[i j k];
        end
    end
end
for i=1:length(point)
    ee=[point(i,:) ' point(i,:) ' point(i,:)'];
    [in,Jang(i,:)] = inWS2(ee,C,E,l,d,th);
end
Jang
MaxJang= [max(Jang);180.*max(Jang)./pi]
MinJang= [min(Jang);;180.*min(Jang)./pi]
DeltaJang= MaxJang-MinJang
```

C.4 Matlab Code for Dynamic Analysis of Robot

The Matlab functions in this section implement the dynamic model developed in Section 6.4 and use it to conduct the dynamic prototype analyses discussed in Section 6.5. DynamicModel.m sets up some of the inertial properties of the robot prototype and fits third order curves to the specified initial and final conditions of the parallel platform and robot wrist. It then calls inWS2.m (Section C.2.4) to determine the parallel mechanism actuator joint angles needed to achieve the moving platform motion. The parallel mechanism actuator joint angles are differentiated twice using dif.m to determine the required angular velocity and angular acceleration of the parallel mechanism actuators. DynamicModel.m then calls wristsim.m to simulate the dynamic behavior of the robot wrist, PlatBal.m to simulate the dynamic behavior of the moving platform, and armBal.m to simulate the dynamic behavior of the upper arms of the parallel mechanism. Most of the code of DynamicModel.m is used to plot the results, which are presented in Appendix E.

C.4.1 DynamicModel.m

```
function DynamicModel

BreastUp=0 %Set to 1 to simulate breast up WOG capture, 0 to simulate
breast down WOG capture
Prototype=3 %Set to 1,2 or 3 depending on the prototype being simulated

t=[0:.001:0.4];
p0=[-(pi/3) pi/3 pi];
%%%%%%%%%%%%%%%%%%%%%%%%%%%%%%%%%%%%%%%%%%%%%%%%%%%%%%%%%%%%%%%%%%%%%%%%
%Third order Polynomial position control For Parallel Mechanism &
"Rotate"
%onstant magnitude acceleration for "Flip"
pin=[-9 -12 -39];
```

```

if BreastUp
    pf=[9 12 -21];
    pwi=pi;
    pwf=0;
    twi= pi;
    twf=pi;
    if Prototype==3
        pin=[-9 -12 -33];
        Pf=[9 12 -15];
    end
end
if BreastUp==0
    pf=[9 12 -36];
    pwi=0;
    pwf=pi;
    twi= pi;
    twf= 0;
    if Prototype==3
        pin=[-9 -12 -33];
        pf=[9 12 -30];
    end
end
vi=[0 -18.2 0];
vf=[0 9.1 0];
dpwi=0;
dpwf=0;
ddtwi=2*(twf-twi)/(0.4^2);
tf=t(length(t));
tm=[1 0 0 0;0 1 0 0;1 tf tf^2 tf^3;0 1 2*tf 3*tf^2];
XYZm=[pin;vi;pf;vf];
XYZc=inv(tm)*XYZm;
pwc=inv(tm)*[pwi dpwi pwf dpwf]';
for i=1:length(t)
    for j=1:3

        p(i,j)=(XYZc(4,j)*(t(i)^3))+(XYZc(3,j)*(t(i)^2))+(XYZc(2,j)*t(i))
+(XYZc(1,j));
        v(i,j)=3*XYZc(4,j)*(t(i)^2)+2*XYZc(3,j)*t(i)+XYZc(2,j);
        a(i,j)=6*XYZc(4,j)*t(i)+2*XYZc(3,j);
    end
    pw(i,1)=pwc(4)*(t(i)^3)+pwc(3)*(t(i)^2)+pwc(2)*t(i)+pwc(1);
    dpw(i,1)=3*pwc(4)*(t(i)^2)+2*pwc(3)*t(i)+pwc(2);
    ddpw(i,1)=6*pwc(4)*t(i)+2*pwc(3);
    tw(i,1)=twi+0.5*ddtwi*(t(i)^2);
    dtw(i,1)=ddtwi*t(i);
    ddtw(i,1)=ddtwi;
end

end
%%%%%%%%%%%%%%%%%%%%%%%%%%%%%%%%%%%%%%%%%%%%%%%%%%%%%%%%%%%%%%%%%%%%%%%%
figure(1);
title('X')
subplot(2,2,1);
plot(t,a(:,1));
title('X Acceleration');
ylabel('in/s^2')
xlabel('s')
subplot(2,2,2);

```

```

plot(t,v(:,1));
title('X Velocity');
ylabel('in/s')
xlabel('s')
subplot(2,2,3);
plot(t,p(:,1));
title('X Position');
ylabel('in')
xlabel('s')
f=figure(1);
saveas(f,'X.jpg')

figure(2);
title('Y')
subplot(2,2,1);
plot(t,a(:,2));
title('Y Acceleration');
ylabel('in/s^2')
xlabel('s')
subplot(2,2,2);
plot(t,v(:,2));
title('Y Velocity');
ylabel('in/s')
xlabel('s')
subplot(2,2,3);
plot(t,p(:,2));
title('Y Position');
ylabel('in')
xlabel('s')
f=figure(2);
saveas(f,'Y.jpg')

figure(3);
title('Z')
subplot(2,2,1);
plot(t,a(:,3));
title('Z Acceleration');
ylabel('in/s^2')
xlabel('s')
subplot(2,2,2);
plot(t,v(:,3));
title('Z Velocity');
ylabel('in/s')
xlabel('s')
subplot(2,2,3);
plot(t,p(:,3));
title('Z Position');
ylabel('in')
xlabel('s')
f=figure(3);
saveas(f,'Z.jpg')

figure(4);
title('thw')
subplot(2,2,1);
plot(t,ddtw);
title('thw Acceleration');

```

```

ylabel('rad/s^2')
xlabel('s')
subplot(2,2,2);
plot(t,dtw);
title('thw Velocity');
ylabel('rad/s')
xlabel('s')
subplot(2,2,3);
plot(t,tw);
title('thw Position');
ylabel('rad')
xlabel('s')

figure(5);
title('pw')
subplot(2,2,1);
plot(t,ddpw);
title('pw Acceleration');
ylabel('rad/s^2')
xlabel('s')
subplot(2,2,2);
plot(t,dpw);
title('pw Velocity');
ylabel('rad/s')
xlabel('s')
subplot(2,2,3);
plot(t,pw);
title('pw Position');
ylabel('rad')
xlabel('s')

if Prototype<3
    e=7;
    c=7+3;
    d=34;
    l=19;
end
if Prototype==3
    e=7;
    c=7+2;
    d=25;
    l=15;
end
th1=zeros(length(p),3);
for i=1:length(p(:,1))
    ee=p(i,:);
    ee=[ee' ee' ee'];
    E = zeros(3);
    E(1,:) = -e.*cos(p0);
    E(2,:) = -e.*sin(p0);
    C=zeros(3);
    C(1,:) =c.*cos(p0);
    C(2,:) =c.*sin(p0);
    [LD(:, :, i), ang]=inWS(ee,C,E,l,d,p0);
    th1(i,:)=ang(1,1:3);
end
dth1=dif(th1,t);

```

```

ddth1=dif(dth1,t);

[Fw Mtw Mpw]=wristsim(a,tw,dtw,ddtw,pw,dpw,ddpw); %Dynamic Simulation
of the wrist
F=PlatBal(a,Fw,LD,Prototype); %Dynamic Simulation of the moving
platform
Ma=armBal(th1,dth1,ddth1,p0,F,l,Prototype); %Dynamic Simulation of
the upper arms
RMS=sqrt(sum(Mpw.^2)/length(Mpw)) %Calculation of the RMS torque
required from the "Rotate" motion generator

figure(5)
subplot(2,2,4)
plot(t,Mpw)
title('pw Actuating Moment (in-lb)')
ylabel('in-lb')
xlabel('t')
f=figure(5);
saveas(f,'pw.jpg')

figure(4)
subplot(2,2,4)
plot(t,Mtw)
title('thw Actuating Moment (in-lb)')
ylabel('in-lb')
xlabel('t')
f=figure(4);
saveas(f,'thw.jpg')

figure(6);
subplot(2,2,1);
plot(t,ddth1(:,1));
title('th11 Acceleration');
ylabel('rad/s^2')
xlabel('t')
subplot(2,2,2);
plot(t,dth1(:,1));
title('th11 Velocity');
ylabel('rad/s')
xlabel('t')
subplot(2,2,3);
plot(t,th1(:,1));
title('th11 Position');
ylabel('rad')
xlabel('t')
subplot(2,2,4)
plot(t,Ma(:,1))
title('th11 Actuating Moment (in-lb)')
ylabel('in-lb')
xlabel('t')
f=figure(6);
saveas(f,'th11.jpg')

figure(7);
subplot(2,2,1);
plot(t,ddth1(:,2));
title('th12 Acceleration');

```

```

ylabel('rad/s^2')
xlabel('t')
subplot(2,2,2);
plot(t,dth1(:,2));
title('th12 Velocity');
ylabel('rad/s')
xlabel('t')
subplot(2,2,3);
plot(t,th1(:,2));
title('th12 Position');
ylabel('rad')
xlabel('t')
subplot(2,2,4)
plot(t,Ma(:,2))
title('th12 Actuating Moment (in-lb)')
ylabel('in-lb')
xlabel('t')
f=figure(7);
saveas(f,'th12.jpg')

figure(8);
subplot(2,2,1);
plot(t,ddth1(:,3));
title('th13 Acceleration');
ylabel('rad/s^2')
xlabel('t')
subplot(2,2,2);

plot(t,dth1(:,3));
title('th13 Velocity');
ylabel('rad/s')
xlabel('t')
subplot(2,2,3);
plot(t,th1(:,3));
title('th13 Position');
ylabel('rad')
xlabel('t')
subplot(2,2,4)
plot(t,Ma(:,3))
title('th13 Actuating Moment (in-lb)')
ylabel('in-lb')
xlabel('t')
f=figure(8);
saveas(f,'th13.jpg')

figure(9);
subplot(2,3,1);
plot(t,Mtw)
title('thw Actuating Moment (in-lb)')
ylabel('in-lb')
xlabel('t')
subplot(2,3,2);
plot(t,Mpw)
title('pw Actuating Moment (in-lb)')
ylabel('in-lb')
xlabel('t')
subplot(2,3,4);

```

```

plot(t, Ma(:,1))
title('th11 Actuating Moment (in-lb)')
ylabel('in-lb')
xlabel('t')
subplot(2,3,5);
plot(t, Ma(:,2))
title('th12 Actuating Moment (in-lb)')
ylabel('in-lb')
xlabel('t')
subplot(2,3,6);
plot(t, Ma(:,3))
title('th13 Actuating Moment (in-lb)')
ylabel('in-lb')
xlabel('t')
f=figure(9);
saveas(f, 'ControlEffort.jpg')

Th11MaxMin=[max(Ma(:,1)) min(Ma(:,1))]
Th12MaxMin=[max(Ma(:,2)) min(Ma(:,2))]
Th13MaxMin=[max(Ma(:,3)) min(Ma(:,3))]
ThwMaxMin=[max(Mtw) min(Mtw)]

ThwMaxMin=[max(Mpw) min(Mpw)]

```

C.4.2 wristsim.m

```

function [F,Mtw,Mpw]=wristsim(a,tw,dtw,ddtw,pw,dpw,ddpw)

Iwog=[26.6 0 0;0 57 0;0 0 57]; %WOG rotational inertia
Iee=[35.74 0 0;0 18.25 0;0 0 21.19]; %end effector rotational
inertia
Iw3=[0.15 0 0;0 0.15 0;0 0 0.11]; %Stainless steel wrist component
rotational inertia
Iw2=[1.12 0 0;0 0.80 0;0 0 1.66]; %Delrin wrist component rotational
inertia
Im=[51.9 0 0;0 51.9 0;0 0 20.4]; %servo motor rotational inertia
mwog=5.5; %WOG mass
mee=2.5; %end effector mass
mw3=0.32; %Stainless Steel wrist component mass
mw2=0.78; %Delrin wrist component mass
mm=10; %Servo motor mass
if prototype == 3
    Im=[33.7 0 0;0 33.7 0;0 0 13.2]; %Servo motor rotational
inertia
    mm=6.5; %Servo motor mass
end
rwog=[1.5 0 7]'; %vector from F to WOG C.M.
ree=[-0.66 0 5.83]'; %vector from F to end effector C.M.
rw3=[0 0 0.67]'; %vector from F to stainless steel wrist component
C.M.
rw2=[0 0 0.1]'; %vector from F to Delrin wrist component C.M.

```

```

rm=[0 0 -4]';          %vector from F to vector motor C.M.
for i=1:length(tw)
    omegag=[0 dtw(i) dpw(i)]';
    alphag=[dpw(i)*dtw(i) ddtw(i) ddpw(i)]';
    omegah=[0 dtw(i) 0]';
    alphah=[0 ddtw(i) 0]';
    Reh=[cos(tw(i)) 0 sin(tw(i));0 1 0;-sin(tw(i)) 0 cos(tw(i))];
    Rhg=[cos(pw(i)) sin(pw(i)) 0;-sin(pw(i)) cos(pw(i)) 0;0 0 1];
    Rgh=[cos(pw(i)) -sin(pw(i)) 0;sin(pw(i)) cos(pw(i)) 0;0 0 1];
    Rhe=[cos(tw(i)) 0 -sin(tw(i));0 1 0;sin(tw(i)) 0 cos(tw(i))];
    wmg=[0 -dpw(i) dtw(i);dpw(i) 0 0;-dtw(i) 0 0];
    wmh=[0 0 dtw(i);0 0 0;-dtw(i) 0 0];
    awog=Reh*a(i,:)'+cross(alphag,Rgh*rwog)+cross(omegag,cross(omegag
,Rgh*rwog));
    aee=Reh*a(i,:)'+cross(alphag,Rgh*ree)+cross(omegag,cross(omegag,R
gh*ree));
    aw3=Reh*a(i,:)'+cross(alphag,Rgh*rw3)+cross(omegag,cross(omegag,R
gh*rw3));
    aw2=Reh*a(i,:)'+cross(alphah,rw2)+cross(omegah,cross(omegah,rw2))
;
    am=Reh*a(i,:)'+cross(alphah,rm)+cross(omegah,cross(omegah,rm));
    F(i,:)=(1/386)*(Rhe*(mwog*awog+mee*aee+mw3*aw3+mw2*aw2+mm*am)+[0
0 mwog+mee+mw3+mw2+mm]')';
    Mwog=(1/386)*(Rgh*Iwog*Rgh'*alphag+wmg*Rgh*Iwog*Rgh'*omegag+cross
(Rgh*rwog,mwog*awog));
    Mee=(1/386)*(Rgh*Iee*Rgh'*alphag+wmg*Rgh*Iee*Rgh'*omegag+cross(Rg
h*ree,mee*aee));
    Mw3=(1/386)*(Rgh*Iw3*Rgh'*alphag+wmg*Rgh*Iw3*Rgh'*omegag+cross(Rg
h*rw3,mw3*aw3));
    Mw2=(1/386)*(Iw2*alphah+wmh*Iw2*omegah+cross(rw2,mw2*aw2));
    Mm=(1/386)*(Im*alphah+wmh*Im*omegah+cross(rm,mm*am));
    M=Mwog+Mee+Mw3+Mw2+Mm;
    Mtw(i,1)=M(2);
    Mpw(i,1)=M(3);
end

```

C.4.3 PlatBal.m

```

function F=PlatBal(a,Fw,LD,Prototype)

if Prototype==1
    mmovingplatform=6.3;    %Mass of the moving platform
    mwristbar=2.8;         %Mass of bars connecting wrist to moving
platform
    mssairmotor=3;        %Mass of "Flip" generating actuator
    mLd1=8.2;             %Mass of linkage connecting L1 to D1
    mLd2=8.2;             %Mass of linkage connecting L2 to D2
    mLd3=2.8;             %Mass of linkage connecting L3 to D3
elseif Prototype==2
    mmovingplatform=3.6;
    mwristbar=1.1;

```

```

        mssairmotor=3;
        mLD1=3.8;
        mLD2=3.8;
        mLD3=2.8;
elseif Prototype==3
        mmovingplatform=3.6;
        mwristbar=0.9;
        mssairmotor=2.7;
        mLD1=3.1;
        mLD2=3.1;
        mLD3=2.3;
end
mp=mmovingplatform+mssairmotor+2*mwristbar+0.5*(mLD1+mLD2+mLD3);
for i=1:length(a);
    gamma=inv(LD(:, :, i))*((1/386)*mp*a(i, :)' + Fw(i, :)' + [0 0 mp]');
    F(i, :, 1)=LD(:, 1, i)*gamma(1);
    F(i, :, 2)=LD(:, 2, i)*gamma(2);
    F(i, :, 3)=LD(:, 3, i)*gamma(3);
    f(i, :)=34*gamma';
end
end

```

C.4.4 armBal.m

```

function Ma=armBal(th1,dth1,ddth1,p0,F,l,Prototype)

if Prototype==1
    ml=[2.6 2.6 2.06];%Mass of bars connecting points Ci to points Li
    md=[8.2 8.2 2.8]; %Mass of bars connecting points Li to points Di
    Iclcm(:, :, 1)=[1.17 0 0;0 90.9 0;0 0 90.6]; %Rotational inertia
of bar connecting C1 to L1
    Iclcm(:, :, 2)=[1.17 0 0;0 90.9 0;0 0 90.6]; %Rotational inertia
of bar connecting C2 to L2
    Iclcm(:, :, 3)=[0.56 0 0;0 71.5 0;0 0 71.5]; %Rotational inertia
of bar connecting C3 to L3
elseif Prototype==2
    ml=[2.6 2.6 2.06];
    ml=ml/2;
    md=[3.8 3.8 2.8];
    Iclcm(:, :, 1)=[1.17 0 0;0 90.9 0;0 0 90.6];
    Iclcm(:, :, 2)=[1.17 0 0;0 90.9 0;0 0 90.6];
    Iclcm(:, :, 3)=[0.56 0 0;0 71.5 0;0 0 71.5];
elseif Prototype ==3
    ml=[2.1 2 .1 1.66];
    md=[3.1 3.1 2.3];
    Iclcm(:, :, 1)=[0.94 0 0;0 47 0;0 0 47];
    Iclcm(:, :, 2)=[0.94 0 0;0 47 0;0 0 47];
    Iclcm(:, :, 3)=[0.45 0 0;0 47 0;0 0 47];
end
Icl(:, :, 1)=Iclcm(:, :, 1)+ml(1)*[0 0 0;0 (l/2)^2 0;0 0
(l/2)^2]+(md(1)/2)*[0 0 0;0 l^2 0;0 0 l^2];

```

```

Icl(:, :, 2)=Iclcm(:, :, 2)+ml(2)*[0 0 0;0 (1/2)^2 0;0 0
(1/2)^2]+(md(2)/2)*[0 0 0;0 1^2 0;0 0 1^2];
Icl(:, :, 3)=Iclcm(:, :, 3)+ml(3)*[0 0 0;0 (1/2)^2 0;0 0
(1/2)^2]+(md(3)/2)*[0 0 0;0 1^2 0;0 0 1^2];
Roi(:, :, 1)=[cos(p0(1)) sin(p0(1)) 0;-sin(p0(1)) cos(p0(1)) 0;0 0 1];
Roi(:, :, 2)=[cos(p0(2)) sin(p0(2)) 0;-sin(p0(2)) cos(p0(2)) 0;0 0 1];
Roi(:, :, 3)=[cos(p0(3)) sin(p0(3)) 0;-sin(p0(3)) cos(p0(3)) 0;0 0 1];
CL=[1 0 0]';
for j=1:length(F)
    for i=1:3
        Ria=[cos(th1(j,i)) 0 -sin(th1(j,i));0 1 0;sin(th1(j,i)) 0
cos(th1(j,i))];
        wmcl=[0 0 dth1(j,i);0 0 0;-dth1(j,i) 0 0];
        dth=[0 dth1(j,i) 0]';
        ddth=[0 ddth1(j,i) 0]';

        M=(1/386)*Icl(:, :, i)*ddth+(1/386)*wmcl*Icl(:, :, i)*dth+cross(CL,Ri
a*Roi(:, :, i)*(F(j, :, i)'+[0 0 -
md(i)/2]')))+cross(0.5*CL,Ria*Roi(:, :, i)*[0 0 -ml(i)]');
        Ma(j,i)=M(2);
    end
end
end

```

C.4.5 dif.m

```

function dw=dif(w,t)

dw(1, :)=(w(2, :)-w(1, :))/(t(2)-t(1));

for i=2:length(w)
    dw(i, :)=(w(i, :)-w(i-1, :))/(t(i)-t(i-1));
end

```

APPENDIX D

WORKSPACE PLOTS FOR THE QUALITATIVE WORKSPACE STUDY

The plots included in this appendix are generated as part of the qualitative workspace study carried out in Section 5.3. Each of the figures in the following pages illustrate how the workspace of the parallel mechanism changes as one, two, or three of the robot parameters are varied. Each quadrant of each figure illustrates the shape and size of the parallel mechanism workspace for the given set of robot parameters. Within each quadrant of each figure are four images. These images are cross sections of the workspace of the robot. The upper left, upper right, and lower left images are the intersections of the parallel mechanism workspace with the $Z = -0.5$, $Z = -1$, and $Z = -1.5$ planes respectively. The lower right image is the intersection of the parallel mechanism workspace with the $X = 0$ plane.

D.1 First Round of Qualitative Workspace Study

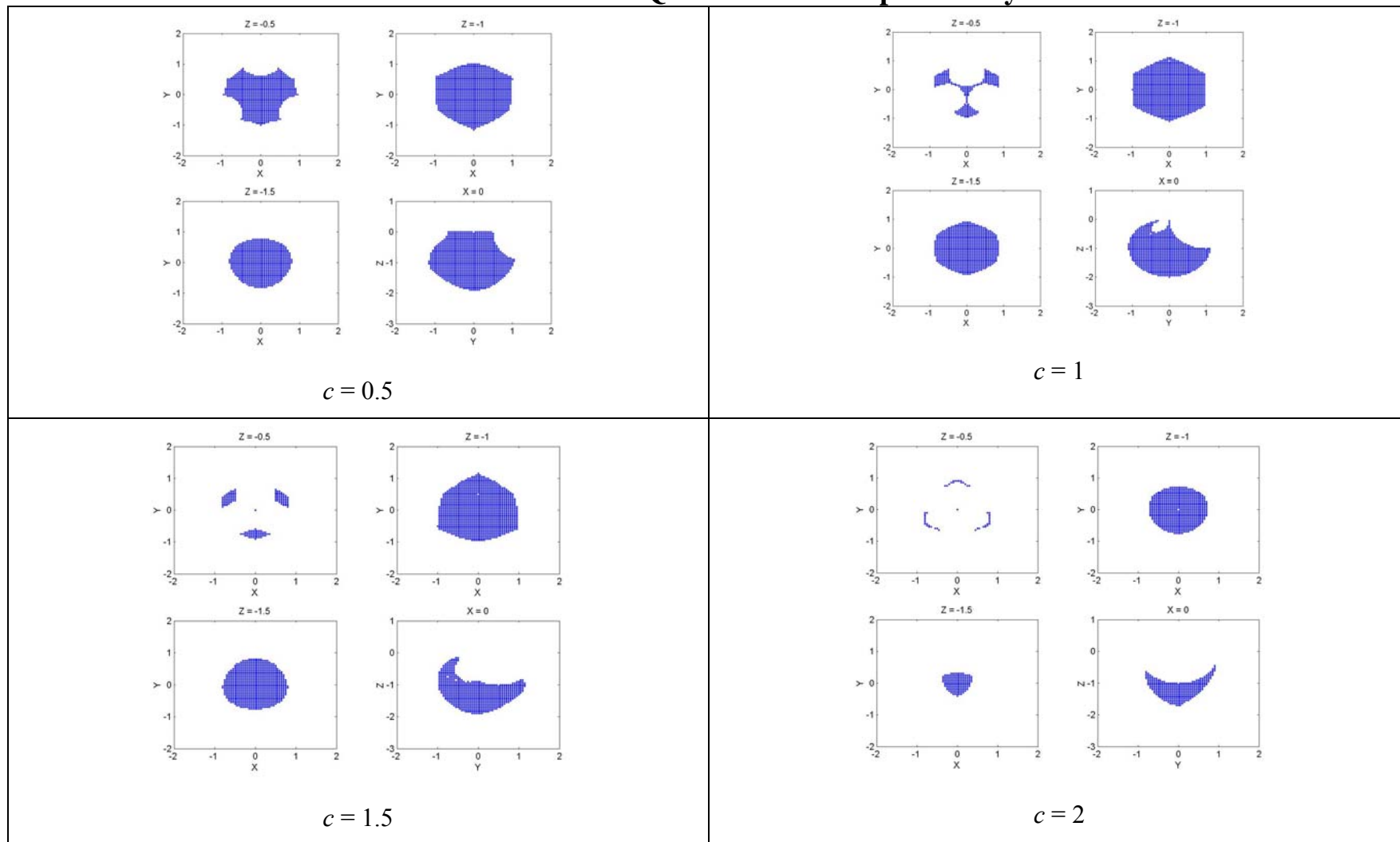


Figure D.1: Variation of c : $l = 1, e = 1, d = 1, \rho_{0i} = [30^\circ, 150^\circ, 270^\circ]$.

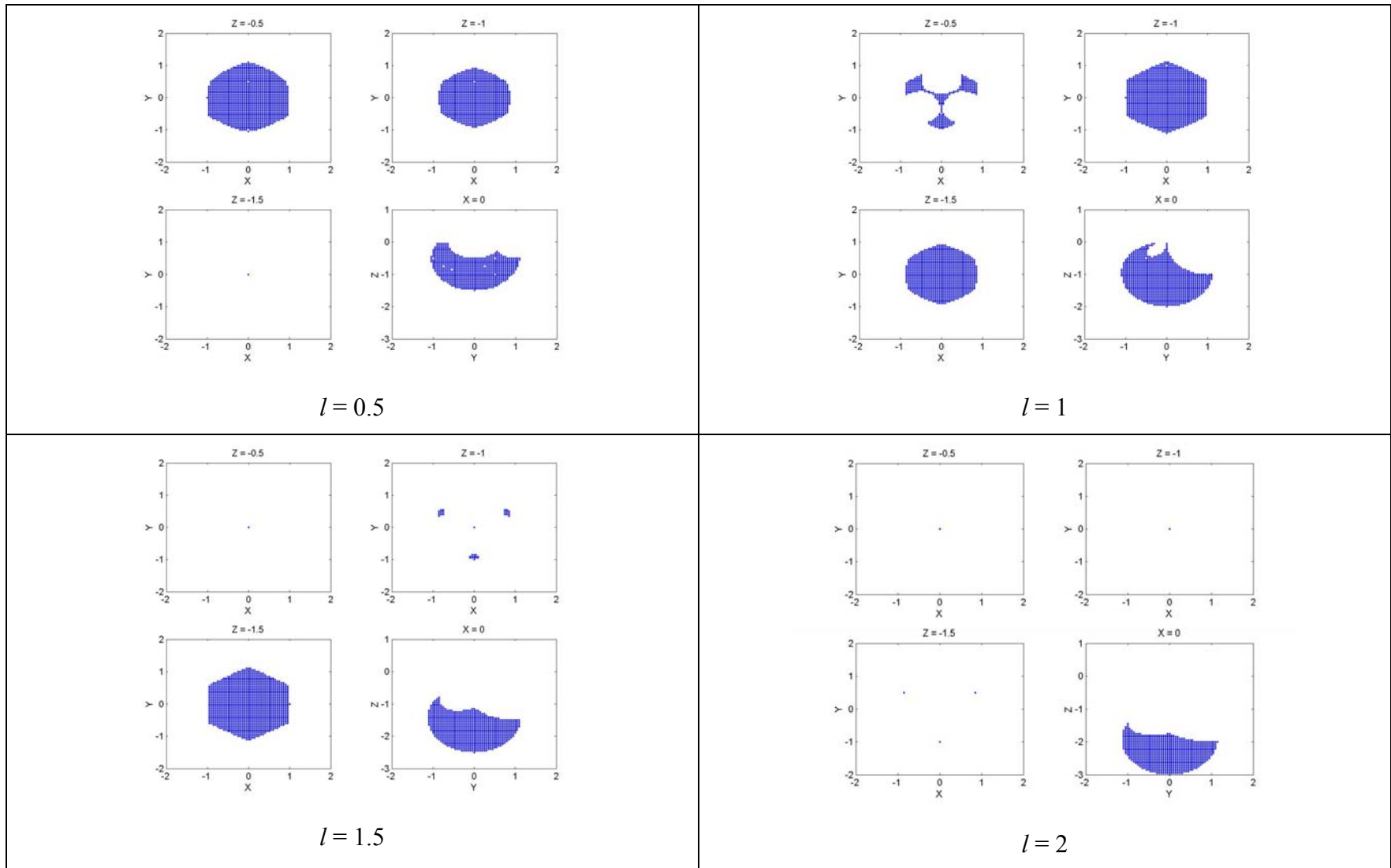


Figure D.2: Variation of l : $c = 1, e = 1, d = 1, \rho_{0i} = [30^\circ, 150^\circ, 270^\circ]$.

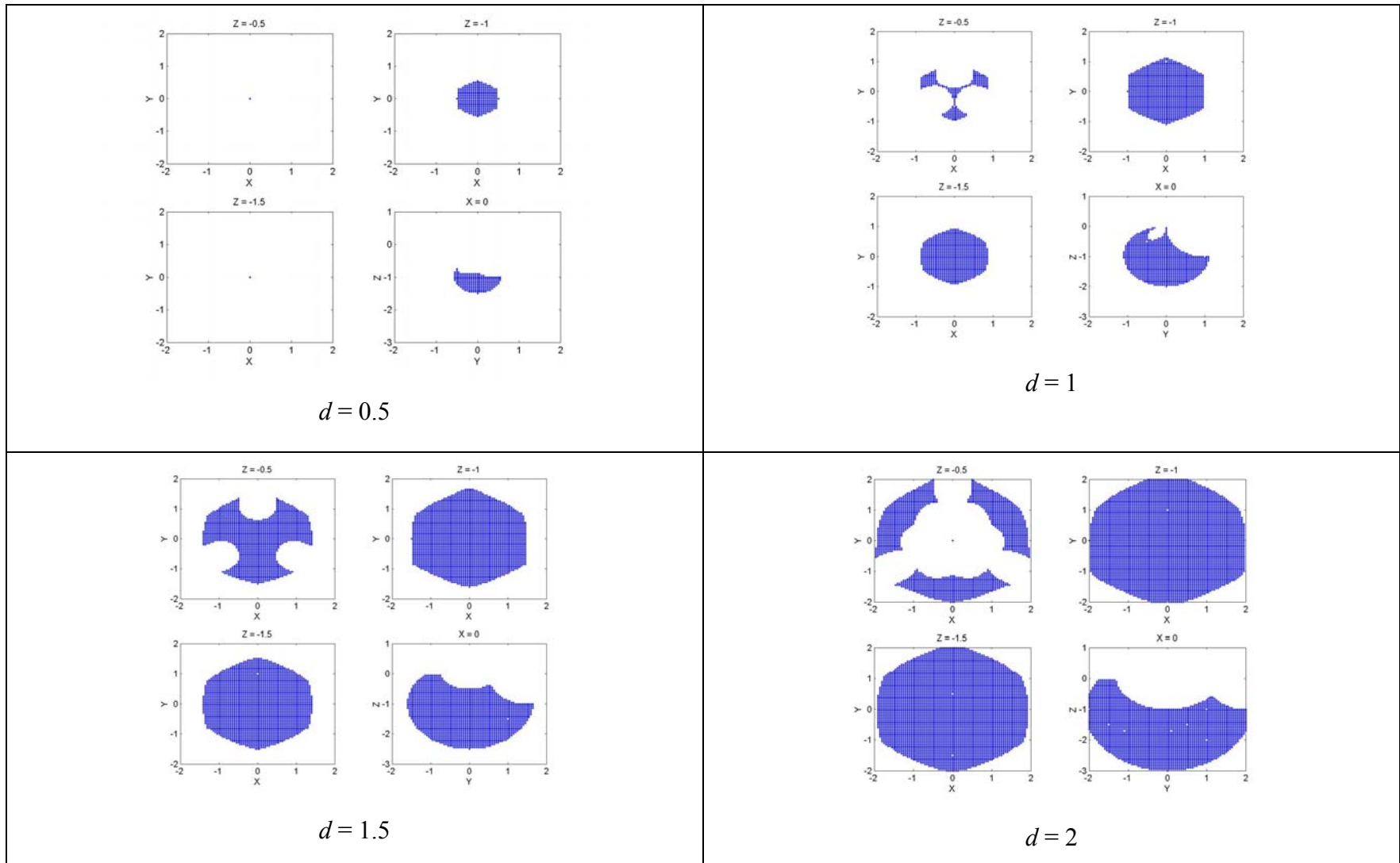


Figure D.3: Variation of d : $l = 1, e = 1, c = 1, \rho_{0i} = [30^\circ, 150^\circ, 270^\circ]$.

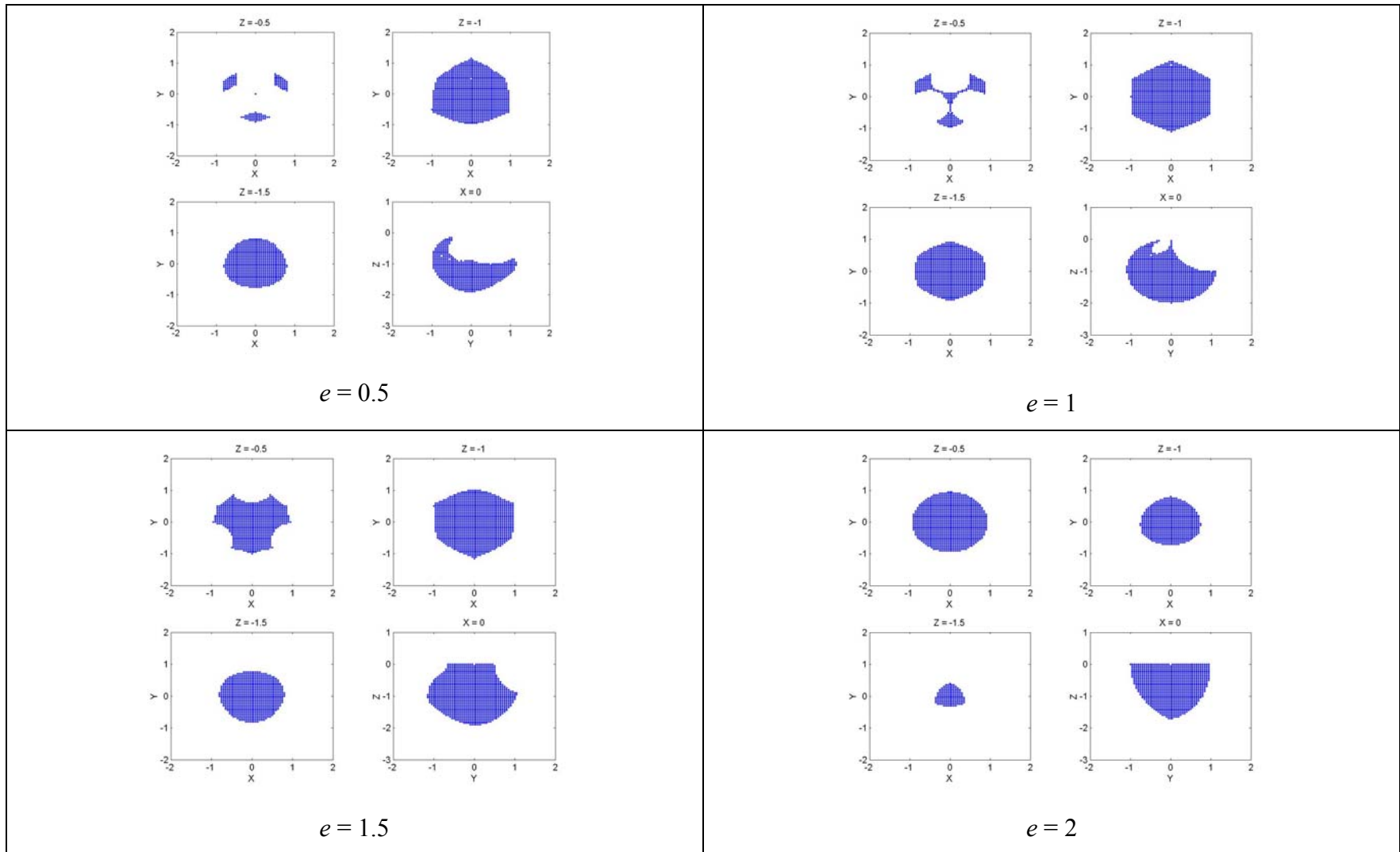


Figure D.4: Variation of e : $l = 1, d = 1, c = 1, \rho_{0i} = [30^\circ, 150^\circ, 270^\circ]$.

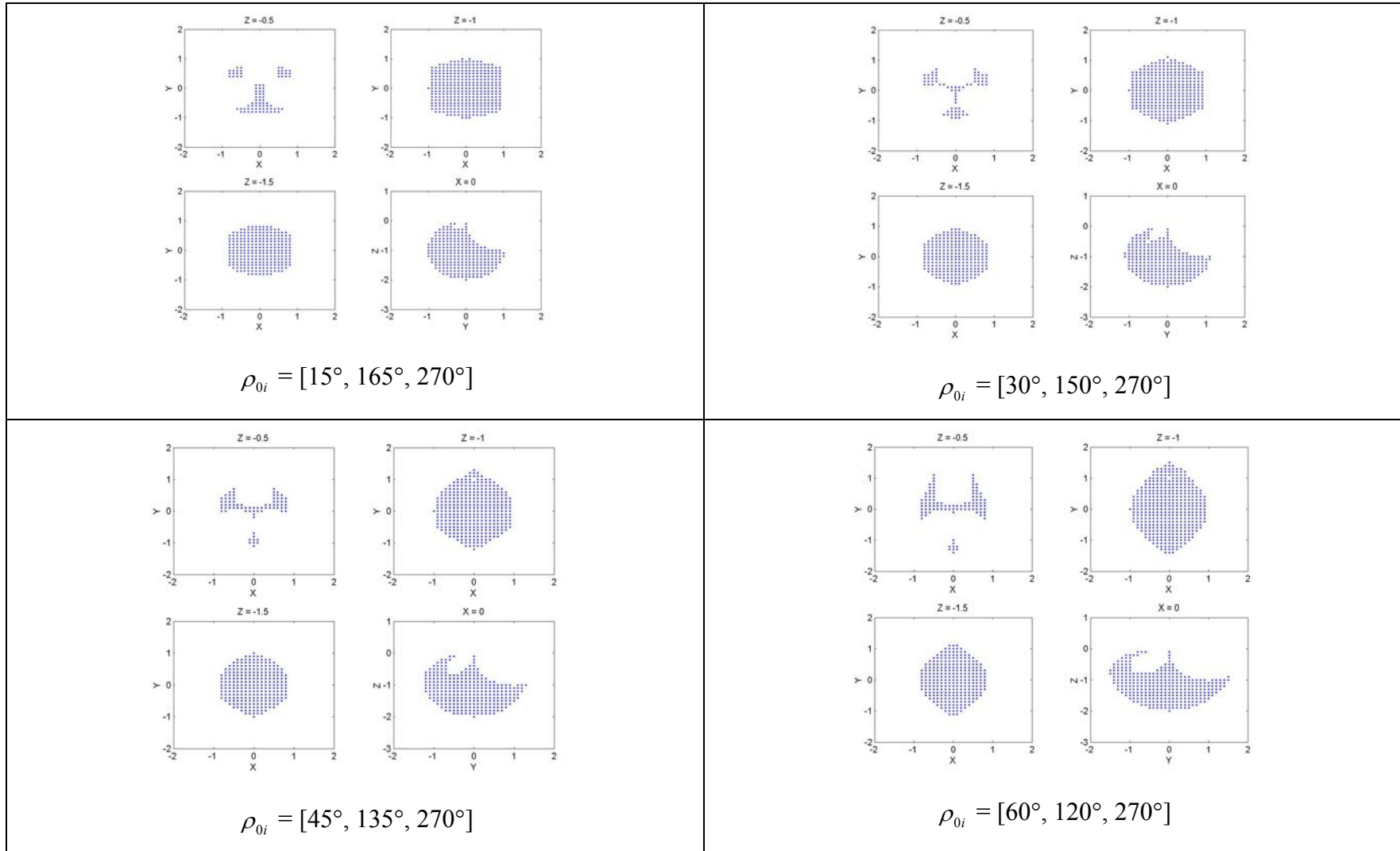


Figure D.5: Variation of ρ_{0i} : $l = 1, e = 1, c = 1, d = 1$.

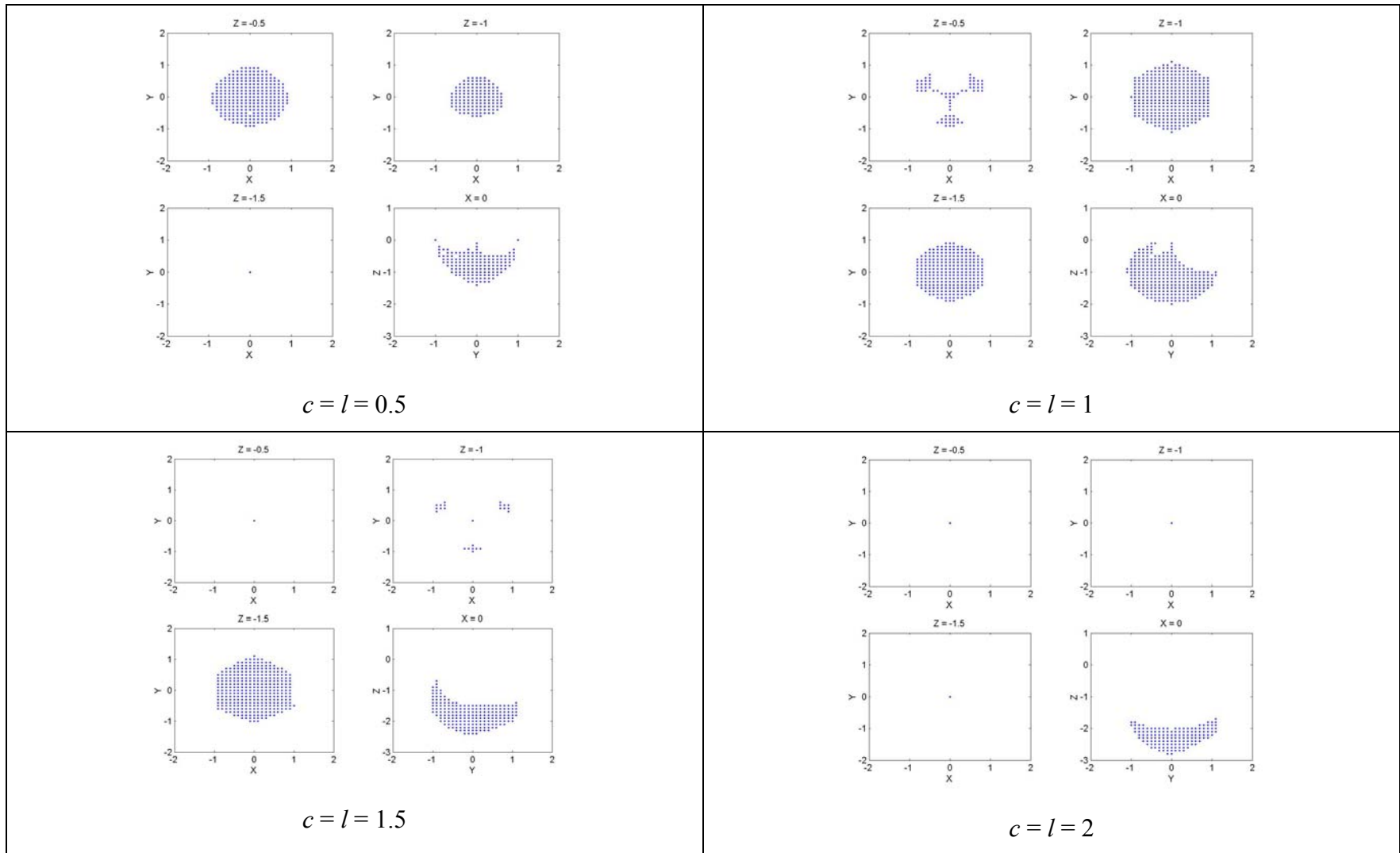


Figure D.6: Variation of c and l : $d = 1$, $e = 1$, $\rho_{0i} = [30^\circ, 150^\circ, 270^\circ]$.

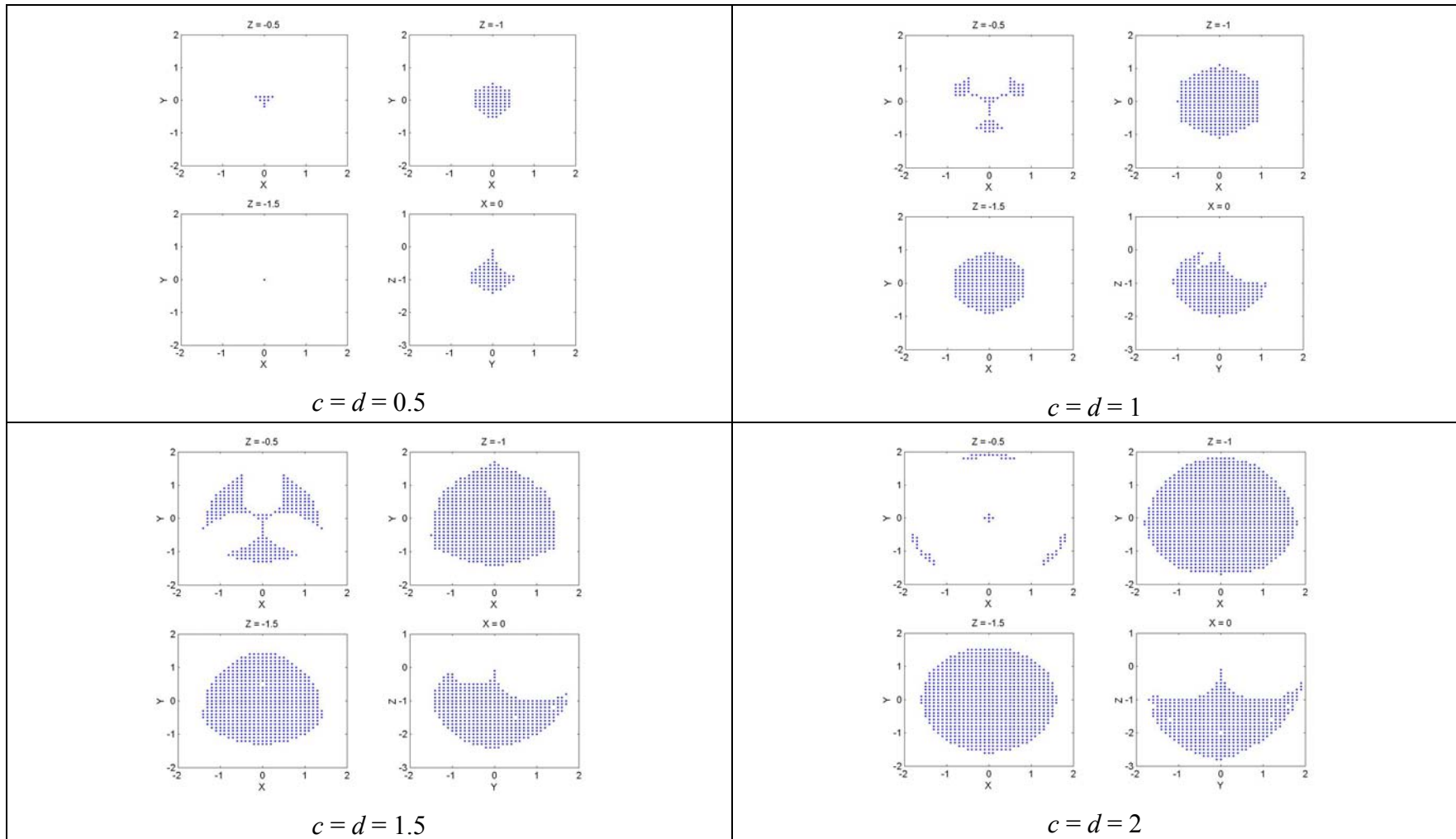


Figure D.7: Variation of c and d : $l = 1$, $e = 1$, $\rho_{0i} = [30^\circ, 150^\circ, 270^\circ]$.

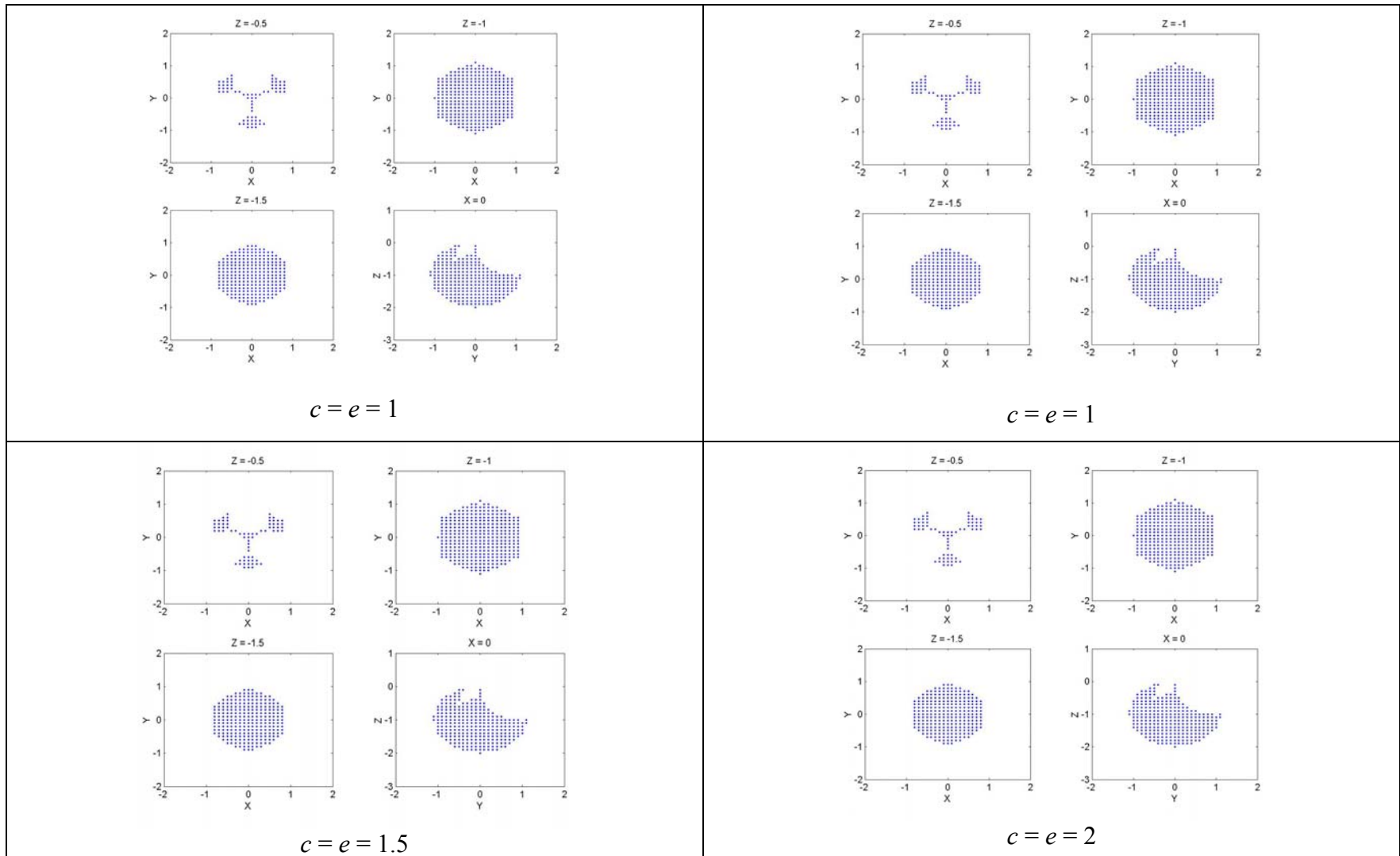


Figure D.8: Variation of c and e : $d = 1$, $l = 1$, $\rho_{0i} = [30^\circ, 150^\circ, 270^\circ]$.

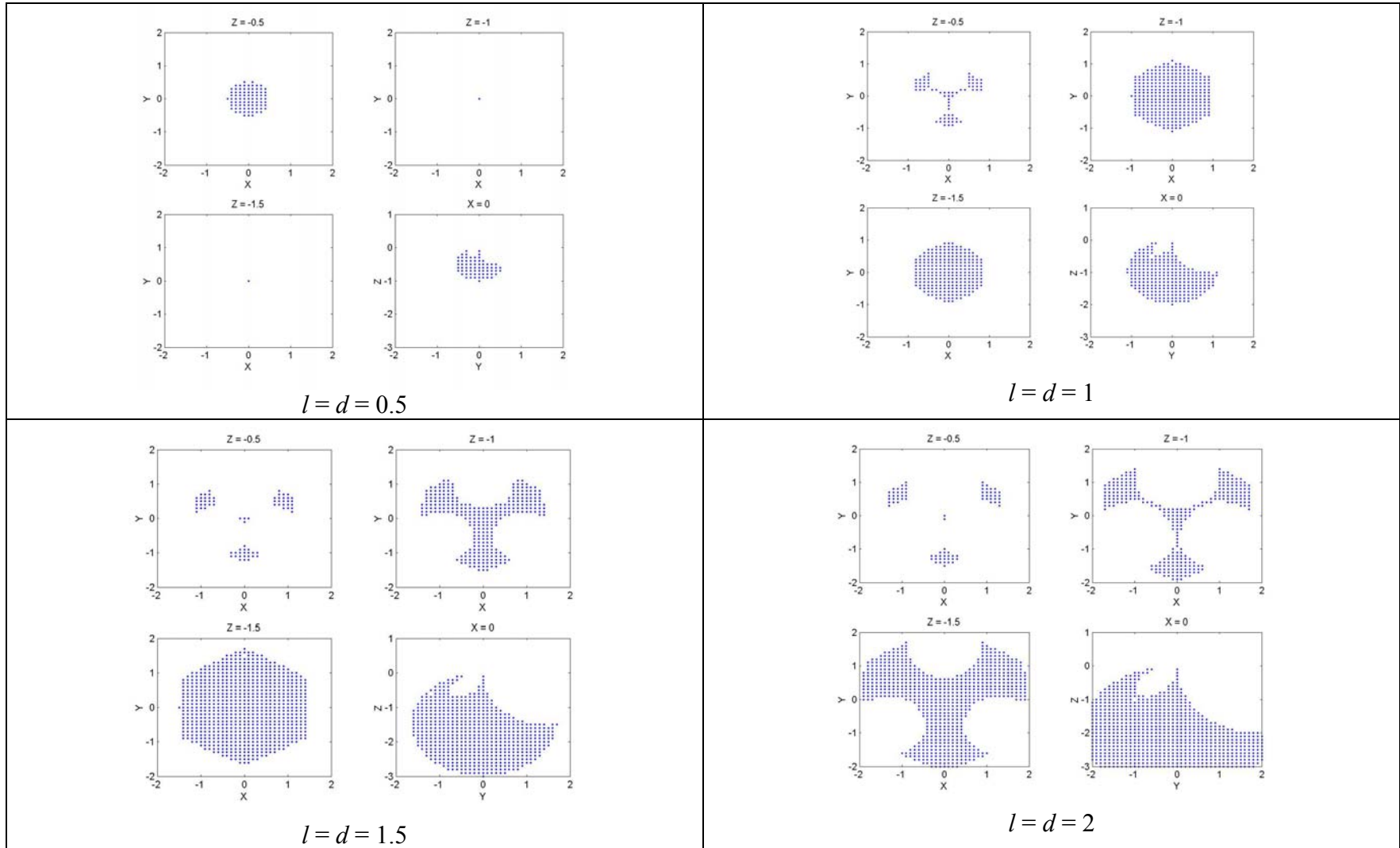


Figure D.9: Variation of l and d : $c = 1, e = 1, \rho_{0i} = [30^\circ, 150^\circ, 270^\circ]$.

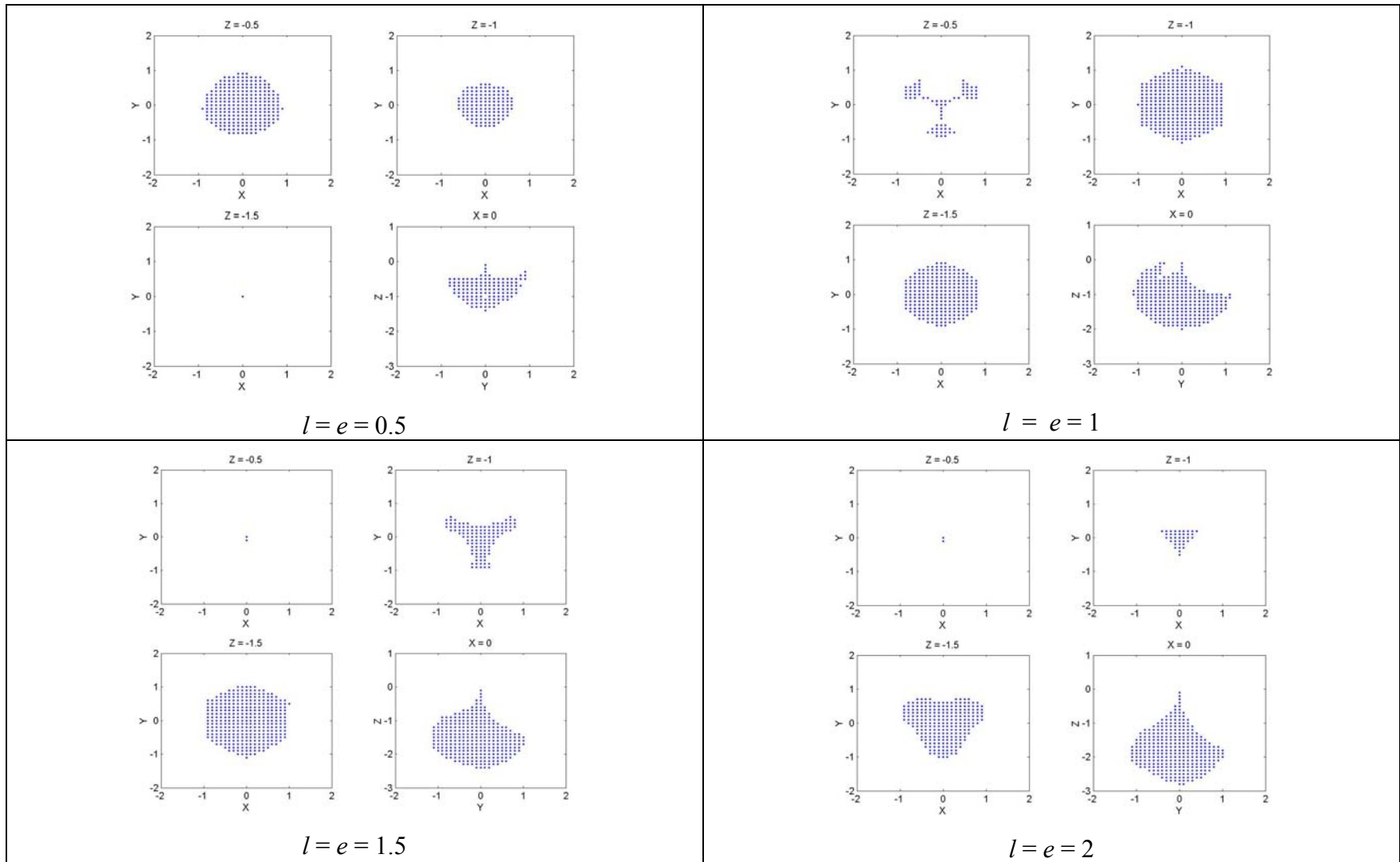


Figure D.10: Variation of l and e : $c = 1$, $d = 1$, $\rho_{0i} = [30^\circ, 150^\circ, 270^\circ]$.

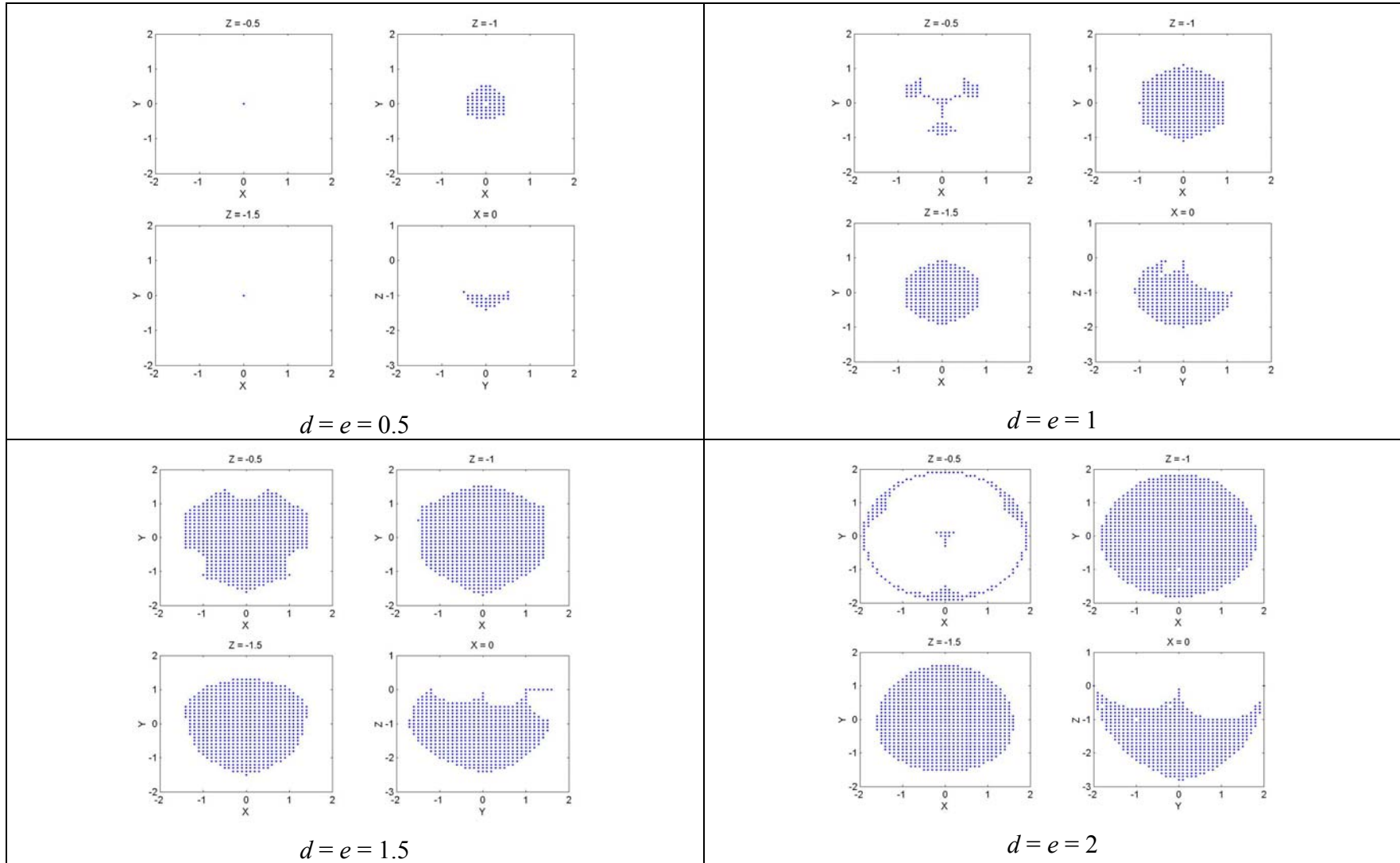


Figure D.11: Variation of d and e : $c = 1, l = 1, \rho_{0i} = [30^\circ, 150^\circ, 270^\circ]$.

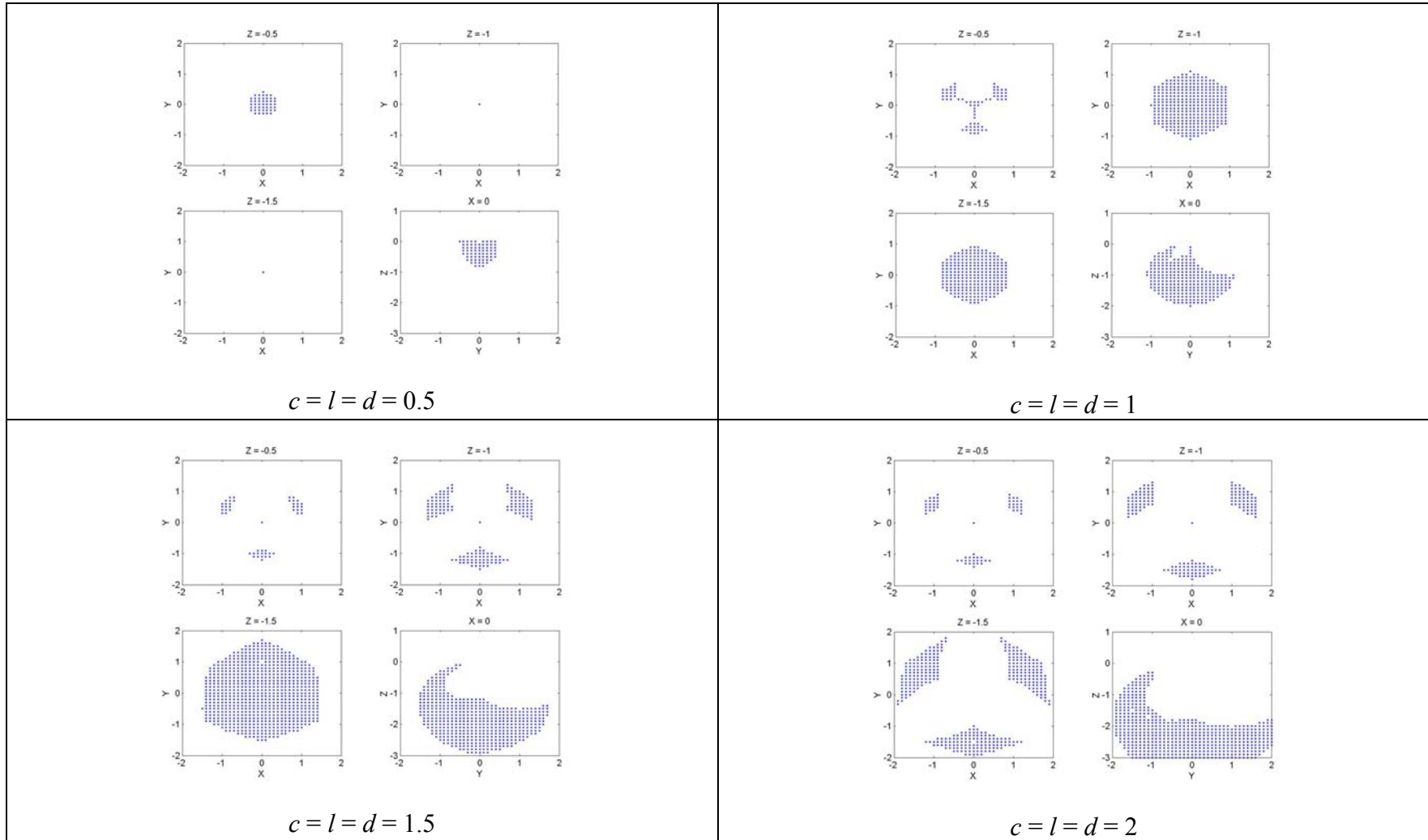


Figure D.12: Variation of c , l and d : $e = 1$, $\rho_{0i} = [30^\circ, 150^\circ, 270^\circ]$.

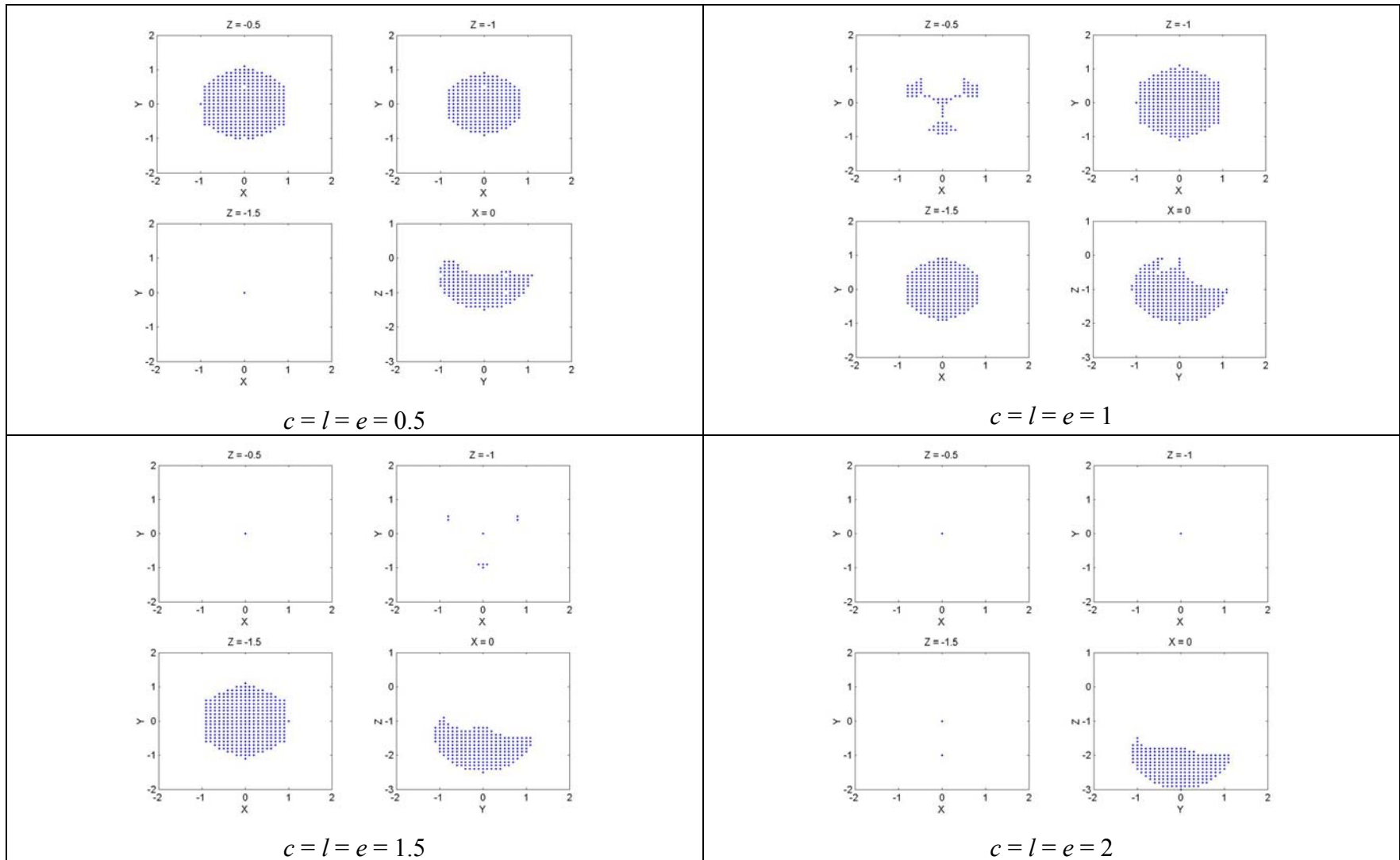


Figure D.13: Variation of c , l and e : $d = 1$, $\rho_{0i} = [30^\circ, 150^\circ, 270^\circ]$.

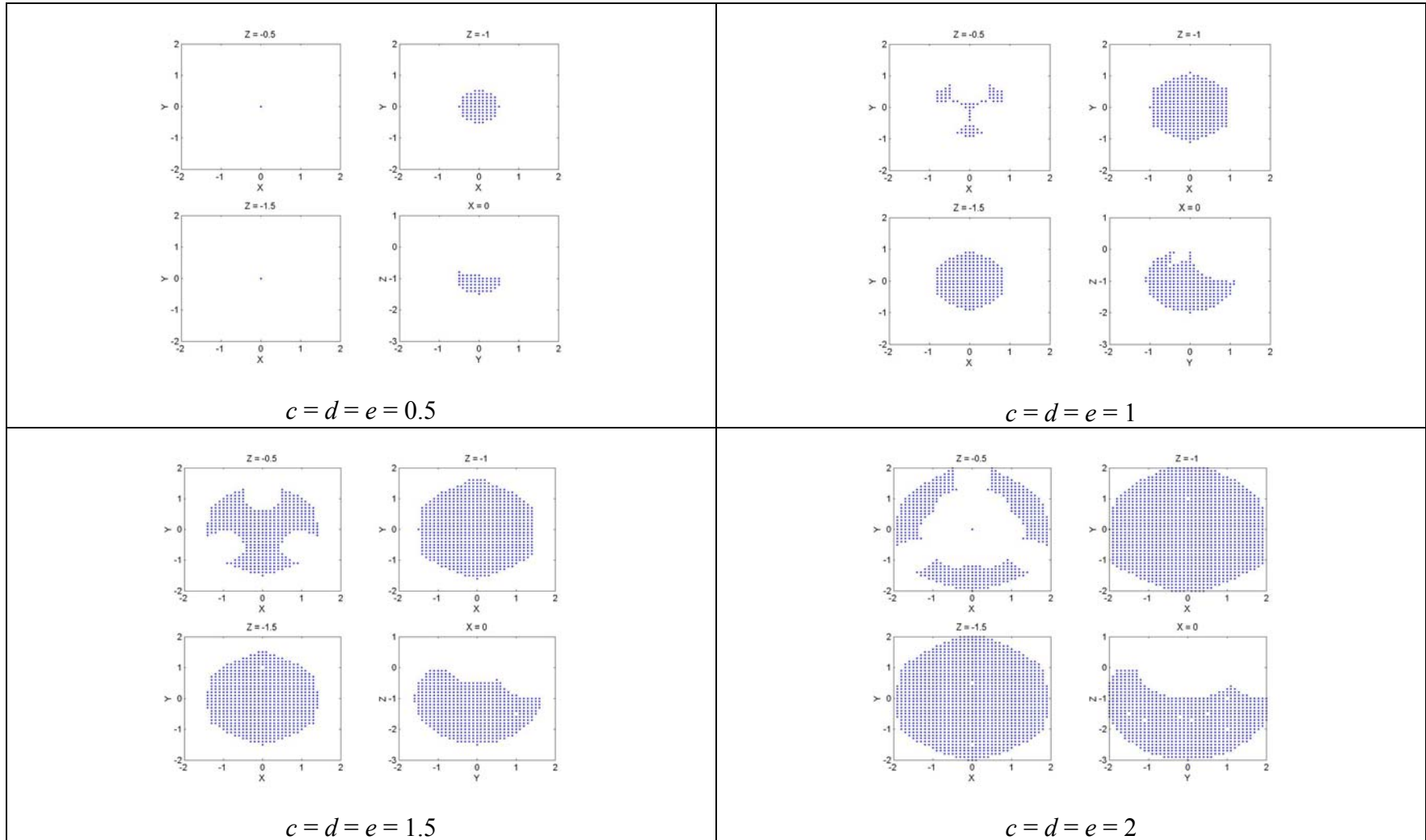


Figure D.14: Variation of c , d and e : $l = 1$, $\rho_{0i} = [30^\circ, 150^\circ, 270^\circ]$.

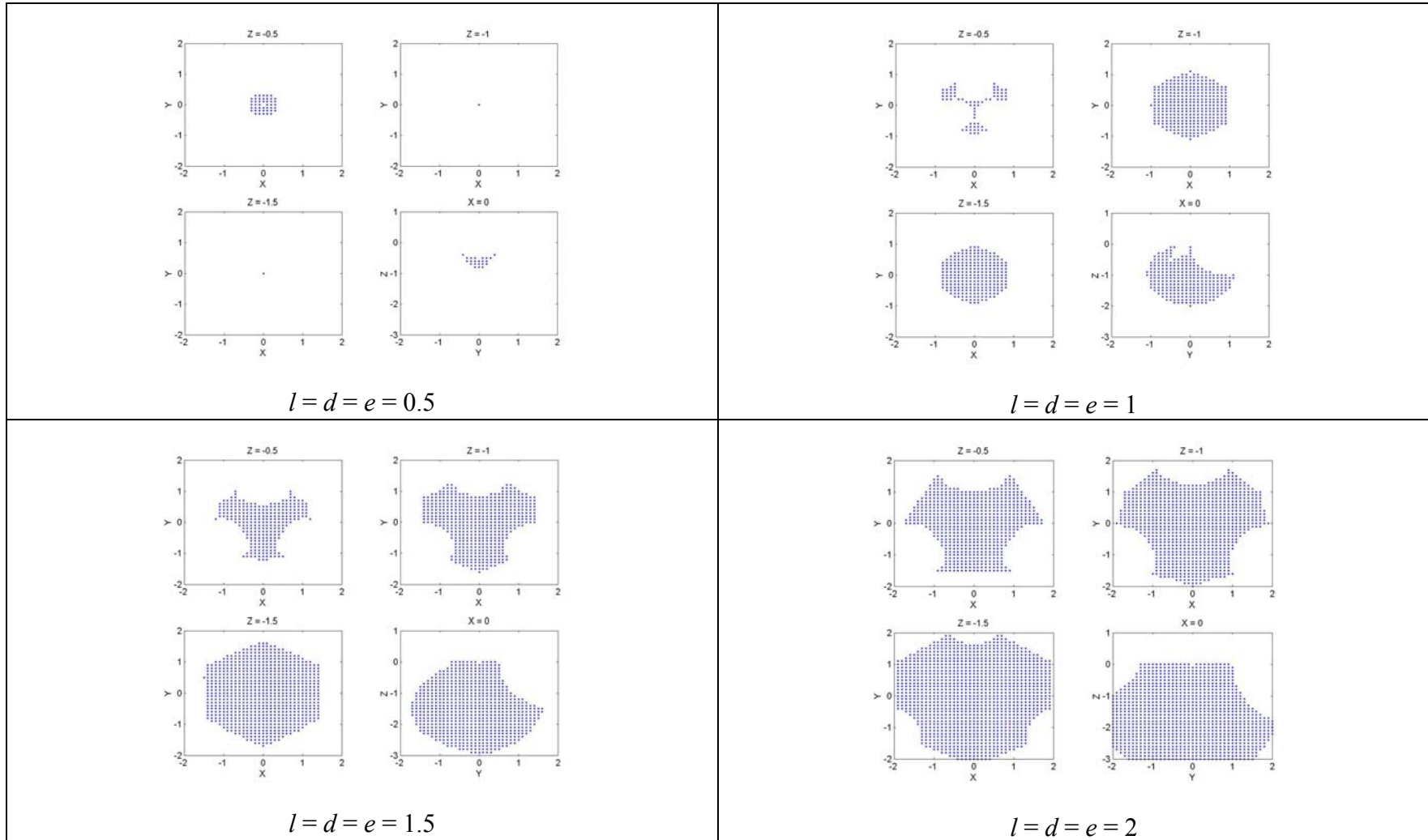


Figure D.15: Variation of l , d and e : $c = 1$, $\rho_{0i} = [30^\circ, 150^\circ, 270^\circ]$.

D.2 Second Round of Qualitative Study, $(c-e)$ is Positive

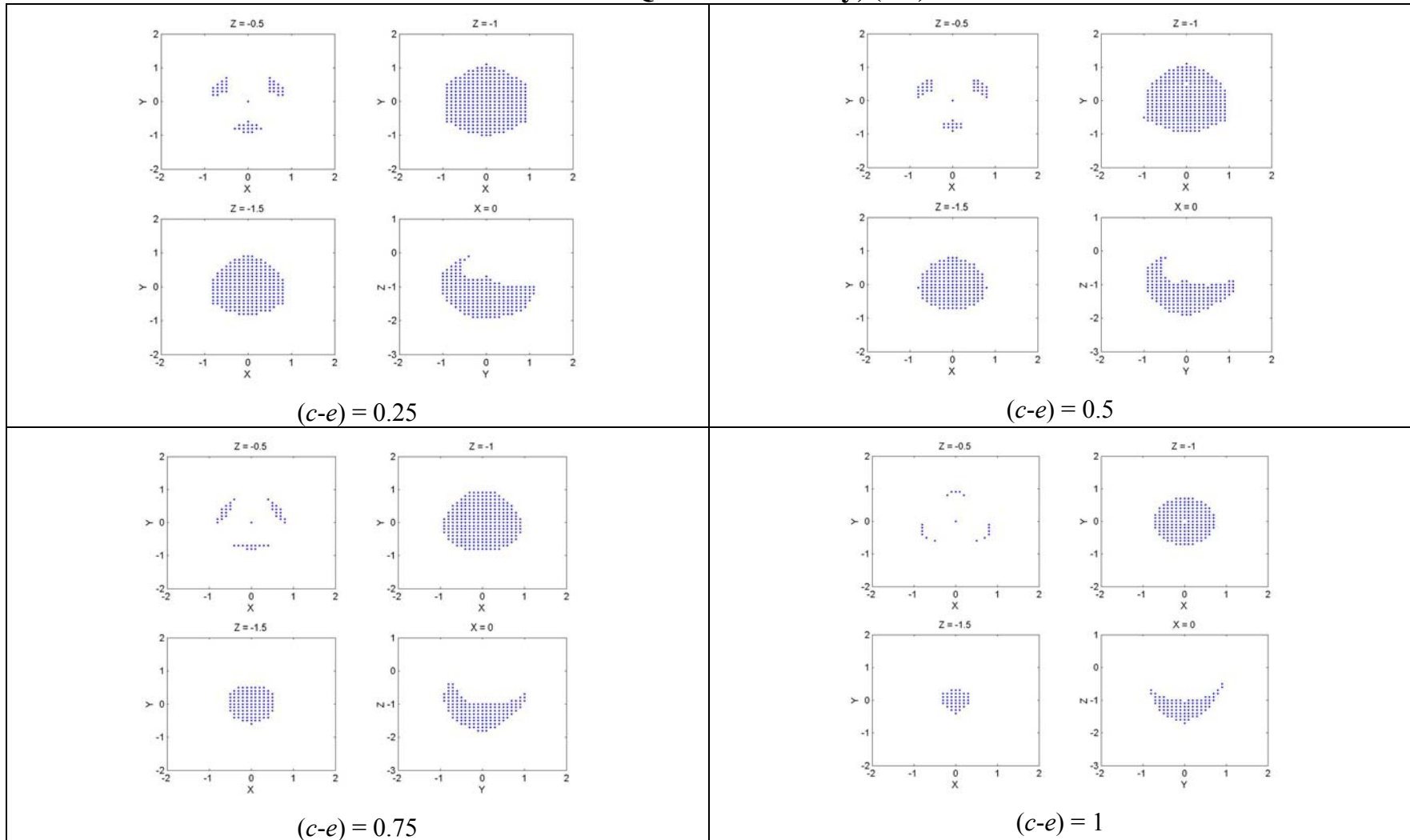


Figure D.16: Positive variation of $(c-e)$: $l = 1, d = 1$.

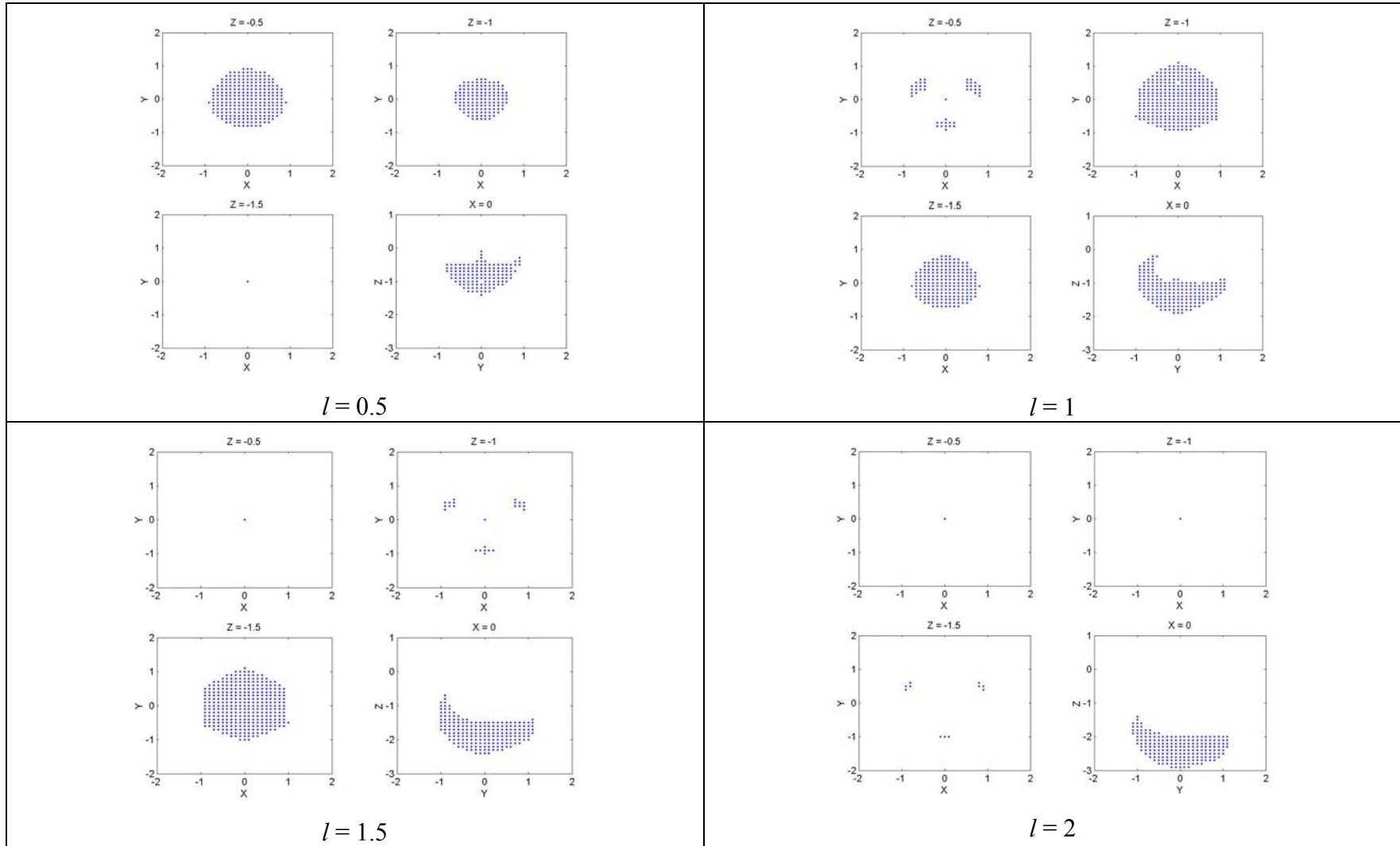


Figure D.17: Variation of l : $(c-e) = 0.5$, $d = 1$.

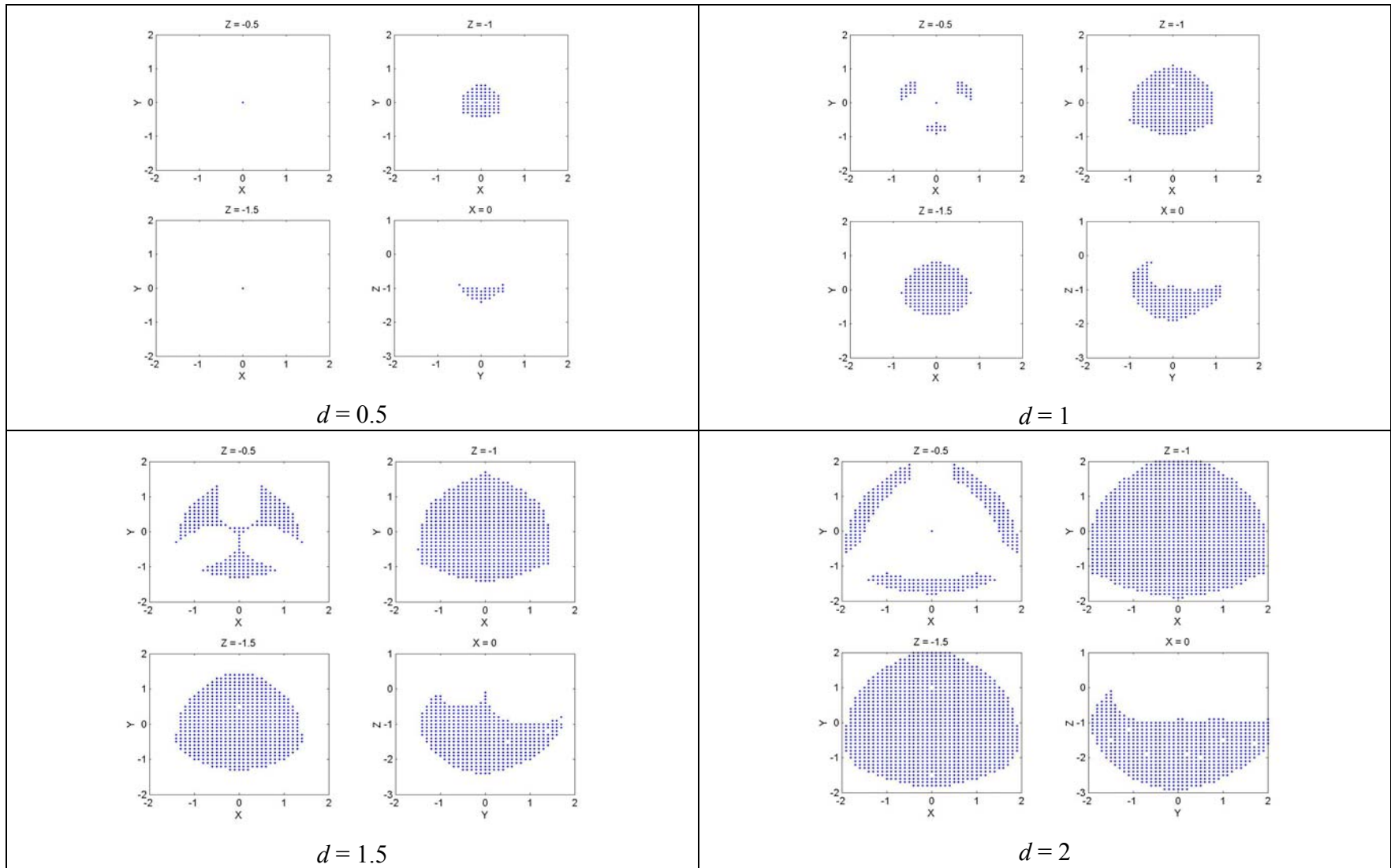


Figure D.18: Variation of d : $(c-e) = 0.5, l = 1$.

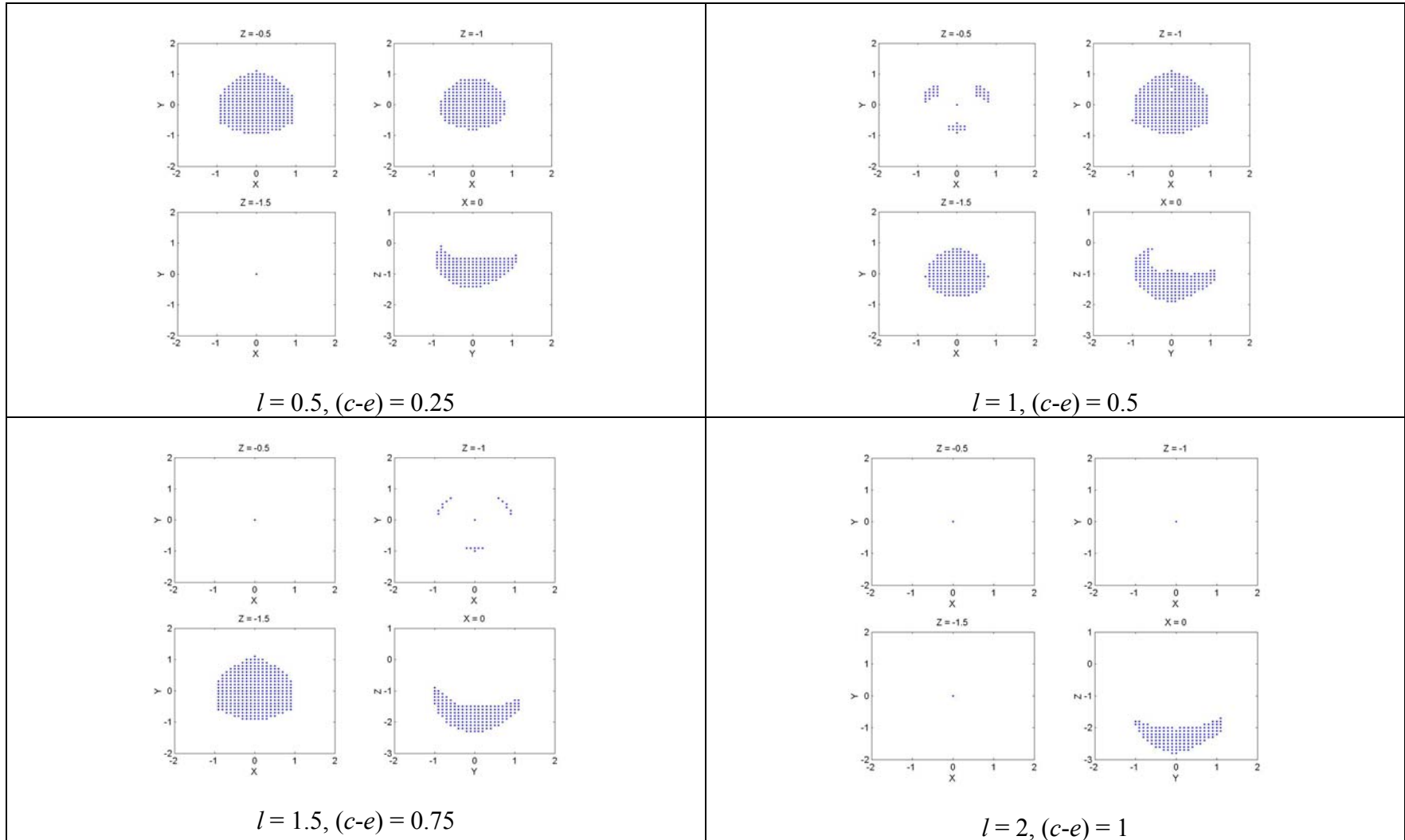


Figure D.19: Variation of l and positive variation of $(c-e)$: $d = 1$.

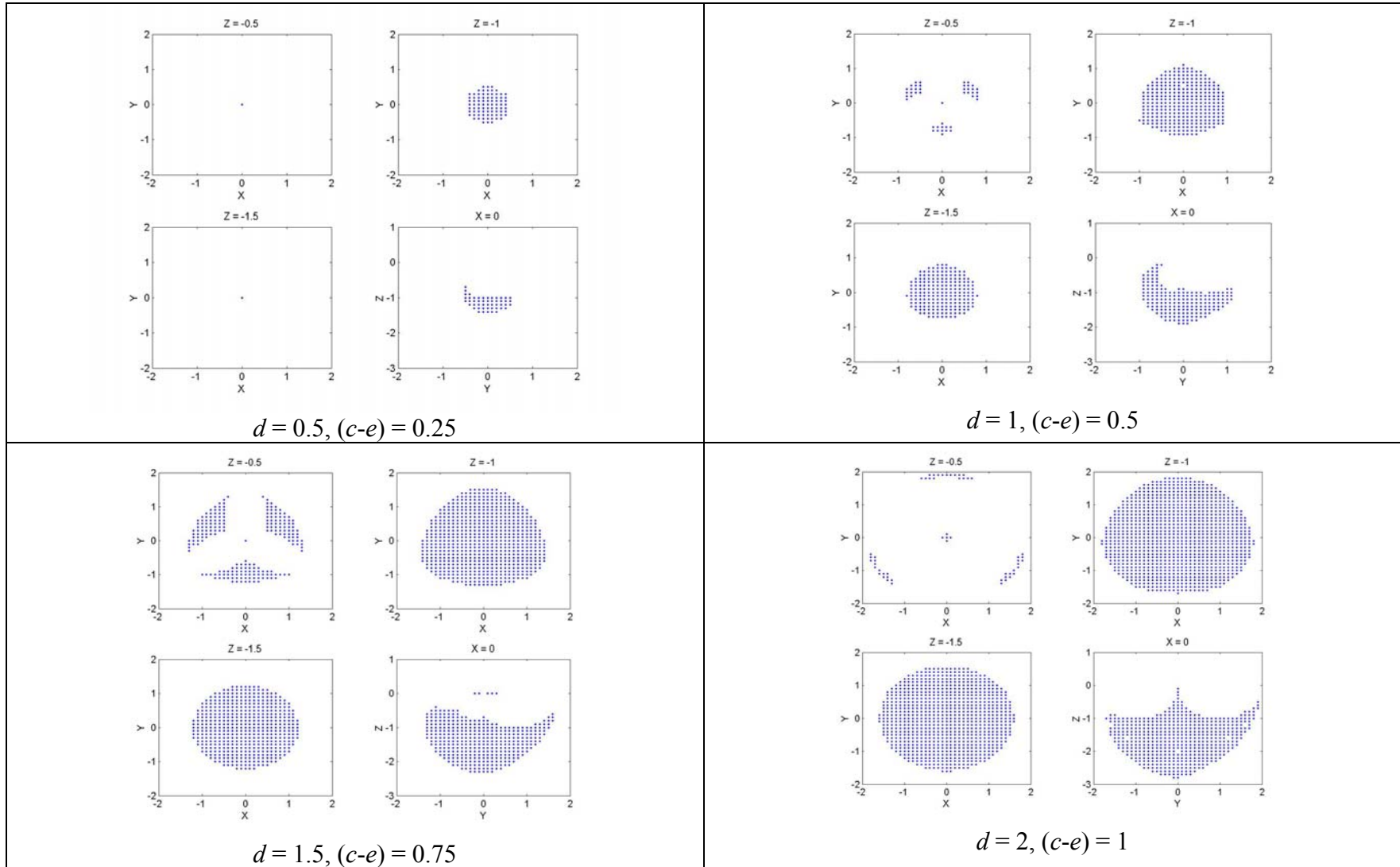


Figure D.20: Variation of d and positive variation of $(c-e)$: $l = 1$.

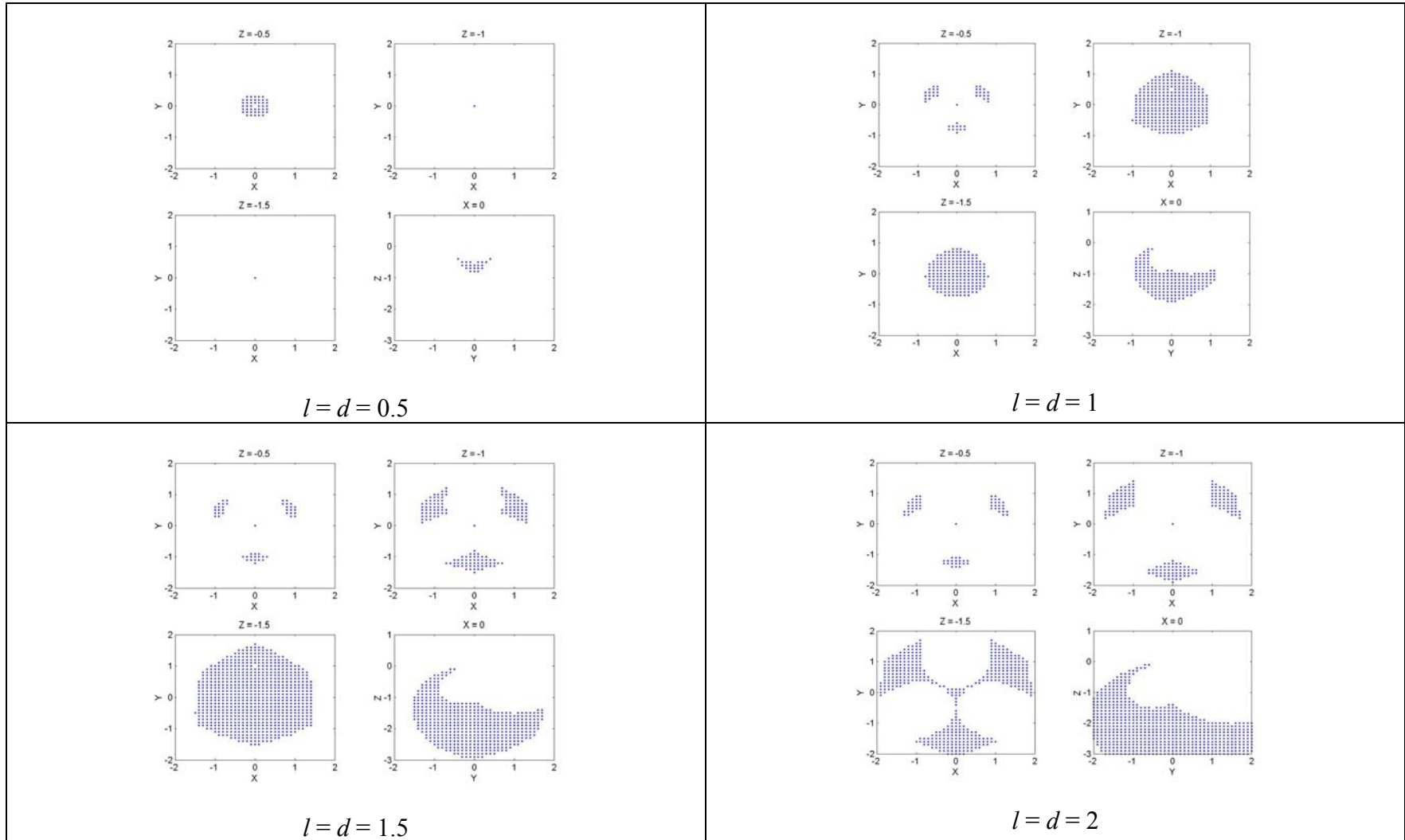


Figure D.21: Variation of l and d : $(c-e) = 0.5$.

D.3 Second Round of Qualitative Study, $(c-e)$ is Negative

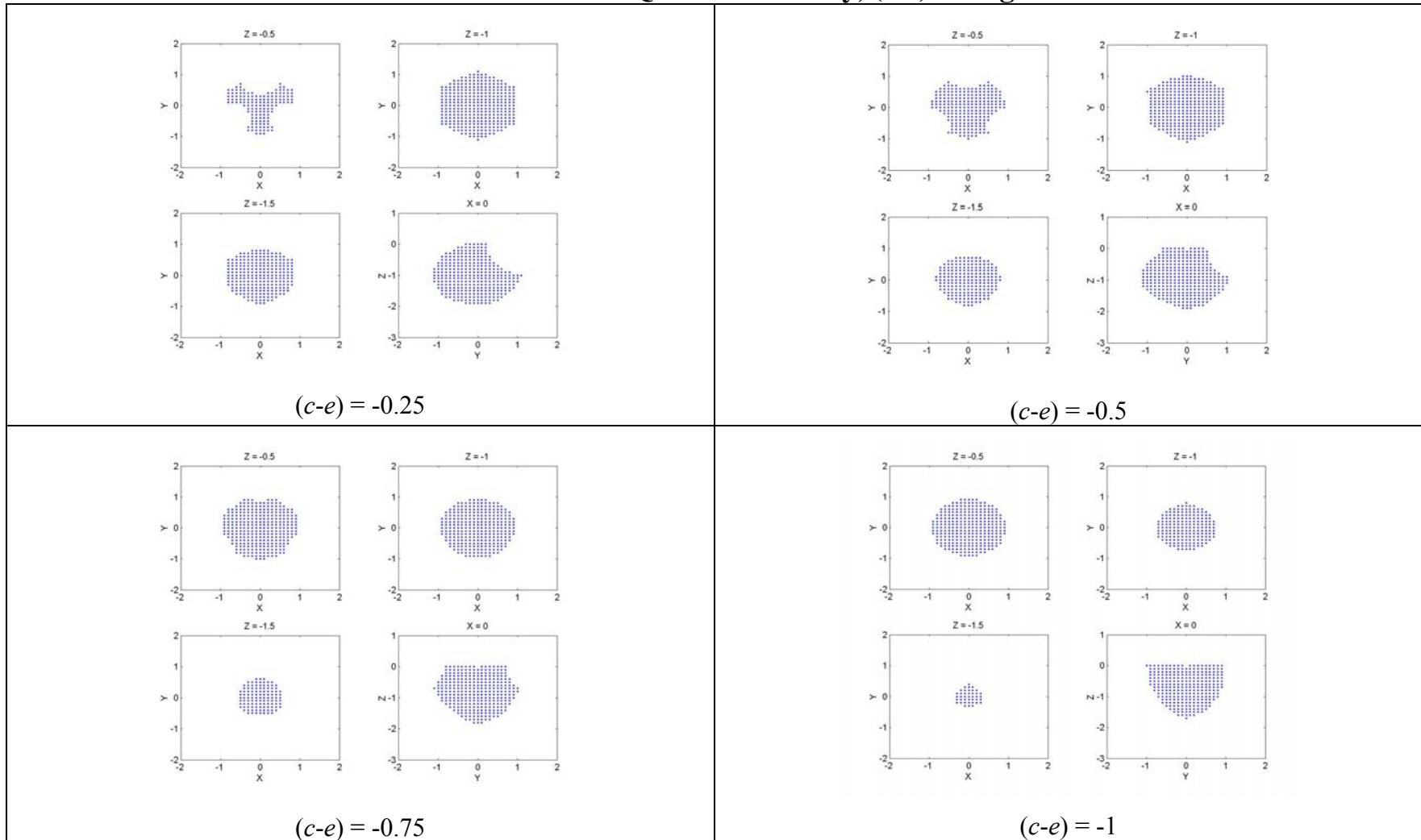


Figure D.22: Negative variation of $(c-e)$: $l = 1, d = 1$.

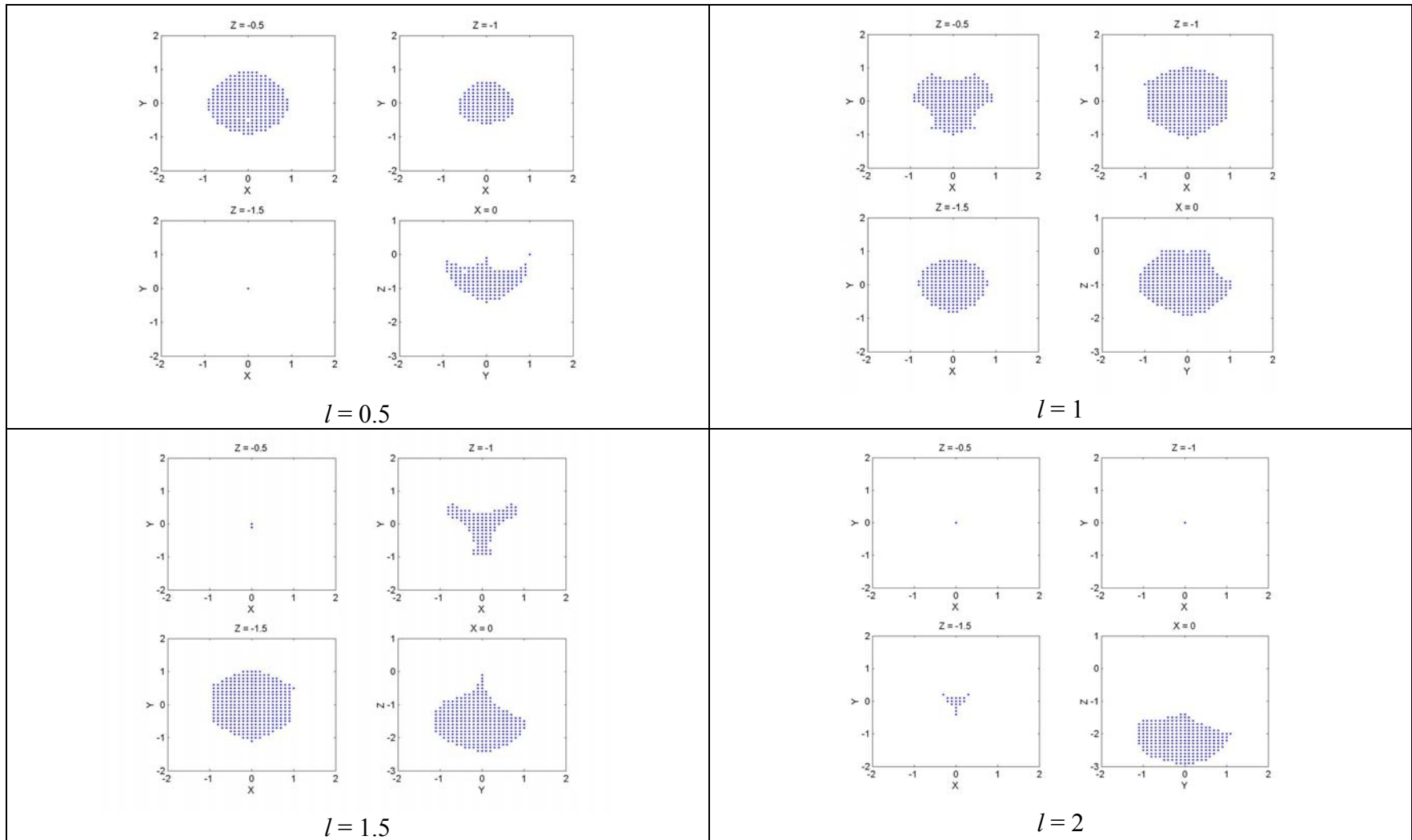


Figure D.23: Variation of l : $d = 1$, $(c-e) = -0.5$.

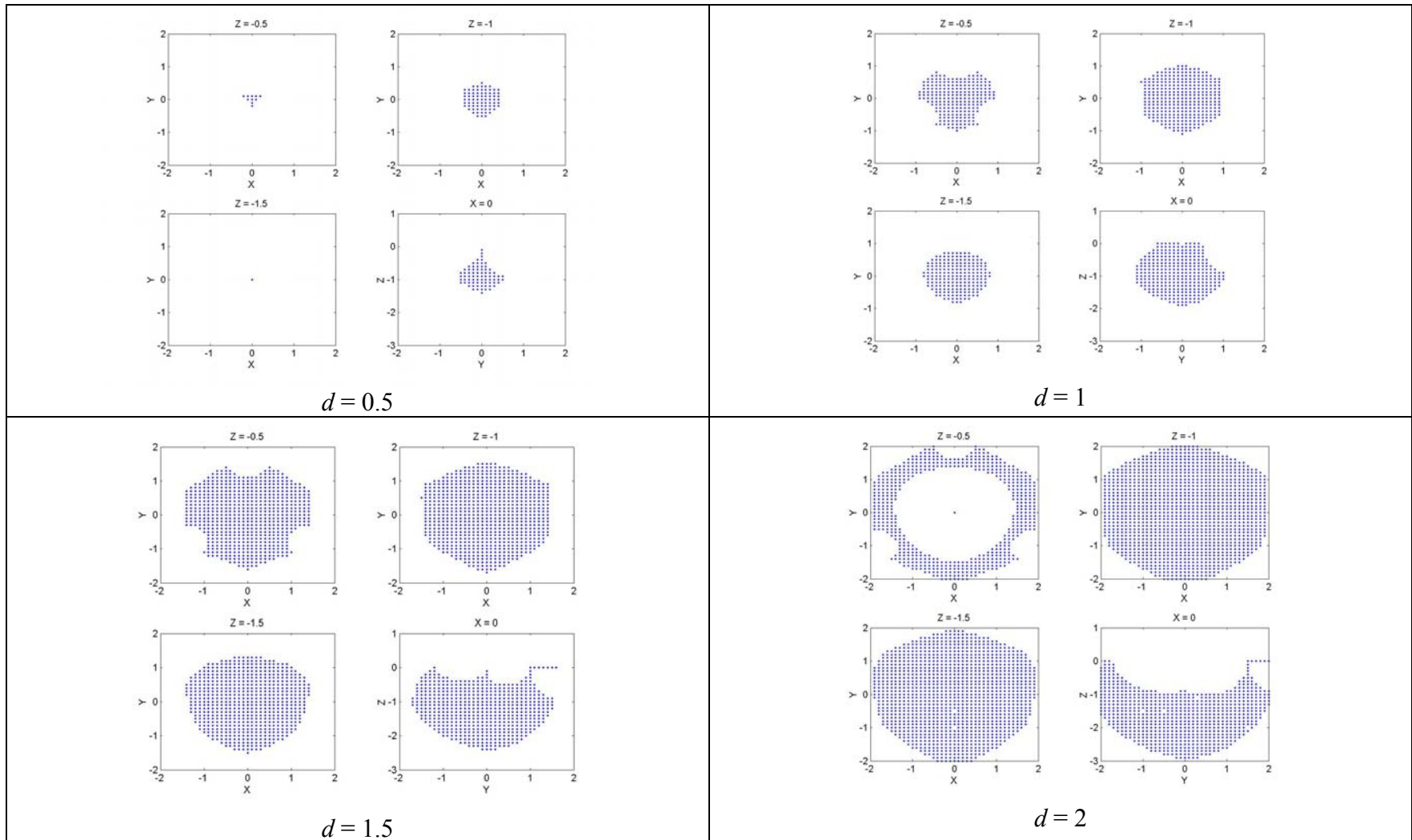


Figure D.24: Variation of d : $l = 1$, $(c-e) = -0.5$.

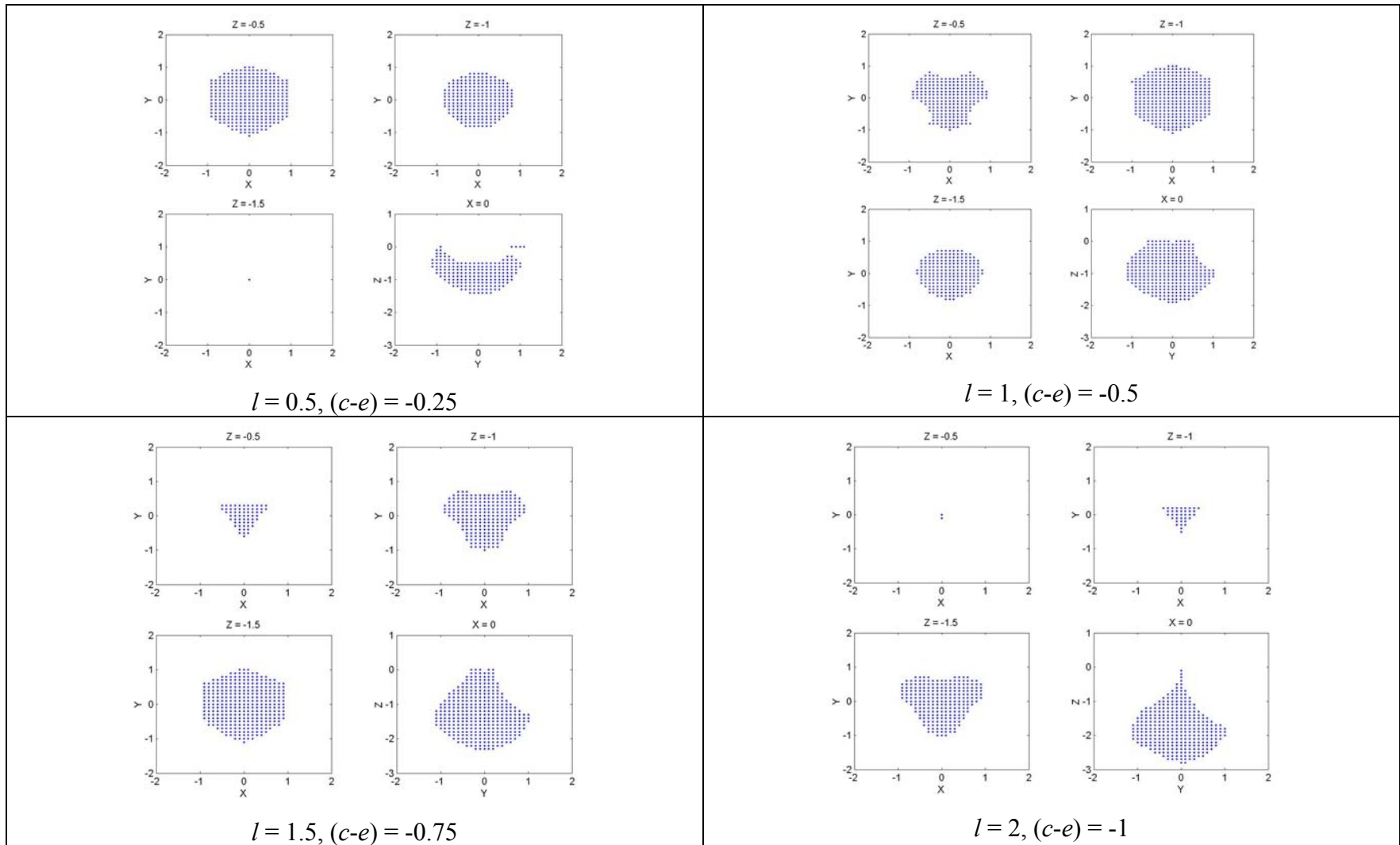


Figure D.25: Variation of l and negative variation of $(c-e)$: $d = 1$.

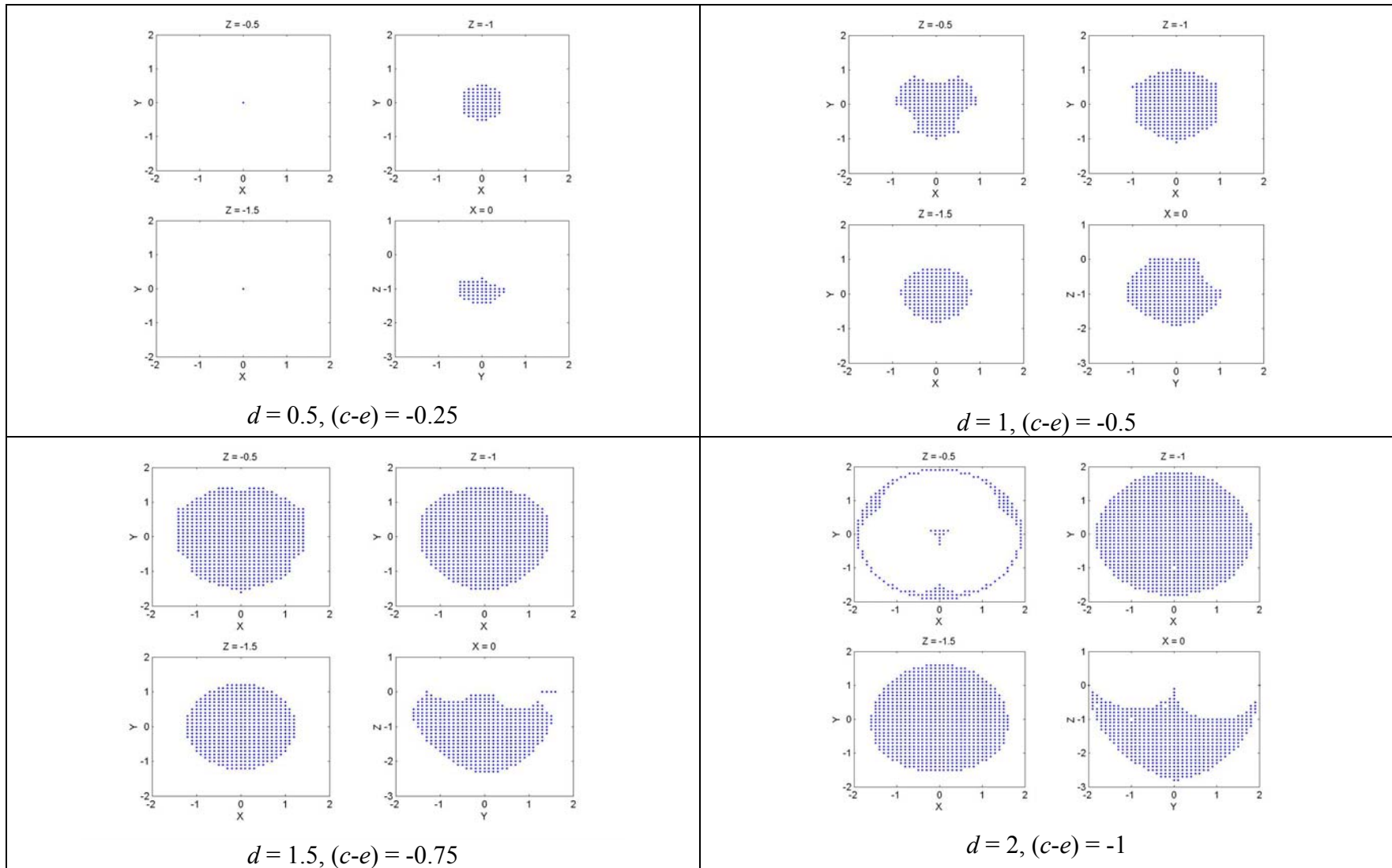


Figure D.26: Variation of d and negative variation of $(c-e)$: $l = 1$.

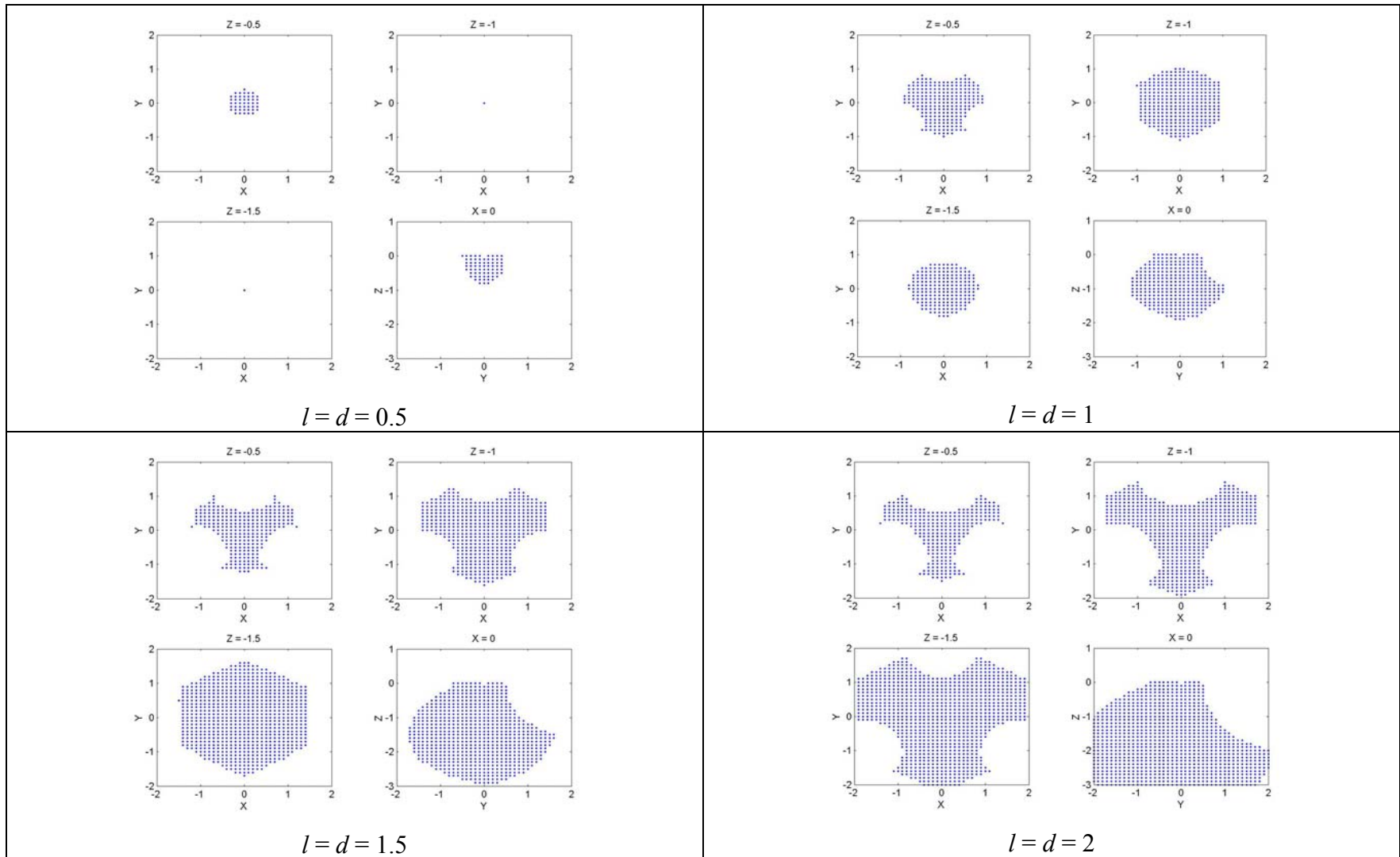


Figure D.27: Variation of l and d : $(c-e) = -0.5$.

APPENDIX E

RESULTS OF THE DYNAMIC ANALYSIS

This appendix contains the results of the dynamic prototype analyses carried out in Sections 6.5.4 through 6.5.6. There are six sections in this appendix corresponding to the six scenarios simulated in Chapter 6. The results in Section E.1 and E.2 correspond to simulations of the first prototype, while Sections E.3 and E.4 correspond to simulations of the second prototype, and Sections E.5 and E.6 correspond to simulations of the third prototype. The odd numbered sections correspond to breast up WOG capture scenario and the even numbered sections correspond to the breast down WOG capture scenario. Within each section there are 8 graphs. The first three display the specified motion of the moving platform in the global X , Y and, Z directions. The next three graphs show the motions the actuators of the parallel mechanism must produce as a consequence of the specified X , Y and Z motion, and the moments that the actuators must produce to achieve that motion. The seventh graph shows the specified motion of the *Flip* generating wrist actuator and the moments required to achieve the motion. The eighth graph shows the specified motion of the *Rotate* generating actuator and the moments required to achieve that motion.

E.1 Dynamic Analysis of First Prototype for Breast Up WOG Acquisition

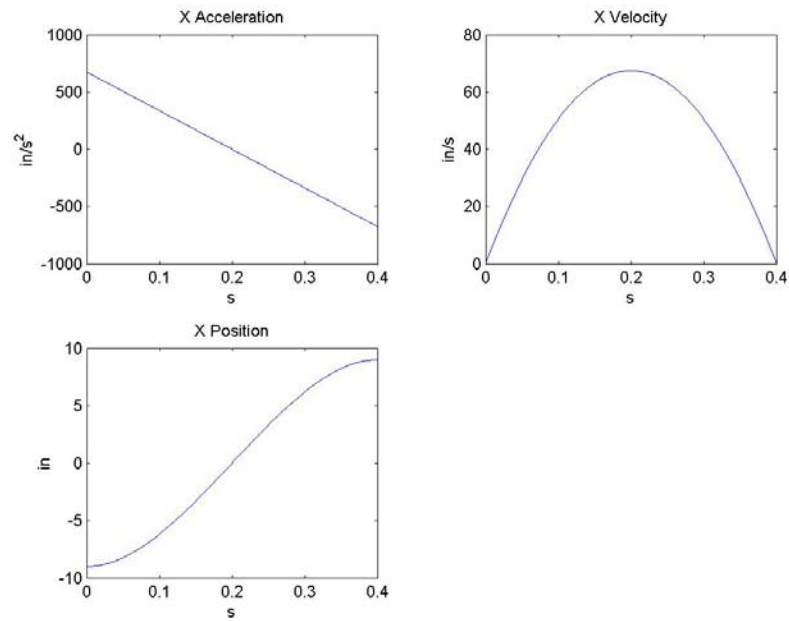


Figure E.1: Motion of the moving platform in the global X direction (1st prototype, breast up).

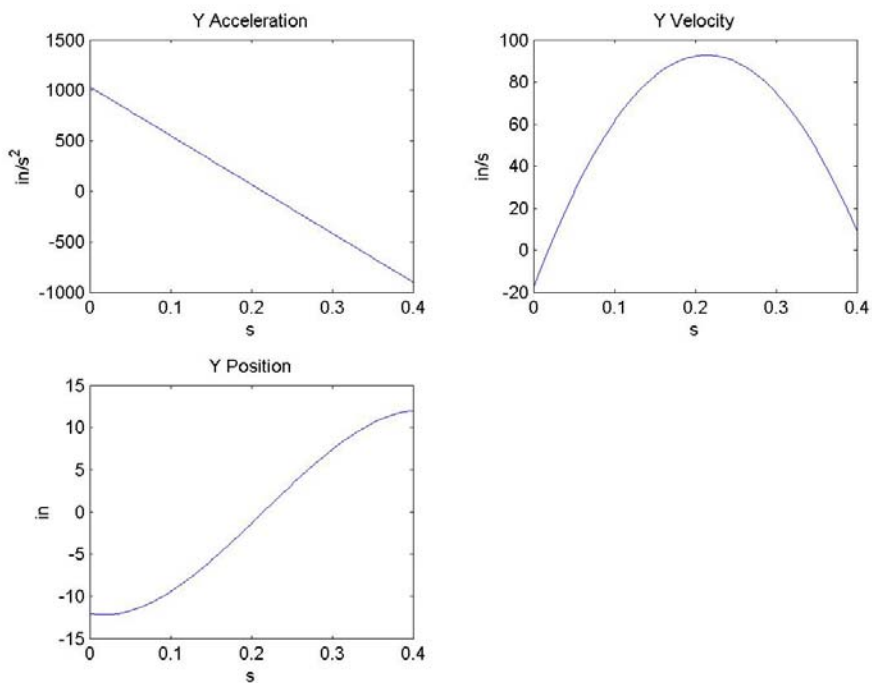


Figure E.2: Motion of the moving platform in the global Y direction (1st prototype, breast up)

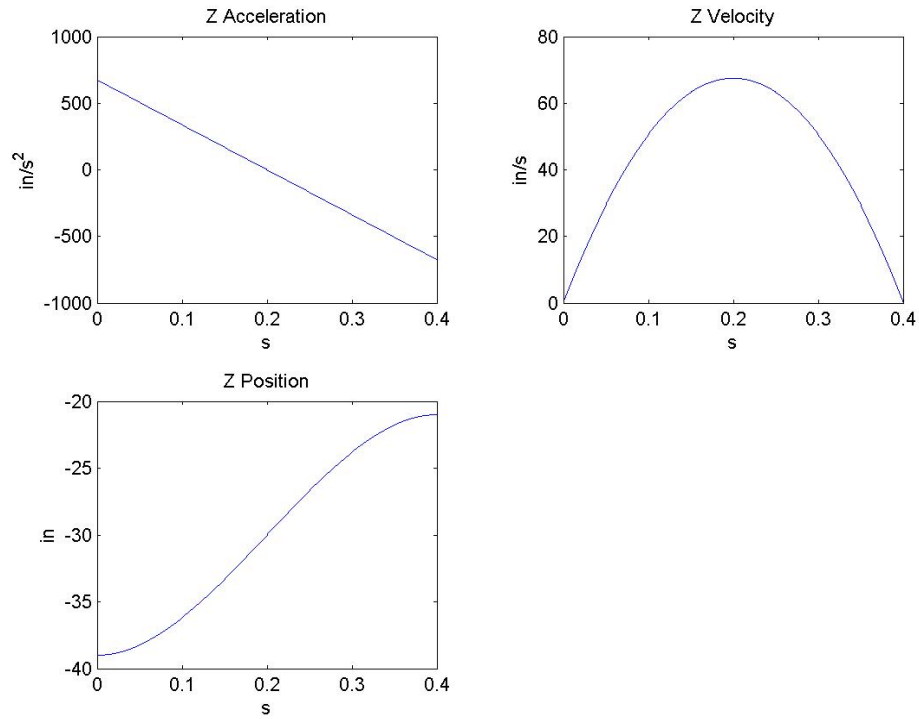


Figure E.3: Motion of the moving platform in the global Z direction (1st prototype, Breast up).

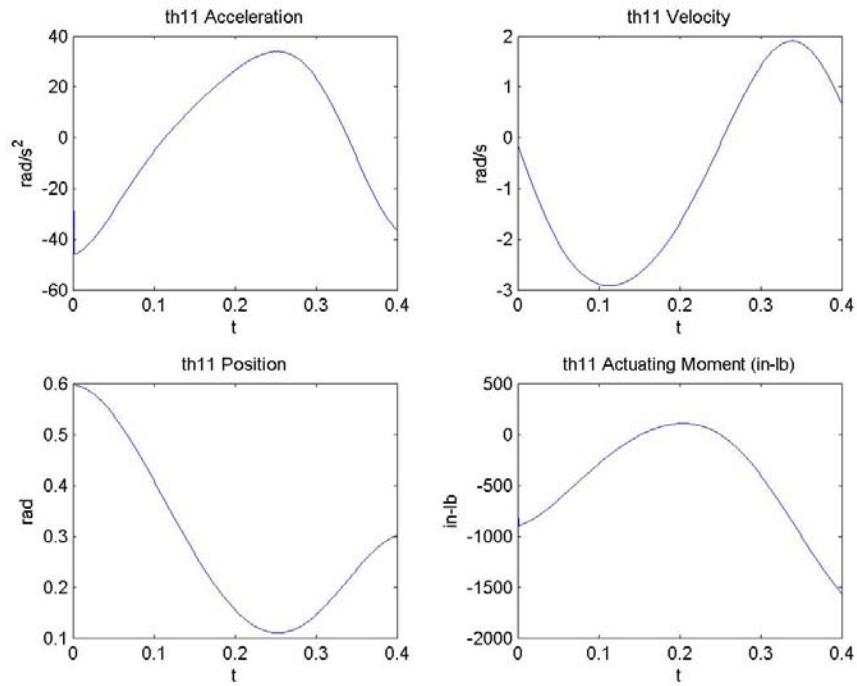


Figure E.4: Motion and moment provided by the parallel mechanism actuator at point C_1 (1st prototype, breast up).

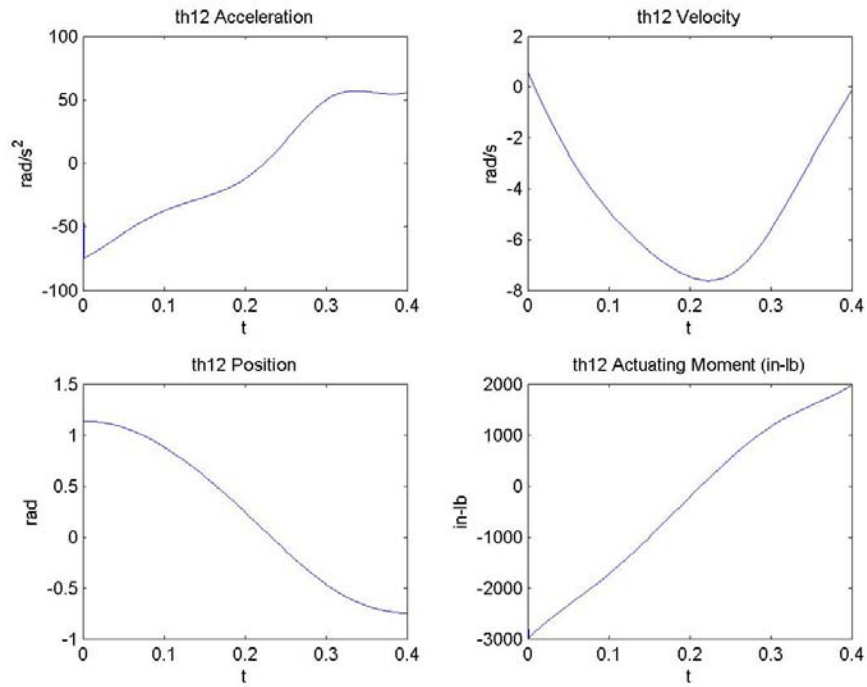


Figure E.5: Motion and moment provided by the parallel mechanism actuator at point C_2 (1st prototype, breast up).

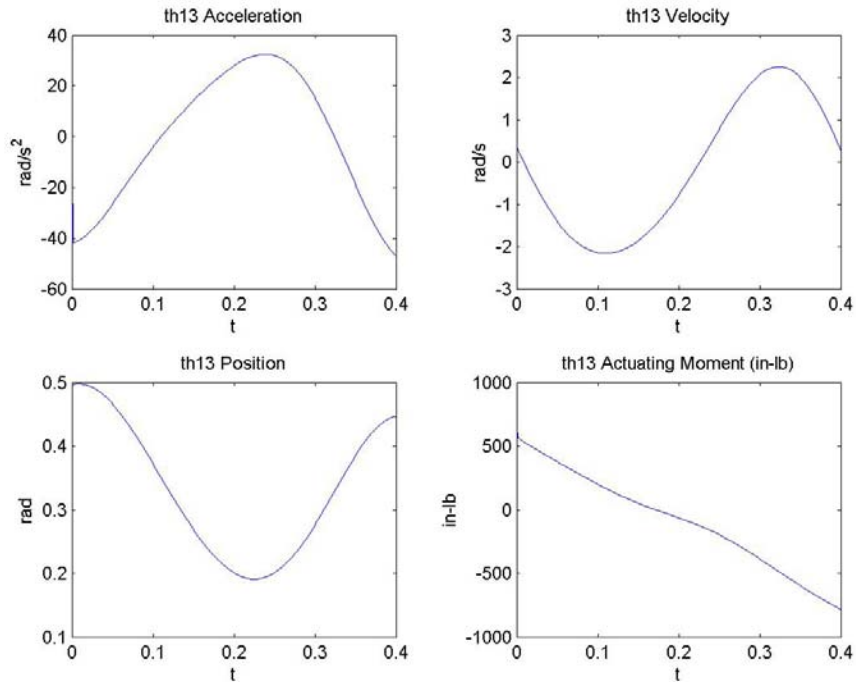


Figure E.6: Motion and moment provided by the parallel mechanism actuator at point C_3 (1st prototype, breast up).

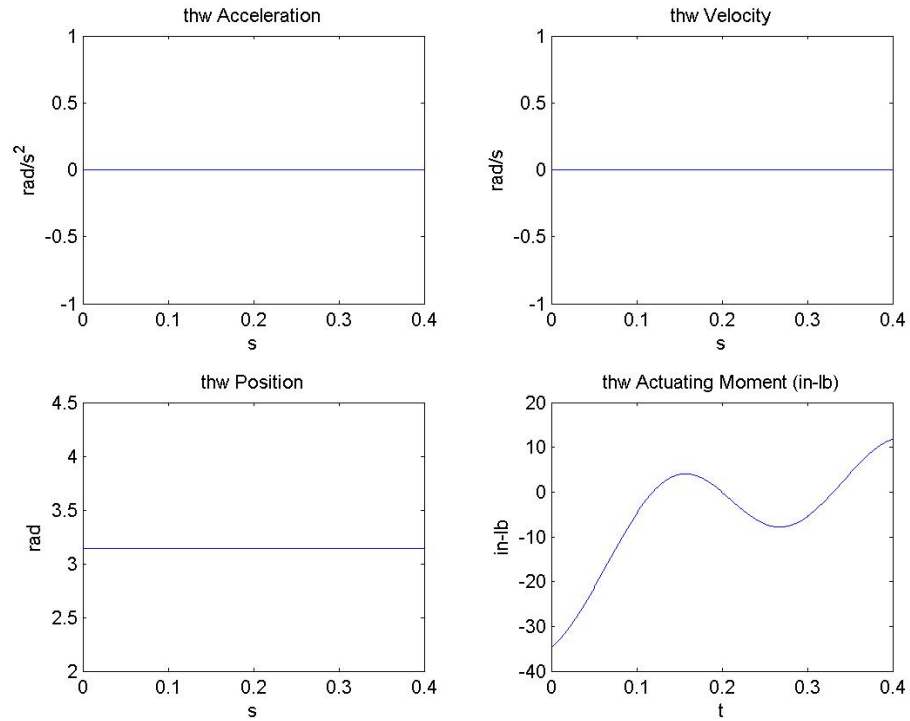


Figure E.7: Motion and moment provided by the *Flip* motion wrist actuator at point F (1st prototype, breast up).

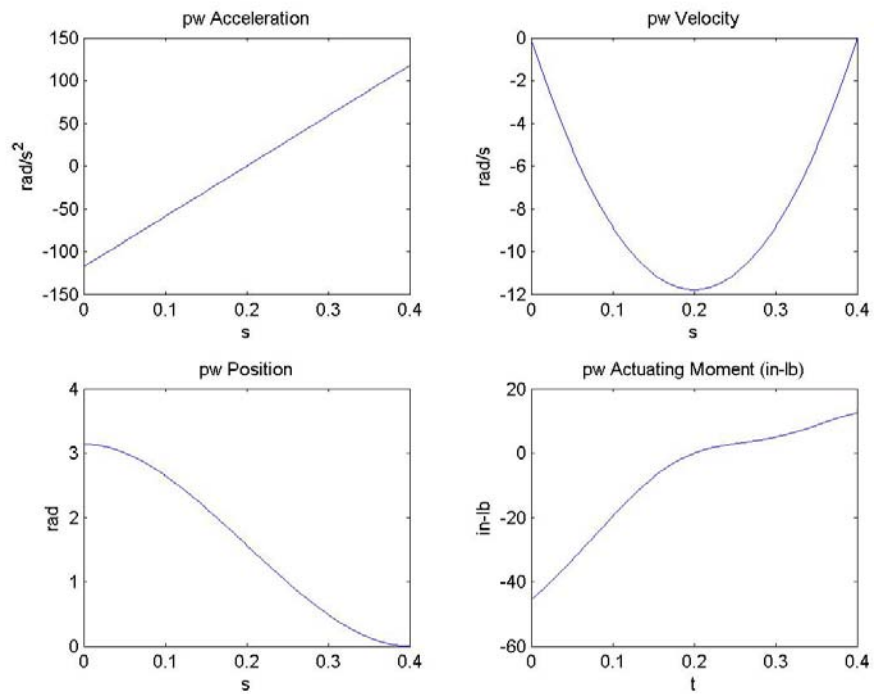


Figure E.8: Motion and moment provided by the *Rotate* motion wrist actuator at point F (1st prototype, breast up).

E.2 Dynamic Analysis of First Prototype for Breast Down WOG Acquisition

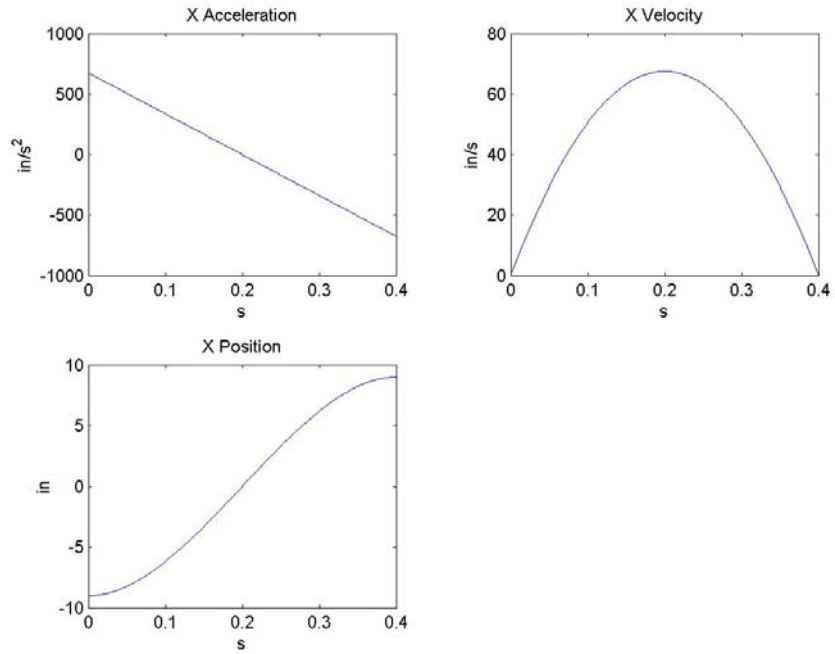


Figure E.9: Motion of the moving platform in the global X direction (1st prototype, breast down).

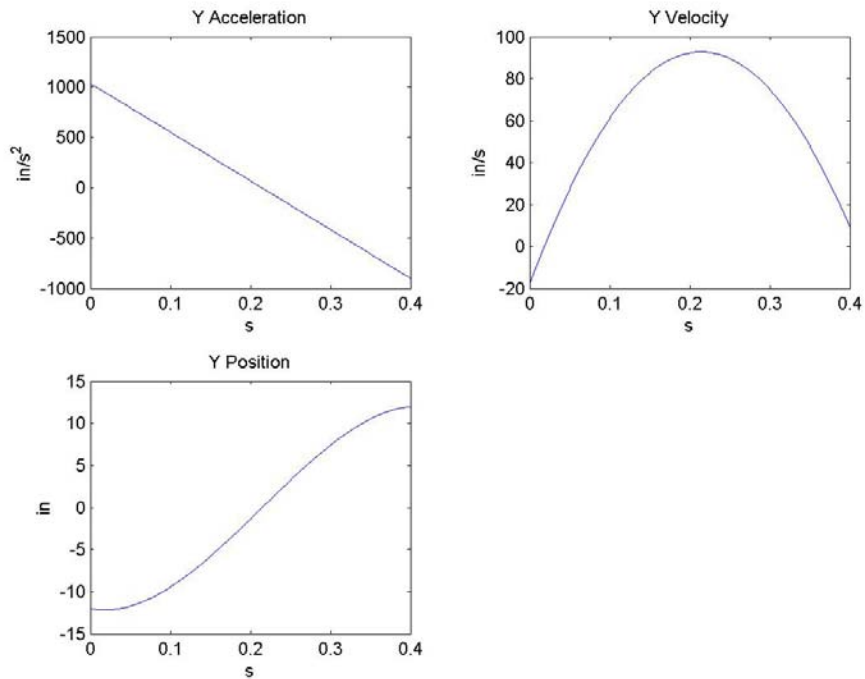


Figure E.10: Motion of the moving platform in the global Y direction (1st prototype, breast down).

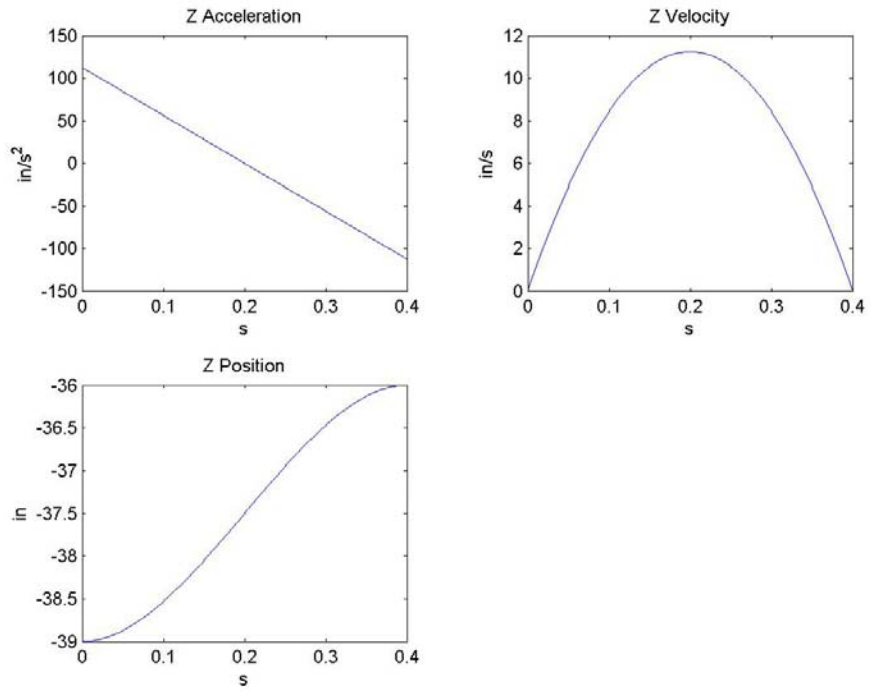


Figure E.11: Motion of the moving platform in the global Z direction (1st prototype, breast down).

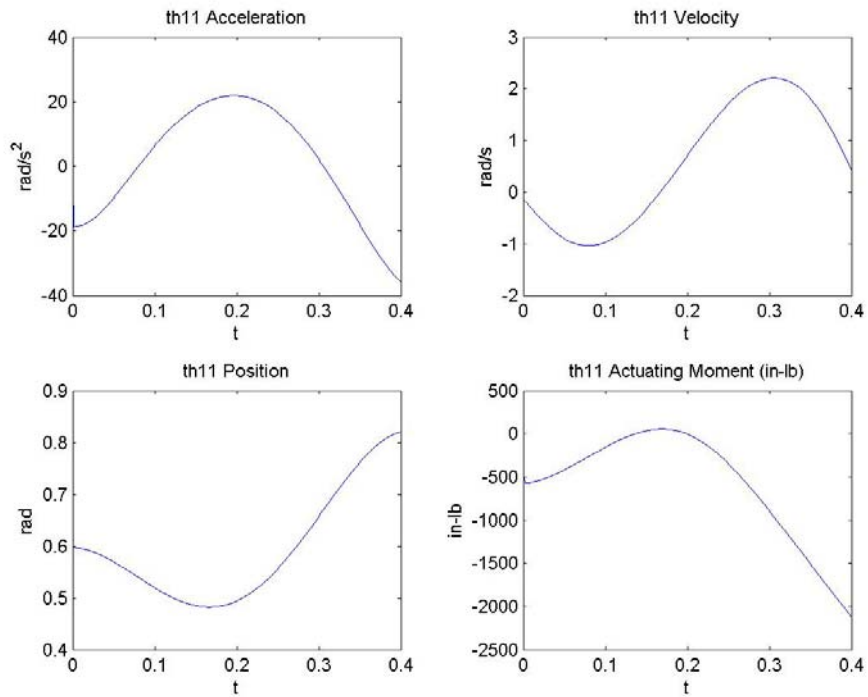


Figure E.12: Motion and moment provided by the parallel mechanism actuator at point C_1 (1st prototype, breast down).

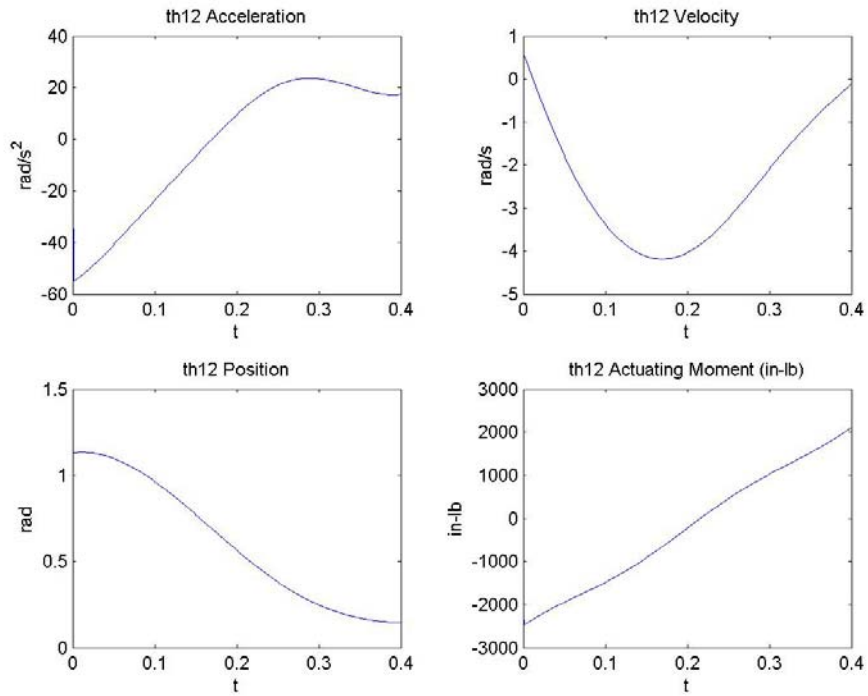


Figure E.13: Motion and moment provided by the parallel mechanism actuator at point C_2 (1st prototype, breast down).

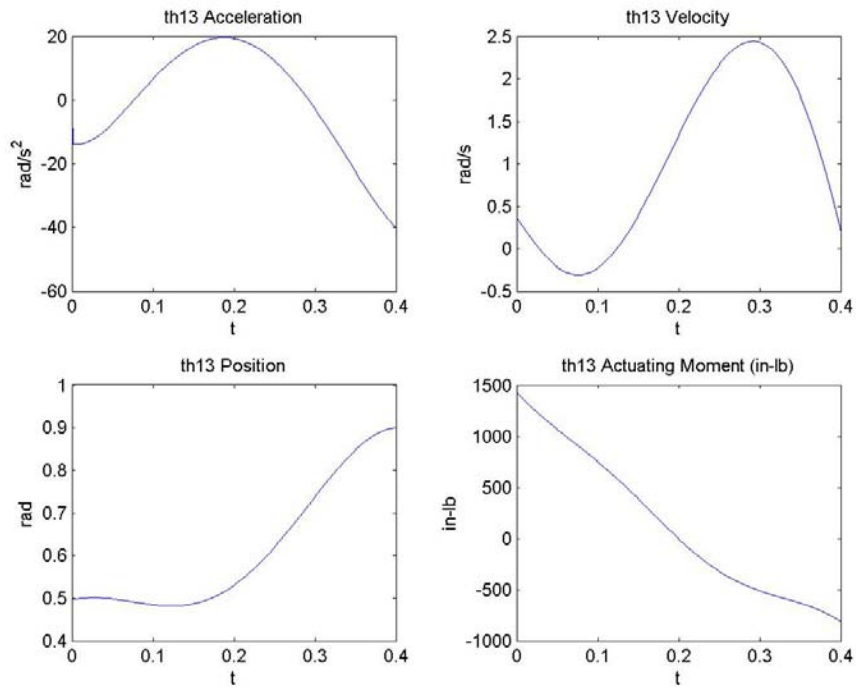


Figure E.14: Motion and moment provided by the parallel mechanism actuator at point C_3 (1st prototype, breast down).

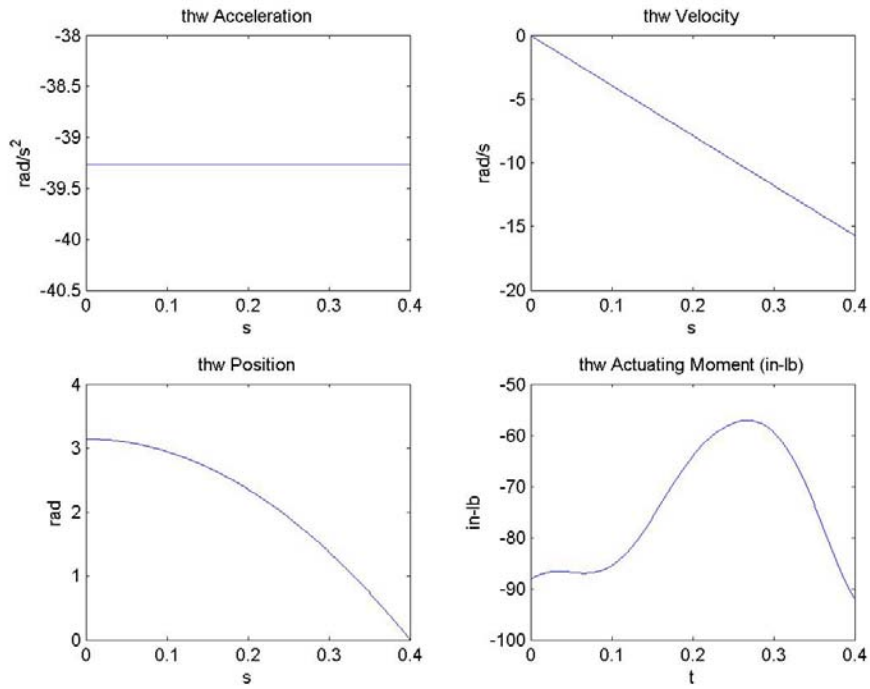


Figure E.15: Motion and moment provided by the *Flip* motion wrist actuator at point *F* (1st prototype, breast down).

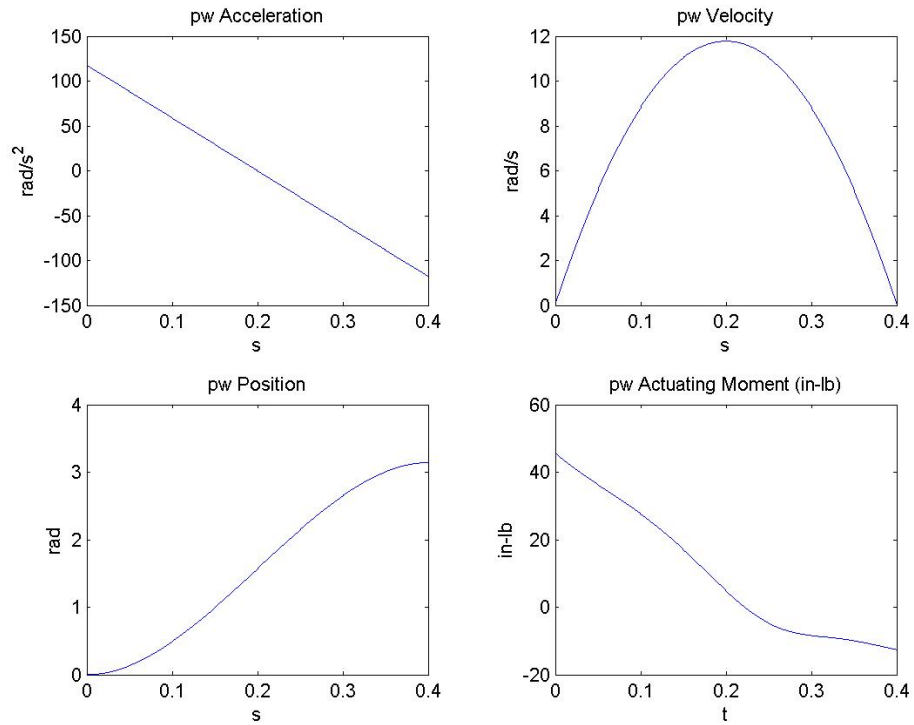


Figure E.16: Motion and moment provided by the *Rotate* motion wrist actuator at point *F* (1st prototype, breast down).

E.3 Dynamic Analysis of Second Prototype for Breast Up WOG Acquisition

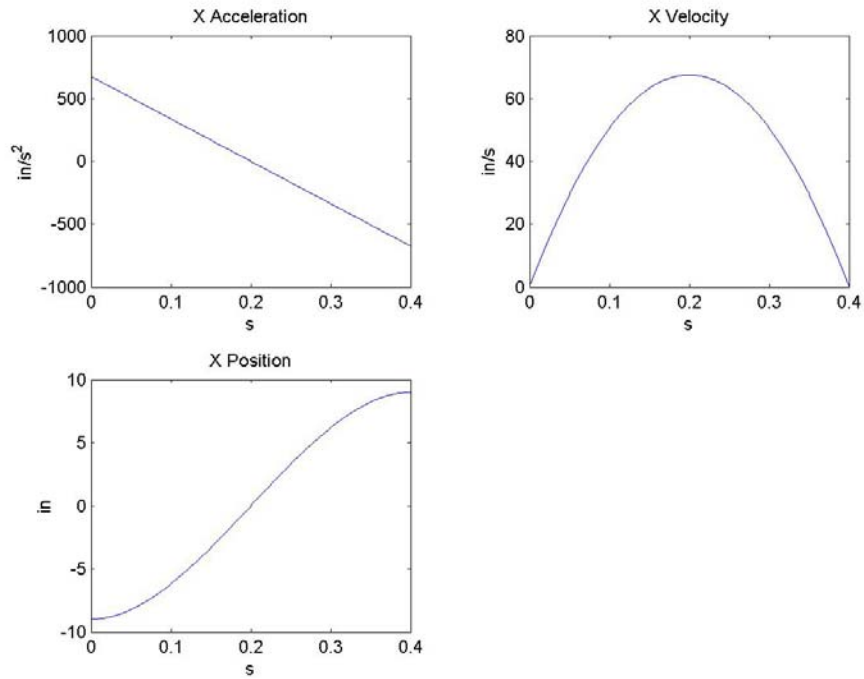


Figure E.17: Motion of the moving platform in the global X direction (2nd prototype, breast up).

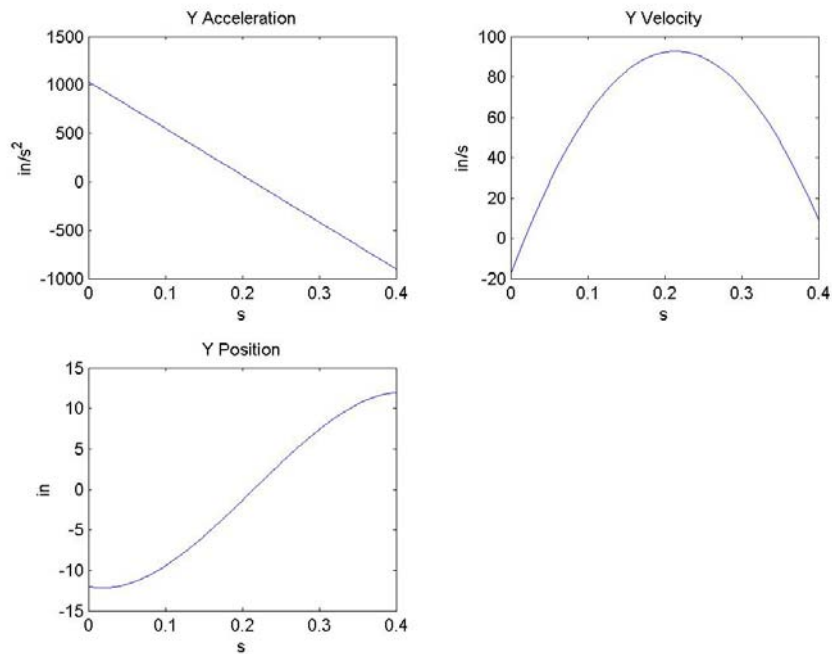


Figure E.18: Motion of the moving platform in the global Y direction (2nd prototype, breast up).

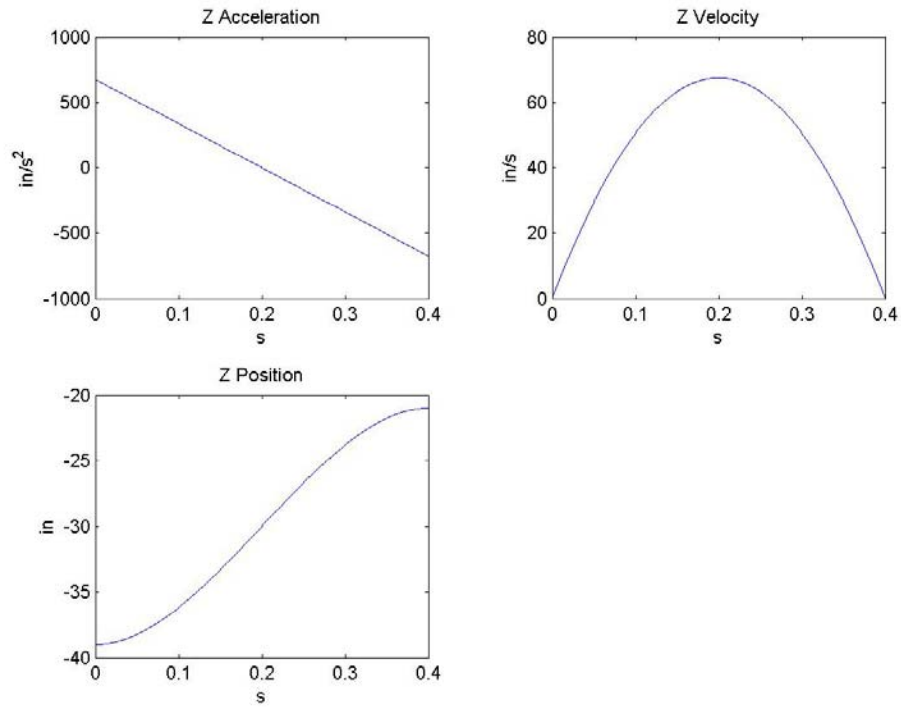


Figure E.19: Motion of the moving platform in the global Z direction (2nd prototype, breast up).

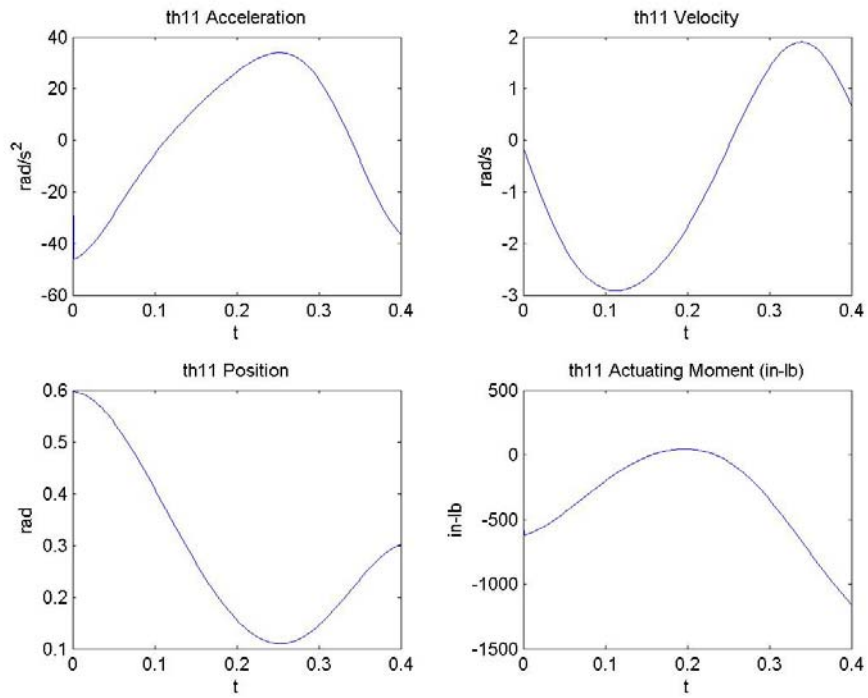


Figure E.20: Motion and moment provided by the parallel mechanism actuator at point C_1 (2nd prototype, breast up).

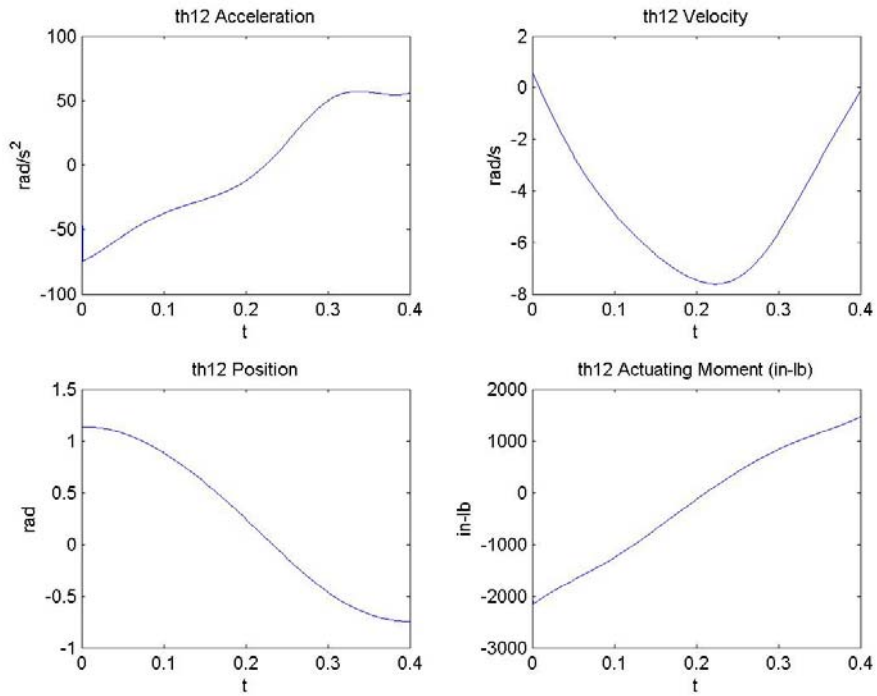


Figure E.21: Motion and moment provided by the parallel mechanism actuator at point C_2 (2nd prototype, breast up).

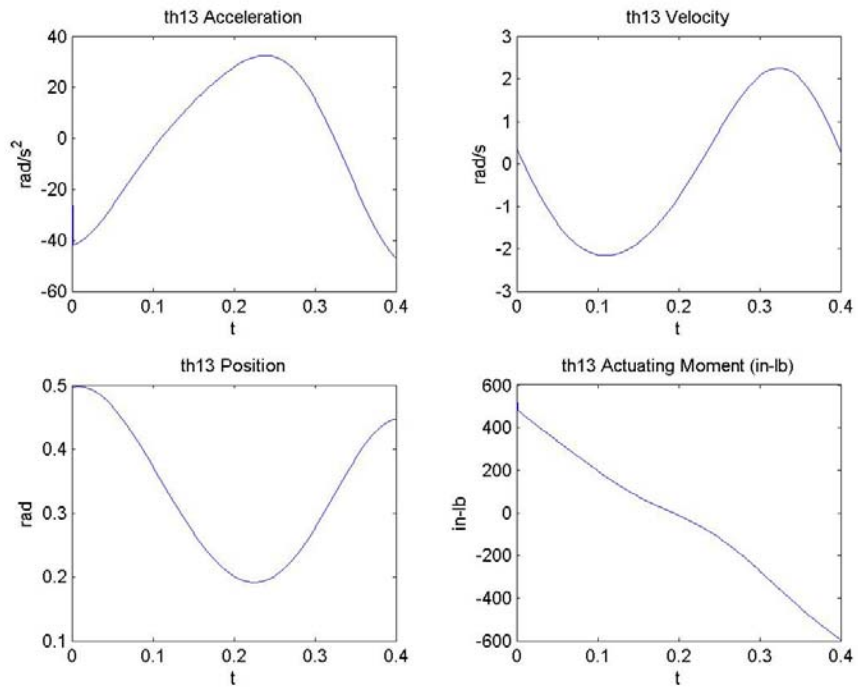


Figure E.22: Motion and moment provided by the parallel mechanism actuator at point C_3 (2nd prototype, breast up).

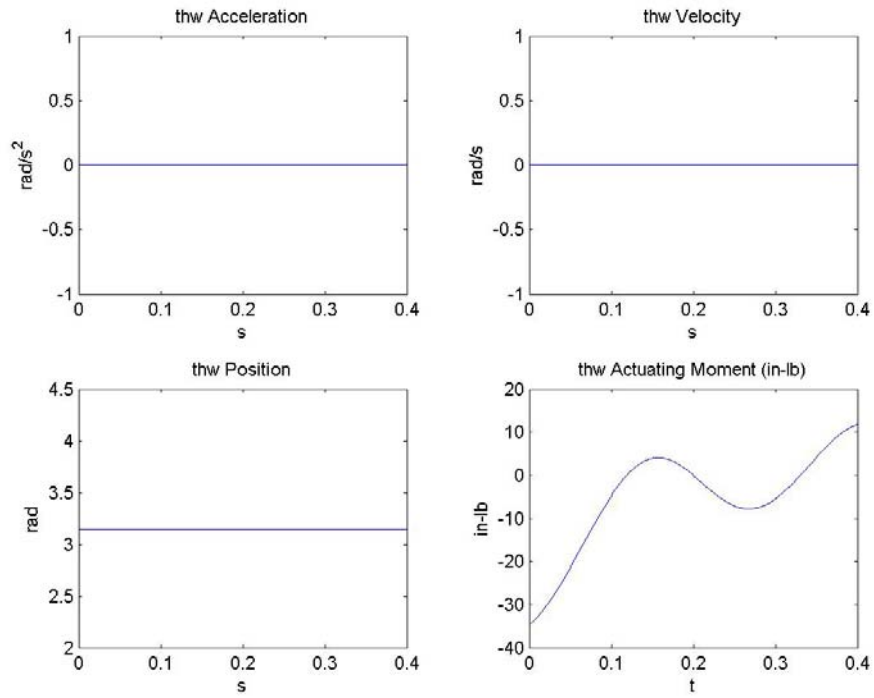


Figure E.23: Motion and moment provided by the *Flip* motion wrist actuator at point F (2nd prototype, breast up).

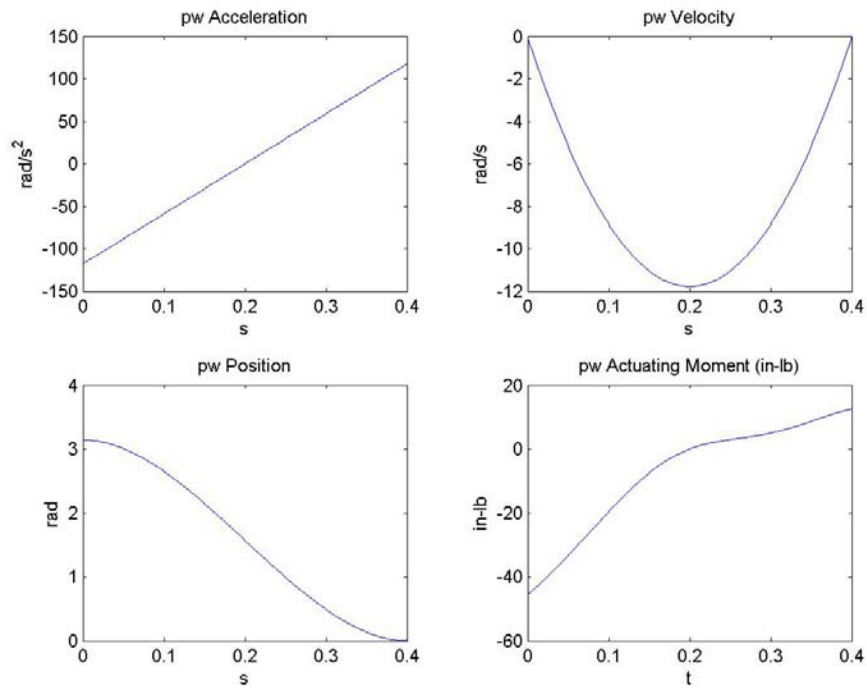


Figure E.24: Motion and moment provided by the *Rotate* motion wrist actuator at point F (2nd prototype, breast up).

E.4 Dynamic Analysis of Second Prototype for Breast Down WOG Acquisition

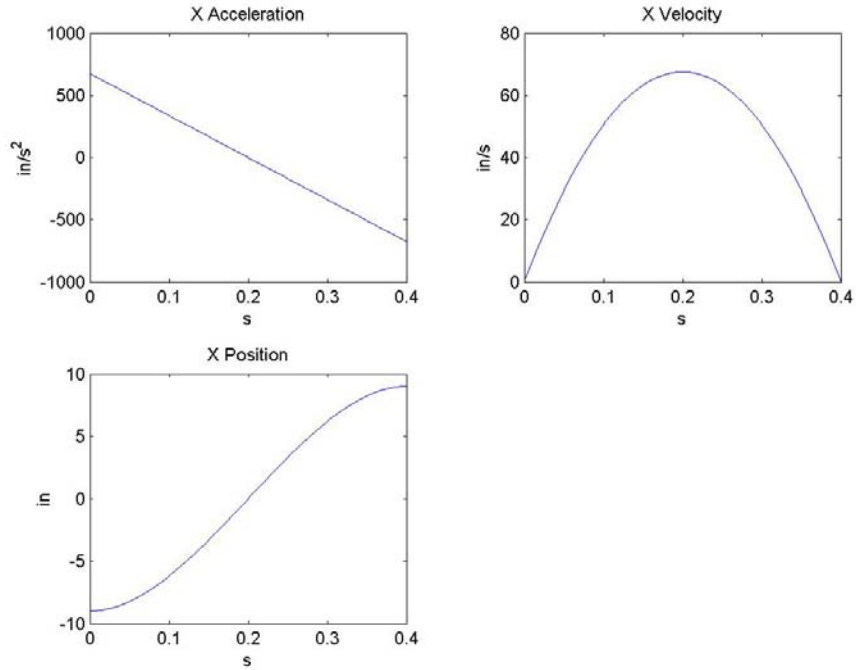


Figure E.25: Motion of the moving platform in the global X direction (2nd prototype, breast down).

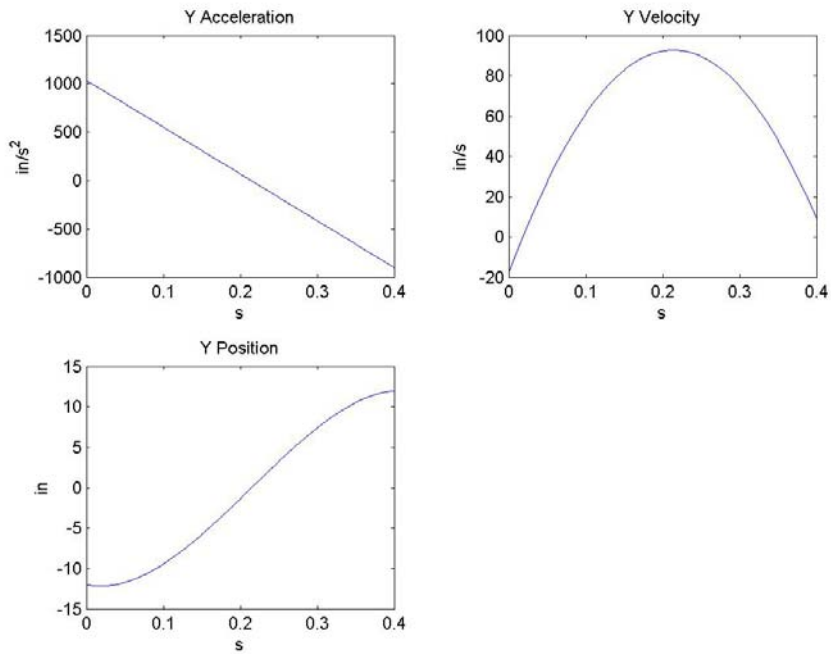


Figure E.26: Motion of the moving platform in the global Y direction (2nd prototype, breast down).

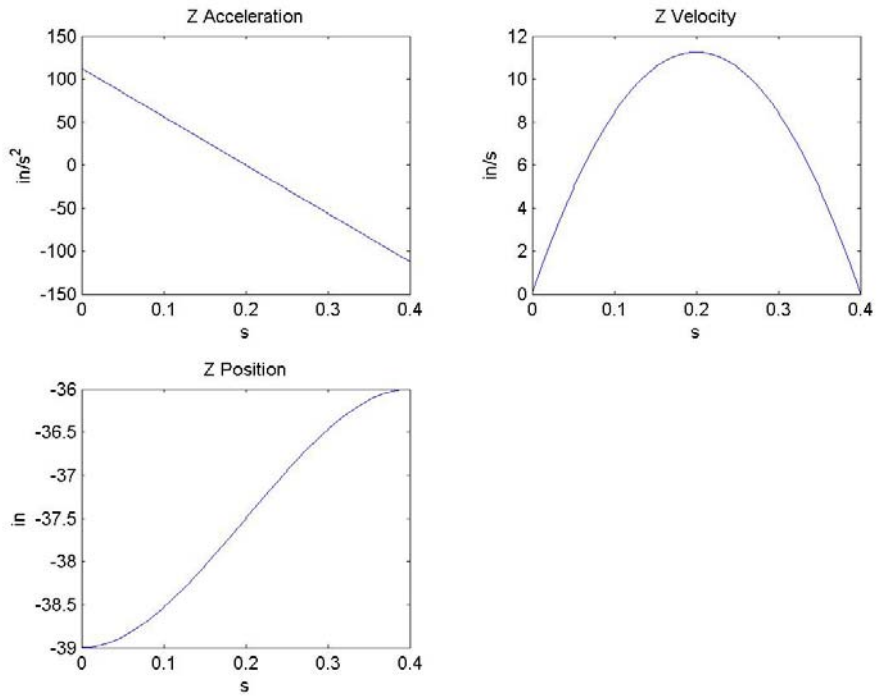


Figure E.27: Motion of the moving platform in the global Z direction (2nd prototype, breast down).

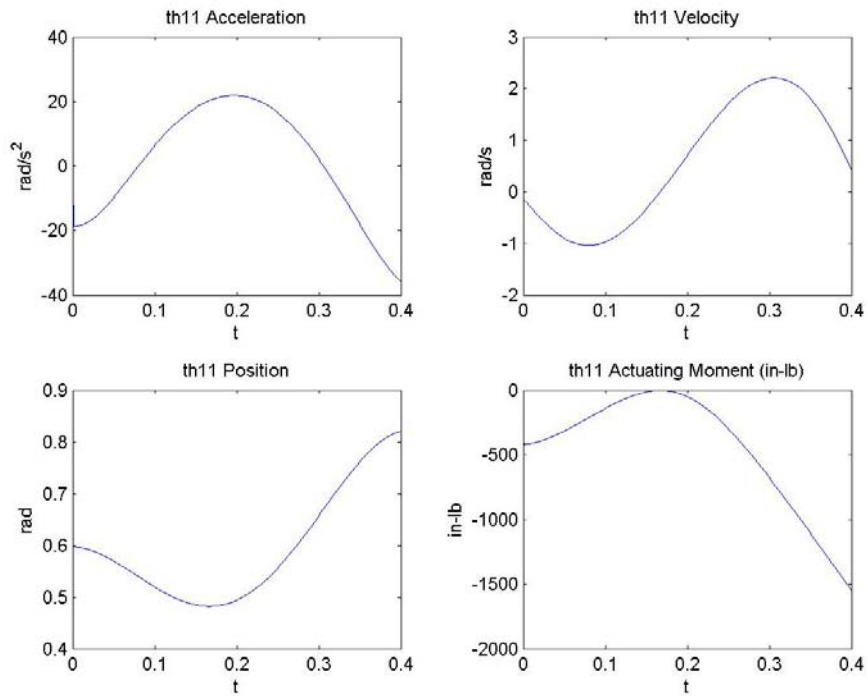


Figure E.28: Motion and moment provided by the parallel mechanism actuator at point C_1 (2nd prototype, breast down).

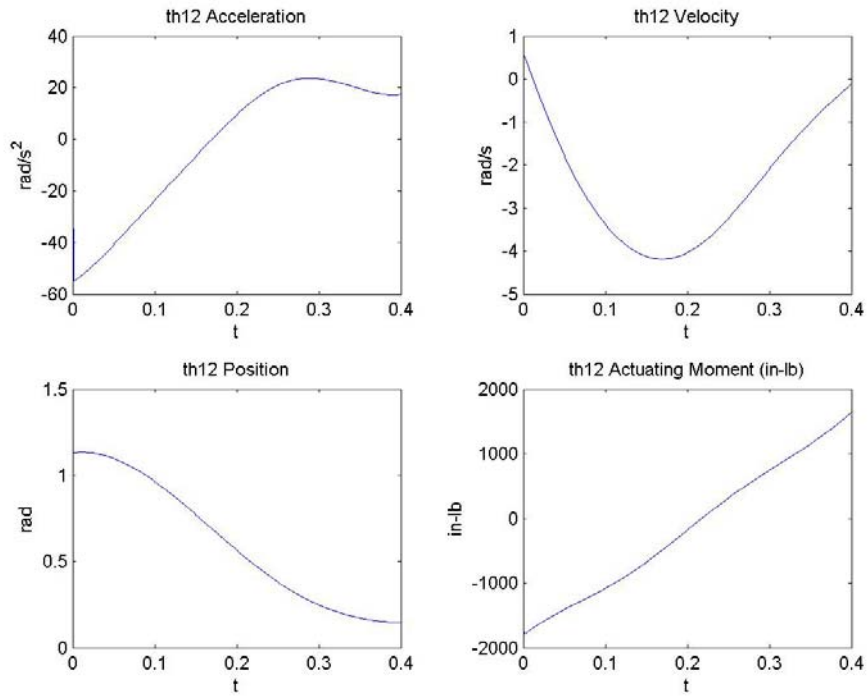


Figure E.29: Motion and moment provided by the parallel mechanism actuator at point C_2 (2nd prototype, breast down).

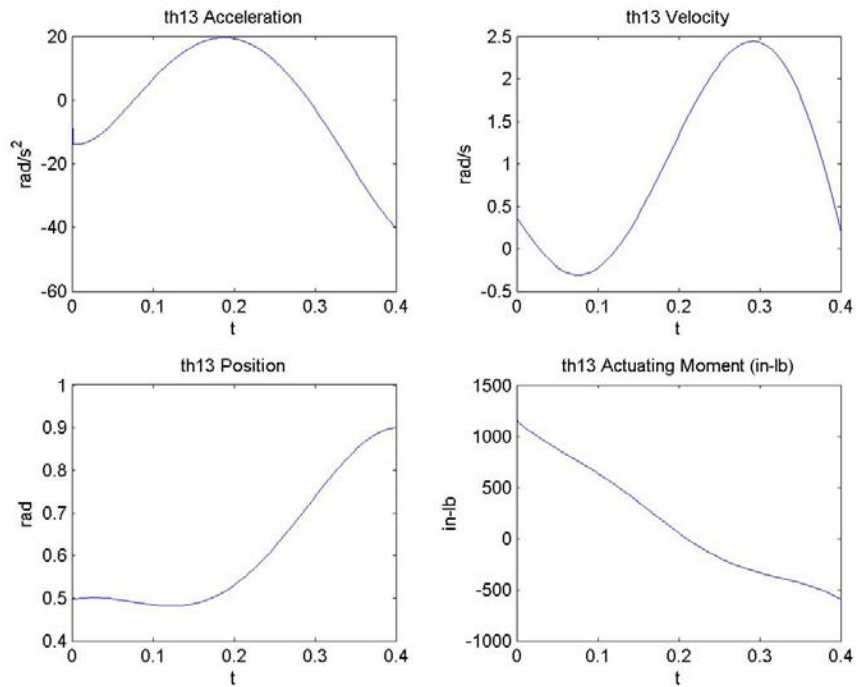


Figure E.30: Motion and moment provided by the parallel mechanism actuator at point C_3 (2nd prototype, breast down).

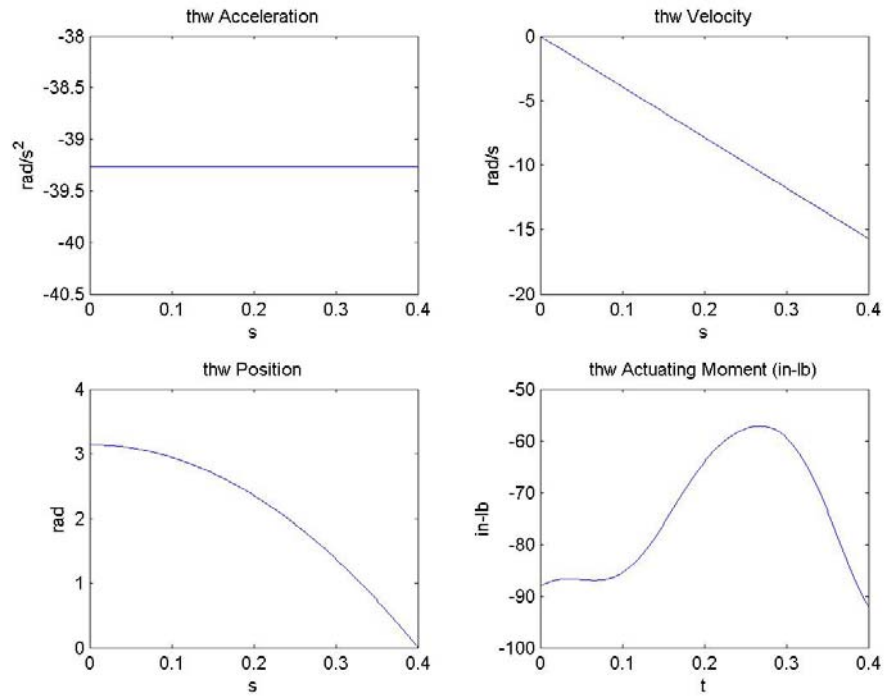


Figure E.31: Motion and moment provided by the *Flip* motion wrist actuator at point *F* (2nd prototype, breast down).

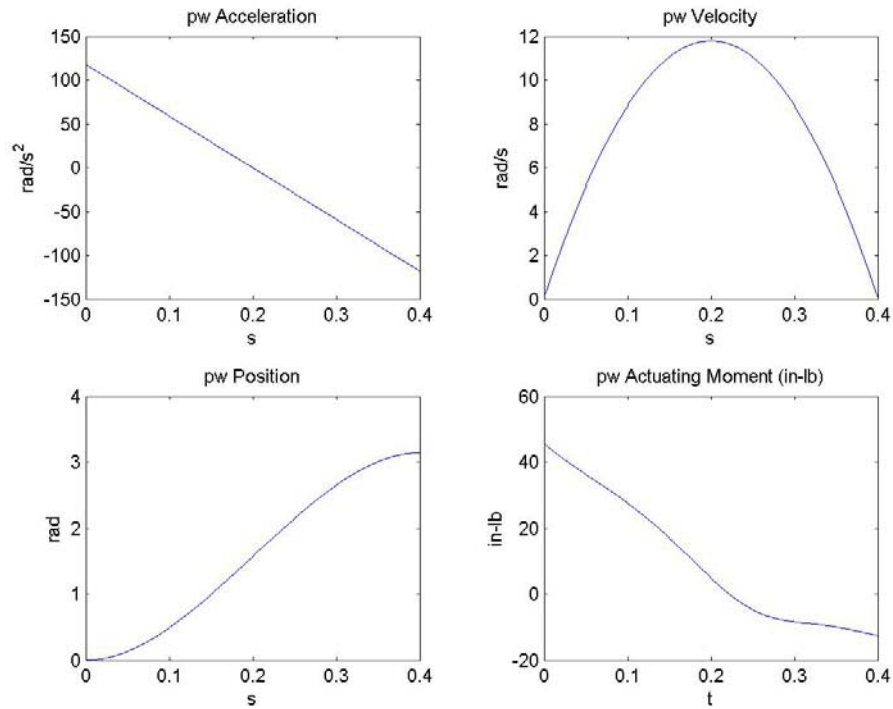


Figure E.32: Motion and moment provided by the *Rotate* motion wrist actuator at point *F* (2nd prototype, breast down).

E.5 Dynamic Analysis of Third Prototype for Breast Up WOG Acquisition

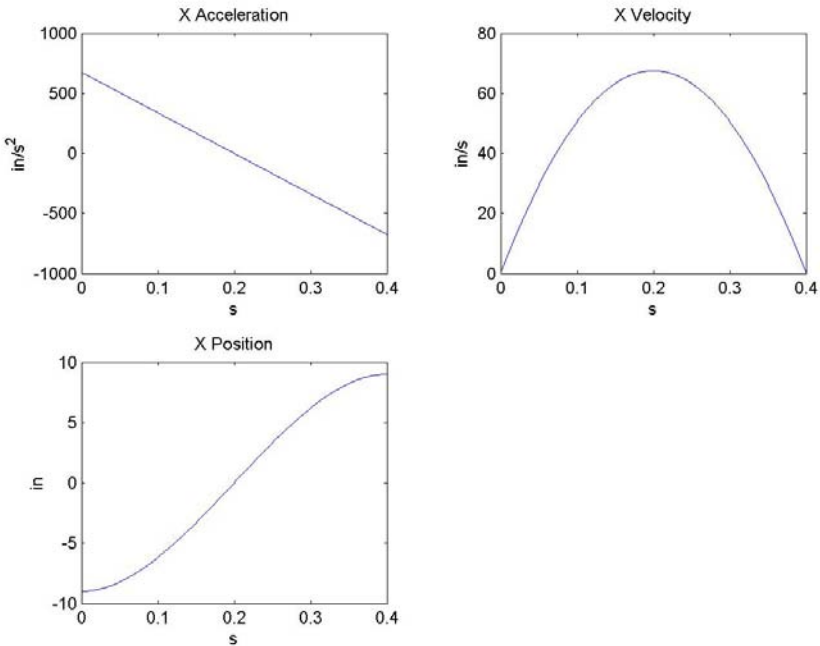


Figure E.33: Motion of the moving platform in the global X direction (3rd prototype, breast up).

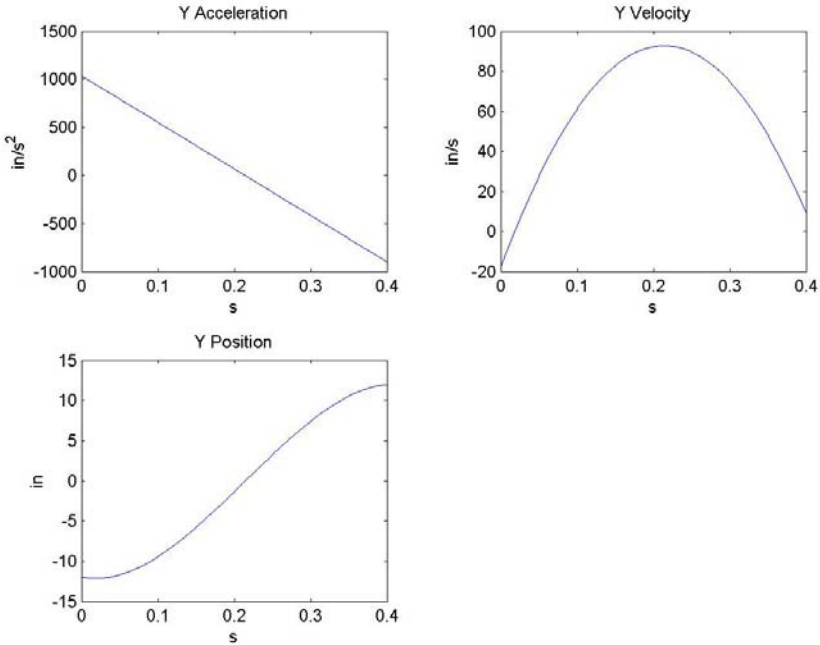


Figure E.34: Motion of the moving platform in the global Y direction (3rd prototype, breast up).

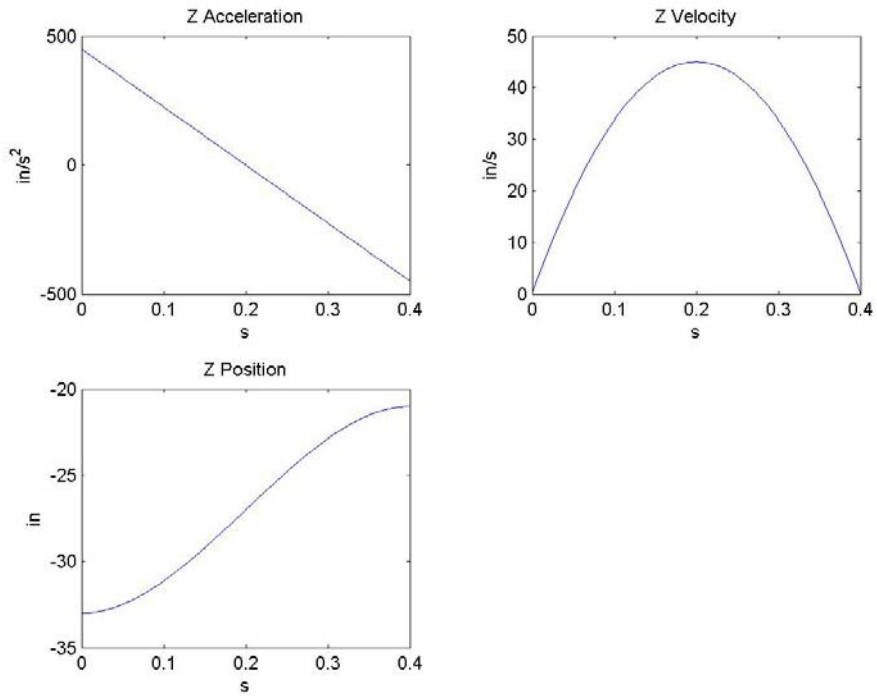


Figure E.35: Motion of the moving platform in the global Z direction (3rd prototype, breast up).

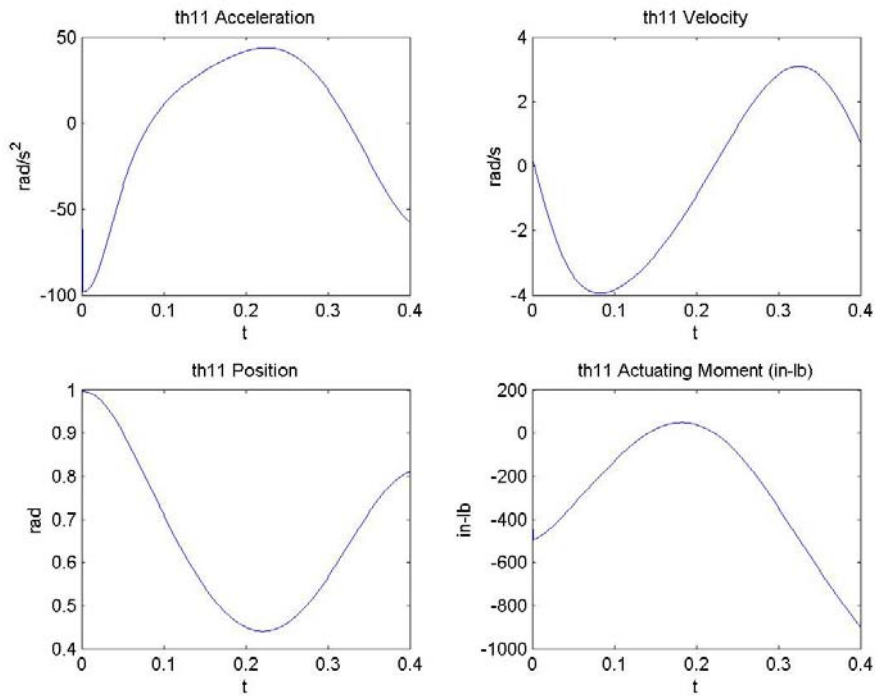


Figure E.36: Motion and moment provided by the parallel mechanism actuator at point C_1 (3rd prototype, breast up).

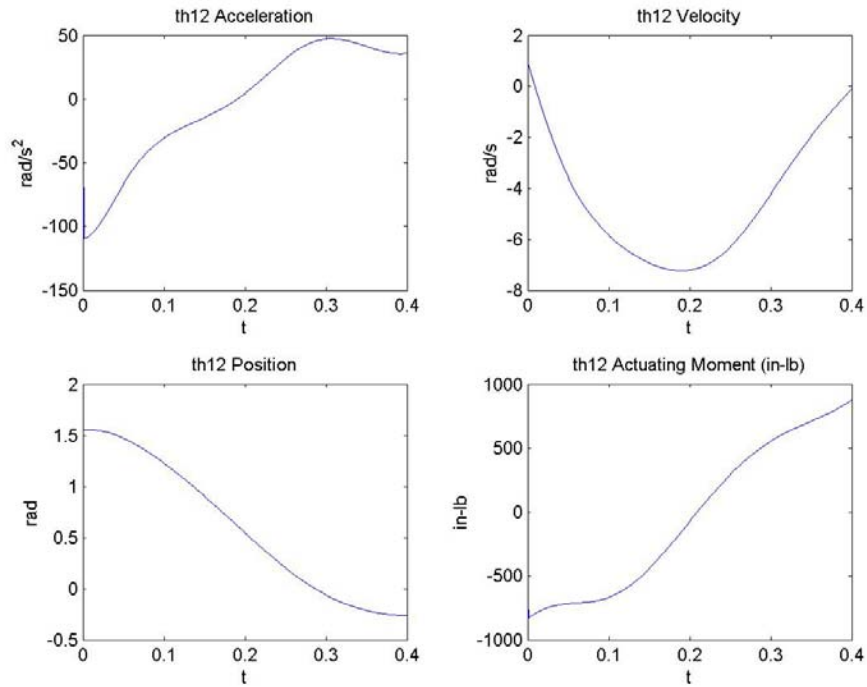


Figure E.37: Motion and moment provided by the parallel mechanism actuator at point C_2 (3rd prototype, breast up).

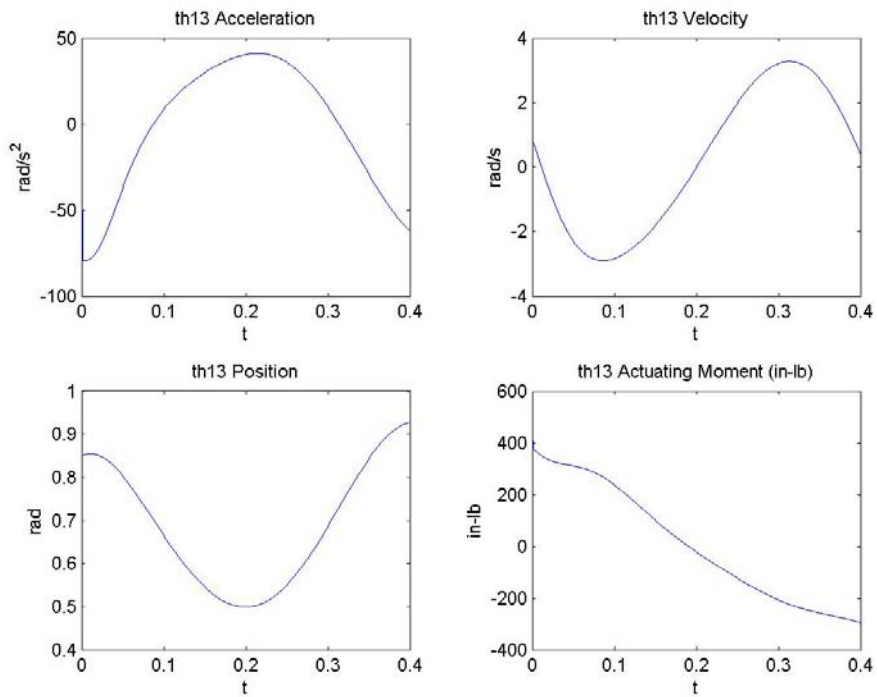


Figure E.38: Motion and moment provided by the parallel mechanism actuator at point C_3 (3rd prototype, breast up).

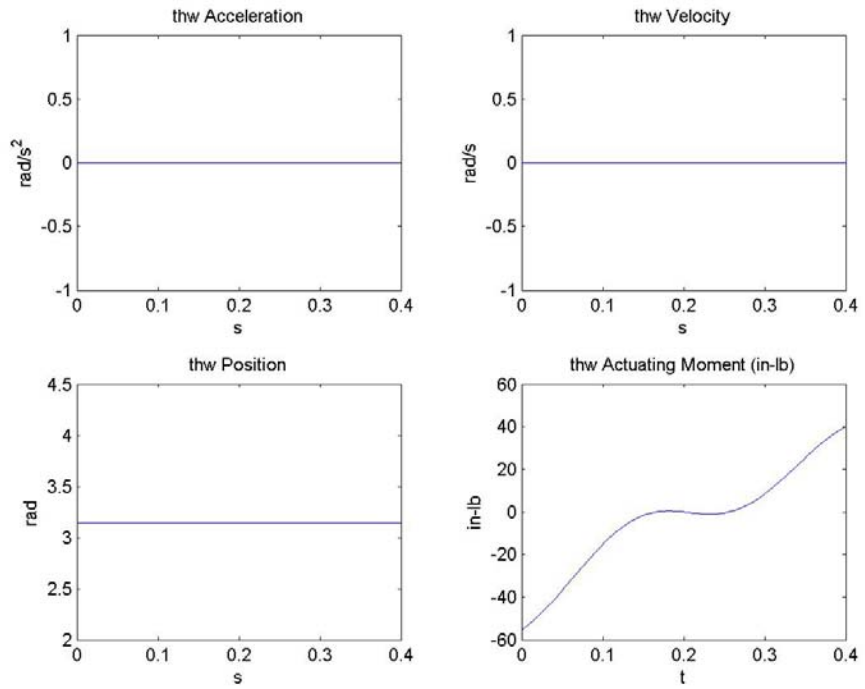


Figure E.39: Motion and moment provided by the *Flip* motion wrist actuator at point *F* (3rd prototype, breast up).

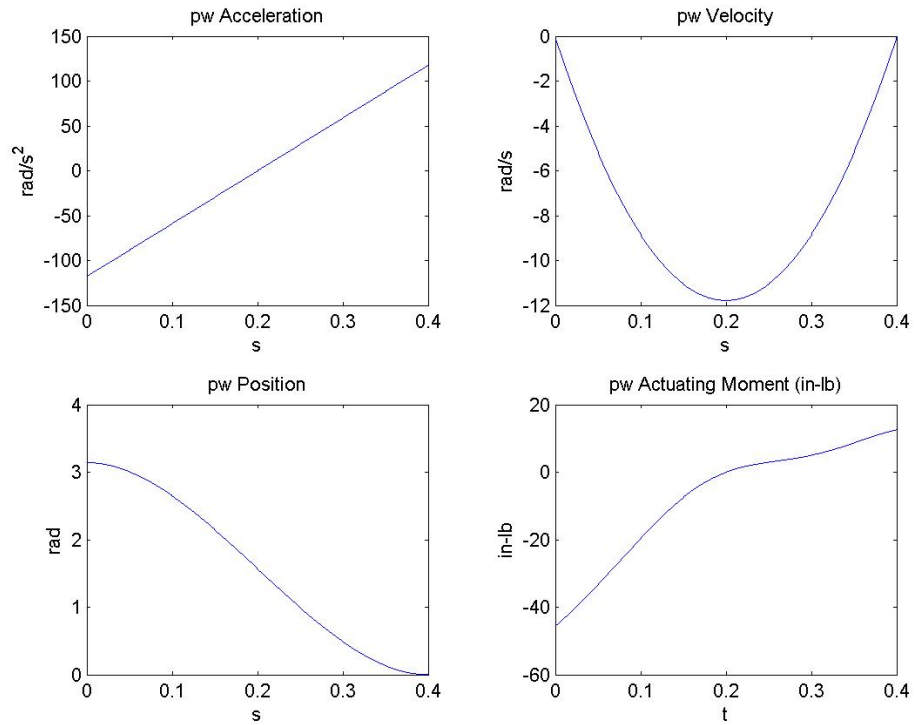


Figure E.40: Motion and moment provided by the *Rotate* motion wrist actuator at point *F* (3rd prototype, breast up).

E.6 Dynamic Analysis of Third Prototype for Breast Down WOG Acquisition

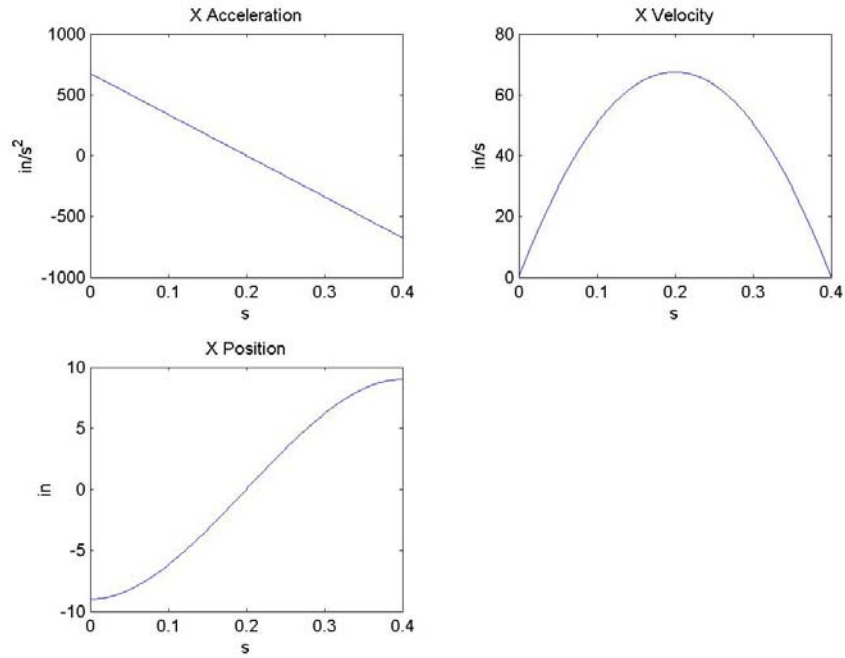


Figure E.41: Motion of the moving platform in the global X direction (3rd prototype, breast down).

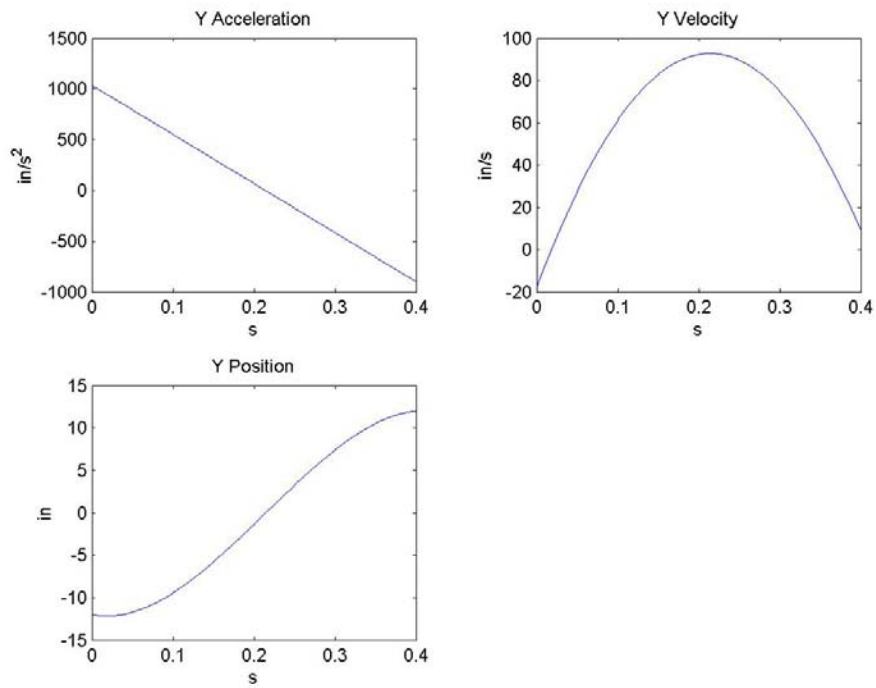


Figure E.42: Motion of the moving platform in the global Y direction (3rd prototype, breast down).

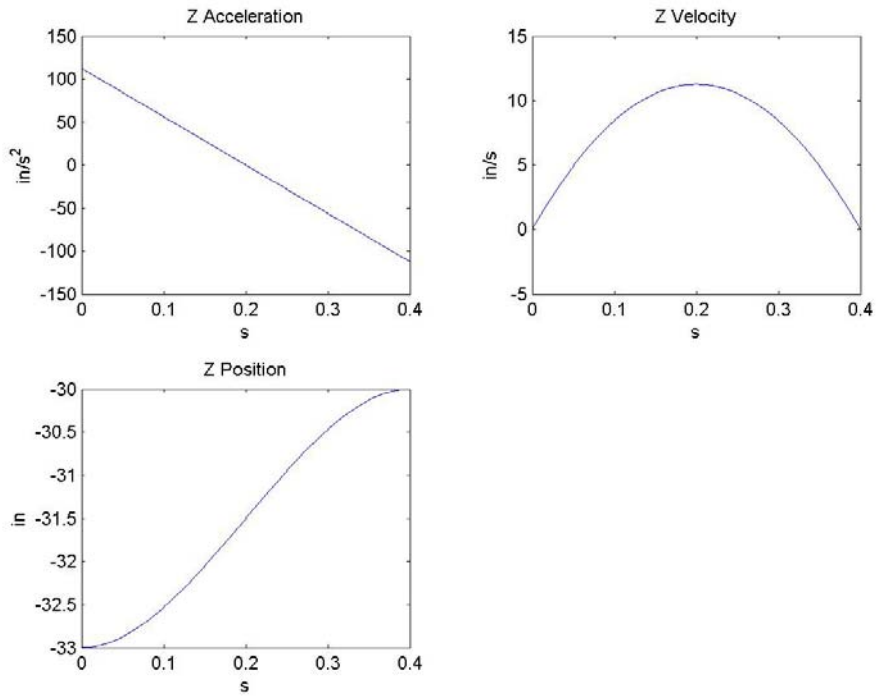


Figure E.43: Motion of the moving platform in the global Z direction (3rd prototype, breast down).

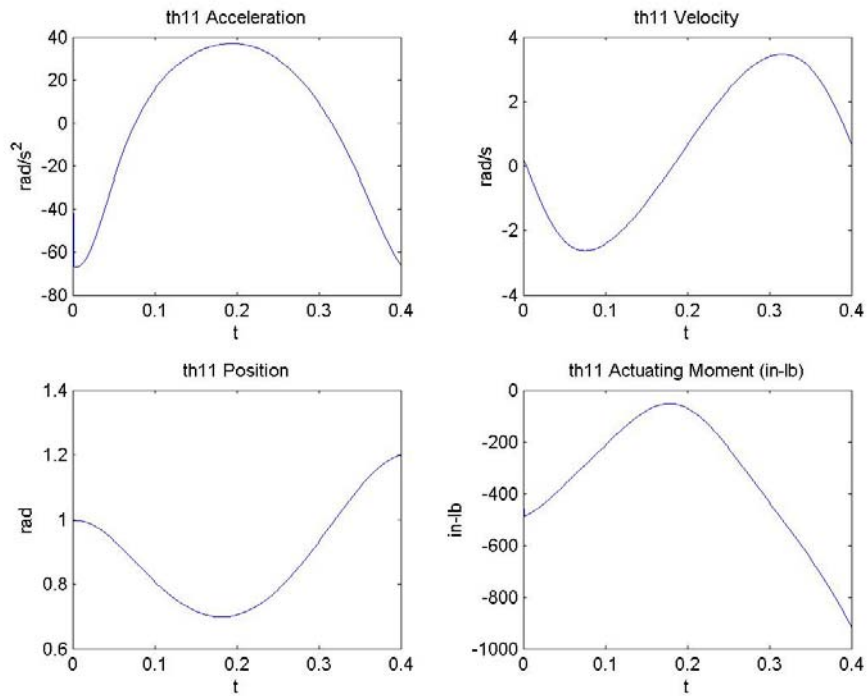


Figure E.44: Motion and moment provided by the parallel mechanism actuator at point C_1 (3rd prototype, breast down).

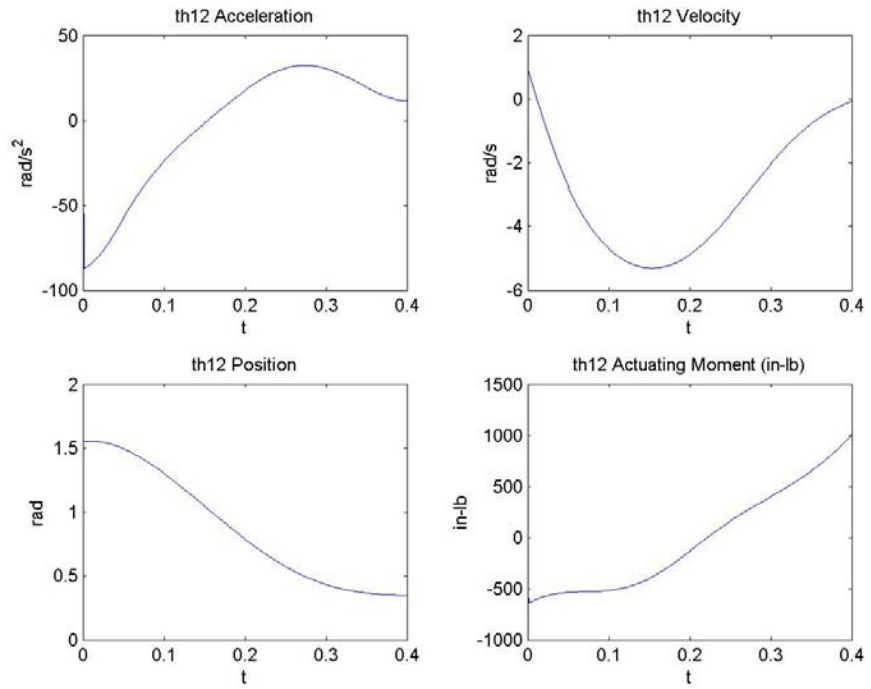


Figure E.45: Motion and moment provided by the parallel mechanism actuator at point C_2 (3rd prototype, breast down).

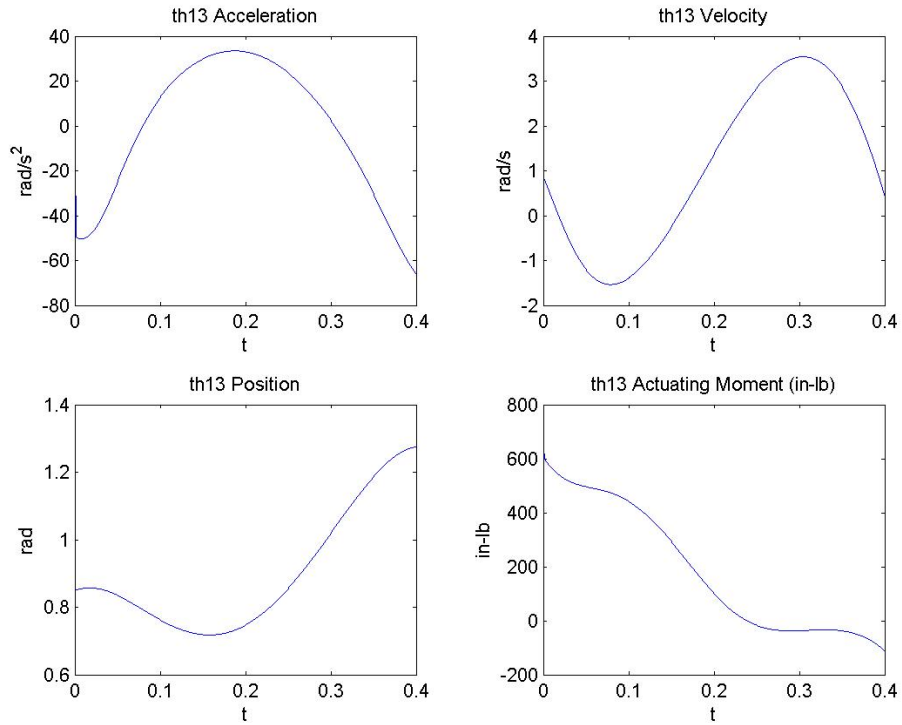


Figure E.46: Motion and moment provided by the parallel mechanism actuator at point C_3 (3rd prototype, breast down).

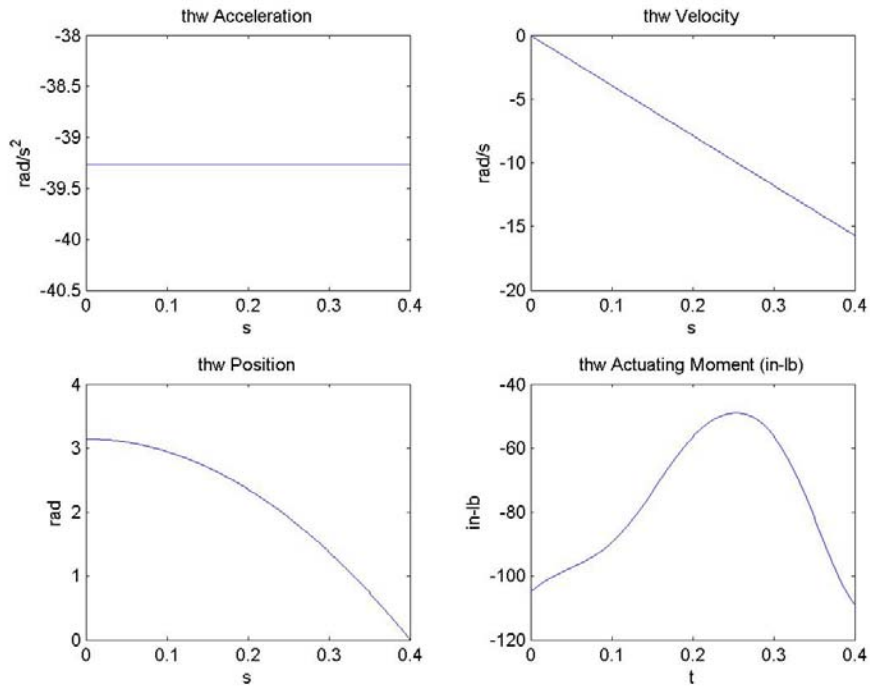


Figure E.47: Motion and moment provided by the *Flip* motion wrist actuator at point *F* (3rd prototype, breast down).

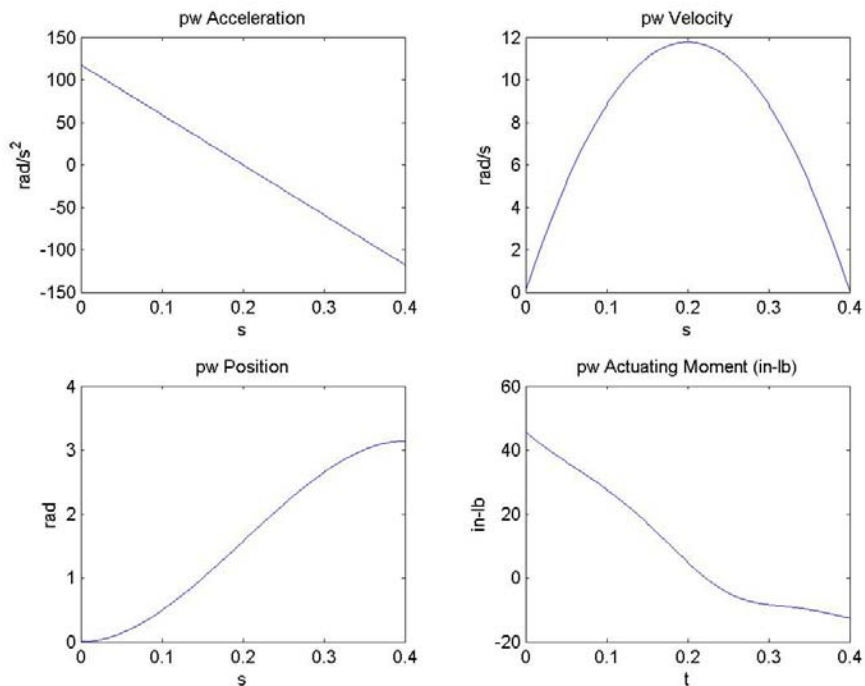


Figure E.48: Motion and moment provided by the *Rotate* motion wrist actuator at point *F* (3rd prototype, breast up).

APPENDIX F

ACTUATOR CUTSHEETS

In Section 6.6 preliminary selections are made for the actuators of the robot. In this appendix the cutsheets for those selections are presented. In Section F.1 the cutsheets for the actuators of the parallel mechanism are presented. The parallel mechanism actuator consists of a 1 hp washdown proof electric vector motor, the Baldor ZDWNM3546T, paired with a Washdown proof 60:1 speed reducer, the Baldor WDFG6032AG. The *Flip* motion of the wrist is provided by a stainless steel airmotor, the Atlas Copco LZB 34RL AR004. The cutsheets for the Atlas Copco LZB 34RL AR004 are presented in Section F.2. Section F.3 contains the cutsheets for the Pacific Scientific PMA 23 Washdown Servo Motor. The PMA 23 provides the *Rotate* motion of the wrist.

F.1 Parallel Mechanism Actuator Cutsheets

Product Overview: ZDWNM3546T



Click for Larger Image

Catalog Number: ZDWNM3546T
Description: 1HP | 1750RPM | 3PH | TENV | 143TC NEMA
Ship Weight: 45 lbs.
List Price: \$1693
Multiplier Symbol: E2

[View Specifications](#)

FEATURES

- Totally Enclosed Non Ventilated (TENV)
- C-Face with base 143TC-254TC
- Supplied with 1024 line count encoder
- Stainless Steel Shaft
- Forsheda® running contact V-ring
- Epoxy coating
- Moisture sealant on bolt heads, between frame and endplate
- ISR® (Inverter Spike Resistant) magnet wire
- Class H Insulated

APPLICATIONS

Vector Drive Washdown. Material handling, packaging equipment in food processing and other wet environments. For adjustable speed applications requiring full torque from zero to base speed.

Figure F.1: Baldor ZDWNM3546T 1 hp washdown vector motor features.

Inverter Drive® and Vector Drive® Washdown Duty Motors Performance Data 230/460 Volt Ratings-TENV Enclosure

60 HZ		BASE SPEED	MAX. SPEED	NEMA FRAME	ENCL	INVERTER CATALOG NO.	VECTOR CATALOG NO.	460 VOLT LINE AMPS				OUTPUT TORQUE LB-FT			% EFFICIENCY LINE POWER	WK ² LB-FT ²	APPROX. WEIGHT LBS	BEARINGS	
HP	KW							IDLE	FL	FL	L.R.	B.D.	FL	L.R.				B.D.	DE
1	0.75	1750	6000	143TC	TENV	IDWNM3546T	ZDWNM3546T	0.81	1.4	3.0	10.0	14.5	85.5	0.14	40	6205	6203		
1.5	1.1	1750	6000	145TC	TENV	IDWNM3554T	ZDWNM3554T	1.2	2.1	4.5	19.8	20.5	87.5	0.21	49	6205	6203		
2	1.5	1725	6000	182TC	TENV	IDWNM3609T	ZDWNM3609T	1.7	2.9	6.0	25.0	30.0	84.0	0.26	68	6206	6205		
3	2.2	1750	3600	184TC	TENV	IDWNM3611T	ZDWNM3611T	1.8	4.0	9.0	22.0	32.0	88.5	0.319	79	6206	6205		
5	3.7	1760	6000	213TC	TENV	IDWNM3707T	ZDWNM3707T	3.4	6.7	14.9	48.0	52.0	89.5	0.74	122	6307	6206		
7.5	5.6	1765	4000	254TC	TENV	IDWNM22937T	ZDWNM22937T	4.0	9.1	22.5	48.6	86.0	91.0	1.75	242	6309	6208		
10	7.5	1765	4000	254TC	TENV	IDWNM22938T	ZDWNM22938T	4.4	12.0	30.0	58.0	114	91.7	2.45	291	6309	6208		

Figure F.2: Baldor ZDWNM3546T 1 hp washdown vector motor performance data.

Inverter Drive® and Vector Drive® Washdown Duty Motors

Baldor's A.C. Inverter Drive® and Vector Drive® Washdown Duty Motors range from 1 to 10 Hp and are suitable for use on conveyors, pumps, and other equipment in the food processing industry. Specifically designed for high pressure washdown applications.



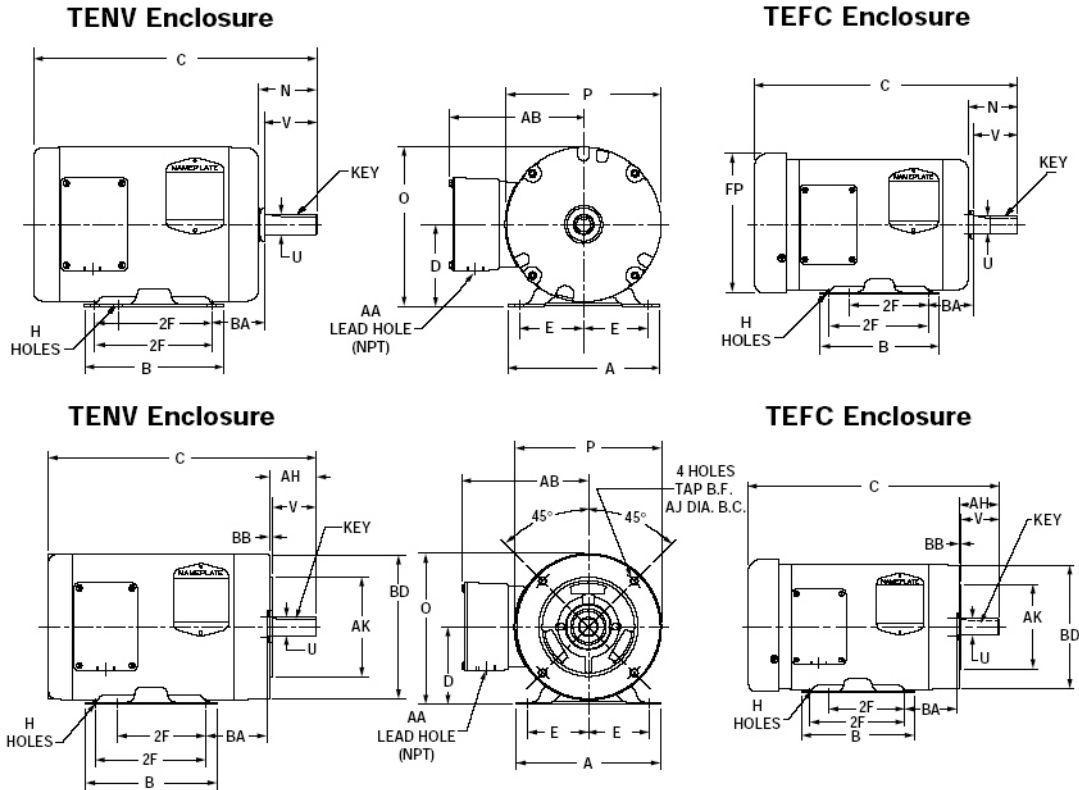
1.5Hp TENV Washdown Vector Drive Motor
Catalog # ZDWNM3554T

Mechanical Design Characteristics

Specification	Description	Frames		
		56	143T 215T	254T 256TC
Nameplate	Nameplate and fasteners stainless steel. Includes base volts and frequency, connection diagrams, blower rating (volts, hertz, phase, and amps), maximum motor speed, rotor inertia and magnetization current	S	S	S
Frame Dimensions	NEMA	S	S	S
Frame Construction	Steel band	S	S	S
	Stainless steel band (Paint Free only)	S	S	S
Multiple Mounting Holes in Base	Multiple mounting holes standard	S	S	S
Endplates	Die cast aluminum with steel bearing inserts	S	S	S
	Treated die cast aluminum with steel bearing inserts (Paint Free only)	S	S	S
Face Mounting	Horizontal	O	O	O
	C-Face (standard on stock motors 56C-256TC)	S	S	S
	D-Flange	O	O	O
Conduit Box & Cover	Die cast aluminum	S		
	Treated die cast aluminum (Paint Free only)		S	S
Gaskets & Sealing	Neoprene gaskets prevent entrance of moisture between the conduit box and frame as well as the lid and conduit box. Joint between the endplates and motor frame is sealed to prevent water entry	S	S	S
Ground Provisions	Inside conduit box for convenience	S	S	S
Lifting Provisions	Eyebolt in frame	S	S	S
Cooling Fan	Non-sparking, glass-filled polypropylene	S	S	S
Rotor Construction	Special high pressure aluminum die cast with low loss electrical steel and special slot configuration. Coated with 2-part epoxy for resistance to corrosion	S	S	S
Balance	Dynamically balanced better than NEMA MG1-1998 specifications.	S	S	S
Shaft Material	Entire shaft is made of 300 series stainless steel for prevention of rust and corrosion	S	S	S
Shaft Seals	A contact lip seal and V-ring type Forsheda rotating seal are provided on the drive-end shaft to prevent entrance of contamination into the bearings.	S	S	S
Drains	Multiple drain hole locations with removable plugs to maximize drainage & minimize water entry	S	S	S
Paint	FDA approved two-part epoxy coated inside and outside to extend motor life and prevent internal corrosion	S	S	S
	No internal or external paint (Paint Free only)	S	S	S
Bearings	Premium grade ball bearings, double shielded	S	S	
	Premium grade ball bearings, open with Lube Lock			S
	Roller bearing on drive end	O	O	O
Bearing Retention	Locked bearings for universal mounting	S	S	S
Bearing Lubrication	Exxon Mobil POLYREX® EM for use in wet environments with resistance to wash-out	S	S	S
Grease Provisions	Regreasable with addition of grease fittings	S	S	S
Limited Warranty	18 months - motors only; 24 months when used with Baldor control	S	S	S

Note: Specifications and Dimensions are subject to change without notice, please contact Baldor for certified information.
S= standard, O= optional

Figure F.3: Baldor ZDWNM3546T 1hp washdown vector motor mechanical characteristics.



Catalog No. starting with "C" = C-face with base.
 Catalog No. starting with "V" = C-face, no base.

NEMA Frame	A	B	D	E	2F	H	N	O	P	U	V	AA	AB	AH	AJ	BF TAP	AK	BA	BB	BD
56	6.50	4.50	3.50	2.44	3.00	0.34	2.44	6.81	6.62	0.625	1.88	0.50	5.22	-	-	3/8-16	-	2.75	-	-
56C	6.50	4.50	3.50	2.44	3.00	0.34	-	6.81	6.62	0.625	1.88	0.50	5.22	2.06	5.88	3/8-16	4.50	2.75	0.12	6.50
143TC	6.50	5.94	3.50	2.75	4.00	0.34	-	6.81	6.62	0.875	2.25	0.50	5.22	2.12	5.88	3/8-16	4.50	2.75	0.12	6.50
143V	6.50	5.94	3.50	2.75	3.00	0.34	2.30	6.81	6.62	0.875	2.25	0.50	5.22	-	-	3/8-16	-	2.75	-	-

Figure F.4: Baldor ZDWNM3546T 1 hp washdown vector motor dimensions.

[Gear Products](#) | [Speed Reducers](#) |
Product Overview: WDFG6032AG



Catalog Number: WDFG6032AG
Description: WDF-932-60-B5-G
Ship Weight: 76 lbs.
List Price: \$961
Multiplier Symbol: GB

[View Specifications](#)

FEATURES

- Epoxy coated cast iron housing
- Stainless steel output shaft and hardware
- BISSC Certified
- Factory fill with Mobile SHC634 synthetic oil
- Sealed housing with pressure compensation chamber
- Chill cast bronze worm gears
- Hardened steel worm
- Ball bearings on input shaft
- Tapered roller bearings on output shaft
- Industry standard mounting dimensionally interchangeable with many other worm gear reducers

APPLICATIONS

Food processing and other applications where units are regularly exposed to high pressure washdown.

Figure F.5: Baldor WDFG6032AG 60:1 washdown gearbox features.



Washdown Right Angle, Quill Type Gear Reducer continued...

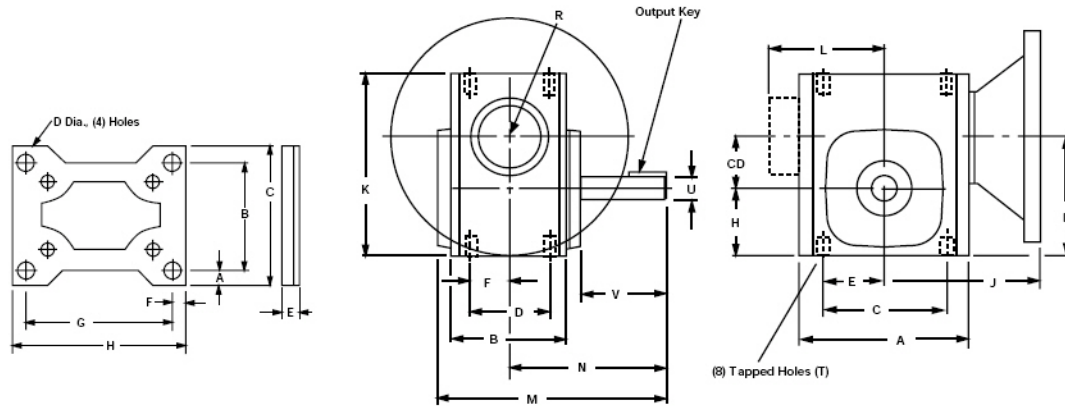
Nominal Output RPM @ 1750 RPM In	Gear Ratio	Continuous Duty Output Torque (In-Lbs) Based on 1750 RPM Motor								Max Input Hp	Max Output Torque Rating In-Lbs	NEMA Motor Mount	Style No.	Catalog No.	Ap'x Shpg. Wgt.
		0.25	0.33	0.5	0.75	1	1.5	2	3						
44	40	174	230							0.33	230	56C	WDF-913-40-B5-G	WDFG4013AG	15
	40	208	275							0.44	317	56C	WDF-915-40-B5-G	WDFG4015AG	25
	40	180	238	360						0.64	461	56C	WDF-918-40-B5-G	WDFG4018AG	25
	40		340	515						0.66	680	56C	WDF-921-40-B5-G	WDFG4021AG	31
	40			521	781					0.99	1030	56C	WDF-924-40-B5-G	WDFG4024AG	38
	40			524	786	1049				1.23	1296	56C	WDF-926-40-B5-G	WDFG4026AG	54
	40					1081	1622	2163		2.20	2374	140TC	WDF-932-40-B7-G	WDFG4032BG	97
35	50	177	234							0.33	234	56C	WDF-913-50-B5-G	WDFG5013AG	15
	50	230	303							0.33	303	56C	WDF-915-50-B5-G	WDFG5015AG	25
	50	222	294							0.49	436	56C	WDF-918-50-B5-G	WDFG5018AG	25
	50	280	370	561						0.58	651	56C	WDF-921-50-B5-G	WDFG5021AG	31
	50		401	608	912					0.83	1014	56C	WDF-924-50-B5-G	WDFG5024AG	38
	50			621	932	1242				1.00	1242	56C	WDF-926-50-B5-G	WDFG5026AG	54
	50				958	1278	1917			1.83	2366	140TC	WDF-932-50-B7-G	WDFG5032BG	97
29	60	218	288							0.33	288	56C	WDF-915-60-B5-G	WDFG6015AG	25
	60	220	290							0.47	413	56C	WDF-918-60-B5-G	WDFG6018AG	25
	60	317	418	634						0.50	634	56C	WDF-921-60-B5-G	WDFG6021AG	31
	60		458	693						0.69	956	56C	WDF-924-60-B5-G	WDFG6024AG	38
	60					1100	1467	2200		1.54	2255	56C	WDF-932-60-B5-G	WDFG6032AG	97

NOTE:
 Service Class I Torque Ratings
 Service Class II Torque Ratings
 Service Class III Torque Ratings

NOTE: Optional Shaft Positions, Base Installation and Motor Mounting available through Mod Express. Refer to a Baldor District Office for pricing and delivery.
 See pages 36 for dimension drawing.
 See page 25 for optional Stainless Steel bases.
 Data subject to change without notice. Contact Baldor for certified data.

Figure F.6: 60:1 Baldor WDFG6032AG washdown gearbox performance.

Right Angle Quill Type Gear Reducer Model F - Basic



Size	C.D.	A	B	C	D	E	F	H	J 56C 140TC	J 180TC	K	L	M	N	P	T TAP SIZE	T DEPTH
913	1.33	4.25	2.88	3.25	2.00	1.63	1.00	1.72	3.94	-	4.65	-	6.03	4.00	3.05	5/16-18	0.62
915	1.54	5.13	3.69	4.19	2.75	2.10	1.38	1.91	4.50	-	5.38	-	6.72	4.31	3.45	5/16-18	0.62
918	1.75	5.56	3.69	4.19	2.75	2.09	1.38	2.06	4.69	-	5.75	-	6.78	4.31	3.81	5/16-18	0.62
921	2.06	6.06	3.81	5.00	2.88	2.50	1.44	2.28	5.07	-	6.38	-	7.22	4.69	4.34	3/8-16	0.75
924	2.38	6.44	4.06	5.00	2.88	2.50	1.44	2.50	5.25	-	6.94	-	7.75	5.09	4.88	3/8-16	0.75
932	3.25	8.92	5.88	7.50	4.00	3.75	2.00	3.50	6.56	7.00	9.38	6.65	10.69	7.06	6.75	7/16-14	0.88

Size	Output Shaft				Motor Size Available (per size and ratio)								Ap'x. Wgt.	
	+0.000, -0.001		W-KEY		10:1	15:1	20:1	30:1	40:1	50:1	60:1	LBS.	OIL CAP.	
913	0.625	2.19	3/16	1.00	B5	B5	B5	B5	B5	B5	B5	13	6.5	
915	0.750	2.06	3/16	1.00	B5	B5	B5	B5	B5	B5	B5	18	10	
918	0.875	2.06	3/16	1.00	B5,B7	B5,B7	B5	B5	B5	B5	B5	21	14	
921	1.000	2.38	1/4	1.25	B5,B7	B5,B7	B5,B7	B5	B5	B5	B5	27	17.5	
924	1.125	2.66	1/4	1.25	B5,B7	B5,B7	B5,B7	B5,B7	B5,B7	B5	B5	33	26.5	
932	1.375	3.44	5/16	2.50	B7,B9	B7,B9	B7,B9	B5,B7	B5,B7	B5,B7	B5,B7	76	67	

Figure F.7: Baldor WDFG6032AG 60:1 washdown gearbox dimensions.

F.2 Flip Motion Generating Wrist Actuator Cutsheets



Figure F.8: Atlas Copco LZW 34RL AR004.

Product data at air pressure 6.3 bar (91 psi) Reversible		
Ordering No.	8411 0339 73	
Model	LZW 34RL AR004-11	
Max. power	0.24	kW
	0.32	hp
Speed at max. power	190	r/min
Torque at max. power	12	Nm
	8.9	lbf. ft
Min. starting torque	13	Nm
	9.6	lbf. ft
Free speed	350	r/min
Air consumption at max. power	8.5	l/s
	18.0	cmf
Weight	1.2	kg
	2.6	lb
Shaft loading code	c	
Lubrication free	Yes	
Comment:	Stainless steel	

Figure F.9: Atlas Copco LZW 34RL AR004 product data.

Atlas Copco Air Motors

Performance curves

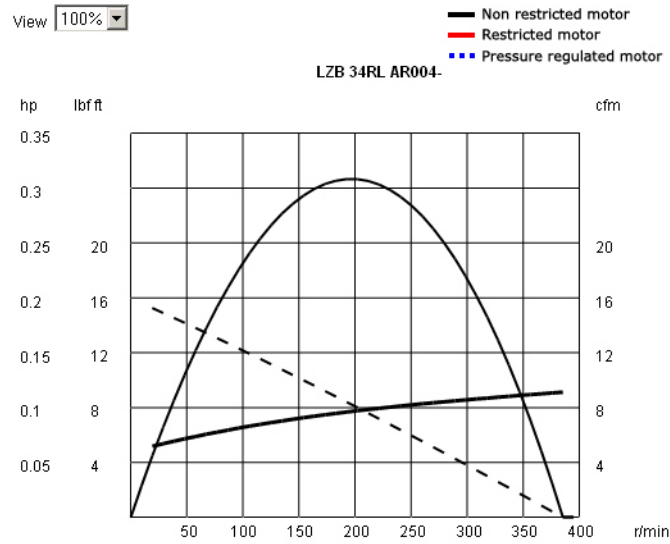


Figure F.10: Atlas Copco LZB 34RL AR004 performance curve: 81 psi.

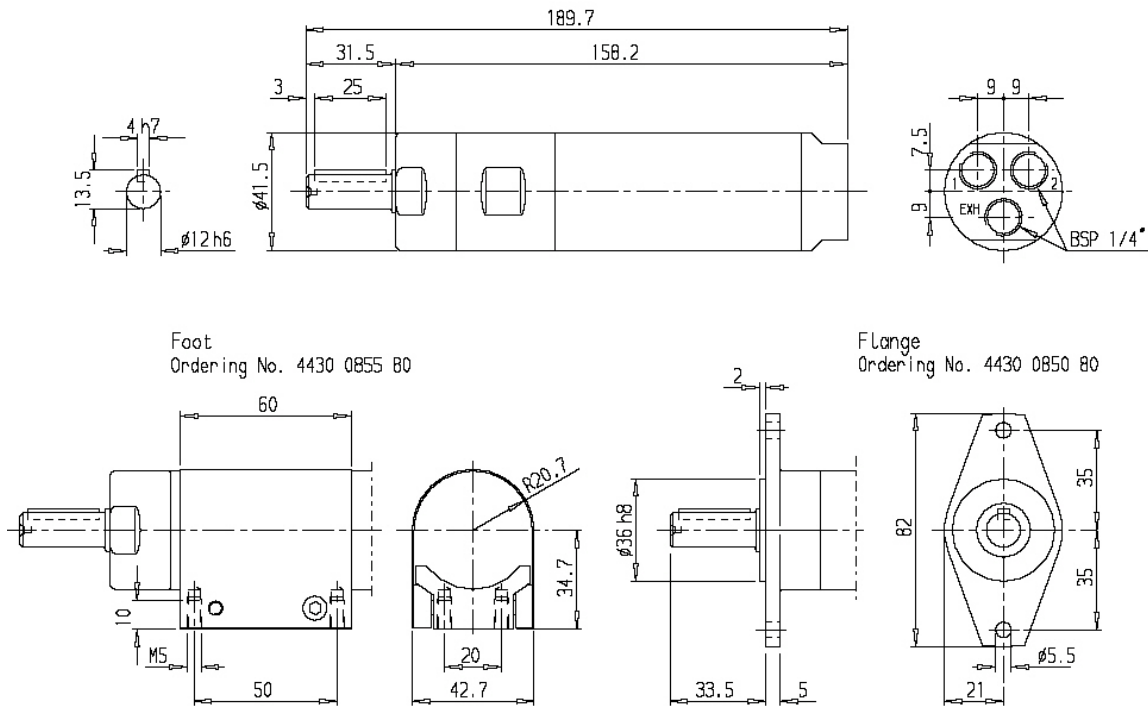


Figure F.11: Atlas Copco LZB 34RL AR004 dimensions.

F.3 Rotate Motion Generating Wrist Actuator Cutsheets

PMA2 SERIES MOTOR



- 6-pole synchronous servomotors
- Neodymium-iron-boron magnets for maximum torque
- 240V ac, 320V dc bus maximum operation
- Available with integral brake
- IP65 or optional IP67 protection
- Anti-cog stator design
- High-quality Interconnectron connectors
- Rated speeds to 7,400 RPM

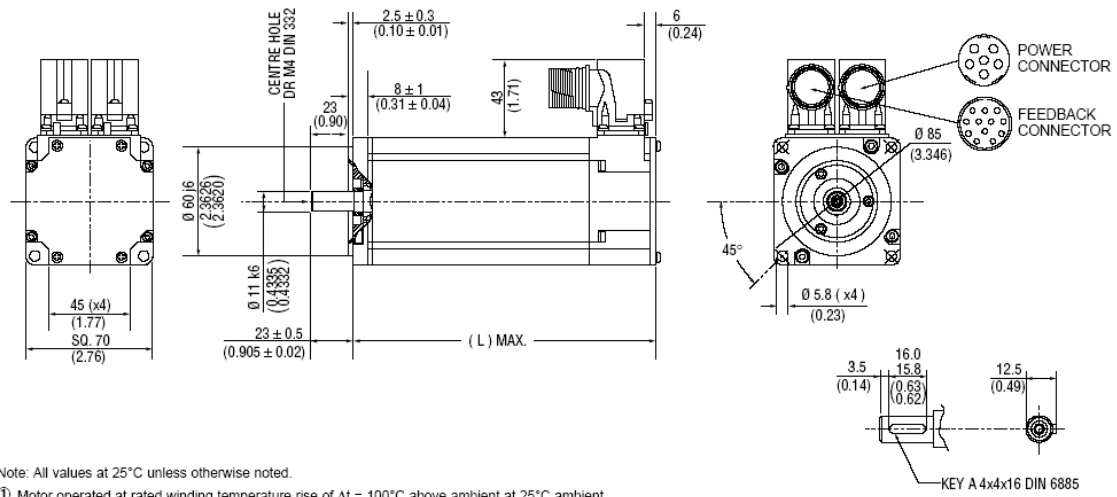
The PMA2 Series motors cover a continuous torque range from 0.5 to 2.6 Nm. These compact motors are well-suited for speed and position control applications requiring maximum performance in minimum space. The PMA2 Series is available with a commutating encoder, in addition to the standard resolver primary feedback, allowing for integration with other control schemes.

RATINGS AND CHARACTERISTICS

Motor parameters and winding data. See system data beginning on page 4 for typical torque/speed performance.

PARAMETER	SYMBOL	UNITS	PMA21	PMA22	PMA23		PMA24		
Continuous stall torque ^{① ② ③}	T_{CS}	Nm (lb.-in.)	0.63 (5.6)	1.3 (11.5)	2 (17.7)		2.6 (23.0)		
Peak torque ^{④ ⑤}	T_{PK}	Nm (lb.-in.)	2.3 (20.4)	4.7 (41.6)	7.2 (63.7)		9.6 (85.0)		
Inertia ^⑥	J_M	$kgm^2 \times 10^{-9}$ (lb.-in.-sec ² × 10 ⁻⁹)	0.022 (0.19)	0.038 (0.34)	0.055 (0.49)		0.072 (0.64)		
Static friction (max.)	T_f	Nm (lb.-in.)	0.016 (0.14)	0.033 (0.29)	0.050 (0.44)		0.065 (0.58)		
Viscous damping coefficient	K_{DV}	Nm/ARPM (lb.-in./ARPM)	0.003 (0.03)	0.006 (0.05)	0.009 (0.08)		0.012 (0.11)		
Thermal resistance	R_{TH}	deg. C/Watt	1.83	1.41	1.13		0.89		
Thermal time constant	τ_{TH}	min.	13.0	15.0	18.0		20.0		
Weight (motor only)	W	kg (lbs.)	1.7 (3.7)	2.3 (5.0)	2.9 (6.4)		3.5 (7.7)		
WINDING DATA			B	B	B	C	D	C	D
Torque constant (RMS)	K_t	Nm/A _{RMS} (lb.-in./A _{RMS})	0.37 (3.3)	0.49 (4.3)	0.74 (6.5)	0.59 (5.2)	0.4 (3.5)	0.79 (7.0)	0.5 (4.4)
Voltage constant (RMS) (I-n)	K_E	V _{RMS} /rad/sec (V _{RMS} /ARPM)	0.23 (2.0)	0.30 (31.2)	0.45 (47.4)	0.36 (37.9)	0.24 (25.4)	0.49 (50.9)	0.31 (31.9)
Continuous stall current ^{① ②}	I_{CS}	A _{RMS}	1.72	2.65	2.7	3.4	5.0	3.3	5.3
Current at peak torque ^⑥	I_{PK}	A _{RMS}	6.88	10.6	10.8	13.6	20.0	13.2	21.2
Resistance (line-to-line)	R_C	Ohms	8.8	4.81	6.1	3.8	1.7	4.6	1.9
Inductance (line-to-line)	L	mH	10.5	7.4	10.6	6.8	3.0	8.9	3.5
Typical Rated Speed @ 240V ac, 320V dc bus	W_R	RPM	6,050	4,650	3,600	4,200	6,400	3,000	4,950
Typical Rated Torque @ 240V ac, 320V dc bus	T_{CR}	Nm (lb.-in.)	0.5 (4.4)	1.06 (9.4)	1.7 (14.6)	1.6 (14.2)	1.4 (12.4)	2.2 (19.5)	2.2 (19.5)

Figure F.12: Pacific scientific PMA 23 washdown servo motor characteristics.



Note: All values at 25°C unless otherwise noted.

- ① Motor operated at rated winding temperature rise of $\Delta t = 100^\circ\text{C}$ above ambient at 25°C ambient. Ratings result of average rating between free air and cold plate mounting. Equivalent to mounting to a 10" x 10" x 1/4" aluminum heat sink.
- ② All tests performed with sinusoidal commutation.
- ③ Theoretical motor maximum.
- ④ Caution: For peak torques or peak currents greater than 4x the continuous rating, consult the factory for thermal considerations.
- ⑤ Add parking brake, if applicable, for total inertia.
- ⑥ Motor with resolver feedback.
- ⑦ Commutating encoder option may reduce continuous torque ratings by up to 10%. Contact factory for details.

CUSTOMER KEY OPTION

Motor	PMA21	PMA22	PMA23	PMA24
L Max	143 (5.6)	168 (6.6)	193 (7.6)	218 (8.6)

mm (in.)
Note: Commutating encoder option adds 15 mm (0.59") to total length.

Figure F.13: Pacific scientific PMA 23 washdown servo motor dimensions.

REFERENCES

- [1] Sciavicco, L. and Siciliano, B. Modeling and Control of Robot Manipulators, Springer-Verlag, London, 2001.
- [2] Merlet, Jean-Pierre, Parallel Robots, Kluwer Academic Publishing, Dordrecht, The Netherlands, 2000.
- [3] Yan, Hong-Sen, Creative Design of Mechanical Devices, Springer-Verlag, Singapore, 1998.
- [4] Shigley, Joseph Edward, Kinematic Analysis of Mechanisms, McGraw-Hill, 1969.
- [5] Khodabandehloo, K. (Editor), Robotics in Meat, Fish and poultry Processing, Blackie Academic & Professional, Chapman & Hall, Glasgow, 1993.
- [6] Socha, Kevin G. Design of a Compliant end Effector for Grasing Non-Rigid Materials, Georgia Institute of Technology, Atlanta, GA, 2003.
- [7] OSHA, *Ergonomics for the Prevention of Musculoskeletal disorders Draft Guidelines for poultry Processing*,
<http://www.osha.gov/ergonomics/guidelines/poultryprocessing/poultryall-in-one.pdf>, 2003.
- [8] Bureau of Labor Statistics, *Industry Injury and Illness Data*,
<http://www.bls.gov/iif/oshsum.htm#01Summary>, 2003.
- [9] McMurray, G.V., Rutheford, R.C., Piepmeier, J.A., Biro, R.F., Holcombe, W.D., Lee, K.M. "Automation in the poultry industry: the application of Human Level Performance Robotics," IEEE/ASME International Conference on Advanced Intelligent Mechatronics '97 , 16-20 June 1997.
- [10] Pahl, G. and Beitz, W., Engineering Design, Springer-Verlag, London, 1996.
- [11] USDA Economic Research Service,
<http://www.ers.usda.gov/data/foodconsumption/datasystem.asp>, 2003.
- [12] Zsombor-Murray, P.J., "Descriptive Geometric Kinematic Analysis of Clavel's "Delta" Robot", www.cim.mcgill.ca/~paul/clavdelt.pdf, September 23, 2003.

- [13] Lee, K.M., “A Three-Degrees-Of-Freedom Micromotion In-Parallel Actuated Manipulator” IEEE Transactions on Robotics and Automation, vol. 7, no. 5, pp. 634-641, October 1991.
- [14] Di Gregario, R., Parenti-Castelli, V., “Mobility Analysis of the 3-UPU Parallel Mechanism Assembled for a Pure Translational Motion”, Proceedings of the IEEE/ASME International Conference on Advanced Intelligent Mechatronics, pp. 520-525, September 19-23, 1999.
- [15] Tsai, L.W., “Kinematics Of a Three-DOF Platform With Three Extensible Limbs”, Recent Advances in Robot Kinematics, Kluwer Academic Publishers, pp. 401-410, Dordrecht, The Netherlands, 1996.
- [16] Di Gregario, R., Parenti-Castelli, V., “A Translational 3-DOF Parallel Manipulator”, Advances in Robot Kinematics: Analysis and Control, Kluwer Academic Publishers, pp. 49-58, Dordrecht, The Netherlands, 1998.
- [17] Shigley, J.E., Kinematic Analysis of Mechanisms, McGraw-Hill, 1969.
- [18] Shigley, J.E., Mechanical Engineering Design, Fifth Edition, McGraw-Hill, 1989.
- [19] Bickford, J. H., Mechanisms for Intermittent Motion, Industrial Press, New York, N.Y., 1972.
- [20] Murray, R. M., A Mathematical Introduction to Robotic Manipulation, CRC, 1994.
- [21] Thomas, F., Torras, C., “A Group –Theoretic Approach to the Computation of Symbolic Part Relations”, IEEE Journal of Robotics and Automation, vol. 4, no. 6, December 1988.
- [22] Sparacino, F., Herve, J.M., “Synthesis of Parallel Manipulators Using Lie-Groups Y-Star and H-Robot”, Proceedings of the 1993 IEEE/Tsukuba International Workshop on Advanced Robotics, pp. 75-80, November 8-9, 1993.
- [23] Herve, J.M., Sparacino, F., “Structural Synthesis of “Parallel” Robot Generating Spatial Translation”, Fifth International Conference on Advanced Robotics, pp. 808-813, June 19-22, 1991.
- [24] Pierot et al., “Fast Parallel Robots”, Journal of Robotic Systems, 8(6):829-840, December 1991.
- [25] NSF, 2002, Hygiene requirements for the design of meat and poultry processing equipment, NSF/ANSI/3-A 1419-1 – 2002.
- [26] Coquemond, C, “Automatic Shackle Loading”, Georgia Tech Research Institute, January 2004.

[27] Celton, O, “Automatic Shackle Loading”, Georgia Institute of Technology, January 2004.

[28] Stamper, R, A Three Degree of Freedom Parallel Manipulator With Only Translational Degrees of Freedom, University of Maryland, College Park, MD, 1997.